Stony Brook University

Characterization of the Spatial and Temporal Variations of Submarine Groundwater Discharge Using Electrical Resistivity and Seepage Measurements

A Dissertation Presented

by

Josephine Miryam Kalyanie Durand

to

The Graduate School

in Partial Fulfillment of the

Requirements

for the Degree of

Doctor of Philosophy

in

Geosciences

(Hydrogeology)

Stony Brook University

August 2014

Stony Brook University

The Graduate School

Josephine Miryam Kalyanie Durand

We, the dissertation committee for the above candidate for the

Doctor of Philosophy degree, hereby recommend

acceptance of this dissertation.

Teng-fong Wong –Dissertation Advisor
Professor, Geosciences

Daniel Davis - Chairperson of Defense
Professor and Chair, Geosciences

Gilbert Hanson
Distinguished Service Professor, Geosciences

Henry Bokuniewicz
Distinguished Service Professor, School of Marine and Atmospheric Sciences

Harold Walker
Professor and Civil Engineering Program Director, Stony Brook University

This dissertation is accepted by the Graduate School

Charles Taber
Dean of the Graduate School

Abstract of the Dissertation

Characterization of the Spatial and Temporal Variations of Submarine Groundwater Discharge Using Electrical Resistivity and Seepage Measurements

by

Josephine Miryam Kalyanie Durand

Doctor of Philosophy

in

Geosciences

(Hydrogeology)

Stony Brook University

2014

Submarine groundwater discharge (SGD) encompasses all fluids crossing the sediment/ocean interface, regardless of their origin, composition or driving forces. SGD provides a pathway for terrestrial contaminants that can significantly impact coastal ecosystems. Overexploitation of groundwater resources can decrease SGD which favors seawater intrusion at depth. Understanding SGD is therefore crucial for water quality and resource management. Quantifying SGD is challenging due to its diffuse and heterogeneous nature, in addition to significant spatio-temporal variations at multiple scales.

In this thesis, an integrated approach combining electrical resistivity (ER) surveys, conductivity and temperature point measurements, seepage rates using manual and ultrasonic seepage meters, and pore fluid salinities was used to characterize SGD spatio-temporal variations and their implications for contaminant transport at several locations on Long Island, NY.

The influence of surficial sediments on SGD distribution was investigated in Stony Brook Harbor. A low-permeability mud layer, actively depositing in the harbor, limits SGD at the shoreline, prevents mixing with seawater and channels a significant volume of freshwater offshore. SGD measured at locations without mud is high and indicates significant mixing

between porewater and seawater. A 2D steady-state density-difference numerical model of the harbor was developed using SEAWAT and was validated by our field observations.

Temporal variations of SGD due to semi-diurnal tidal forcing were studied in West Neck Bay, Shelter Island, using a 12-hr time-lapse ER survey together with continuous salinity and seepage measurements in the intertidal zone. The observed dynamic patterns of groundwater flux and salinity distribution disagree with published standard transient state numerical models, suggesting the need for developing more specific models of non-homogeneous anisotropic aquifers.

SGD distribution and composition were characterized in Forge River, a tidal river that experiences chronic hypoxia due to nitrogen contamination. We found that nitrogen speciation and concentration are linked to different SGD regimes. Near shore sandy zones with high SGD show little nitrate reduction and constitute the major source of nitrogen input to surface waters. Offshore areas rich in silt and organic matter exhibit low SGD and higher denitrification. Dredging activities have altered the sediment distribution and subsequently have created preferential flow paths focusing freshwater discharge into the center of the river.

For Stony Brook Harbor study presented in chapter 2, I acquired, processed and interpreted the electrical resistivity and seepage meter data. Caitlin Young helped during collection of manual seepage data and Joseph Tamborski provided assistance for the mud mapping. The piezometers were installed for a parallel study focusing on denitrification but allowed me to collect and use porewater salinity measurements. Teng-fong Wong and Gilbert Hanson helped with the preparation of the manuscript. Design, simulations and result interpretation of the numerical model presented in chapter 3 were done without external contribution. Data presented in chapter 4 were collected with the help of Neal Stark and Jonathan Wanlass. I performed the processing, analysis and data interpretation. Teng-fong Wong assisted with the preparation of the manuscript. For chapter 5, Neal Stark assisted with the electrical resistivity data acquisition and collected all the water samples in Forge River. Ronald Paulsen provided help with the preparation of the report.

Dedication Page

To the Earth, for being:

a never-ending source of wonders,

a spring of breath-taking beauty

and a constant provider of infinite mysteries.

À Dany, pour tout et plus encore…

Frontispiece

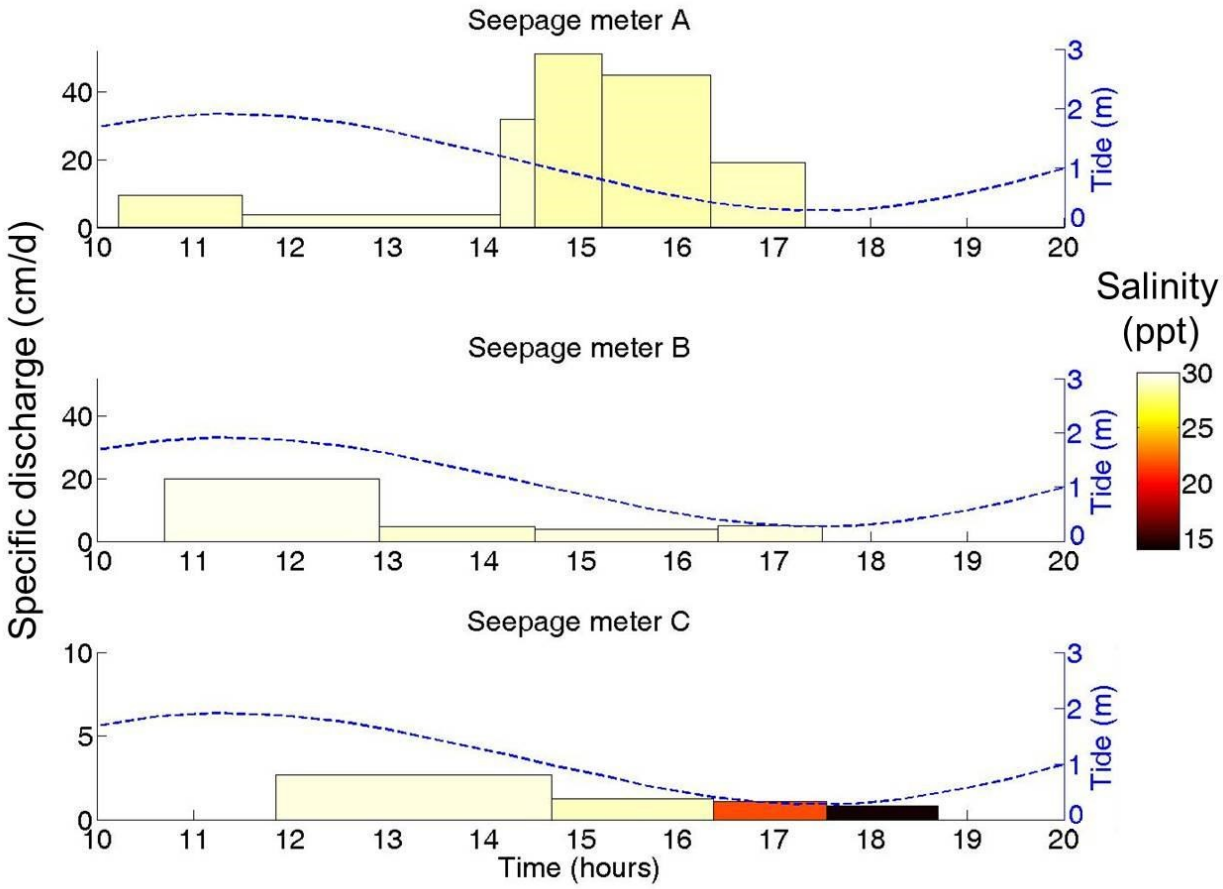

Salinity and flow rates measurements from manual seepage meters in Stony Brook Harbor, NY. The meters A, B and C were placed at 1, 20 and 22 m offshore of the low tide mark, respectively. Each square represents a sampling interval: the base shows the sampling duration in hours, the square height the seepage rate in cm/d and the color the salinity. The blue dotted line indicates the tidal level, in m. Note the different scale for the seepage meter C.

Table of Contents

List of Figures

List of Tables

List of Abbreviations

AGI: Advanced Geosciences Incorporation

BCF: Bloc-Centered Flow (package)

BOD: Biological Oxygen Demand

DRN: Drain (package)

DT: Temperature Difference

ER: Electrical Resistivity

FSI: Freshwater-Seawater Interface

GHB: General Head Boundary (package)

L2: Euclidian norm

MLLW: Mean Lower Level of Water

ORP: Oxydo-Reduction Potential

PBC: Periodic Boundary Condition (package)

RMSE: Root Mean Square Error

SCDHS: Suffolk County Department of Health Services

SCOR: Scientific Committee on Oceanic Research

SGD: Submarine Groundwater Discharge

SM: Seepage Meter

TKN: Total Kjeldhal Nitrogen

USM: Ultrasonic Seepage Meter

Acknowledgments

I am mostly grateful to my advisor Teng-fong Wong for his guidance and the insightful conversations that we shared. He allowed me to work on challenging topics and let me lead my own investigations while giving useful advice when needed. I am also thankful to my committee members Dan Davis, Gil Hanson, Henry Bokuniewicz and Harold Walker for their stimulating discussions and valuable comments on my dissertation.

I would like to thank the Bureau of Water Resources of the Suffolk County Department of Health Services for making the field equipment available and assisting in data collection, especially Jonathan Wanlass and Ronald Paulsen. Neal Stark was also key in the field data acquisition.

I am grateful to Daniel O'Rourke and Chris Smith for the opportunity to work as a consultant, with Cornell Cooperative Extension and CDM Smith, on a project that is part of my thesis.

I am sincerely appreciative of the support and help from Caitlin Young and Joe Tamborski in data collection from both the field and the laboratory. Thanks to you, I now cherish epic memories involving manual seepage meters… I cannot thank Joe enough for proof-reading my manuscript and helping with the English.

I am thankful to the personnel of the main office: Owen, Laura, Yvonne, Diane and Loretta who were always there to help. They provided precious and benevolent advice regarding my adaptation to this country, assistance with the paperwork and any kind of worries.

The Stony Brook adventure would not have been so enjoyable without my labmates Cecilia, Wei and Yuntao, my friend and delightful office mate Anna and the geosciences students, especially Cong-Cong and Hui.

I am deeply grateful to Anibal for his presence and affection along the way. He reminded me every day of the beauty of knowledge and the amazement that science can bring. Thanks to him, I have grown into an even more confident and determined woman.

Finally, I would like to thank my family for their unconditional love and support. They always encouraged me to go forward and never doubted my success.

Publications

Stark NH, **Durand JM**, Wong T-f, Wanlass J, Paulsen R 'Submarine Groundwater Discharge in Relation to the Occurrence of Submerged Aquatic Vegetation, Data Report for Site 1, Three Mile Harbor' 2012 Prepared for the *Peconic Estuary Program of the Suffolk County Department of Health Services.*

Stark NH, **Durand JM**, Wong T-f, Wanlass J, Paulsen R 'Submarine Groundwater Discharge in Relation to the Occurrence of Submerged Aquatic Vegetation, Data Report for Site 2, Gardiners Bay' 2012 Prepared for the *Peconic Estuary Program of the Suffolk County Department of Health Services.*

Stark NH, **Durand JM**, Wong T-f, Wanlass J, Paulsen R 'Submarine Groundwater Discharge in Relation to the Occurrence of Submerged Aquatic Vegetation, Data Report for Site 3, Cedar Point' 2012 Prepared for the *Peconic Estuary Program of the Suffolk County Department of Health Services.*

Stark NH, **Durand JM**, Wong T-f, Wanlass J, Paulsen R 'Submarine Groundwater Discharge in Relation to the Occurrence of Submerged Aquatic Vegetation, Data Report for Site 4, Bullhead Bay' 2012 Prepared for the *Peconic Estuary Program of the Suffolk County Department of Health Services.*

Durand JM, Paulsen R. 'Flow Patterns and Nutrient Loading Associated With Submarine Groundwater Discharge in Forge River and Wills Creek', Report, January, 2014, Prepared for CDM Smith and Town of Brookhaven.

Chapter 1: Introduction

Introduction

The most general definition of submarine groundwater discharge (SGD) encompasses all fluids crossing the sediment/ocean interface regardless of their origin, driving-force or composition [*Burnett et al.*, 2003]. SGD is widely recognized as an important water exchange process between land and sea [*Bokuniewicz*, 1980; *Howarth et al.*, 1996; *Taniguchi et al.*, 2002; *Valiela et al.*, 1978] over different spatial and temporal scales [*Bratton*, 2010; *Michael et al.*, 2003; *Michael et al.*, 2005]. Historically, volume of SGD has been computed as input from all potential sources in the water cycle. Unfortunately, quantitative estimates of SGD so obtained are subject to cumulative errors from the determination of precipitation, evapotranspiration and river runoff. While its volume might be small compared to surface water discharge, SGD can transport high nutrient concentrations which significantly impact coastal water quality [*Johannes*, 1980; *Moore et al.*, 2008; *Slomp and Van Cappellen*, 2004; *Zektser et al.*, 2006]. The mixing of fresh and saline waters creates geochemically active zones in the sediments [*Moore*, 1999; *Moore and Shaw*, 1998; *Valiela and Delia*, 1990]. Understanding SGD is therefore crucial for the quantification of chemical fluxes from coastal aquifers to the ocean and the assessment of water quality for mitigation [*Charette and Buesseler*, 2004; *Valiela et al.*, 1992]. Furthermore, a large part of the population living near the ocean relies on groundwater; overexploitation lowers the terrestrial hydraulic gradient, one of SGD drivers, increasing the risk of seawater intrusion and threatening coastal groundwater resources [*Bear*, 1999; *Post*, 2005].

In the field, a variety of seepage meters (SM) have been developed to obtain direct seepage measurements. They include: manual SM [*Lee*, 1977], ultrasonic SM [*Paulsen et al.*, 2001], heat pulse SM [*Krupa et al.*, 1998; *Taniguchi and Fukuo*, 1993], continuous heat flow SM [*Taniguchi and Iwakawa*, 2001], electromagnetic SM [*Rosenberry and Morin*, 2004] and dye seepage SM [*Sholkovitz et al.*, 2003]. Due to its highly diffuse and heterogeneous nature, and its spatio-temporal variations at a variety of scales, it is recommended to integrate more than one technique that can collectively cover multiple scales [*Burnett et al.*, 2006]. Complementary data can be obtained from natural tracers, including U-Th series nuclides [*Charette et al.*, 2008], methane [*Bugna et al.*, 1996], helium [*Top et al.*, 2001] and Si [*Hwang et al.*, 2005]. Geophysical methods, such as electrical resistivity, can provide information about SGD distribution [*T*

Stieglitz et al., 2008b]. More recently, thermal imaging has been used to obtain regional high-resolution SGD maps [*Johnson et al.*, 2008].

To evaluate fluxes of water and solute related to SGD, it is critical to quantify the relative contributions of fresh and circulated SGD, and the dynamics of their interaction. Numerical models have contributed to deeper understanding of SGD dynamics, and its dependence on various factors: the aquifer beach slope [*Ataie-Ashtiani et al.*, 1999; *Mango et al.*, 2004; *Mao et al.*, 2006], the inland hydraulic gradient [*Prieto and Destouni*, 2005; *Robinson et al.*, 2007a], tidal forcing [*Li et al.*, 1999; *Robinson et al.*, 2006], wave set-up [*Xin et al.*, 2010], seasonal variations [*Michael et al.*, 2005], sea-bed topography [*Konikow et al.*, 2013], heat or density-driven convection [*Kohout*, 1960; 1965], bioirrigation [*Martin et al.*, 2004], sea level rise [*Gonneea et al.*, 2013], storm events [*Robinson et al.*, 2014] and interannual climate oscillations [*Anderson and Emanuel*, 2010].

Nutrients supplied by SGD have been implicated in coastal eutrophication and algal blooms which are recurring problems on Long Island's shore. Most freshwater entering Long Island Sound from the north shore of Long Island is estimated to come from SGD [*Koppelman et al.*, 1976]. Quantifying the nutrient load to Long Island water bodies requires a better understanding of the dynamics of SGD. Three fundamentally different hydrogeological systems on Long Island have been selected for my thesis research.

Simulations of groundwater flow in various bays and lakebeds suggest that shoreline geometry and coastal configuration can accentuate the hydraulic gradient, increasing discharge by as much as a factor of five [*Cherkauer and McKereghan, 1991*]. SGD should therefore be similarly enhanced in embayments relative to straight-face beaches. On the north shore of Long Island, embayments represent a significant amount of shoreline: 11 bays and harbors account for a total of 257 km of shoreline, on an island only 190 km long [*Koppelman et al., 1976*]. Characterizing SGD in embayments is therefore crucial to quantify groundwater seepage more accurately at a regional scale. What are the characteristics of SGD occurring in embayments? This question is addressed in the study on Stony Brook Harbor, NY.

A Sea Grant project entitled 'Sources and Fate of Nitrogen in North Shore Embayments' focused on studying SGD and associated nitrogen fluxes in Stony Brook Harbor, Port Jefferson

Harbor and East Setauket Harbor. Chapter 2 presents the characterization of the hydrogeological framework and SGD distribution in Stony Brook Harbor, which guided the geochemical analyses presented in [*Young*, 2013]. The study integrated multiple hydrologic and geophysical techniques: flow measurements using ultrasonic and manual seepage meters, point conductivity and temperature measurements using a Trident Probe, electrical resistivity surveys and water quality data through pore water sampling. Data from this study highlight the spatial heterogeneity of SGD linked to low-permeability sediment distribution in the harbor.

To further investigate geological control on SGD through the existence of such a low permeability layer, a comparative 2D density-difference numerical model was developed using SEAWAT [*Guo and Langevin*, 2002]. Chapter 3 describes the conceptual model and its implementation and compares the hydraulic head and salinity distribution between 2 versions of the steady-state model with and without the low-permeability mud layer.

Data from Forge River and Stony Brook Harbor, as well as several other sites in the Peconic Estuary [*Stark et al.*, 2012a; b; c; d] and Port Jefferson Harbor all indicate that the dynamics of SGD is intimately related to tidal loading. When taking into account dynamic boundaries representing tides and waves, groundwater flow and solute transport models predict multiple freshwater-seawater interfaces more complex than previously thought. The boundaries are composed of three main parts: a shallow saline advective cell in the intertidal zone, an offshore deep saline convection cell traditionally called the saltwater wedge, and a relatively thin zone of freshwater discharge between them [*Robinson et al., 2006*]. To what extent can these numerical models realistically reproduce field observations of hydrogeological complexities and variations in porewater salinity distribution due to tidal forcing? To address this question, I chose to image the intertidal zone of a sandy coastal aquifer, in West Neck Bay (Shelter Island, NY) during a semi-diurnal tidal cycle. This second location was selected because SGD in West Neck Bay had been extensively studied in a comparative experiment led by working group 112 of the Scientific Committee on Oceanic Research (SCOR) [*Anonymous*, 2002; *Burnett et al.*, 2006; *Dulaiova et al.*, 2006; *Paulsen et al.*, 2004; *Sholkovitz et al.*, 2003; *Stieglitz et al.*, 2008b; *Stieglitz et al.*, 2007] and in other previous studies [*O'Rourke*, 2000; *Paulsen et al.*, 1998]. This study, presented in chapter 4, combined stationary time-lapse ER surveys and direct seepage measurements at the sediment/water interface in the intertidal and subtidal zones. Some data suggested the existence

of a confining unit at that site, but its extent and properties were not characterized [*Stieglitz et al.*, 2007]. A second goal of this study was to investigate if deeper ER vertical cross-sections could image the spatial extent of that confining layer under the beach.

The third site is the Forge River, on the south shore of Long Island, which has suffered chronic hypoxia due to nitrogen contamination, entering the system through groundwater. A study involving Cornell Cooperative Extension at Suffolk County, CDM Smith and the town of Brookhaven aimed at mapping SGD distribution and quantifying different nitrogen species concentrations in groundwater along Forge River's banks and under the river bottom. The overall objective was to quantify the naturally-occurring reduction of nitrogen load from groundwater to the river across the hyporheic zone specifically, at two locations on the Forge River itself, and along one of its tributaries, Wills Creek [*Durand and Paulsen*, 2014]. Chapter 5 includes a more detailed description of all the equipment used during all the studies presented in this thesis. The results obtained along Forge River banks are presented and interpreted to distinguish three main zones with specific SGD regimes and nitrogen content and attenuation.

The major findings of this thesis on the three hydrogeologic systems are summarized in chapter 6. The chapters are intended to be read as independent units. However, chapter 3 constitutes a numerical study based on data and observations detailed in chapter 2. Chapter 2 was submitted to *Water Resources Research* under the title "Effect of a mud cap on submarine groundwater discharge in Stony Brook Harbor, NY" by Josephine Durand, Caitlin Young, Gilbert Hanson and Teng-fong Wong, and has been revised taking into account critical comments of the reviewers. Chapter 4 is in preparation for submission. Chapter 5 is extracted from a more extensive report, prepared for CDM Smith and the Town of Brookhaven and published with the title "Flow Patterns and Nutrient Loading Associated with Submarine Groundwater Discharge in Forge River and Wills Creek" by Josephine Durand and Ronald Paulsen.

For Stony Brook Harbor study presented in chapter 2, I acquired, processed and interpreted the electrical resistivity and seepage meter data. Caitlin Young helped during collection of manual seepage data and Joseph Tamborski provided assistance for the mud mapping. The piezometers were installed for a parallel study focusing on denitrification [*Young*, 2013] but allowed me to collect and use porewater salinity measurements. Teng-fong Wong and

Gilbert Hanson helped with the preparation of the manuscript. Design, simulations and result interpretation of the numerical model presented in chapter 3 were done without external contribution. Data presented in chapter 4 were collected with the help of Neal Stark and Jonathan Wanlass. I performed the processing, analysis and data interpretation. Teng-fong Wong assisted with the preparation of the manuscript. For chapter 5, Neal Stark assisted with the electrical resistivity data acquisition and collected all the water samples in Forge River. Ronald Paulsen provided help with the preparation of the report.

References

Anderson, W. P., and R. E. Emanuel (2010), Effect of interannual climate oscillations on rates of submarine groundwater discharge, *Water Resources Research*, *46*(5).

Anonymous (2002), Submarine Groundwater discharge assessment intercomparison experiment, , International Hydrological Program (IHP), Scientific Commitee on Oceanic Research (SCOR), Land Ocean Interactions in the Coastal Zone (LOICZ), *Report*, 26 pp.

Ataie-Ashtiani, B., R. Volker, and D. Lockington (1999), Tidal effects on sea water intrusion in unconfined aquifers, *Journal of Hydrology*, *216*(1-2), 17-31.

Bear, J. (1999), *Seawater intrusion in coastal aquifers: Concepts, methods, and practices*, Springer Netherlands.

Bokuniewicz, H. (1980), Groundwater seepage into Great South Bay, New York, *Estuarine and Coastal Marine Science*, *10*(4), 437-444.

Bratton, J. F. (2010), The three scales of submarine groundwater flow and discharge across passive continental margins, *The Journal of Geology*, *118*(5), 565-575.

Bugna, G. C., J. P. Chanton, J. E. Cable, W. C. Burnett, and P. H. Cable (1996), The importance of groundwater discharge to the methane budgets of nearshore and continental shelf waters of the northeastern Gulf of Mexico, *Geochimica et Cosmochimica Acta*, *60*(23), 4735-4746.

Burnett, W. C., H. Bokuniewicz, M. Huettel, W. S. Moore, and M. Taniguchi (2003), Groundwater and pore water inputs to the coastal zone, *Biogeochemistry*, *66*(1-2), 3-33.

Burnett, W. C., et al. (2006), Quantifying submarine groundwater discharge in the coastal zone via multiple methods, *Science of the Total Environment*, *367*(2-3), 498-543.

Charette, M., W. Moore, and W. Burnett (2008), Uranium-and thorium-series nuclides as tracers of submarine groundwater discharge, *U-Th series nuclides in aquatic systems. Elsevier*, 155-191.

Charette, M. A., and K. O. Buesseler (2004), Submarine groundwater discharge of nutrients and copper to an urban subestuary of Chesapeake Bay (Elizabeth River), *Limnology and Oceanography*, 376-385.

Cherkauer, D. S., and P. F. McKereghan (1991), Ground-Water Discharge to Lakes: Focusing in Embayments, *Ground Water*, *29*(1), 72-80.

Dulaiova, H., W. C. Burnett, J. P. Chanton, W. S. Moore, H. Bokuniewicz, M. A. Charette, and E. Sholkovitz (2006), Assessment of groundwater discharges into West Neck Bay, New York, via natural tracers, *Continental Shelf Research*, *26*(16), 1971-1983.

Durand, J. M., and R. Paulsen (2014), Flow Patterns and Nutrient Loading Associated with Submarine Groundwater Discharge in Forge River and Wills Creek, prepared for CDM Smith and the Town of Brookhaven. *Report, 83 pp.*

Gonneea, M. E., A. E. Mulligan, and M. A. Charette (2013), Climate-driven sea level anomalies modulate coastal groundwater dynamics and discharge, *Geophysical Research Letters*, *40*(11), 2701-2706.

Howarth, R. W., et al. (1996), Regional nitrogen budgets and riverine N & P fluxes for the drainages to the North Atlantic Ocean: Natural and human influences, *Biogeochemistry*, *35*(1), 75-139.

Hwang, D.-W., G. Kim, Y.-W. Lee, and H.-S. Yang (2005), Estimating submarine inputs of groundwater and nutrients to a coastal bay using radium isotopes, *Marine Chemistry*, *96*(1), 61-71.

Johannes, R. (1980), Ecological significance of the submarine discharge of groundwater, *MARINE ECOL.- PROG. SER.*, *3*(4), 365-373.

Johnson, A. G., C. R. Glenn, W. C. Burnett, R. N. Peterson, and P. G. Lucey (2008), Aerial infrared imaging reveals large nutrient-rich groundwater inputs to the ocean, *Geophysical Research Letters*, *35*(15), L15606.

Kohout, F. (1960), Cyclic flow of salt water in the Biscayne aquifer of southeastern Florida, *Journal of Geophysical Research*, *65*(7), 2133-2141.

Kohout, F. (1965), Section of geological sciences: a hypothesis concerning cyclic flow of salt water related to geothermal heating in the floridan aquifer*,†, *Transactions of the New York Academy of Sciences*, *28*(2 Series II), 249-271.

Konikow, L., M. Akhavan, C. Langevin, H. Michael, and A. Sawyer (2013), Seawater circulation in sediments driven by interactions between seabed topography and fluid density, *Water Resources Research*, *49*(3), 1386-1399.

Koppelman, L. E., P. K. Weyl, M. G. Gross, and D. S. Davies (1976), *The urban sea: Long Island Sound*, viii+223 pp., Praeger Publishers, New York.

Krupa, S. L., T. V. Belanger, H. H. Heck, J. T. Brock, and B. J. Jones (1998), Krupaseep—The next generation seepage meter, *Journal of Coastal Research*, 210-213.

Lee, D. R. (1977), A device for measuring seepage flux in lakes and estuaries, *Limnology and Oceanography*, 140-147.

Li, L., D. Barry, F. Stagnitti, and J. Parlange (1999), Submarine groundwater discharge and associated chemical input to a coastal sea, *Water Resources Research*, *35*(11), 3253-3259.

Mango, A. J., M. W. Schmeeckle, and D. J. Furbish (2004), Tidally induced groundwater circulation in an unconfined coastal aquifer modeled with a Hele-Shaw cell, *Geology*, *32*(3), 233-236.

Mao, X., P. Enot, D. Barry, L. Li, A. Binley, and D. S. Jeng (2006), Tidal influence on behaviour of a coastal aquifer adjacent to a low-relief estuary, *Journal of Hydrology*, *327*(1-2), 110-127.

Martin, J. B., J. E. Cable, P. W. Swarzenski, and M. K. Lindenberg (2004), Enhanced Submarine Ground Water Discharge from Mixing of Pore Water and Estuarine Water, *Ground Water*, *42*(7), 1000-1010.

Michael, H. A., J. S. Lubetsky, and C. F. Harvey (2003), Characterizing submarine groundwater discharge: A seepage meter study in Waquoit Bay, Massachusetts, *Geophys. Res. Lett*, *30*(6), 1297.

Michael, H. A., A. E. Mulligan, and C. F. Harvey (2005), Seasonal oscillations in water exchange between aquifers and the coastal ocean, *Nature*, *436*(7054), 1145-1148.

Moore, W. S. (1999), The subterranean estuary: a reaction zone of ground water and sea water, *Marine Chemistry*, *65*(1), 111-125.

Moore, W. S., and T. J. Shaw (1998), Chemical signals from submarine fluid advection onto the continental shelf, *Journal of Geophysical Research: Oceans (1978–2012)*, *103*(C10), 21543-21552.

Moore, W. S., J. L. Sarmiento, and R. M. Key (2008), Submarine groundwater discharge revealed by 228Ra distribution in the upper Atlantic Ocean, *Nature Geoscience*, *1*(5), 309-311.

O'Rourke, D. (2000), Quantifying specific discharge into West Neck Bay, Shelter Island, New York using a three-dimensional finite-difference groundwater flow model and continuous measurements with an ultrasonic seepage meter, 88 pp, State University of New York, Stony Brook.

Paulsen, R., C. Smith, and T.-f. Wong (1998), Defining freshwater outcrops in West Neck Bay, Shelter Island, New York using direct contact resistivity measurements and transient underflow measurements, paper presented at Geology of Long Island and Metropolitan New York, Stony Brook, NY, USA, April, 18th 1998.

Paulsen, R. J., C. F. Smith, D. O'Rourke, and T. F. Wong (2001), Development and evaluation of an ultrasonic ground water seepage meter, *Ground Water*, *39*(6), 904-911.

Paulsen, R. J., D. O'Rourke, C. F. Smith, and T. F. Wong (2004), Tidal Load and Salt Water Influences on Submarine Ground Water Discharge, *Ground Water*, *42*(7), 990-999.

Post, V. (2011), A new package for simulating periodic boundary conditions in MODFLOW and SEAWAT, *Computers & Geosciences*, *37*(11), 1843-1849.

Post, V. E. A. (2005), Fresh and saline groundwater interaction in coastal aquifers: Is our technology ready for the problems ahead?, *Hydrogeology Journal*, *13*(1), 120-123.

Prieto, C., and G. Destouni (2005), Quantifying hydrological and tidal influences on groundwater discharges into coastal waters, *Water resources research*, *41*(12).

Robinson, C., B. Gibbes, and L. Li (2006), Driving mechanisms for groundwater flow and salt transport in a subterranean estuary, *Geophys. Res. Lett*, *33*, L03402.

Robinson, C., L. Li, and D. Barry (2007b), Effect of tidal forcing on a subterranean estuary, *Advances in Water Resources*, *30*(4), 851-865.

Robinson, C., P. Xin, L. Li, and D. A. Barry (2014), Groundwater flow and salt transport in a subterranean estuary driven by intensified wave conditions, *Water Resources Research*, *50*(1), 165-181.

Rosenberry, D. O., and R. H. Morin (2004), Use of an electromagnetic seepage meter to investigate temporal variability in lake seepage, *Groundwater*, *42*(1), 68-77.

Sholkovitz, E., C. Herbold, and M. Charette (2003), An automated dye-dilution based seepage meter for the time-series measurement of submarine groundwater discharge, *Limnol. Oceanogr. Methods*, *1*, 16-28.

Slomp, C. P., and P. Van Cappellen (2004), Nutrient inputs to the coastal ocean through submarine groundwater discharge: controls and potential impact, *Journal of Hydrology*, *295*(1), 64-86.

Stark, N., J. M. Durand, T.-f. Wong, J. Wanlass, and R. Paulsen (2012a), Submarine Groundwater Discharge in Relation to the Occurrence of Submerged Aquatic Vegetation, Data Report for Site 1, Three Mile Harbor, prepared for the Peconic Estuary Program of the Suffolk County Department of Health Services, *Report.*

Stark, N., J. M. Durand, T.-f. Wong, J. Wanlass, and R. Paulsen (2012b), Submarine Groundwater Discharge in Relation to the Occurrence of Submerged Aquatic Vegetation, Data Report for Site 2, Gardiners Bay, prepared for the Peconic Estuary Program of the Suffolk County Department of Health Services, *Report.*

Stark, N., J. M. Durand, T.-f. Wong, J. Wanlass, and R. Paulsen (2012c), Submarine Groundwater Discharge in Relation to the Occurrence of Submerged Aquatic Vegetation, Data Report for Site 3, Cedar Point., prepared for the Peconic Estuary Program of the Suffolk County Department of Health Services, *Report.*

Stark, N., J. M. Durand, T.-f. Wong, J. Wanlass, and R. Paulsen (2012d), Submarine Groundwater Discharge in Relation to the Occurrence of Submerged Aquatic Vegetation, Data Report for Site 4, Bullhead Bay, prepared for the Peconic Estuary Program of the Suffolk County Department of Health Services, *Report.*

Stieglitz, T., J. Rapaglia, and H. Bokuniewicz (2008b), Estimation of submarine groundwater discharge from bulk ground electrical conductivity measurements, *Journal of Geophysical Research*, *113*(C8), C08007.

Stieglitz, T. C., J. Rapaglia, and S. C. Krupa (2007), An effect of pier pilings on nearshore submarine groundwater discharge from a (partially) confined aquifer, *Estuaries and coasts*, *30*(3), 543-550.

Taniguchi, M. (2002), Tidal effects on submarine groundwater discharge into the ocean, *Geophysical Research Letters*, *29*(12).

Taniguchi, M., and Y. Fukuo (1993), Continuous Measurements of Ground-Water Seepage Using an Automatic Seepage Meter, *Groundwater*, *31*(4), 675-679.

Taniguchi, M., and H. Iwakawa (2001), Measurements of submarine groundwater discharge rates by a continuous heat-type automated seepage meter in Osaka Bay, Japan, *Journal of Groundwater Hydrology*, *43*(4), 271-278.

Taniguchi, M., W. C. Burnett, J. E. Cable, and J. V. Turner (2002), Investigation of submarine groundwater discharge, *Hydrological Processes*, *16*(11), 2115-2129.

Taniguchi, M., W. C. Burnett, H. Dulaiova, E. A. Kontar, P. P. Povinec, and W. S. Moore (2006), Submarine groundwater discharge measured by seepage meters in Sicilian coastal waters, *Continental Shelf Research*, *26*(7), 835-842.

Top, Z., L. E. Brand, R. D. Corbett, W. Burnett, and J. Chanton (2001), Helium and radon as tracers of groundwater input into Florida Bay, *Journal of Coastal Research*, 859-868.

Valiela, I., and C. Delia (1990), Special issue-groundwater inputs to coastal waters-introduction, edited, Kluwer Academic Publ Spuiboulevard 50, Po Box 17, 3300 Aa Dordrecht, Netherlands.

Valiela, I., J. M. Teal, S. Volkmann, D. Shafer, and E. J. Carpenter (1978), Nutrient and particulate fluxes in a salt marsh ecosystem: Tidal, *Limnol. Oceanogr*, *23*(4), 798-812.

Valiela, I., K. Foreman, M. LaMontagne, D. Hersh, J. Costa, P. Peckol, B. DeMeo-Andreson, C. D'Avanzo, M. Babione, and C. H. Sham (1992), Couplings of watersheds and coastal waters: sources and consequences of nutrient enrichment in Waquoit Bay, Massachusetts, *Estuaries and Coasts*, *15*(4), 443-457.

Xin, P., C. Robinson, L. Li, D. A. Barry, and R. Bakhtyar (2010), Effects of wave forcing on a subterranean estuary, *Water Resources Research*, *46*(12), W12505.

Young, C. R. (2013), *Fate of Nitrogen during Submarine Groundwater Discharge into Long Island North Shore Embayments*. Doctoral dissertation. Stony Brook University, 165 pp.

Zektser, I. S., L. G. Everett, and R. G. Dzhamalov (2006), *Submarine groundwater*, CRC Press Inc.

Chapter 2: Effect of a surficial low permeability mud layer on submarine groundwater discharge: a case study in Stony Brook Harbor, New York

Abstract

Characterization of submarine groundwater discharge (SGD) in a tidally-dominated, low-energy environment was performed in Stony Brook Harbor, on the north shore of Long Island, NY. Our integrated approach combined: point electrical conductivity measurements, 2D electrical resistivity surveys, manual and ultrasonic seepage measurements and porewater sampling. Embayment-wide reconnaissance of sediment conductivity at 60 cm depth throughout the harbor reveals significant heterogeneities in porewater salinity distribution and identified two significantly contrasting sites. At the first study site, freshwater discharge is channeled 65 m offshore with seepage rates varying from 3-30 cm/d. At the second site, the intertidal zone comprises a superficial mixing cell overlying a zone of more diffuse mixing with high SGD rates ranging from 30-110 cm/d. Offshore discharge is approximately 3 cm/d. The difference in SGD between the two sites is attributed to the presence of a low-permeability mud layer at the bottom of the harbor. The mud layer locally confines groundwater flow and channels freshwater offshore. SGD percolated through the mud layer is estimated to represent approximately 30% volume of the SGD calculated for the near shore area. Surficial mud deposits control the distribution, magnitude and degree of mixing of fresh SGD with overlying seawater, and their spatial distribution should be taken into account for regional scale SGD calculations.

1. Introduction

Submarine groundwater discharge (SGD) is widely recognized as an important water exchange process between land and sea [*Bokuniewicz*, 1980; *Howarth et al.*, 1996; *Taniguchi et al.*, 2002; *Valiela et al.*, 1978] over different spatial and temporal scales [*Bratton, 2010]*. While its volume might be small compared to surface water discharge, SGD can transport high nutrient concentrations which significantly impact coastal water quality *[Johannes, 1980; Moore et al., 2008; Slomp and Van Cappellen, 2004; Zektser et al., 2006*]. Understanding nutrient flow paths towards the ocean is crucial for water quality assessment and mitigation [*Charette and Buesseler*, 2004; *Valiela et al.*, 1992].

Due to the highly diffuse and heterogeneous nature of SGD, different methods have been developed to quantify SGD, including manual and automatic seepage meters, geochemical tracers and hydrological modeling *[Burnett et al., 2006; Michael et al., 2003*]. It has been shown that SGD pathways can modify porewater chemistry through mixing and interactions with sediments *[Bratton et al., 2004; Kroeger and Charette, 2008*] or by affecting solute residence time [*Kuan et al., 2012*].

Simulations of groundwater flow in various bays and lakebeds suggest that shoreline geometry and coastal configuration can accentuate the hydraulic gradient, increasing discharge by as much as a factor of five [*Cherkauer and McKereghan, 1991*]. SGD should therefore be enhanced in embayments relative to straight-face beaches. Moreover, embayments are common and they can represent a significant amount of shoreline: on the north shore of Long Island, for instance, 11 bays and harbors account for a total of 257 km of shoreline, while the length of Long Island is only 190 km [*Koppelman et al., 1976*]. Characterizing SGD in embayments is therefore crucial for quantifying groundwater seepage more accurately at a regional scale.

Harbors and bays possess curved shorelines providing protection from winds, waves and currents. The decrease in energy between the ocean and an embayment can lead to deposition of marine muds, fine-grained sediments of relatively low-permeability which can impact SGD distribution. Multiple studies have focused on the influence of geologic heterogeneities on SGD at various scales [*Bokuniewicz et al.*, 2008; *Michael et al.*, 2011; *Mulligan et al.*, 2007; *Russoniello et al.*, 2013], and on the role of shallow confining units [*Bratton et al., 2002; Stieglitz et al.,* 2007]. However, the influence of low permeability layers resulting from active

deposition above the aquifer/ocean interface still need to be investigated *[Bratton et al.,* 2007]. Improved understanding of freshwater fluxes will help quantify groundwater contribution to non-point source pollution and identify potential remediation techniques. This information can provide zone managers with valuable data for water quality control and coastal management.

The purpose of this study is twofold. Building on the legacy from *Taylor and Cherkauer* [1984], my first objective is to characterize the hydrogeological framework and SGD distribution in Stony Brook Harbor, a meso-tidal embayment typical of many in the north Atlantic, through an integrated approach using multiple geophysical techniques. We have adopted the protocol outlined by Paulsen et al., [2008]. Point conductivity measurements using a direct-push probe, inserted 0.6 m into the sediments, were used to perform an embayment-wide reconnaissance of areas with fresh porewater and identify two areas of interest. These two locations were studied more thoroughly with stationary electrical resistivity (ER) surveys that provide vertical 2D sections of high spatial resolution, as proxies of groundwater salinity distribution [*Stieglitz et al.*, 2008b; *Taniguchi et al.*, 2007; *Weinstein et al.*, 2007]. Water sampling using piezometer wells [*Charette and Allen*, 2006] provided in-situ salinity readings to supplement the two previous methods. Seepage measurements from ultrasonic [*Paulsen et al.*, 2001] and manual [*Lee, 1977*] seepage meters were used to determine the spatial heterogeneity of SGD rates.

The second objective of this study is to map out the spatial distribution of SGD and characterize its temporal variations in order to elucidate the discharge mechanisms in a harbor setting. I observed two scenarios, with and without the presence of the low-permeability mud layer. I conclude that in Stony Brook Harbor a thin surficial low-permeability mud layer, likely to be found in many other low-energy coastal environments, controls SGD distribution and magnitude by partially confining the flow close to the shore, channeling freshwater offshore where it percolates slowly throughout the surficial mud layer. This study suggests that, independent from the underlying geological stratigraphy, active sedimentation of fine particles can have a significant impact on SGD rate and distribution. I recommend investigating the presence of such a layer in similar low-energy coastal environments prior to any SGD study, and characterizing its spatial extent and sediment properties before attempting any regional SGD estimates.

2. Study site

Stony Brook Harbor is a shallow, salt-marsh estuary located on the North shore of Long Island, New York (Figure 1a). The area of the Harbor and its major tributary, West Meadow Creek, is about 4.8 km^2, which includes about 3.0 km^2 of open water and 1.8 km^2 of islands and marshes. The average depth of water at mean low tide is 0.9 m. The harbor is separated from Long Island Sound by two baymouth bars, Long Beach and West Meadow Beach, and connected to the Sound by a 130 m narrow inlet at its northeastern corner [*Robbins,* 1977].

The bottom of the harbor consists of glacial sand and gravel *[Buxton and Modica,* 1992]. The surface sediments are a mix of fine-grained to coarse-grained sand with localized pockets of gravel. Stony Brook Harbor is a low-energy tidally dominated environment. The grain size distribution within the harbor follows the tidal current force: finer grain sediments are found the farthest from the inlet [*Park,* 1985].

Monitoring by the New York State Department of Environmental Conservation (NYDEC) indicates a harbor average salinity of 26 ±2 except for the Head of the Harbor, where the influx of freshwater from springs and groundwater lowers the salinity to 15 at low tide [*Robbins,* 1977]. The shallowness of the harbor and the large tidal range keep the harbor waters vertically well mixed. Tidal oscillations in the harbor are dominated by a semidiurnal lunar tide, with a mean tidal range of ~1.9 m at the harbor mouth and ~1.8 m at the head of the harbor.

The drainage basin of Stony Brook Harbor is highly vegetated and relatively small, covering 18 km^2 [*Robbins,* 1977], with negligible precipitation runoff [*Gross,* 1972]. West Meadow Creek, the major tributary of the harbor, is located at the northeast of the harbor and discharges about 300 m from the inlet, far from our main study site. The influence of West Meadow Creek and Mills Creek, as well as other potential smaller or intermittent sources was not studied in the present work, as they are not the main focus of the study - but should be investigated in the future regarding mass balance calculations at the scale of the harbor.

The upland region surrounding the harbor is composed of glacial drift deposited during the most recent stage of glaciation. These deposits are part of the Harbor Hill moraine, a ridge that runs east-west along almost the entire length of Long Island, forming the hilly topography of the north shore. The elevation of the moraine that covers most of the area around the harbor varies in

height from 15 to 45 m. This moraine is mostly made of till with some stratified sand and gravel [*Robbins,* 1977]. A detailed description of the geology of the area is available in [*Lubke*, 1964].

Two study sites were selected in the southwestern portion of the harbor (Figure1a) for detailed investigations. Site 1 was studied using electrical resistivity (ER) surveys, ultrasonic and manual seepage meters, and piezometers (Figure 1b). Site 2, located approximately 40 m south of site 1 along the same shore, was studied using piezometers, ER surveys and ultrasonic seepage meters (Figure 1c). Pore water extracted from the piezometers was analyzed for salinity using a hand held YSI 556 multiprobe. The mean horizontal hydraulic gradient was estimated to be 0.07, one located on the shore and another 184 m inland. The beach slope in the intertidal zone is 0.05 (or 2.3°), as determined by a laser topography survey. At site 1, the beach is composed of three sedimentological areas; a high-tide zone of medium-to-coarse sand, a mid-tide zone of *Spartina Alterniflora* marsh, and a low-tide medium-to-fine grain sand zone. The beach is 40 m wide and is completely inundated during spring tide when the tidal variation amplitude reaches 2 m. At site 2, the beach sand grades from high tide to low tide sand with a much smaller mid-tide marsh zone. The presence of an organic-rich mud layer was observed at site 1, beyond the sand and marshes located close to the shore and its thickness reaches 85 cm at 60 m from the shore. The mud layer is not observed at site 2, at the same distance from the shore. A grain size distribution analysis from this layer, using a Malverne Mastersizer 2000 laser diffractometer, indicates medium-to-coarse grained silt with d_{50} of 0.03 mm.

The software ProChart Navigator used to predict tidal levels uses the mean lower level of water (MLLW) as a datum. As the low-tide mark position varied during each field campaign, I chose to use the MLLW as reference. The comparison between the tidal predictions and the actual water level changes in Stony Brook Harbor for 7 consecutive days allowed me to estimate the position of the MLLW, which was marked with a stake and used as a reference for all surveys.

3. Methods

3.1 Trident

The Trident probe is a direct-push instrument, developed to screen and assess offshore areas where groundwater may be discharging to the surface water body [*Chadwick et al.*, 2003]. The

Trident integrates two sets of measurements. One subsurface probe is equipped with two sensors to measure the sediment bulk conductivity and temperature, a second probe is equipped with two sensors to measure the surface water conductivity and temperature in the vicinity of the Trident probe, and two pore water samplers. In this study, measurement depth is fixed at 60 cm below the sediment-water interface, or less if the sediments do not allow full penetration. Conductivity is measured using pairs of electrodes organized as a Wenner array. The temperature sensor has a measurement range of -5 to +35 °C with an accuracy of 0.001 °C, and a resolution of 0.00025 °C.

Trident stations were used in a preliminary study, forming 6 transects across the Harbor for a total of 28 sample points (Figure 2). Data were collected between 3/28/2011 and 4/11/2011 mostly during ebbing tides. Locations with maximum temperature and conductivity contrast between overlying water and porewater were further studied for collection of resistivity and piezometer data.

3.2 Electrical resistivity data acquisition and inversion

The electrical resistivity (ER) of a porous medium is controlled by its saturation, porosity, clay content and the electrical resistivity of the electrolyte in the pore space [*Olhoeft,* 1981; *Telford et al*., 1990]. In a fully saturated medium without clay, the inferred electrical resistivity can be linearly related to the electrolyte resistivity if the porosity is homogeneous. In particular, a relatively high electrical resistivity would imply a relatively low salinity, probably due to the influx of fresh SGD [*Swarzenski et al*., 2007]. ER surveys have been widely used to identify freshwater plumes [*Cross et al., 2010; Dimova et al., 2012; Manheim et al., 2004; Swarzenski et al.*, 2006; *Taniguchi et al*., 2007, among others].

In this study, ER imaging was performed using an Advanced Geosciences Inc. (AGI) SuperSting 8-channel receiver R8 resistivity meter. The SuperSting system used a cable 33 m long with 56 electrodes separated by 0.61 m. Measurements were made using a dipole-dipole configuration. Reciprocal measurements were collected using an inverse Schlumberger setting. Both data sets were stacked together to perform a joint, finite-element inverse analysis. For resistivity surveys, the depth of investigation (DOI) depends on the length of the cable and type of array. On land, the instrument can probe down to ~20% of the electrode spread depth. In

marine settings, however, part of the signal is lost due to the highly conductive seawater layer and the DOI is reduced. Characterizing the DOI is necessary before any interpretation [*Oldenburg and Li*, 1999].

Data were analyzed using the software package EarthImager 2D [*AGI*, 2009], and inverted using an Occam's smooth inversion [*Constable et al.*, 1987]. The inversion provides the optimal estimation of ER spatial distribution for a given profile. An average apparent resistivity model was used as a starting model for the inversion, as it limited the apparition of high frequency artifacts. Levels of noise above 4% for individual electrodes reflected insufficient coupling with the ground and were therefore filtered prior to inversion [*AGI*, 2009]. Land topography was measured using a level laser and bathymetry profile was acquired using a sonic depth sounder during the resistivity acquisition. A pressure logger placed in the water allowed the measurement of water column pressure changes due to tidal variations. Errors in the estimation of the water column depth can significantly affect the inversion [*Day-Lewis et al*., 2006]. The inversion was performed using the average water depth measured during acquisition. A sensitivity analysis showed that the inversion yielded satisfactory results for water column variations under 0.25 m. The overlying water depth resistivity was fixed as the average of the Trident surface resistivity values measured along the ER line. To provide ground-truthing information, resistivity sections were converted to conductivity sections and compared with the piezometer transects [*Henderson et al*., 2010].

Two ER surveys, T1, and T2, were acquired at site 1 and 2, respectively, perpendicular to the shoreline on 5/31/2011 at high tide and an additional double-cable survey T1-2 was acquired at site 1 on 7/23/11.

3.3 Seepage meters

SGD at selected locations was quantified using ultrasonic seepage meters (USM) developed by Paulsen et al. [2001]. SGD was captured in a steel collection chamber or funnel with a square cross section of 0.21 m^2, inserted approximately 0.1 m into the sediments. The meter is capable of measuring SGD at rates as low as ±0.1 μm/s (0.86 cm/d), for several days with a sampling period of 15 minutes. To ensure the reproducibility of the results, two funnels were deployed simultaneously, spaced a few meters apart from each other at every measurement

point. Unfortunately, in 2 cases, only one funnel provided reliable data due to electronic problems or mud snails lodged in the flow tube.

At site 1, funnel F1 was deployed on 7/22/11 at approximately 23 m from the MLLW. At site 2, 3 funnels were deployed: F2 on 5/20/11 at 40 m from the MLLW, F3 and F4 on 7/23/11, at 50 and 55 m from MLLW, respectively. Seepage meters were located along the ER transects; seepage measurements were taken every 15 minutes for at least 4 days (Figure 1b).

Three manual seepage meters [*Lee*, 1977] A, B and C were deployed on 8/14/2012, at 33, 42 and 54 m from the first piezometer P1-0, respectively (Figure 1b). SGD rates and water samples were collected for 6 hours, going from high to low tide. Seepage meters F1, B and C were implanted in muddy areas while seepage meters A, F2, F3 and F4 were placed in sandy areas.

3.4 Piezometers

Two porewater piezometer transects were performed at each site. Piezometer names include a number indicating their cross shore distance (in m) from the first piezometer taken as the origin of the profile (Figure 1b and c). Porewater samples were collected using an AMS Retract-A-Tip sampling system [*Charette and Allen*, 2006]. LDPE tubing (Grainger, I.D 0.64 cm) was rinsed with deionized water (18.2 mΩ) and connected to a peristaltic pump (Cole-Parmer) using low gas permeability Viton tubing (Masterflex). Samples were collected at depths ranging from 0.5 – 10 m beneath the sediment surface. The sampling interval varied between 0.5 and 1 m, depending on field salinities measured with the YSI probe. Piezometer transects were acquired around low tide from 5/31/11 to 6/7/11 and from 5/12/11 to 5/20/11 at site 1 and 2, respectively.

3.5 Mud layer mapping and sediment core analysis

A detailed mud layer profile was acquired during the ER survey at site 1. To get an estimate of the representativeness of site 1 observations throughout the harbor, the aerial extent of the mud layer in the southern portion of the harbor was surveyed manually via kayaks using a graduated PVC pole. In the deeper portions of the harbor, the thickness of the mud is a lower bound as the penetration of the pole into the mud was limited by the pole length, the manual push and the kayak stability. Measurements were started at low tide along the west shore of the harbor, and finished close to high tide along the east shore. A natural neighbor interpolation was

calculated in ArcMap 10.0 (n=53, Figure 9). The apparent thinning of the mud on the east shore could be an artifact of the acquisition as flooding tide limited the accessible depth when the east shore was reached. Visual inspection confirmed that the mud layer was continuous in the center of the harbor, thinner towards the shore and progressively disappeared below the low tide mark around the lower half of the harbor. It is unlikely that the mud extends into the northern portion of the harbor based on a previous sediment map of the harbor [*Robbins*, 1977], dredged channels and the higher level of energy observed there, thus, that portion was not sampled. Acoustic methods could be more efficient and accurate for mapping the extent of the mud layer in the whole harbor [*Murphy III et al*., 2011], however, the shallowness severely restricts boat access and exact mapping of the mud layer was beyond the scope of this study.

Collection of sediment cores using a Geoprobe was unsuccessful due to the shallowness of the harbor and the high compressibility of the sediments. Superficial core samples were taken manually at site 1, using PVC cylinders, in the sandy portion close to the shore and in the mud farther offshore. Porosity and permeability were measured in the lab using standard methods of weighting the samples saturated and dry, and of falling head [*Marshall et al.*, 1996], respectively.

4. Results

4.1 Stony Brook Harbor bulk conductivity and temperature anomalies

At the end of March, groundwater is warmer than surface water and the average temperature is ~11°C whereas the opposite is true at the beginning of April. The Trident measurements indicate that bulk temperatures varied between 5-9°C during data collection (Figure 2a). The bulk temperatures are colder in the northern half of the harbor, likely indicating mixing with surface water (Figure 2a and b), whereas the warmest temperatures are located along the shore in the southern part of the harbor. The warming of surface water was attributed to the winter/spring seasonal changes during the two weeks of acquisition (Figure 2b). Surface temperatures are more variable, ranging from 3°C on the first days of acquisition, on the northern Trident profiles, to 13°C on the last day of acquisition for the two stations located at 73.18°W, 40.9025°N. Calculating the temperature difference (DT) between the bulk and the surface temperatures reveals areas of strong contrast which can indicate freshwater discharge (Figure 2a) [*Anderson*, 2005; *Befus et al.*, 2013]. Note that one of the two stations located at 73.18°W,

40.905°N did not record bulk temperature (empty circle on Figure 2a), and therefore the high corresponding positive DT is only an artifact (Figure 2c). Most temperature differences vary within ± 1 °C, but 3 stations show a clear signal: one with a positive DT in the northern part of the harbor, and two with highly negative DT values on the western shore of the harbor. The station with a positive DT indicates the presence of freshwater in the sediments at 60 cm depth; however, this signal is not confirmed by the conductivity plot (figure 2d). The two stations along the western shore coincide with low bulk conductivities, under 10,000 µS/cm, suggesting a strong fresh SGD signal. In the center of the harbor, bulk conductivity values are ~ 30,000 µS/cm, which indicates that bottom sediments are saturated with seawater. Intermediate conductivities around 20,000 µS/cm are visible mostly in the south-eastern and the western shore of the harbor, indicating mixing between surface water (conductivity of ~38,000 µS/cm) and fresh groundwater (conductivity of <5,000 µS/cm), showing agreement with the temperature measurements. The two stations with the strongest fresh SGD signal were chosen for further investigation.

4.2 Electrical conductivity

Results of the single-cable ER surveys for sites 1 and 2 are presented in Figure 3. There are some apparent differences in porewater salinity distribution between each site. At site 1, conductivities around 5,000 µS/cm, indicative of brackish water, are found in the intertidal zone, for $0 < x < 9$ m. This zone is limited to 2 m depth below grade in the intertidal portion of the section and becomes thinner ~ 1 m offshore. This zone seems to extend further offshore but appears discontinuous or attenuated around x ~22 m and x> 29 m. Under this zone, low conductivity values under 2,000 µS/cm are visible on the whole section, suggesting that mixing is localized, and that freshwater is channeled as far as 20 m offshore of the MLLW. Conductivity exhibits values as low as 80 µS/cm at depths greater than 6 m. However, this portion of the ER surey should not be over-interpreted as the sensitivity of the model decreases with depth. Note that electrode #42 (x~25 m) was removed on transect T1 as it presented a high level of noise; the removal created a narrow resistive patch visible under the missing electrode.

The double-cable transect presented similar features: a zone of low conductivity is present on the whole length of the section between 2 and 9 m depth (Figure 4). A thin layer of high conductivities is visible under the ER cable and is an artifact of the inversion. Due to the

length of this survey, 67 m, acquisition time is close to 3h. A water level variation of approximately 0.4 m during acquisition was enough to create high frequency artifacts on the inverted section. In this case, the accuracy of the inversion is more limited as the average water column is less representative. The other conductive area visible at depth on transect T1-2 could also be an artifact of the inversion as the model is not very sensitive to the data below 10 m depth (as determined by a DOI analysis). However, additional porewater salinity measurements from a temporary piezometer located at x ~ 34 m are in agreement with the ER section and confirm that freshwater is channeled horizontally at site 1 and that salinity increases at depth from 0.99 at z = 7.4 m to 8.3 at z = 10 m below grade.

At site 2 (Figure 3b), intermediate conductivity values ranging from 3,000 - 13,000 µS/cm are observed in the first 12 m horizontally, down to 7 m depth, and offshore down to 3 m depth below grade. This indicates the intertidal mixing zone is more developed at site 2 than at site 1 and that mixing occurs on most of the section. At depth greater than 3 m, low conductivities are visible in the center of the section which could be some fresher water driven from land that did not get mixed in the intertidal zone.

The classical salt wedge usually present in the subtidal zone [*Glover*, 1959; *Kohout*, 1960] is not visible on any of the ER images. At site 1, the FSI appears horizontal. This shows that, at least in this harbor, the numerical predictions of salinity distribution for straight beach faces do not apply.

4.3 Piezometer transects

To compare the conductivity sections to the piezometer profiles, it is necessary to convert the bulk conductivities into electrolyte conductivities using Archie's law [*Archie*, 1942].

$$F = \frac{\sigma_w}{\sigma_o} = \varphi^{-m}$$

Where F is the formation factor [dimensionless], σ_w and σ_o the conductivity of the saturating fluid and the saturated porous medium, respectively [µS/cm], φ the porosity [dimensionless] and m the cementation factor [dimensionless].

Utilizing the sand porosity of 0.4 determined with the sediment core analyses at site 1, and assuming a cementation factor of 1.3, typical of unconsolidated sands, I obtain a formation

factor or 3.3. Porewater conductivities from the piezometer transects are superimposed to the ER inverted sections converted to electrolyte conductivities (Figure 5). Piezometer conductivities are in good agreement with the ER surveys; however, there are also some discrepancies.

At site 1, both methods show a superficial mixing cell overlying freshwater but the mixing cell imaged by the piezometers penetrates deeper than predicted by the ER survey (Figure 5a). At site 2, details in conductivity variations shown on the ER survey are not apparent on the piezometer profile (Figure 5b). The piezometer conductivities are generally higher than the electrolyte conductivities computed from the ER sections. This is most likely due to a temperature effect from pumping. Before being measured with the YSI probe, the pore fluid is pumped to the surface and is warmed up by both the friction in the tube and exposure to the sun. Measured temperatures were as high as 30°C which is obviously abnormal for porewater and significantly increases conductivity values. According to the practical salinity scale from 1978 [*Lewis and Perkin*, 1981], measured temperatures and conductivities are used to compute salinity for the standard conditions: at temperature of 15°C and for pressure of 1 atm; salinity profiles presented here are therefore not affected by the temperature issue.

Salinity profiles are presented in (Figure 6). At site 1, salinities between P1-0 and P1-19 range from 10 to 20 in the intertidal zone (Figure 6a), indicating a superficial zone of mixing down to a maximum depth of 5 m. Beneath the superficial mixing zone, groundwater is mostly fresh with salinity less than 5 at depth and offshore from the MLLW, suggesting that mixing is strongly localized in the shallow tidal circulation zone. This superficial mixing cell overlays a zone of channelized freshwater that extends at least to a depth of 10 m below grade.

At site 2 (Figure 6b), piezometers P2-0 and P2-8 have freshwater salinity values of 2 or less at depths greater than 2 m beneath the sediment surface. Wells P2-15, P2-23, P2-30 have salinities above 10 at all depths revealing diffuse mixing beyond the intertidal zone. Maximum salinity values are found between 0 - 4 m depth in the intertidal zone in wells P2-8 and P2-15, showing strong seawater infiltration and mixing due to the tide. The mid to high salinities observed at well P2-15 are unexpected, and might be the result of a local heterogeneity in the sediments that enhances infiltration of seawater at high tide. We also note that salinity values reach a minimum of 12, before rising again at depths greater than 4 m, marking a transition to the

deep saline zone at site 2. The differences in porewater salinity distribution revealed by the ER surveys are confirmed by the piezometer profiles.

4.4 Seepage measurements

4.4.1 Ultrasonic seepage meters

At site 1, the specific discharge measured at the end of May 2011, by funnel F1 is very low, with an average of 3.6 cm/d (Figure 7a). The flow rate exhibits two high peaks at the beginning of the recording period that do not match any precipitation event and may be artifacts triggered by the disturbance of the mud layer during installation. Higher rates averaging 10 cm/d are visible on day 3, as a consequence of the 0.51 cm precipitation falling that day. A Fourier transform analysis confirmed the visible absence of correlation between SGD and tidal stage.

At site 2, seepage rates measured in May by funnel F2 are very high, with an average of 61.3 cm/d (Figure 7b). Seepage rates vary from -83.3 to 274.9 cm/d, with the latter magnitude close to the highest values measured on Long Island [*Paulsen et al.*, 2004] and other locations throughout the world [*Russoniello et al.*, 2013; *Stieglitz et al.*, 2008a; *Taniguchi et al.*, 2002]. The relationship between tidal stage and SGD is not consistent over time: from 5/19 to 5/21 high tide coincides with a peak in SGD and from 5/21 to 5/25 high tide coincides with a local minimum in an overall SGD peak. This is highly unusual and does not fit the general case where a negative correlation is observed between the tides and SGD [*Paulsen et al.*, 2004; *Taniguchi and Iwakawa*, 2004; *Taniguchi et al.*, 2006]. Both tidal and seepage signals have a period of 12.42 hours corresponding to the principal lunar semi-diurnal M_2, and a period of 6.21 hours corresponding to shallow water over tide of the principal lunar M_4, as revealed by a Fourier transform analysis. The seepage measurement period also coincides with a transition from spring tide to neap tide, which adds another trend to the resulting tidal signal. The complexity of the tidal signal could explain the complexity of SGD recorded at this site.

Funnels F3 and F4 exhibit relatively high average seepage rates: 109.3 cm/d and 29.8 cm/d, respectively. The approximation of an exponential decay of SGD with respect to distance from shore does not apply at this site [*Bokuniewicz*, 1980; *Mc Bride and Pfannkuch*, 1975]. Both funnels were placed approximately 40 m offshore of the MLLW, and did not reside within the intertidal zone. SGD in F3 shows strong variations but they do not seem to be related to the tide. SGD in F4 does not vary much and does not exhibit any correlation with the tide either. A

frequency analysis of both SGD signals confirmed the absence of tidal correlation. It is therefore reasonable to assume a relatively high freshwater component in the discharge at site 2, as the high seepage rates observed are not the result of intertidal seawater circulation.

The variety of behaviors recorded at site 2 suggests that SGD at that location is controlled by the interaction between several factors. The complexity of the tidal signal might be partially responsible for the unusual SGD response. The lack of consistent relation with the tide in time and space points toward transient processes. The mud layer has different porosity, permeability and compressibility from the underlying sand. Transient storage in the mud layer could be another explanation for the unusual observations at site 2 (Figure 9). Unfortunately, my current data do not allow me to provide a more definitive answer regarding SGD control at this location.

4.4.2 Manual seepage meters

At site 1, seepage meter A, located 11 m offshore of the MLLW was closest to the intertidal zone with average rates of 23 cm/d, correlated with tidal stage. Seepage meter B, 20 m from MLLW, was closest to the ultrasonic seepage meter F1, with similar flow rates of < 5 cm/d (Figure 8). Seepage meter C, located 32 m offshore of MLLW, has the lowest SGD values (less than 3 cm/d). Neither B nor C shows any correlation between discharge and tidal level.

Water from the seepage meter bags was analyzed for temperature, conductivity and salinity using a YSI probe (Figure 8). Salinity values for A and B were close to those of seawater throughout the sampling period and presented no sign of freshening, suggesting that the discharge was mostly circulated seawater. For seepage meter C, the furthest from the shore, freshening was observed close to low tide. We observed a salinity minimum of 15, in comparison with 30 measured at high tide.

SGD calculated using ^{222}Rn measurements from a surface water sample collected in the center of the harbor was ~5 cm/d (Joe Tamborski, pers. comm.), which is in agreement with the 3 cm/d average rate measured with the ultrasonic and manual seepage meters implanted in the mud. Remote sensing techniques such as thermal infrared imaging could provide insight into the distribution of SGD at the scale of the harbor [*Johnson et al.*, 2008].

Along a 50 m profile perpendicular to the shore, the mud layer was observed to appear a few meters below the low tide mark, and its thickness to increase towards the center of the

harbor. It reached a maximum thickness of 85 cm close to seepage meter C, but decreased at about 50 cm beyond. The differences in rates between the three manual seepage meters were not just linked to their relative distances to the shore, but also to the kind of sediments they were implanted in.

4.4.3 Sediment core analysis

Sediment core analyses indicated porosities of 40% for the sand and 62% for the mud. The aquifer porosity might be slightly different, as the measurements were made on a core that did not include pebbles, cobblers or mollusks present in the intertidal area. Hydraulic conductivity measurements using the standard falling head method yielded values of 0.1 m/d and 1.5 10^{-3} m/d for the sand and the mud, respectively. The vertical hydraulic conductivity for the sand is two orders of magnitude smaller than the value typically adopted in numerical models for Long Island [*Buxton and Modica*, 1992], whereas the value for the mud is in very good agreement with empirical values for unconsolidated silt [*Fetter*, 2001]. The mud layer is characterized by a high porosity and very low permeability, which explains the strong difference in flow regimes observed between site 1 and 2 as no difference was found in the sand properties and the hydraulic gradient is unlikely to vary significantly between these two places.

5. Discussion

5.1 Conceptual models

I hypothesize that the observed mud layer acts as a low-permeability cap and influences groundwater flow. A conceptual model is used to discuss the different flow and mixing scenarios with or without the cap (Figure 10).

For the sandy portions of the shore without the mud cap, as seen for $0 < x < 14$ m at site 1 and all along site 2, the features identified are similar to those previously observed and predicted by numerical simulations: the intertidal zone comprises a shallow mixing zone with high salinity resulting from seawater intrusion and circulation from tidal dynamics [*Robinson et al*., 2006]. The shallow seawater circulation cell overlays fresher water and therefore salinity decreases as depth increases. Measured SGD rates are high close to the shore and low offshore; however the expected exponential decrease is not observed *[Mc Bride and Pfannkuch*, 1975].

When the mud cap is present (Figure9b), as seen at site 1 for x > 14 m offshore of the MLLW, groundwater is hydraulically isolated from the overlying seawater, which prevents mixing and strongly limits SGD rates. Freshwater from land is channeled and directed offshore as a result of the low permeability mud cap. SGD rates through the cap are very small and do not seem to be correlated with the tides. The mud layer is not observed in the intertidal zone, and therefore, a superficial mixing cell can develop [*Robinson et al*., 2006]. The influence of the cap can also explain the relatively high seepage rates measured at site 2, relatively far from the shore. The cap confines SGD to a large area by reducing vertical fluxes; hydraulic potential builds and porewater flows horizontally to greater distances than expected. This agrees with mathematical models of seepage in lake beds tested for different localization of low permeability bottom sediments [*Mc Bride and Pfannkuch*, 1975] as well as direct field observations *[Hirsch and Randazzo*, 2000]. A similar effect was observed by *Bokuniewicz* [1980], in Great South Bay on Long Island, where his seepage meter measurements indicated the presence of a superficial clay layer that significantly decreased SGD and funneled discharge further offshore. *Michael et al*. [2005] observed an organic-rich muck layer that influenced vertical hydraulic gradients in Waquoit Bay, MA. Discontinuities in the mud layer can explain the very high flow rates observed offshore at site 2 and the variability of seepage rates at similar distances from the shore. [*Russoniello et al*., 2013] also observed a fresh water plume beneath low permeability areas in an estuarine setting where paleovalleys were filled in by mud and peat deposits.

5.2 Stony Brook Harbor SGD

Seepage rates measured in Stony Brook Harbor are similar to other values reported in the literature, but the range in rates measured at the same distance from the shore is unprecedented. Low rates of 3 cm/d measured in the mud cap are close to those measured by *Bokuniewicz* [1980] in Great South Bay, where sediments are composed of a mix of sand and clay. Higher rates of 26 cm/d measured in the intertidal zone are close to those reported at Osaka Bay, Japan [*Taniguchi et al*., 2002] where seepage meters were implanted in muddy sands. The very high rates measured at site 2 are close to the 73.7-105.2 cm/d reported in Barbados, West Indies in a sandy environment [*Lewis*, 1987]. Our range of values is similar to the wide range observed in Shelter Island, NY where sediments are composed of mostly sand, gravel and silt with seepage rates varying from 14 cm/d to 225cm/d depending on the tidal level [*Paulsen et al.*, 2004].

Contrary to what is predicted, neither of our two sites exhibits an exponential decay with distance from the shore.

This study shows that sediments heterogeneity can significantly modify the flow pattern and that the presence of a discontinuous mud cap controls SGD, and introduces significant lateral heterogeneities in SGD distribution and rates. The observations at site 1 indicate a freshwater-seawater interface structure very different from what was predicted by numerical simulations [*Robinson et al*., 2006]: a superficial mixing cell is observed in the intertidal zone but no localized zone of freshwater discharge was seen below the low tide mark. Before any attempt to compute chemical transport and mass balances in such an environment, it is necessary to accurately map the extent of the mud cap for the whole harbor and identify the relative importance of sites similar to site 1 versus site 2, where the mud layer is present but begins further offshore. Accounting for only one of these two scenarios would yield erroneous estimates.

The preliminary muck thickness mapping shows that the mud layer extends throughout the southern part of the harbor (Figure 9). This agrees with other previous studies of sediment grain-size distribution, where the very-fine particles were localized in the lowest energy part of the harbor [*Robbins,* 1977]. The apparent thinning towards the north is only an artifact of the interpolation as the center of the harbor was more difficult to survey from a kayak.

If one attempts to make a general estimate of the amount of SGD discharging through the intertidal sand, assuming an average rate measured by our manual seepage meter A of 26 cm/d for, with an average discharge zone of 20 m and a shoreline of 18,000 m, SGD discharging at the shoreline would be ~ 93,600 m^3/d. Based on our map of the mud layer and on a complete map of sediment grain-size distribution throughout the harbor from [*Robbins,* 1977], we can assume that the mud layer is present in half of the harbor area. If we assign it a discharge rate of 3 cm/d, as measured by our manual and ultrasonic seepage meters and confirmed by the 222Rn measurements, with a mean low tide area of 950,000 m^2, we obtain an additional SGD volume of 28,500 m^3/d. This would imply that an extra volume of ~30% the shoreline SGD is released through the mud layer, in the center of the harbor. Salinity data in seepage meters suggest that the freshwater content is higher in SGD discharging through the mud. The mud cap is not restricting the total amount of SGD entering the harbor but rather redistributing it. It is likely that

freshwater partially confined by the mud layer will have strong discharge rates at the northern limit of the mud, where the bottom sediments become coarse and more permeable but also at any discontinuity of the cap. By limiting the mixing before discharge and by redistributing the seepage areas, the mud influences also residence times and groundwater flow paths, impacting nutrients fate.

5.3 Implications for water and nutrients budgets

Nutrient concentrations in discharge water will be affected by differences in both discharge rate and sediment structure. In the simple case (Figure 10a), with no cap, the freshwater from land undergoes a diffuse mixing process that extends offshore and at depth as observed with salinity measurements [*Li et al.*, 1999]. In this scenario, nutrients originating from oxygenated freshwater are rapidly diluted with infiltrating seawater, before being discharged to the surface. A lack of sediment bound carbon, as exhibited by medium-to-coarse grained sands in this zone, precludes the development of hypoxic conditions along groundwater flow paths. This prevents nitrogen attenuation mechanisms, such as microbial denitrification and anammox. Therefore, in this case we could expect high nutrient loading surface waters [*Slomp and Van Cappellen*, 2004].

Implications for nutrient budgets in areas with a mud cap are significantly different. The cap is primarily composed of mud and silt sediments with high organic content. Fresh oxygenated groundwater discharging through these sediments undergoes rapid oxygen depletion, which could facilitate nutrient removal via denitrification, anammox and phosphate sorption onto clay particles. Although discharge rates through the mud cap are at least an order of magnitude lower than through sandy intertidal sediments, our map and a previous sediment distribution analysis [*Robbins*, 1977] indicate that the mud cap is widespread throughout the harbor (Figure2), and therefore, both discharge scenarios should be accounted for.

These findings have significant implications for nitrogen fluxes and mass balance at the scale of the harbor. The extent of the mud cap is controlling not only the volume and location of the freshwater seeps, but it also affects the residence time of groundwater chemical species. To be accurate and representative, nutrients budgets should take the spatial extent of the layer into account. Chemical analyses have also revealed significant differences in nitrogen species concentrations between these two locations [*Young*, 2013], showing how crucial it is to

understand the hydrogeological framework before studying chemical reactions and species distribution.

5.4 Sources of error

The Trident probe can be a useful tool to identify zones of fresh SGD. The portability of the probe and the short time span required for the measurements allows one to cover a large area in a relatively small amount of time. During this study, dissolved gas measurements needed to be performed as soon as possible after the end of the winter [*Young*, 2013] which constrained the timeframe for the Trident screening. Using the Trident at the winter/spring transition limited the use of temperature signal as a fresh SGD indicator as strong temperature variations on a few days was enough to create artifacts on the temperature signal. This might have prevented identification of other strong fresh SGD areas. In the future, it will be best to use the Trident probe away from seasonal transitions to ensure a temporal consistency in temperature measurements.

ER surveys can be a helpful tool to image fluid distribution in the ground as fluid conductivities can vary up to 6 orders of magnitude in coastal settings. However, ER performances can be limited by various factors that must be taken into account prior to any interpretation. In general, the sensitivity of the model decreases with depth and therefore, the DOI must be assessed for each specific setting. For our double-cable ER survey we found that the long time period required for acquisition was problematic, as the tides caused the water column thickness to vary by 0.4 m during data collection, enough to produce noise and create artifacts during the inversion. The beach topography and the broad tidal range in Stony Brook Harbor limited the use of long ER surveys. Surveys planning and forward modeling can help design better suited surveys for a particular setting, but the EI2D is limited by its forward modeling options, as it does not allow to include topography and underwater electrodes.

Direct pore-water analysis can be an appropriate way to constrain an inversion or check the ER results [*Henderson et al*., 2010]. The piezometer transects provided *in situ* salinity measurements that enabled us to distinguish between areas with different salt content and compare them to the ER sections. Unfortunately, the comparison was limited by the time discrepancies between acquisition campaigns for each method and precipitation events occurring

during piezometer data collection. The ER surveys represented snapshots, over 45 minutes, of the fluid distribution at high tide, whereas the piezometer transects were done point by point during 8 consecutive days each, at various tidal levels.

As described in details by Young [2013], a cluster monitoring well was installed in the intertidal zone, between piezometers P1-7 and P1-19 (Figure 1b). Individual wells were screened at a constant interval of 0.9 m (3'), screen length was 0.15 m. Ten sampling depths varied between 0.91 to 9.1 meters below grade, with a 0.9 m interval. Samples were collected daily between 9:30 am to 10:30am EST, 27 day period between 9/26/11 and 10/25/11. The analysis of the sample shows that salinities are consistent over time at a given depth [*Young*, 2013]: the salinity structure appears stable over two spring-neap tidal cycles, which allows us to compare our resistivity and piezometer profiles in spite of the time discrepancies in acquisition. The direct conductivity comparison was hindered by a temperature effect resulting from the pumping and exposure to the surface before measurements. This could be prevented by having C/T probes directly into the piezometers which was not possible for this study.

Due to the diffuse nature of SGD, seepage meter measurements can vary significantly at various scales [*Michael et al*., 2003; *Michael et al*., 2005; *Rosenberry*, 2008; *Russoniello et al*., 2013; *Shaw and Prepas*, 1989]. Concurrent measurements are therefore necessary to ensure the validity of the measurements. Due to technical difficulties, I was unable to obtain a grid of seepage data but isotopes derived fluxes provided estimates that were in agreement with our seepage data (Joe Tamborski, pers. comm.). The slightly higher rate measured above the mud can be the result of the spatial integration of Rn measurements or due to SGD annual variations during the two-year time span between seepage and Rn measurements.

Manual and ultrasonic seepage meters were also in very good agreement. In high energy settings, flow can be enhanced around the seepage meters due to hydrodynamic interactions [*Shaw and Prepas*, 1989; *Shinn et al*., 2002], but fluxes were sufficiently high to ignore these and our sites were wave and current free thus limiting the Bernoulli effect [*Cable et al.*, 2006; *Corbett and Cable*, 2003]. During installation of the manual seepage meters, there is always some surface water that is trapped into the sediments and interpreting the salinity in the seepage bags as that of SGD would be erroneous. Seepage rates as low as measured in the manual seepage C (< 3cm/d) were insufficient to entirely flush the seepage meter during the period of

observation. However, the significant freshening observed confirms the presence of fresh water far into the subtidal zone and supports the hypothesis that freshwater is channeled from land towards the center of the harbor by the low permeability mud layer.

6. Conclusion

Our integrated approach using a direct-push probe, electrical resistivity surveys, piezometer transects and seepage meter measurements was successful in identifying the complexity of SGD characteristics at large and small scales in Stony Brook Harbor. The comparison between the results of different methods revealed remarkable agreement. Piezometer transects validated the reliability of electrical resistivity surveys in a challenging environment such as tidally dominated harbors.

This study emphasizes that the distribution of SGD in embayments differs from numerical predictions for straight beach faces when low-permeability bottom sediments are present. The deposition of fine particle mud layers is likely to happen in many places where there is a significant loss of energy from the ocean. SGD can be distributed throughout the whole harbor and not just close to the shore, as models predict. A superficial low permeability mud layer can control groundwater flow and affect pathways and residence times which will have implications both on water budgets and on chemical reactions and therefore nutrients budgets. The channeling of freshwater offshore as a result of the mud layer could also be enhanced by the curvature of the shore that would focus groundwater towards the center of the harbor. More investigations on the effect of low permeability mud layers and shoreline curvature are necessary, as well as the study of their joint effect on SGD. Numerical modeling more specific to bay environments would be very beneficial to determine what characteristics a mud layer would impact groundwater flow, and to make these results more applicable to other settings. We recommend investigating the presence of such layer in similar low-energy coastal environments prior to any SGD study and characterizing its extent and properties before attempting any regional SGD estimates.

Acknowledgments

The study at Stony Brook University was partially funded by the NY Seagrant Research Program, through the grant –R/CTP-44-NYCT. We are grateful to the Office of Water Resources of Suffolk County Health Department for providing technical assistance in the field, including

the installation of monitoring wells within the study area. The data acquisition would not have been possible without the significant contributions of F. Basile, M. Buzby, E. Ericksen, R. Milito, R. Paulsen, N. Stark, L. Velasquez, M. Velasquez and J. Wanlass.

References

AGI (2009), Instruction Manual for EarthImager 2D, Version 2.4.0, Resistivity and IP Iversion Software, Austin, Texas, *Report.*

Anderson, M. P. (2005), Heat as a ground water tracer, *Groundwater*, *43*(6), 951-968.

Archie, G. (1942), The electrical resistivity log as an aid in determining some reservoir characteristics, *Trans. AIME*, *146*(99), 54-62.

Befus, K. M., M. B. Cardenas, D. V. Erler, I. R. Santos, and B. D. Eyre (2013), Heat transport dynamics at a sandy intertidal zone, *Water Resources Research*, *49*(6), 3770-3786.

Bokuniewicz, H. (1980), Groundwater seepage into Great South Bay, New York, *Estuarine and Coastal Marine Science*, *10*(4), 437-444.

Bokuniewicz, H., M. Taniguchi, T. Ishitoibi, M. Charette, M. Allen, and E. A. Kontar (2008), Direct measurements of submarine groundwater discharge (SGD) over a fractured rock aquifer in Flamengo Bay Brazil, *Estuarine Coastal and Shelf Science*, *76*(3), 466-472.

Bratton, J. F. (2010), The three scales of submarine groundwater flow and discharge across passive continental margins, *The Journal of Geology*, *118*(5), 565-575.

Bratton, J. F., S. M. Colman, E. R. Thieler, and R. R. Seal (2002), Birth of the modern Chesapeake Bay estuary between 7.4 and 8.2 ka and implications for global sea-level rise, *Geo-Marine Letters*, *22*(4), 188-197.

Bratton, J. F., J. K. Böhlke, F. T. Manheim, and D. E. Krantz (2004), Ground Water Beneath Coastal Bays of the Delmarva Peninsula: Ages and Nutrients, *Ground Water*, *42*(7), 1021-1034.

Bratton, J. F., W. Sanford, C. Langevin, M. Polemio, and P. Povinec (2007), The importance of shallow confining units to submarine groundwater flow, paper presented at Proceedings of the Symposium" A New Focus on Groundwater-Seawater Interactions" at the 24th General Assembly of the International Union of Geodesy and Geophysics, Perugia, Italy, 2-13 July 2007., IAHS Press.

Burnett, W. C., et al. (2006), Quantifying submarine groundwater discharge in the coastal zone via multiple methods, *Science of the Total Environment*, *367*(2-3), 498-543.

Buxton, H. T., and E. Modica (1992), Patterns and rates of ground-water movement on Long Island, New York, *Ground Water*, *V. 30*(No. 6), p. 857-866.

Cable, J. E., J. B. Martin, and J. Jaeger (2006), Exonerating Bernoulli? On evaluating the physical and biological processes affecting marine seepage meter measurements, *Limnology and Oceanography: Methods*, *4*, 172-183.

Chadwick, D. B., A. Gordon, J. Groves, C. Smith, R. Paulsen, and B. Harre (2003), New tools for monitoring coastal contaminant migration, *Sea technology*, *44*(6), 17-22.

Charette, M. A., and K. O. Buesseler (2004), Submarine groundwater discharge of nutrients and copper to an urban subestuary of Chesapeake Bay (Elizabeth River), *Limnology and Oceanography*, 376-385.

Charette, M. A., and M. C. Allen (2006), Precision Ground Water Sampling in Coastal Aquifers Using a Direct-Push, Shielded-Screen Well-Point System, *Ground Water Monitoring & Remediation*, *26*(2), 87-93.

Cherkauer, D. S., and P. F. McKereghan (1991), Ground-Water Discharge to Lakes: Focusing in Embayments, *Ground Water*, *29*(1), 72-80.

Constable, S. C., R. L. Parker, and C. G. Constable (1987), Occam's inversion: A practical algorithm for generating smooth models from electromagnetic sounding data, *Geophysics*, *52*(3), 289-300.

Corbett, D. R., and J. E. Cable (2003), Seepage meters and advective transport in coastal environments: Comments on "Seepage meters and Bernoulli's revenge" by EA Shinn, CD Reich, and TD Hickey. 2002. Estuaries 25: 126–132, *Estuaries and Coasts*, *26*(5), 1383-1387.

Cross, V., D. S. Foster, and J. F. Bratton (2010), Continuous resistivity profiling and seismic-reflection data collected in 2006 from the Potomac River estuary, Virginia and Maryland*Rep.*

Day-Lewis, F., E. White, C. Johnson, J. Lane Jr, and M. Belaval (2006), Continuous resistivity profiling to delineate submarine groundwater discharge--examples and limitations, *The Leading Edge*, *25*(6), 724.

Dimova, N. T., P. W. Swarzenski, H. Dulaiova, and C. R. Glenn (2012), Utilizing multichannel electrical resistivity methods to examine the dynamics of the fresh water–seawater interface in two Hawaiian groundwater systems, *Journal of Geophysical Research*, *117*(C2), C02012.

Fetter, C. (2001), Applied Hydrogeology (4 th), edited, New Jersey.

Gardner, L. R., and A. M. Wilson (2006), Comparison of four numerical models for simulating seepage from salt marsh sediments, *Estuarine, Coastal and Shelf Science*, *69*(3), 427-437.

Gibbes, B., C. Robinson, L. Li, and D. Lockington (2007), Measurement of hydrodynamics and pore water chemistry in intertidal groundwater systems, *Journal of Coastal Research, SI*, *50*, 884-894.

Glover, R. (1959), The pattern of fresh-water flow in a coastal aquifer, *Journal of Geophysical Research*, *64*(4), 457-459.

Gross, M. G. (1972), Characteristics and environmental quality of six north shore bays: Nassau and Suffolk Counties, Long Island, New York*Rep. 14*, Stony Brook, New York: Marine Science Research Center, State University of New York.

Henderson, R. D., F. D. Day-Lewis, E. Abarca, C. F. Harvey, H. N. Karam, L. B. Liu, and J. W. Lane (2010), Marine electrical resistivity imaging of submarine groundwater discharge: sensitivity analysis and application in Waquoit Bay, Massachusetts, USA, *Hydrogeology Journal*, *18*(1), 173-185.

Hirsch, J., and A. Randazzo (2000), Hydraulic seepage within an astatic karst lake, North-Central Florida'.

Howarth, R. W., et al. (1996), Regional nitrogen budgets and riverine N & P fluxes for the drainages to the North Atlantic Ocean: Natural and human influences, *Biogeochemistry*, *35*(1), 75-139.

Johannes, R. (1980), Ecological significance of the submarine discharge of groundwater, *MARINE ECOL.- PROG. SER.*, *3*(4), 365-373.

Johnson, A. G., C. R. Glenn, W. C. Burnett, R. N. Peterson, and P. G. Lucey (2008), Aerial infrared imaging reveals large nutrient-rich groundwater inputs to the ocean, *Geophysical Research Letters*, *35*(15), L15606.

Kohout, F. (1960), Cyclic flow of salt water in the Biscayne aquifer of southeastern Florida, *Journal of Geophysical Research*, *65*(7), 2133-2141.

Koppelman, L. E., P. K. Weyl, M. G. Gross, and D. S. Davies (1976), *The urban sea: Long Island Sound*, viii+223 pp., Praeger Publishers, New York.

Kroeger, K., and M. Charette (2008), Nitrogen biogeochemistry of submarine groundwater discharge, *Limnology and Oceanography*, *53*(3), 1025-1039.

Kuan, W. K., G. Jin, P. Xin, C. Robinson, B. Gibbes, and L. Li (2012), Tidal influence on seawater intrusion in unconfined coastal aquifers, *Water Resources Research*, *48*(2), W02502.

Lee, D. R. (1977), A device for measuring seepage flux in lakes and estuaries, *Limnology and Oceanography*, 140-147.

Lewis, E., and R. Perkin (1981), The practical salinity scale 1978: Conversion of existing data, *Deep Sea Research Part A. Oceanographic Research Papers*, *28*(4), 307-328.

Lewis, J. B. (1987), Measurements of groundwater seepage flux onto a coral reef: Spatial and temporal variations, *Limnology and Oceanography*, *32*(5), 1165-1169.

Li, L., D. Barry, F. Stagnitti, and J. Parlange (1999), Submarine groundwater discharge and associated chemical input to a coastal sea, *Water Resources Research*, *35*(11), 3253-3259.

Manheim, F. T., D. E. Krantz, and J. F. Bratton (2004), Studying ground water under Delmarva coastal bays using electrical resistivity, *Groundwater*, *42*(7), 1052-1068.

Marshall, T. J., J. W. Holmes, and C. W. Rose (1996), *Soil physics*, Cambridge University Press.

Mc Bride, M. S., and H. O. Pfannkuch (1975), The distribution of seepage within lakebeds, *Jounral of Research of U.S. Geological Survey*, *3*(5), 8.

Michael, H. A., J. S. Lubetsky, and C. F. Harvey (2003), Characterizing submarine groundwater discharge: A seepage meter study in Waquoit Bay, Massachusetts, *Geophys. Res. Lett*, *30*(6), 1297.

Michael, H. A., A. E. Mulligan, and C. F. Harvey (2005), Seasonal oscillations in water exchange between aquifers and the coastal ocean, *Nature*, *436*(7054), 1145-1148.

Michael, H. A., M. A. Charette, and C. F. Harvey (2011), Patterns and variability of groundwater flow and radium activity at the coast: a case study from Waquoit Bay, Massachusetts, *Marine Chemistry*, *127*(1), 100-114.

Moore, W. S., J. L. Sarmiento, and R. M. Key (2008), Submarine groundwater discharge revealed by 228Ra distribution in the upper Atlantic Ocean, *Nature Geoscience*, *1*(5), 309-311.

Mulligan, A. E., R. L. Evans, and D. Lizarralde (2007), The role of paleochannels in groundwater/seawater exchange, *Journal of hydrology*, *335*(3), 313-329.

Murphy III, W., W. B. Ward, B. Boyd, G. Fleming, W. Murphy IV, R. Nolen-Hoeksema, M. Art, and D. A. Rosales (2011), High-resolution shallow geophysics and geology in the Hudson-Raritan Estuary Ecosystem Restoration, New Jersey, *The Leading Edge*, *30*(2), 182-190.

Oldenburg, D. W., and Y. Li (1999), Estimating depth of investigation in dc resistivity and IP surveys, *Geophysics*, *64*(2), 403-416.

Olhoeft, G. (1981), Electrical properties of rocks, *Physical properties of rocks and minerals*, *2*, 298-305.

Park, M. J. (1985), Prediction of tidal hydraulics and sediment transport patterns in Stony Brook Harbor, State University of New York, Stony Brook.

Paulsen, R. J., C. F. Smith, D. O'Rourke, and T. F. Wong (2001), Development and evaluation of an ultrasonic ground water seepage meter, *Ground Water*, *39*(6), 904-911.

Paulsen, R. J., D. O'Rourke, C. F. Smith, and T. F. Wong (2004), Tidal Load and Salt Water Influences on Submarine Ground Water Discharge, *Ground Water*, *42*(7), 990-999.

Paulsen, R. J., C. F. Smith, J. Wanlass, and N. H. Stark (2008), Forge River Groundwater Flow Rate and Nutrient Contaminant Load Site Investigation Draft Report*Rep.*, 67 pp, Suffolk County Department of Health Services.

Robbins, S. K. (1977), Stony Brook Harbor: an interdisciplinary analysis., *Special report Rep. 9*, SUNY Stony Brook, Marine Sciences Research Center.

Robinson, C., B. Gibbes, and L. Li (2006), Driving mechanisms for groundwater flow and salt transport in a subterranean estuary, *Geophys. Res. Lett*, *33*, L03402.

Rosenberry, D. O. (2008), A seepage meter designed for use in flowing water, *Journal of Hydrology*, *359*(1), 118-130.

Russoniello, C. J., C. Fernandez, J. F. Bratton, J. F. Banaszak, D. E. Krantz, A. S. Andres, L. F. Konikow, and H. A. Michael (2013), Geologic effects on groundwater salinity and discharge into an estuary, *Journal of Hydrology*, *498*, 1-12.

Shaw, R., and E. Prepas (1989), Anomalous, short-term influx of water into seepage meters, *Limnology and Oceanography*, *34*(7), 1343-1351.

Shinn, E. A., C. D. Reich, and T. D. Hickey (2002), Seepage meters and Bernoulli's revenge, *Estuaries*, *25*(1), 126-132.

Slomp, C. P., and P. Van Cappellen (2004), Nutrient inputs to the coastal ocean through submarine groundwater discharge: controls and potential impact, *Journal of Hydrology*, *295*(1), 64-86.

Stieglitz, T., M. Taniguchi, and S. Neylon (2008a), Spatial variability of submarine groundwater discharge, Ubatuba, Brazil, *Estuarine Coastal and Shelf Science*, *76*(3), 493-500.

Stieglitz, T., J. Rapaglia, and H. Bokuniewicz (2008b), Estimation of submarine groundwater discharge from bulk ground electrical conductivity measurements, *Journal of Geophysical Research*, *113*(C8), C08007.

Stieglitz, T. C., J. Rapaglia, and S. C. Krupa (2007), An effect of pier pilings on nearshore submarine groundwater discharge from a (partially) confined aquifer, *Estuaries and coasts*, *30*(3), 543-550.

Swarzenski, P. W., F. W. Simonds, A. J. Paulson, S. Kruse, and C. Reich (2007), Geochemical and geophysical examination of submarine groundwater discharge and associated nutrient loading estimates into Lynch Cove, Hood Canal, WA, *Environmental Science & Technology*, *41*(20), 7022-7029.

Swarzenski, P. W., W. C. Burnett, W. J. Greenwood, B. Herut, R. Peterson, N. Dimova, Y. Shalem, Y. Yechieli, and Y. Weinstein (2006), Combined time-series resistivity and geochemical tracer techniques to examine submarine groundwater discharge at Dor Beach, Israel, *Geophysical Research Letters*, *33*(24).

Taniguchi, M. (2002), Tidal effects on submarine groundwater discharge into the ocean, *Geophysical Research Letters*, *29*(12).

Taniguchi, M., and H. Iwakawa (2004), Submarine groundwater discharge in Osaka Bay, Japan, *Limnology*, *5*(1), 25-32.

Taniguchi, M., W. C. Burnett, J. E. Cable, and J. V. Turner (2002), Investigation of submarine groundwater discharge, *Hydrological Processes*, *16*(11), 2115-2129.

Taniguchi, M., T. Ishitobi, W. C. Burnett, and G. Wattayakorn (2007), Evaluating ground water–sea water interactions via resistivity and seepage meters, *Ground Water*, *45*(6), 729-735.

Taniguchi, M., W. C. Burnett, H. Dulaiova, E. A. Kontar, P. P. Povinec, and W. S. Moore (2006), Submarine groundwater discharge measured by seepage meters in Sicilian coastal waters, *Continental Shelf Research*, *26*(7), 835-842.

Taylor, R. W., and D. S. Cherkauer (1984), The application of combined seismic and electrical measurements to the determination of the hydraulic conductivity of a lake bed, *Groundwater Monitoring & Remediation*, *4*(4), 78-85.

Telford, W. M., L. Geldart, and R. E. Sheriff (1990), *Applied geophysics*, Cambridge Univ Pr.

Valiela, I., J. M. Teal, S. Volkmann, D. Shafer, and E. J. Carpenter (1978), Nutrient and particulate fluxes in a salt marsh ecosystem: Tidal, *Limnol. Oceanogr*, *23*(4), 798-812.

Valiela, I., K. Foreman, M. LaMontagne, D. Hersh, J. Costa, P. Peckol, B. DeMeo-Andreson, C. D'Avanzo, M. Babione, and C. H. Sham (1992), Couplings of watersheds and coastal waters: sources and consequences of nutrient enrichment in Waquoit Bay, Massachusetts, *Estuaries and Coasts*, *15*(4), 443-457.

Weinstein, Y., W. C. Burnett, P. W. Swarzenski, Y. Shalem, Y. Yechieli, and B. Herut (2007), Role of aquifer heterogeneity in fresh groundwater discharge and seawater recycling: An example from the Carmel coast, Israel, *Journal of Geophysical Research-Oceans*, *112*(C12).

Wilson, A. M., and L. R. Gardner (2006), Tidally driven groundwater flow and solute exchange in a marsh: numerical simulations, *Water Resources Research*, *42*(1).

Young, C. R. (2013), *Fate of Nitrogen during Submarine Groundwater Discharge into Long Island North Shore Embayments*. Doctoral dissertation. Stony Brook University, 165 pp. http://www.geo.sunysb.edu/reports/cyoung-phd-thesis.pdf

Zektser, I. S., L. G. Everett, and R. G. Dzhamalov (2006), *Submarine groundwater*, CRC Press Inc.

Figures and captions

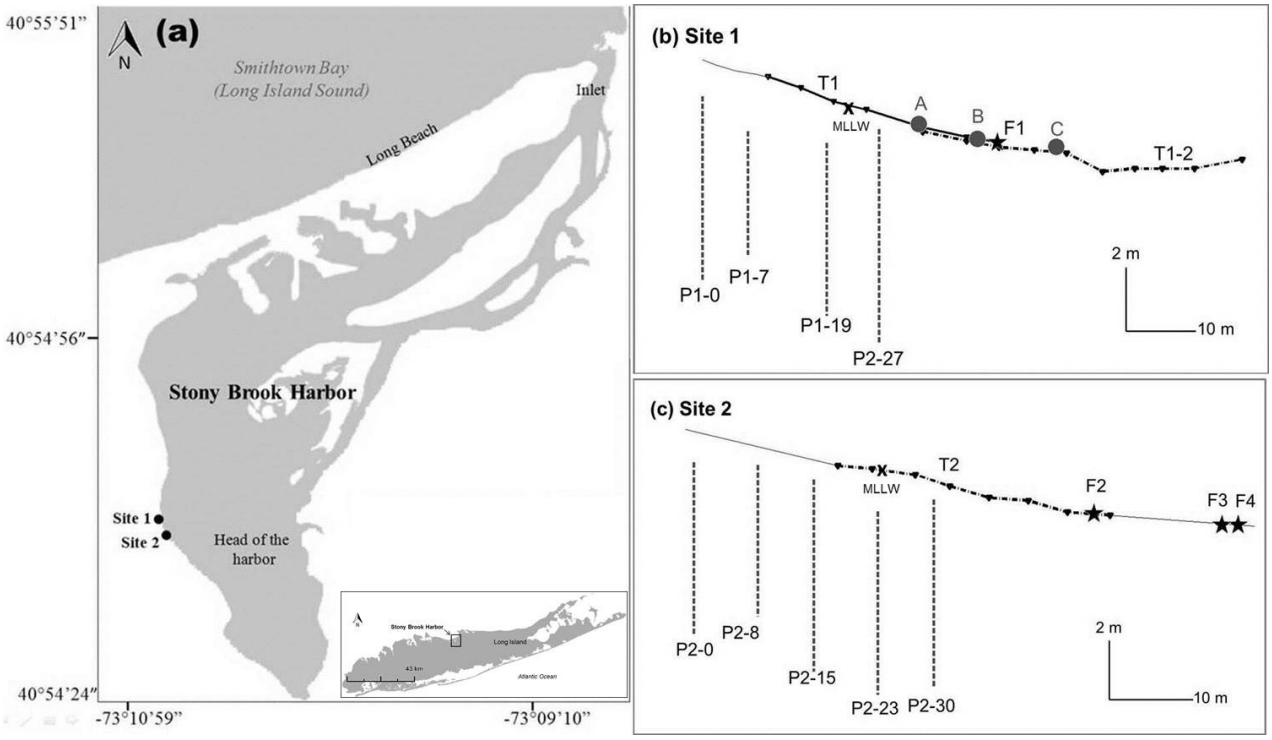

Figure 1. (a) Site map of Stony Brook Harbor and inclusion of general location. (b) Cross section of relative positions of the different measurements at site 1. (c) Cross section of relative positions of the different measurements at site 2. The vertical black dotted lines indicate the piezometer wells. The number following the P indicates the site and the number after the hyphen, the distance from the first piezometer. The grey dots show the positions of the manual seepage meters. The stars, F, indicate the positions of the ultrasonic seepage meter funnels. The electrical resistivity transects, T, are plotted as solid or dotted lines with black inverted triangles. The black cross (x) indicate the position of the mean lower level of water (MLLW). The high tide mark would be landward of the first piezometer at each site. The sections are presented with 5x vertical exaggeration.

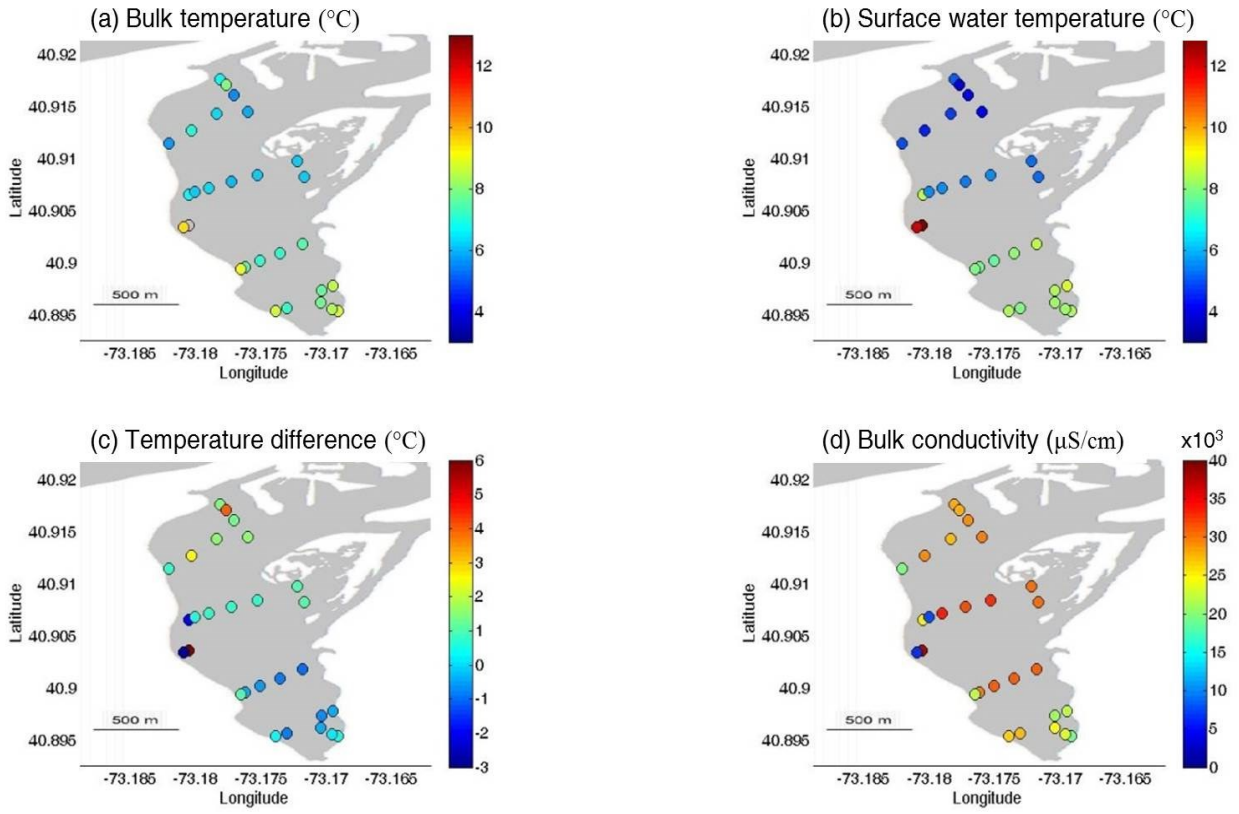

Figure 2. Site map of the Trident probe transects realized between 3/28/11 and 4/11/11 across Stony Brook Harbor. (a) Bulk temperature of sediments at 60 cm depth, in °C. (b) Surface water temperature, in °C. (c) Temperature difference between porewater and surface water

$\Delta T = T_{porewater} - T_{surface\ water}$, in °C. (d) Sediments bulk conductivity, in µS/cm, at 60 cm depth.

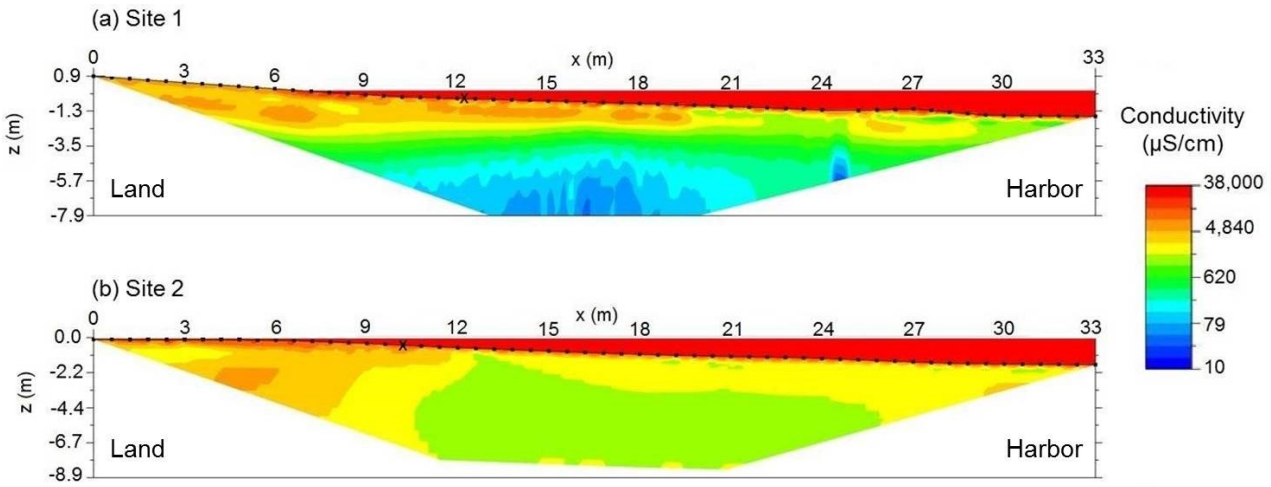

Figure 3. Inverted conductivity sections at site 1 (a) and site 2 (b), in µS/cm. The black line indicates the position of the cable, the dots locate the electrodes and the black crosses (x) show the position of the MLLW. The high tide marks are landward of both profiles. Colors are plotted on a log scale. RMS values are 6.03% and 6.13% for sections at site1 and 2, respectively.

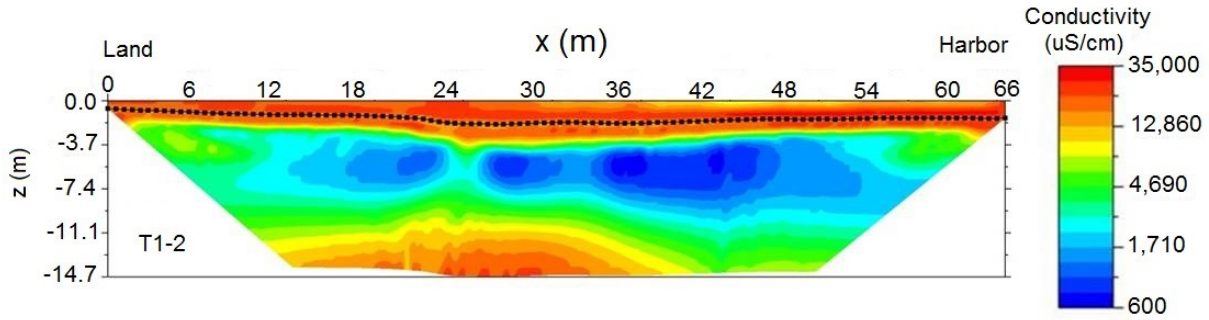

Figure 4. Inverted conductivity section of the double-cable transect T1-2 at low tide at site 1. Conductivities are plotted on a log scale, in µS/cm. The black dotted line indicates the position of the cable with the electrodes. The MLLW mark was located a couple of meters landward of the profile. The RMS value is 7.68%.

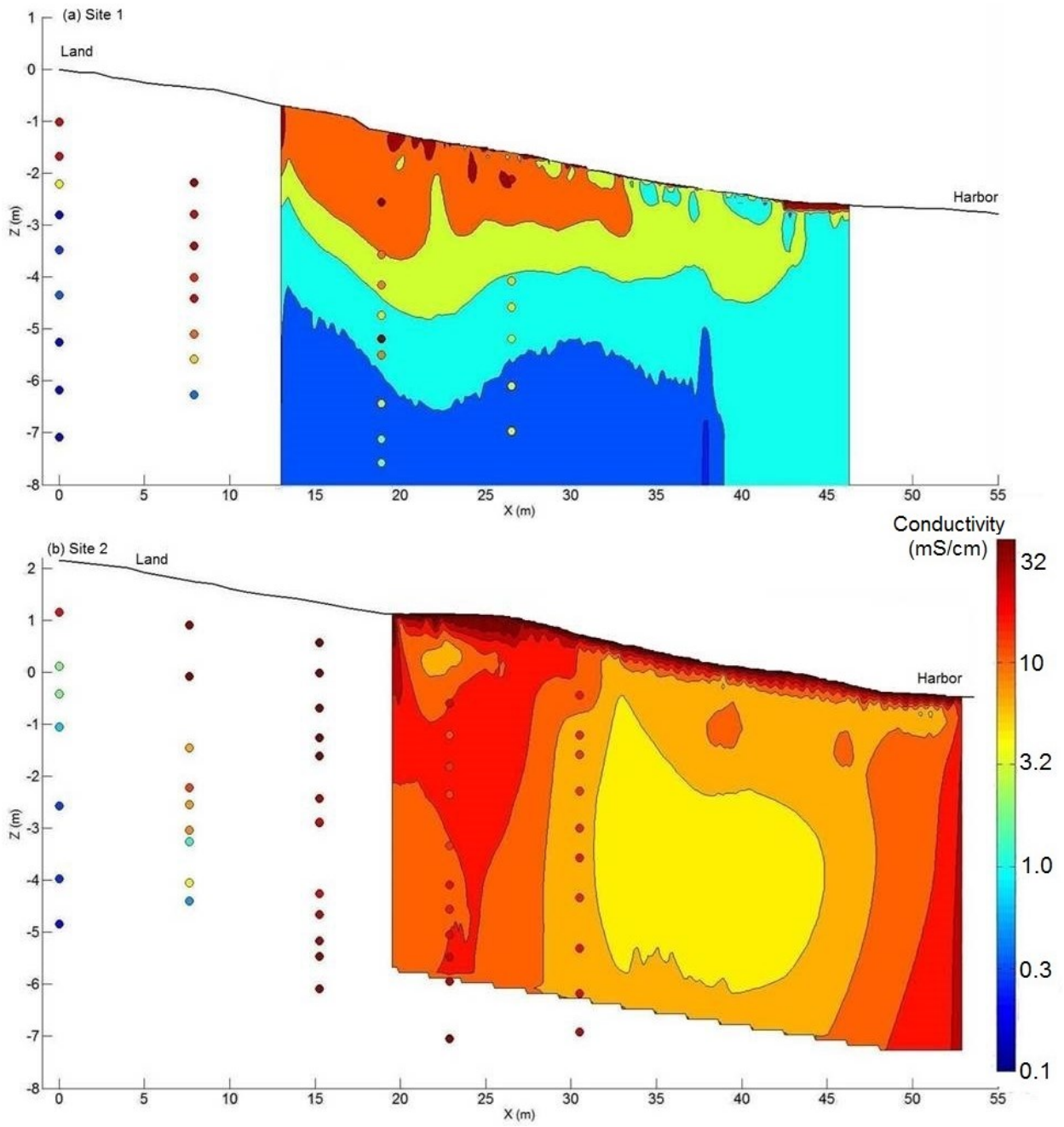

Figure 5. Comparison of piezometer pore water conductivities and inverted conductivity sections at sites 1 (a) and 2 (b). Conductivities are plotted on a log scale. Topography is indicated with a black solid line.

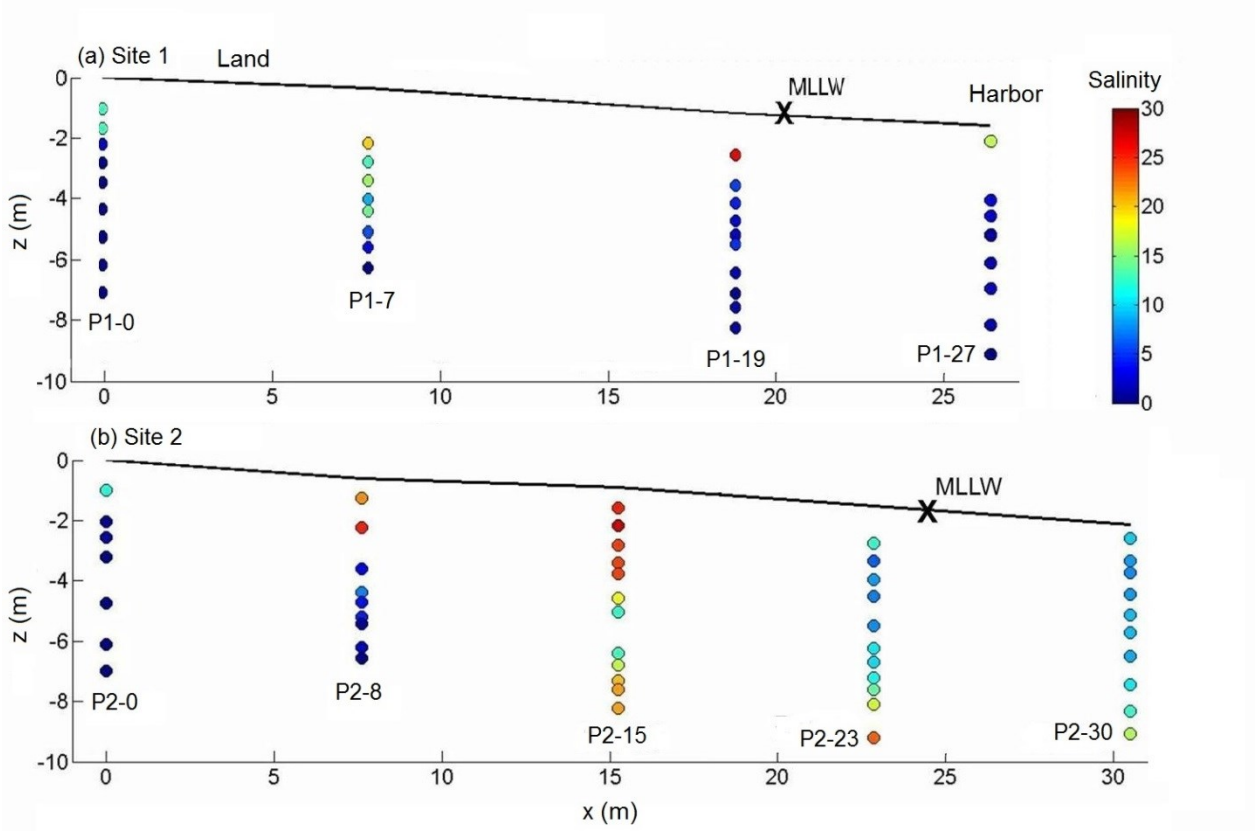

Figure 6. Salinity measurements for the piezometer transects at site 1 (a) and site 2 (b). The dots show the locations of porewater samples. Colors indicate the value of salinity. The cross (x) marks the position of the mean lower level of water (MLLW). The high tide marks would be a couple of meters landward of the profiles.

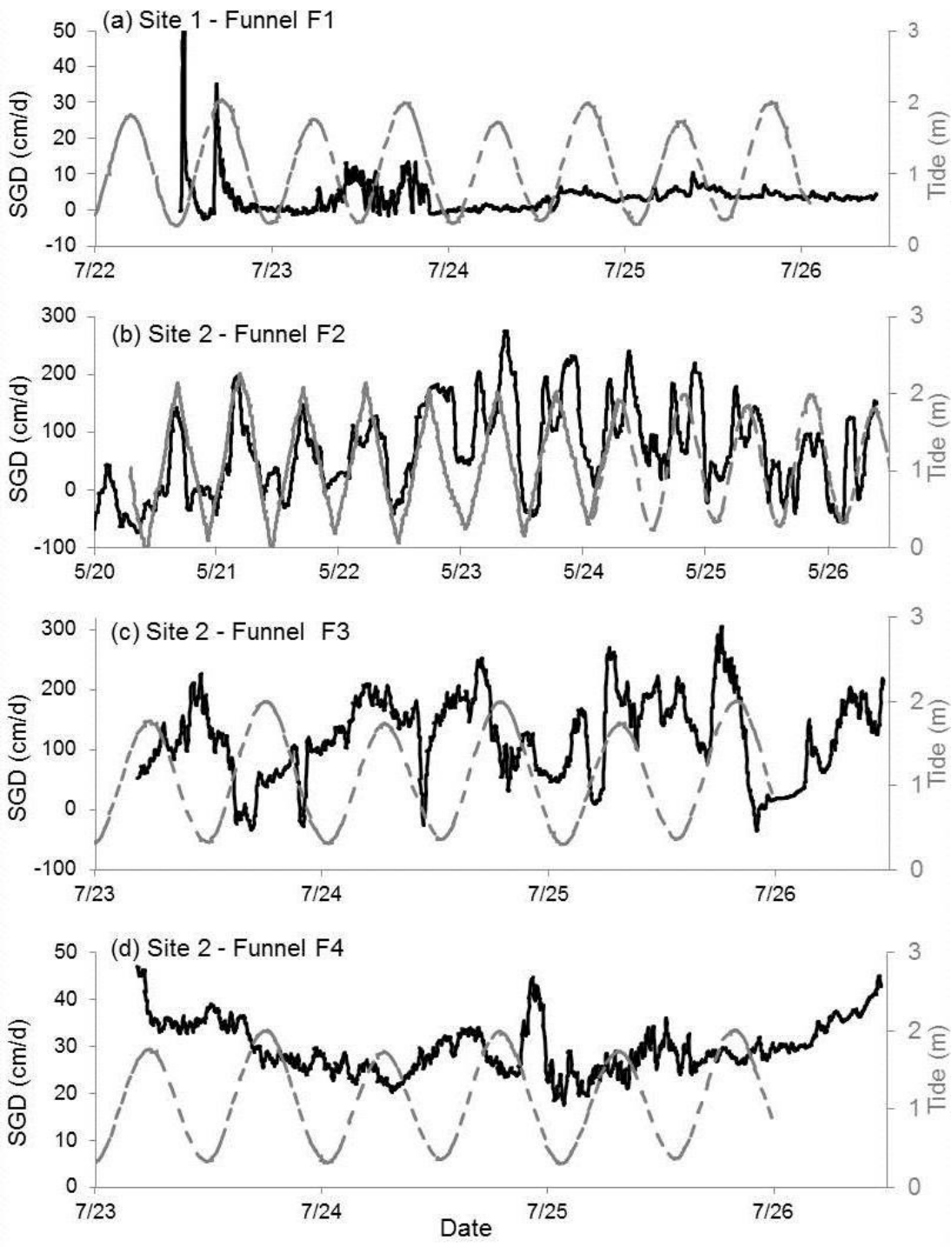

Figure 7. Four-point moving averages of specific discharge measurements by the ultrasonic seepage meters, in cm/d, at site 1: funnel 1 (a) implanted at 25 m offshore of the MLLW from 7/22/11 to 7/26/11, and site 2: funnel 2 (b) implanted at 30 m offshore of the MLLW from 5/20/11 to 5/26/11, funnel 3 (c) implanted at 40 m offshore of the MLLW from 7/23/11 to 7/26/11 and funnel 4 (d), implanted at 45 m offshore of the MLLW from 7/23/11 to 7/26/11. The grey dotted lines indicate measured tidal level, in m.

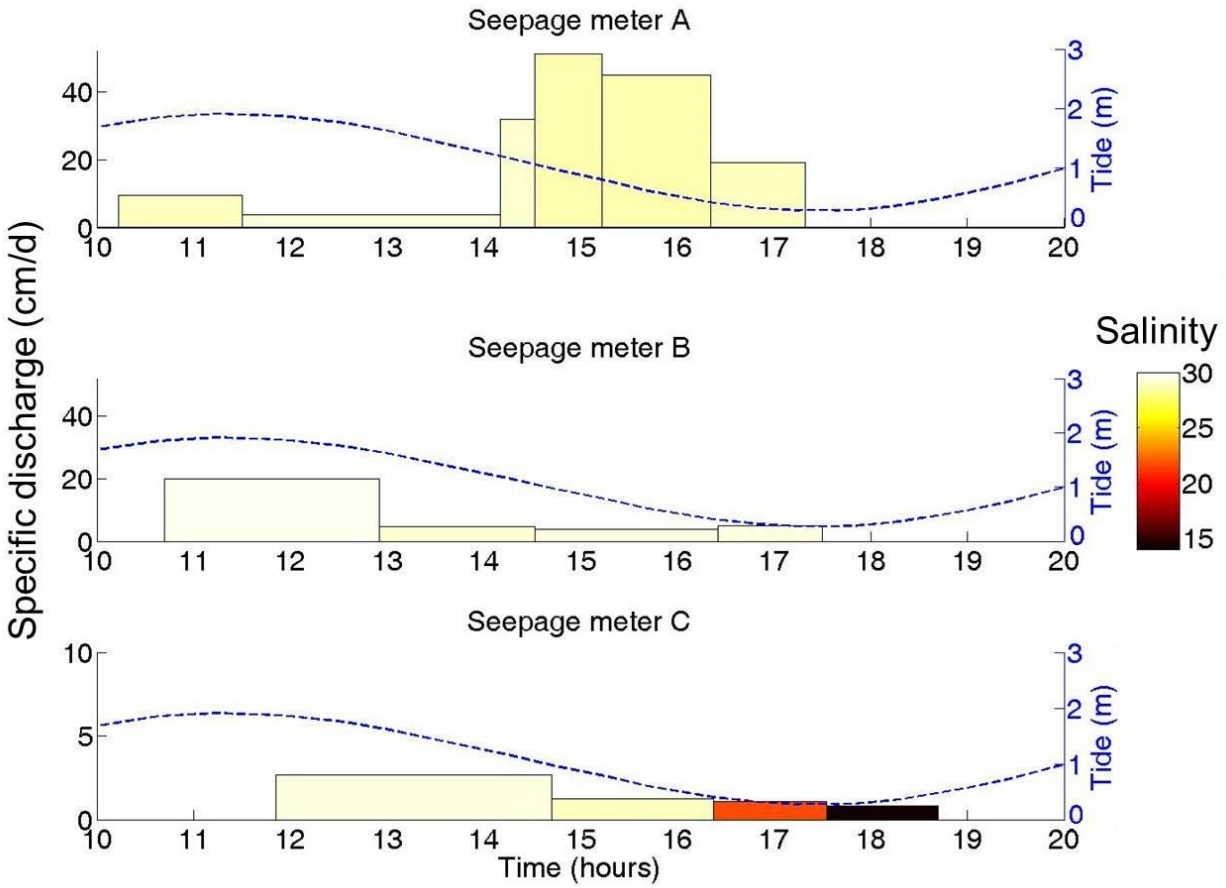

Figure 8. Salinity and specific discharge measurements from the manual seepage meters at site 1. Seepage meters A, B and C were placed at 1, 20 and 22 m offshore of the low tide mark, respectively. Each rectangle represents a sampling bag: the base shows the sampling duration in hours, the height the seepage rate in cm/d and the color the salinity. The blue dotted line indicates the tidal level, in m. Note the different scale for the seepage meter C.

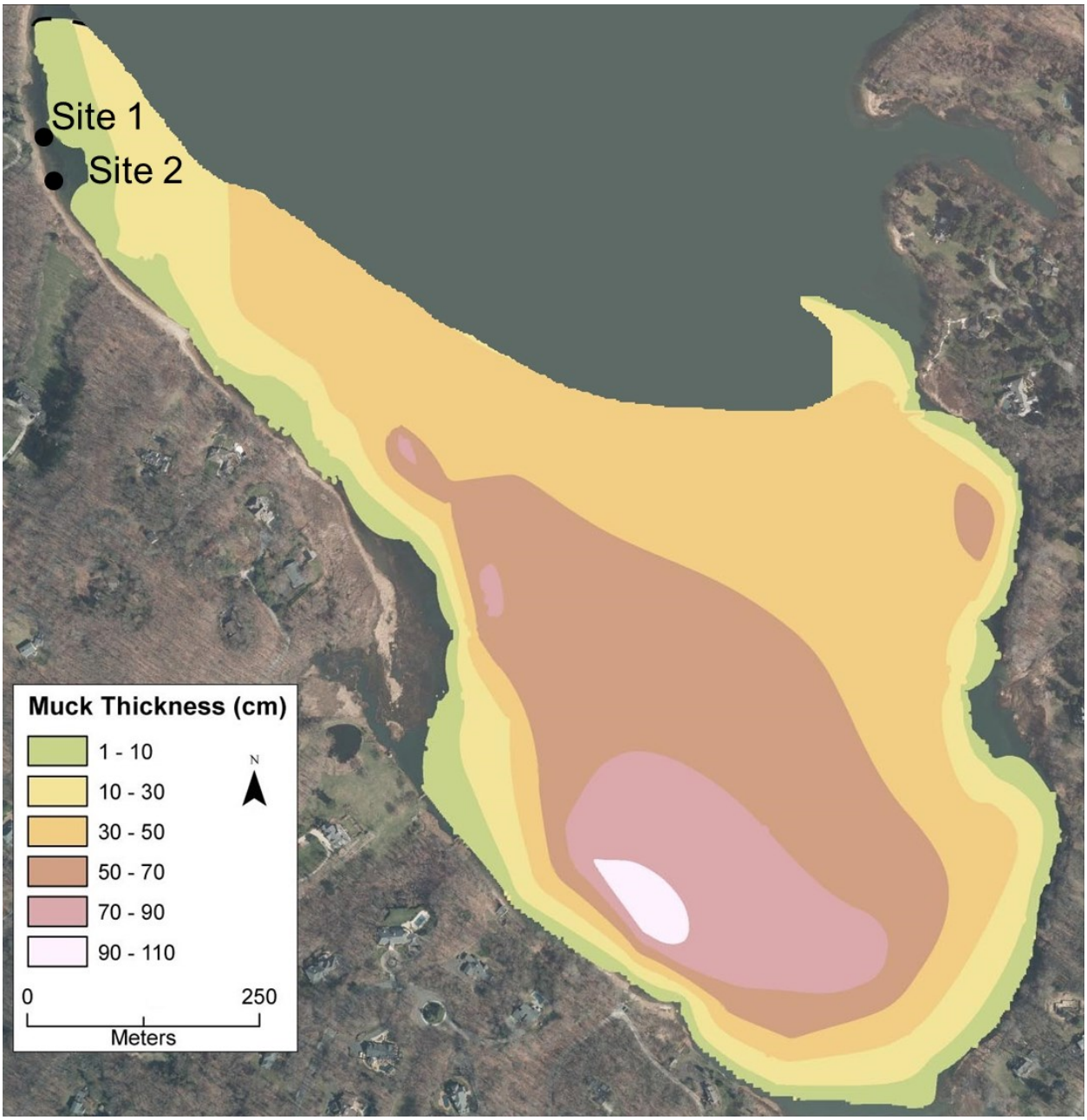

Figure 9: Interpolated map of the mud thickness in the southern portion of Stony Brook Harbor, in cm, and relative locations of sites 1 and 2.

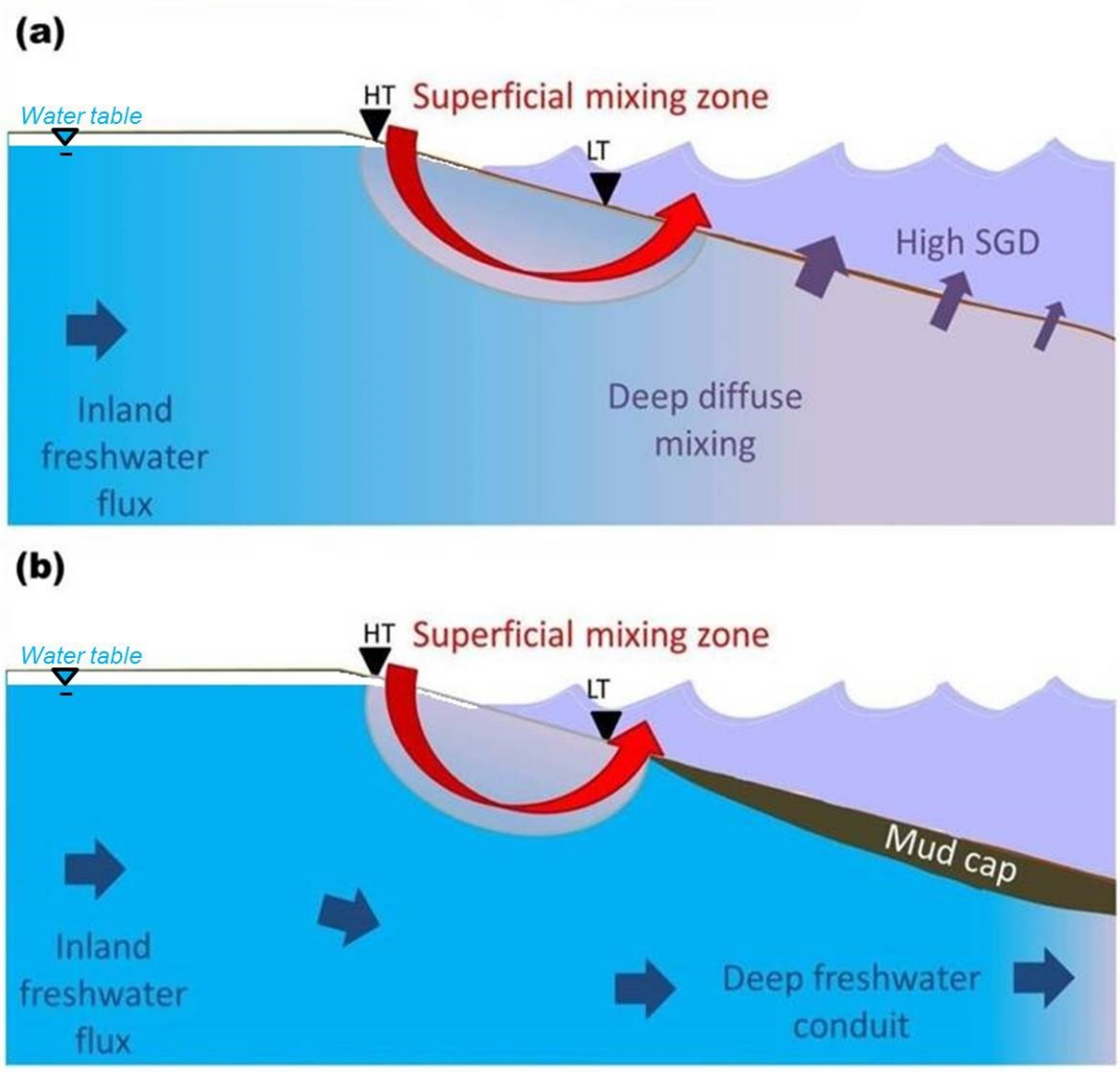

Figure 10. Conceptual model of groundwater fluxes in the absence (a) or presence (b) of a mud cap. HT and LT indicate the high tide and low tide marks, respectively. The cap limits the vertical flow and thus controls the extent of infiltration, mixing and circulation of seawater.

Chapter 3: Groundwater flow and solute transport modeling of a coastal unconfined sandy aquifer: application to Stony Brook Harbor

Abstract

A field study of spatial distribution of submarine groundwater discharge (SGD) in Stony Brook Harbor, NY suggested that it is controlled by a low-permeability mud layer, spreading throughout approximately a third of the harbor area. Published numerical models developed for homogeneous, isotropic unconfined aquifers with tidal forcing are in discrepancy with observations at Stony Brook Harbor. Active sedimentation of fine particle is common in low energy environments; it is therefore of interest to investigate the role of such a layer using a more specific model. Comparative 2D SEAWAT density-difference groundwater flow and transport models were developed. Steady-state simulations with and without the mud layer were able to reproduce field observations. A 50 cm thick layer with a hydraulic conductivity of 0.01 m/d at the surface of the sediments is sufficient to significantly alter the hydraulic gradient and salinity distribution under the mud.

1. Introduction

With about 44% of the current world population living within 150 km of the coasts, pressure on coastal groundwater resources and seawater intrusion constitute major concerns that need to be addressed [*Bear*, 1999]. Predicting the freshwater-seawater interface (FSI) position and dynamics is therefore crucial. Empirically, the Ghyben-Herzberg relation states that the FSI should be found at a depth equal to 40 times the hydraulic head on land, with sea level as reference [*Badon-Ghyben*, 1888; *Herzberg*, 1901]. Hydrodynamic equilibrium predicts the existence of a saltwater wedge limiting a density-driven convection cell model [*Cooper Jr*, 1959; *Glover*, 1959; *Kohout*, 1960]. Recently, improved numerical models have allowed the inclusion of dynamic boundary conditions, such as waves and tides, that lead to predictions of a more complex FSI [*Robinson et al.*, 2006; *Robinson et al.*, 2007a; *Robinson et al.*, 2007b; *Robinson et al.*, 2007c]. Current numerical models indicate that the FSI should have three main components: a superficial mixing cell located in the intertidal zone, a freshwater discharge area close to the low tide mark and the saltwater wedge. The size and position of these features are contingent upon the relative importance of several factors: the inland hydraulic gradient, the slope of the beach, the tidal and wave amplitude [*Robinson et al.*, 2007b].

Submarine groundwater discharge (SGD) encompasses all fluids that cross the sediment ocean interface, regardless of their origin or composition [*Burnett et al.*, 2003]. This means that SGD includes fresh water derived from inland hydraulic gradient, intrusion of seawater and any discharge of circulated seawater, no matter what the driving force is. Studying SGD in coastal settings is challenging due to the highly dynamic boundary conditions and variety of physical drivers responsible for different SGD components. Numerical simulations have proved very useful in isolating and studying the effects of individual variables, as well as various combinations of factors. A stronger hydraulic gradient sharpens the FSI and pushes it offshore [*Prieto and Destouni*, 2005; *Robinson et al.*, 2007a]. Tides and waves influence the chemistry of SGD by enhancing the circulated seawater fraction [*Gibbes et al.*, 2008a; *Gibbes et al.*, 2008b; *Li et al.*, 1999; *Robinson et al.*, 2007a; *Robinson et al.*, 2007b; *Xin et al.*, 2010]. An inclined beach slope intensifies seawater intrusion at high tidal levels [*Ataie-Ashtiani et al.*, 1999; *Mango et al.*, 2004; *Mao et al.*, 2006], while spring-neap tides and seasonal recharge cycles influence the position of the FSI and the associated chemical loading on longer time scales [*Michael et al.*,

2005; *Turner et al.*, 1997]. Interactions with the seabed topography can also enhance SGD [*Konikow et al.*, 2013]. Field and laboratory measurements coupled with numerical simulations suggested that the pathways SGD takes through the different parts of the FSI may influence the associated chemical reactions by affecting solute residence time [*Beck et al.*, 2007a; *Gibbes et al.*, 2008a; *Gibbes et al.*, 2008b; *Kuan et al.*, 2012; *Mulligan and Charette*, 2006].

Realistic modeling of the hydrologic system would require not only the representation of dynamic boundaries but also several other factors such as density variations, spatial variability and diffusivity of phenomena [*Burnett et al.*, 2006; *Michael et al.*, 2003; *Michael et al.*, 2005], heterogeneities, processes in the unsaturated zone [*Heiss et al.*, 2014] and scale dependent processes [*Bratton*, 2010; *Smith*, 2004]. The interactions among these variables still need further investigations. Most current numerical models are limited to isotropic, homogeneous aquifers with straight beach faces. This idealized case might not be suitable for understanding regional scale SGD, including harbors and bays. First, a concave shoreline is known to focus groundwater flow [*Cherkauer and McKereghan*, 1991; *Lewandowski et al.*, 2013; *Winter and Pfannkuch*, 1984]. The existence of fine-particle low-permeability layer was investigated using flow nets, but it has only been modeled for lakes where there are no density-driven or changes in water level due to tides and waves [*Mc Bride and Pfannkuch*, 1975]. Second, the loss of energy between the ocean and an embayment can deposit layers of fine particles or mud, with porosity and permeability that are significantly different from the ones of the coastal aquifer. Analytical models investigating the influence of a low permeability layer in lakes concluded that discharge is focused at the shore independently of the layer [*Mc Bride and Pfannkuch*, 1975], but our field observations at Stony Brook Harbor suggest otherwise (see chapter 2). To study SGD at larger scales, it is necessary to characterize SGD distribution in embayments, as they do represent a significant portion of the shoreline. The first step, presented here, focuses on studying the influence of a low-permeability mud layer on SGD distribution in Stony Brook Harbor, NY. To my knowledge, this is the first attempt at developing a 2D density-difference groundwater flow and transport model for a heterogeneous aquifer.

SEAWAT is a density-dependent code [*Guo and Langevin*, 2002] that allows the simulation of freshwater-seawater interactions in coastal environments by coupling the functionalities of the groundwater simulator MODFLOW [*Harbaugh et al.*, 2000] and the solute transport code

MT3DMS [*Zheng and Wang*, 1999b]. It is used here to simulate SGD in an unconfined sandy aquifer with a sloping beach. With this model, we show that SGD distribution is controlled by the spatial extent of a mud layer. A layer as thin as 50 cm is enough to substantially change SGD amplitude, composition and location by modifying the hydraulic gradient and restricting mixing with seawater.

2. Mathematical model

Several assumptions are made while developing the governing equation of groundwater flow and solute transport in SEAWAT. It is assumed that Darcy's law is valid, which means that the flow is laminar. The standard expression for specific storage in a confined aquifer is applicable. Fick's law of diffusion is valid and isothermal conditions prevail. Active cells are assumed to be fully saturated with water and finally, a fully miscible liquid phase of very small compressibility is assumed [*Guo and Langevin*, 2002; *Langevin et al.*, 2003].

SEAWAT uses the concept of equivalent freshwater head. In a saline groundwater environment, heads vary with pressure, elevation and density. To prevent increased complexity of governing equations, all heads are converted to freshwater heads by applying a density-dependent correction (Equation 1).

$$h_f = \frac{\rho}{\rho_f} h + \frac{\rho - \rho_f}{\rho_f} Z \qquad \text{(Equation 1)}$$

where h is the head [L], h_f is the equivalent freshwater head [L], ρ is the density of saline aquifer water [ML^{-3}], ρ_f is the density of freshwater [ML^{-3}] and Z is the elevation above 0 [L].

The basis of the governing equation for ground-water flow is the conservation of mass for fluid and solute (Equation 2):

$$-\nabla \cdot (\rho \vec{q}) + \bar{\rho} q_s = \frac{\partial (\rho n_e)}{\partial t} \qquad \text{(Equation 2)}$$

where ρ is the fluid density [ML^{-3}], $\vec{q}$ is the specific discharge vector [LT^{-1}], $\bar{\rho}$ is the density of water entering from a source or leaving through a sink [ML^{-3}], q_s is the volumetric flow rate per unit volume of aquifer representing sources and sinks [T^{-1}], n_e is the effective porosity [dimensionless], and t is time [T].

Using the chain rule, differentiating with respect to time and pressure, identifying the compressibility factors for the porous medium and the fluid, the flow equation becomes (Equation 3):

$$-\nabla.(\rho\vec{q}) + \bar{\rho}q_s = \rho S_p \frac{\partial P}{\partial t} + n_e \frac{\partial \rho}{\partial C}\frac{\partial C}{\partial t} \qquad \text{(Equation 3)}$$

where P is the pore fluid pressure [$ML^{-1}T^{-2}$], C is the solute concentration [ML^{-3}], and S_p is the specific storage in terms of pressure [$M^{-1}LT^{-2}$]. Details of the calculations are available in the SEAWAT user manual [*Guo and Langevin*, 2002].

The specific discharge used in the flow equation is calculated using Darcy's law for each direction, assuming that the axes are in alignment with the principal permeability directions and expressing the heads in term of equivalent freshwater heads, yields the governing equation for saturated density-dependent groundwater flow (Equation 4):

$$\nabla \cdot \left[\rho K_f \left(\nabla \cdot h_f + \frac{\rho - \rho_f}{\rho_f}.\nabla z\right)\right] = \rho S_f \frac{\partial h_f}{\partial t} + n_e \frac{\partial \rho}{\partial t} - \rho_s q_s \qquad \text{(Equation 4)}$$

where z is the vertical coordinate directing upward [L], K_f is the equivalent freshwater hydraulic conductivity [LT^{-1}], h_f is the equivalent freshwater head [L], ρ is the fluid density [ML^{-3}], ρ_f is the freshwater fluid density [ML^{-3}], S_f is the equivalent freshwater storage coefficient [L^{-1}], t is time [T], n_e is the effective porosity, ρ_s and q_s are the density and flow rate per unit volume of aquifer of the sources and sinks, respectively.

In SEAWAT, transport is coupled to groundwater flow. The governing equation for salt transport is (Equation 5):

$$\frac{\partial (n_e C)}{\partial t} = \nabla \cdot (n_e D \nabla C) - \nabla \cdot (n_e \vec{v} C) - q_s C_s \qquad \text{(Equation 5)}$$

where C is the concentration of dissolved salt [ML^{-3}], D is the hydrodynamic dispersion coefficient tensor [L^2T^{-1}], $\vec{v}$ the pore water velocity [LT^{-1}], and C_s is the concentration of dissolved salt from the sources/sinks [ML^{-3}] [*Zheng and Wang*, 1999a].

A state equation relates the fluid density to its salt concentration (Equation 6).

$$\rho = \rho_f + \frac{\partial \rho}{\partial C} C \qquad \text{(Equation 6)}$$

where $\frac{\partial \rho}{\partial C}$ is known to be approximately 0.7143 with C and ρ expressed in kg/m^3 and for C varying between 0 and 35 kg/m^3, the value of seawater.

SEAWAT does not directly simulate unsaturated flow and it accounts for water table fluctuations by using a drying/ wetting function. This approach inactivates cells when heads drop lower than the cell bottom elevation. Inactivated cells can be reactivated if the head in neighboring cells reaches a certain threshold.

3. Conceptual model and implementation

An important aspect of groundwater flow modeling in coastal settings is the ability to reproduce the formation of a seepage face, a result of water table oscillations due to decoupling with sea level. During ebb tide, because sea level drops faster than the water table can follow, a decoupling occurs between the water table level and sea level, which leads to the creation of a seepage face [*Turner et al.*, 1997]. During flood tide, when sea level rises faster than the water table, a landward tilt creates a water table over-height. Simulations that do not account for the seepage face can underestimate groundwater and solute fluxes to coastal water bodies [*Robinson et al.*, 2007a].

Recent studies have focused on determining the best way to represent the changing boundary condition along the sloping beach [*Mulligan et al.*, 2011; *Post*, 2011; *Robinson et al.*, 2007b]. With SEAWAT, it is possible to define boundaries with changing head and concentrations over time, but implementing them along a sloping beach is not straightforward. Three main approaches have been described:

- The High-*K* approach is based on an explicit simulation of the ocean. The model is divided in 2 zones: the aquifer and the ocean. The ocean is represented with a porosity of 1 and a very high hydraulic conductivity [*Robinson et al.*, 2006; *Robinson et al.*, 2007b]. This is the most intuitive approach; however, it is numerically intensive and the high contrast of hydraulic properties at the interface creates strong numerical oscillations that prevent model convergence in many cases [*Mulligan et al.*, 2011].
- In the GHB/DRN approach, oceans cells are inactive. The seepage face is simulated using a drain function (DRN package) at the top of the model. The ocean time-varying

head is imposed through a general head boundary at the top of the model for the part under water (GHB package) with fixed seawater salinity. Computations are faster as the grid is reduced, but implementing the tidal variation in terms of boundary conditions is laborious. Cell located at the sediment/ocean interface become no flow cells if the ocean is not explicitly represented. This means that no SGD can occur. To allow fluid to cross the interface, cells must either be assigned to a drain boundary (DRN) that allows water to exit the aquifer, if they are exposed, or to a variable flux head (GHB) boundary that allows fluid to enter or exit, otherwise. The GHB value depends on the relative heads between the aquifer and the ocean, and therefore, on the cell position along the beach slope. Thus, a tidal variation must be decomposed in small time-steps during which the ocean head is constant. For each variation in water level bigger than a cell thickness, the DRN and GHB boundaries need to be adapted. Generating these files therefore require some automation.

- The PBC approach is the most recent method. It involves a recently developed SEAWAT package that includes the definition of a periodic boundary condition using a sinusoidal head signal. The ocean cells are also inactive and the head is applied directly at the top of the aquifer cells. The boundary condition is dynamically updated during the simulation based on a user-defined tidal signal that can include several tidal constituents. This package allows for the development of a dynamic seepage face whose position is iteratively updated during the simulation, thus overcoming a strong limitation of the original SEAWAT program [*Post*, 2011].

Developing a satisfactory transient model with tidal boundary conditions is not trivial. Due to the amount and complexity of the processes involved, a model cannot accurately represent all of the previously noted variables. In Stony Brook Harbor, tidal forcing is the main factor acting on SGD on a short time scale (i.e. days). My goal was therefore to develop 2D models of two adjacent sites: one similar to an unconfined sandy coastal aquifer and one with a surficial low-permeability mud layer with tidal loading. The first step of such process is to obtain a reliable steady-state model that can then be used as the initial state from which time-varying conditions can be added. Our preliminary results, i.e. Stony Brook steady-state 2D numerical models are presented here for site 1 and site 2, with and without the mud layer, respectively.

4. Stony Brook model description and parameters

My model focuses on the Upper Glacial Aquifer, a sandy unconfined aquifer limited at its base by an impermeable clay unit found at approximately 30 m depth. The simulated domain measures 160 m x 32 m. The finite-difference grid is composed of rectangular blocks with 1 row, 66 columns and 40 layers. The vertical discretization is non-uniform and increases towards the bottom. The columns widths range from 1.25 to 5 m and the layer height from 0.3 to 5 m. Dimensions of the blocks vary to create a more refined mesh centered on the intertidal zone, so as to provide enough accuracy around the zone of interest while limiting the computational time (Figure 11). Column width and layer height vary linearly away from the refined mesh to ensure a smooth grid that facilitates model convergence.

The beach slope was measured using a laser topography survey. A detailed muck layer was observed along site 1; the mud starts at 5 m below the low tide mark, at x ~ 90 m. The mud thickness increases offshore non-monotonically. The maximum thickness measured was ~ 0.85 m, but the average thickness on the profile was 0.5 m.

The model boundary conditions are presented in (Figure 12). No recharge through precipitation is simulated at the top of the model. The seaward vertical boundary and the bottom horizontal boundary of the model are no flow boundaries. The landward vertical boundary is a constant head and constant concentration boundary. For the steady-state model, the seawater level is stable and the ocean boundary is simply represented by a constant head and fixed concentration boundary. For the transient model, the boundary must change with time to reflect the water level variations.

SEAWAT uses the preconditioned conjugate-gradient solver (PCG package) for which convergence is determined by using the head-change and residual criteria chosen by the user. Based on publications reporting better model convergence, we chose to use the block-centered flow package (BCF), even though it may overestimate vertical flow by a factor up to 2 for partially saturated cells [*Mulligan et al.*, 2011]. For the transport simulation, limited numerical dispersion was reported using the implicit finite-difference method with upstream weighting. Cell rewetting is set to occur only from below (for better convergence) when the computed head in an inactive cell rises above 1% of the cell thickness [*Mulligan et al.*, 2011].

Core sediment analyses indicate a porosity of 62% in the mud and 40% in the sand. Standard falling head measurements on mud sediment cores estimated vertical hydraulic conductivity to be ~1.5×10^{-3} m/d, which is in good agreement with average reported values for silt 10^{-4} to 10^{-2} m/d [*Fetter*, 2001]. Care was taken to limit the perturbation of the sediment core during sampling, but due to the texture of the mud this was very difficult. The mud appeared as a fluidized layer and was therefore represented as an isotropic layer i.e. horizontal and vertical hydraulic conductivities are assumed equal. Hydraulic conductivities for the sand were fixed at K_h = 50 m/d and K_v = 5 m/d. These values are similar to that reported by *Buxton and Modica* [1992]: K_h = 70 and K_v = 7 m/d, but somewhat smaller as the latter values were high enough to create convergence issues, unless the grid was very fine, in which case computational power and time were problematic. Dispersivities were not characterized for the upper glacial aquifer, and were assumed to be uniform and isotropic following the literature [*Robinson et al.*, 2007b]. All models parameters and boundary condition values are summarized in Table 1.

5. Model results

Head and salinity distributions obtained for the steady state simulations are presented in figures 13 and 14, respectively. Simulations were run with appreciably different initial conditions (initial hydraulic heads of 0 and 1.5 m and initial salinities of 0.1 and 30) and different grid discretization (cells 2 times smaller or larger) to test the sensitivity of the results. No difference was observed between results.

In the case of a regular sandy unconfined coastal aquifer, the hydraulic heads slowly decrease towards the ocean (Figure 13a). Close to the land boundary, the equipotential lines are subvertical as they are controlled by the vertical constant head boundary. This means that fluxes close to land will be mostly horizontal. Due to the 10:1 anisotropy of the aquifer, groundwater flows horizontally on most of the section. The equipotentials become more inclined towards the harbor due to the horizontal sea level boundary, which means that fluxes right at the sediments interface will be primarily subvertical. The space between equipotential lines does not vary significantly, signifying that the hydraulic gradient decreases progressively from land to the harbor. The strongest fluxes are found along the beach slope, landward of the shoreline.

When the mud layer is present (Figure 13b), however, the head distribution is different. Close to the land boundary, the equipotentials are similar. The transition between vertical to horizontal equipotentials occurs much closer to land. The 0.2 and 0.1 m equipotentials have a semi-ellipsoidal shape centered on the low tide mark, i.e. x ~ 85 m and are much closer indicating a stronger hydraulic gradient. At depth below 10 m, the hydraulic gradient is much weaker and therefore, there is almost no horizontal flow under the harbor. The vertical flux is focused in the intertidal area, before the beginning of the mud layer at x ~ 90 m. Under the mud, for 90 < x < 160 m, the 0.1 and 0.2 equipotential lines are completely horizontal and follow the muds lower limit. The lines are indiscernible, indicating an even stronger hydraulic gradient created by the very low permeability of the layer. Overall, groundwater velocities are smaller. These results demonstrate that a 0.5 m thin mud layer with a hydraulic conductivity of 0.001 m/d, similar to the one observed in Stony Brook Harbor, can have a significant impact on SGD distribution in the intertidal zone and farther offshore.

The differences observed in head distribution are also visible on the salinity section (Figure 14). Without the mud layer, the typical saltwater wedge develops due to the higher density of seawater (Figure 14a). A shallow mixing zone 1-2 m thick develops on the beach slope for 70 < x < 100 m where mixing between fresh groundwater and overlying seawater creates a salinity close to 5. The transition zone is approximately 5 m wide and thickens at depth, which could be due to lower flow velocities or just an artifact of the grid coarsening. Dispersion is delicate to model as it is scale-dependent and therefore difficult to estimate accurately. It is also linked to the discretization of the grid and should therefore not be over-interpreted without further study. To achieve convergence, the model without the mud calculated a few salinity values above 30 at the interface (30.6) which modified the color range. For ease of comparison, the color bar scales are the same but the salty portion of the first model appears in a lighter shade of red.

The salt water wedge is also visible on the second model and is almost identical to the previous model. A small difference exists close the sediment interface; the lateral extent of the superficial diffusion mixing zone is limited by the presence of the mud layer offshore, starting at x ~ 90 m. Further offshore, freshwater from land is channeled horizontally under the mud and mixes with seawater, creating an elongated zone of intermediate salinities ~ 5-10 close to the

surface that progressively increase at depth to reach 30 salinity under 15 m below the mud bottom.

This is in agreement with the observations made in Stony Brook Harbor, where an offshore piezometer well recorded a salinity of 8 at x ~150 m and z ~ 15 m. Manual seepage meters implanted in offshore muddy areas recorded the presence of freshwater, and the ultrasonic seepage meters located in areas without mud layers displayed very high rates. This agrees with both the salinity distribution predicted by the model and the strong vertical hydraulic gradient under the mud.

6. Conclusion

A simplified 2D steady-state model of Stony Brook Harbor shows that a low permeability mud layer as thin as 0.5 m is enough to significantly affect SGD distribution and composition. The numerical predictions are in good agreement with salinity observations collected in the field.

The next step of this work would be to develop a transient model by including a dynamic boundary condition for tidal sea level variations. This would allow more direct comparisons between numerical predictions and electrical resistivity sections, piezometer salinity data and seepage meter measurements in the intertidal zone. Several factors may result in the discrepancy between field observations and numerical results, such as unsaturated flow and sediment compressibility in tidal marshes [*Gardner and Wilson*, 2006; *Wilson and Gardner*, 2006], local variations of porosity in sediments due to marshes roots and bioturbation. A sensitivity analysis of the mud layer characteristics, i.e. thickness and permeability would help determine in which conditions the mud layer can be neglected and when it is crucial to include it in SGD studies.

Porewater chemical analyses performed at our two sites identified two regimes of denitrification linked to SGD flowpaths: discharge through the sandy sediments or through the mud layer. It should be possible to couple the transport simulation to a particle tracking algorithm that would provide a better understanding of the flow paths and residence time of nutrients carried by the inland freshwater. This could help understand the nutrients fluxes into the harbor and validate the hypothesis on nitrate fate [*Young*, 2013].

Future work will include the development of a 3D model that will enable the simulation of the impact of the mud layer, the concave shoreline and the density-driven phenomena. By including sediment heterogeneities, shoreline concavity and density-driven phenomena with numerical modeling, the results of this study will highlight the fundamental differences between the functional discharge mechanisms of coastal embayments with respect to ocean shorelines. Improved quantification of SGD in coastal embayments will allow for more improved nutrient mass balances. This methodology can be applied to any shallow, low-energy environment with significantly differing surficial sediment regimes. A cohesive, regional modeling approach would serve as an excellent complement to thermal infrared remote sensing techniques, allowing researchers to better locate and quantify SGD on a larger scale, where field measurements may be limited and/or not logistically practical [*Johnson et al.*, 2008; *Kelly et al.*, 2013].

References

Ataie-Ashtiani, B., R. Volker, and D. Lockington (1999), Tidal effects on sea water intrusion in unconfined aquifers, *Journal of Hydrology*, *216*(1-2), 17-31.

Badon-Ghyben, W. (1888), Notes on the probable results of well drilling near Amsterdam, *Tijdschrift van het Koninklijk Inst. van Ing. Den Haag*, 21.

Bear, J. (1999), *Seawater intrusion in coastal aquifers: Concepts, methods, and practices*, Springer Netherlands.

Beck, A. J., Y. Tsukamoto, A. Tovar-Sanchez, M. Huerta-Diaz, H. J. Bokuniewicz, and S. A. Sañudo-Wilhelmy (2007b), Importance of geochemical transformations in determining submarine groundwater discharge-derived trace metal and nutrient fluxes, *Applied Geochemistry*, *22*(2), 477-490.

Bratton, J. F. (2010), The three scales of submarine groundwater flow and discharge across passive continental margins, *The Journal of Geology*, *118*(5), 565-575.

Burnett, W. C., H. Bokuniewicz, M. Huettel, W. S. Moore, and M. Taniguchi (2003), Groundwater and pore water inputs to the coastal zone, *Biogeochemistry*, *66*(1-2), 3-33.

Burnett, W. C., et al. (2006), Quantifying submarine groundwater discharge in the coastal zone via multiple methods, *Science of the Total Environment*, *367*(2-3), 498-543.

Buxton, H. T., and E. Modica (1992), Patterns and rates of ground-water movement on Long Island, New York, *Ground Water*, *V. 30*(No. 6), p. 857-866.

Cherkauer, D. S., and P. F. McKereghan (1991), Ground-Water Discharge to Lakes: Focusing in Embayments, *Ground Water*, *29*(1), 72-80.

Cooper Jr, H. H. (1959), A hypothesis concerning the dynamic balance of fresh water and salt water in a coastal aquifer, *Journal of Geophysical Research*, *64*(4), 461-467.

Fetter, C. (2001), Applied Hydrogeology (4 th), edited, New Jersey.

Gardner, L. R., and A. M. Wilson (2006), Comparison of four numerical models for simulating seepage from salt marsh sediments, *Estuarine, Coastal and Shelf Science*, *69*(3), 427-437.

Gibbes, B., C. Robinson, L. Li, D. Lockington, and H. Li (2008a), Tidally driven pore water exchange within offshore intertidal sandbanks: Part II numerical simulations, *Estuarine, Coastal and Shelf Science*, *80*(4), 472-482.

Gibbes, B., C. Robinson, H. Carey, L. Li, and D. Lockington (2008b), Tidally driven pore water exchange in offshore intertidal sandbanks: Part I. Field measurements, *Estuarine, Coastal and Shelf Science*, *79*(1), 121-132.

Glover, R. (1959), The pattern of fresh-water flow in a coastal aquifer, *Journal of Geophysical Research*, *64*(4), 457-459.

Guo, W., and C. D. Langevin (2002), *User's Guide to SEWAT: A Computer Program for Simulation of Three-Dimensional Variable-Density Ground-Water Flow*, United States Geological Survey.

Harbaugh, A. W., E. R. Banta, M. C. Hill, and M. G. McDonald (2000), *MODFLOW-2000, the US Geological Survey modular ground-water model: User guide to modularization concepts and the ground-water flow process*, US Geological Survey Reston, VA, USA.

Heiss, J. W., W. J. Ullman, and H. A. Michael (2014), Swash zone moisture dynamics and unsaturated infiltration in two sandy beach aquifers, *Estuarine, Coastal and Shelf Science*, *143*, 20-31.

Herzberg, D. (1901), *Die wasserversorgung einiger nordseebäder*.

Johnson, A. G., C. R. Glenn, W. C. Burnett, R. N. Peterson, and P. G. Lucey (2008), Aerial infrared imaging reveals large nutrient-rich groundwater inputs to the ocean, *Geophysical Research Letters*, *35*(15), L15606.

Kelly, J. L., C. R. Glenn, and P. G. Lucey (2013), High-resolution aerial infrared mapping of groundwater discharge to the coastal ocean, *Limnol. Oceanogr.: Methods*, *11*, 262-277.

Kohout, F. (1960), Cyclic flow of salt water in the Biscayne aquifer of southeastern Florida, *Journal of Geophysical Research*, *65*(7), 2133-2141.

Konikow, L., M. Akhavan, C. Langevin, H. Michael, and A. Sawyer (2013), Seawater circulation in sediments driven by interactions between seabed topography and fluid density, *Water Resources Research*, *49*(3), 1386-1399.

Kuan, W. K., G. Jin, P. Xin, C. Robinson, B. Gibbes, and L. Li (2012), Tidal influence on seawater intrusion in unconfined coastal aquifers, *Water Resources Research*, *48*(2), W02502.

Langevin, C. D., W. B. Shoemaker, and W. Guo (2003), *MODFLOW-2000, the US Geological Survey Modular Ground-Water Model--Documentation of the SEAWAT-2000 Version with the Variable-Density Flow Process (VDF) and the Integrated MT3DMS Transport Process (IMT)*, US Department of the Interior, US Geological Survey.

Lewandowski, J., K. Meinikmann, T. Ruhtz, F. Pöschke, and G. Kirillin (2013), Localization of lacustrine groundwater discharge (LGD) by airborne measurement of thermal infrared radiation, *Remote Sensing of Environment*, *138*, 119-125.

Li, L., D. Barry, F. Stagnitti, and J. Parlange (1999), Submarine groundwater discharge and associated chemical input to a coastal sea, *Water Resources Research*, *35*(11), 3253-3259.

Mango, A. J., M. W. Schmeeckle, and D. J. Furbish (2004), Tidally induced groundwater circulation in an unconfined coastal aquifer modeled with a Hele-Shaw cell, *Geology*, *32*(3), 233-236.

Mao, X., P. Enot, D. Barry, L. Li, A. Binley, and D. S. Jeng (2006), Tidal influence on behaviour of a coastal aquifer adjacent to a low-relief estuary, *Journal of Hydrology*, *327*(1-2), 110-127.

Mc Bride, M. S., and H. O. Pfannkuch (1975), The distribution of seepage within lakebeds, *Jounral of Research of U.S. Geological Survey*, *3*(5), 8.

Michael, H. A., J. S. Lubetsky, and C. F. Harvey (2003), Characterizing submarine groundwater discharge: A seepage meter study in Waquoit Bay, Massachusetts, *Geophys. Res. Lett*, *30*(6), 1297.

Michael, H. A., A. E. Mulligan, and C. F. Harvey (2005), Seasonal oscillations in water exchange between aquifers and the coastal ocean, *Nature*, *436*(7054), 1145-1148.

Michael, H. A., M. A. Charette, and C. F. Harvey (2011), Patterns and variability of groundwater flow and radium activity at the coast: a case study from Waquoit Bay, Massachusetts, *Marine Chemistry*, *127*(1), 100-114.

Mulligan, A. E., and M. A. Charette (2006), Intercomparison of submarine groundwater discharge estimates from a sandy unconfined aquifer, *Journal of Hydrology*, *327*(3-4), 411-425.

Mulligan, A. E., C. Langevin, and V. E. A. Post (2011), Tidal Boundary Conditions in SEAWAT, *Ground Water*.

Post, V. (2011), A new package for simulating periodic boundary conditions in MODFLOW and SEAWAT, *Computers & Geosciences*, *37*(11), 1843-1849.

Prieto, C., and G. Destouni (2005), Quantifying hydrological and tidal influences on groundwater discharges into coastal waters, *Water resources research*, *41*(12).

Robinson, C., B. Gibbes, and L. Li (2006), Driving mechanisms for groundwater flow and salt transport in a subterranean estuary, *Geophys. Res. Lett*, *33*, L03402.

Robinson, C., L. Li, and H. Prommer (2007a), Tide-induced recirculation across the aquifer-ocean interface, *Water Resources Research*, *43*(7), W07428.

Robinson, C., L. Li, and D. Barry (2007b), Effect of tidal forcing on a subterranean estuary, *Advances in Water Resources*, *30*(4), 851-865.

Robinson, C., B. Gibbes, H. Carey, and L. Li (2007c), Salt-freshwater dynamics in a subterranean estuary over a spring-neap tidal cycle, *Journal of Geophysical Research*, *112*(C9), C09007.

Smith, A. J. (2004), Mixed convection and density-dependent seawater circulation in coastal aquifers, *Water Resources Research*, *40*(8).

Turner, I. L., B. P. Coates, and R. I. Acworth (1997), Tides, waves and the super-elevation of groundwater at the coast, *Journal of Coastal Research*, 46-60.

Wilson, A. M., and L. R. Gardner (2006), Tidally driven groundwater flow and solute exchange in a marsh: numerical simulations, *Water Resources Research*, *42*(1).

Winter, T., and H. Pfannkuch (1984), Effect of anisotropy and groundwater system geometry on seepage through lakebeds: 2. Numerical simulation analysis, *Journal of Hydrology*, *75*(1), 239-253.

Xin, P., C. Robinson, L. Li, D. A. Barry, and R. Bakhtyar (2010), Effects of wave forcing on a subterranean estuary, *Water Resources Research*, *46*(12), W12505.

Young, C. R. (2013), *Fate of Nitrogen during Submarine Groundwater Discharge into Long Island North Shore Embayments*. Doctoral dissertation. Stony Brook University, 165 pp. http://www.geo.sunysb.edu/reports/cyoung-phd-thesis.pdf

Zheng, C., and P. P. Wang (1999a), MT3DMS, *A modular three-dimensional multi-species transport model for simulation of advection, dispersion and chemical reactions of contaminants in groundwater systems*.

Zheng, C., and P. P. Wang (1999b), MT3DMS: a modular three-dimensional multispecies transport model for simulation of advection, dispersion, and chemical reactions of contaminants in groundwater systems; documentation and user's guide*Rep.*, DTIC Document.

Tables

Table 1. Stony Brook Harbor model parameters

Parameter	Value	Unit
Longitudinal dispersivity	0.5	m
Transversal dispersivity	0.05	m
Freshwater concentration	0.1	kg/m^3
Seawater concentration	30	kg/m^3
Constant head boundary	0.5	m
Diffusion coefficient	10^{-9}	m^2/d
Sand horizontal hydraulic conductivity	50	m/d
Sand vertical hydraulic conductivity	5	m/d
Mud horizontal hydraulic conductivity	0.001	m/d
Mud vertical hydraulic conductivity	0.001	m/d
Sand porosity	0.4	
Mud porosity	0.62	
Mud layer thickness	0.5	m

Figures and captions

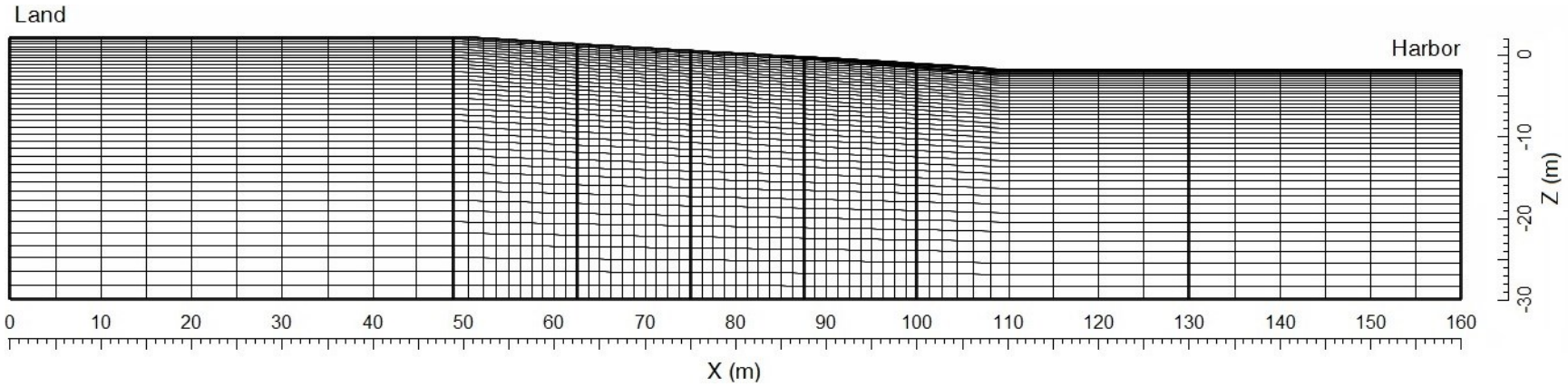

Figure 11. Grid mesh of Stony Brook harbor numerical SEAWAT model. The mud layer starts at x ~ 90 m, and appears as a bold line at the top of the sediments.

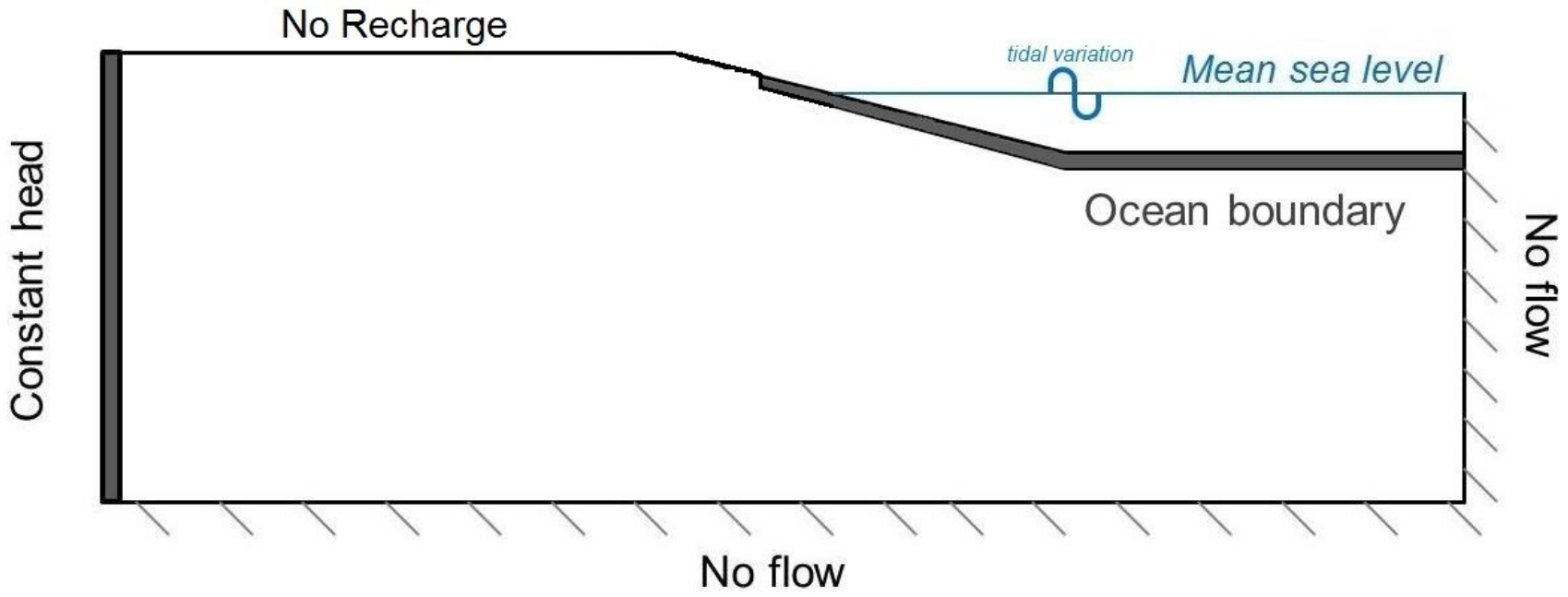

Figure 12. Boundary conditions of a 2D density-difference numerical model of an unconfined coastal aquifer with a sloping beach.

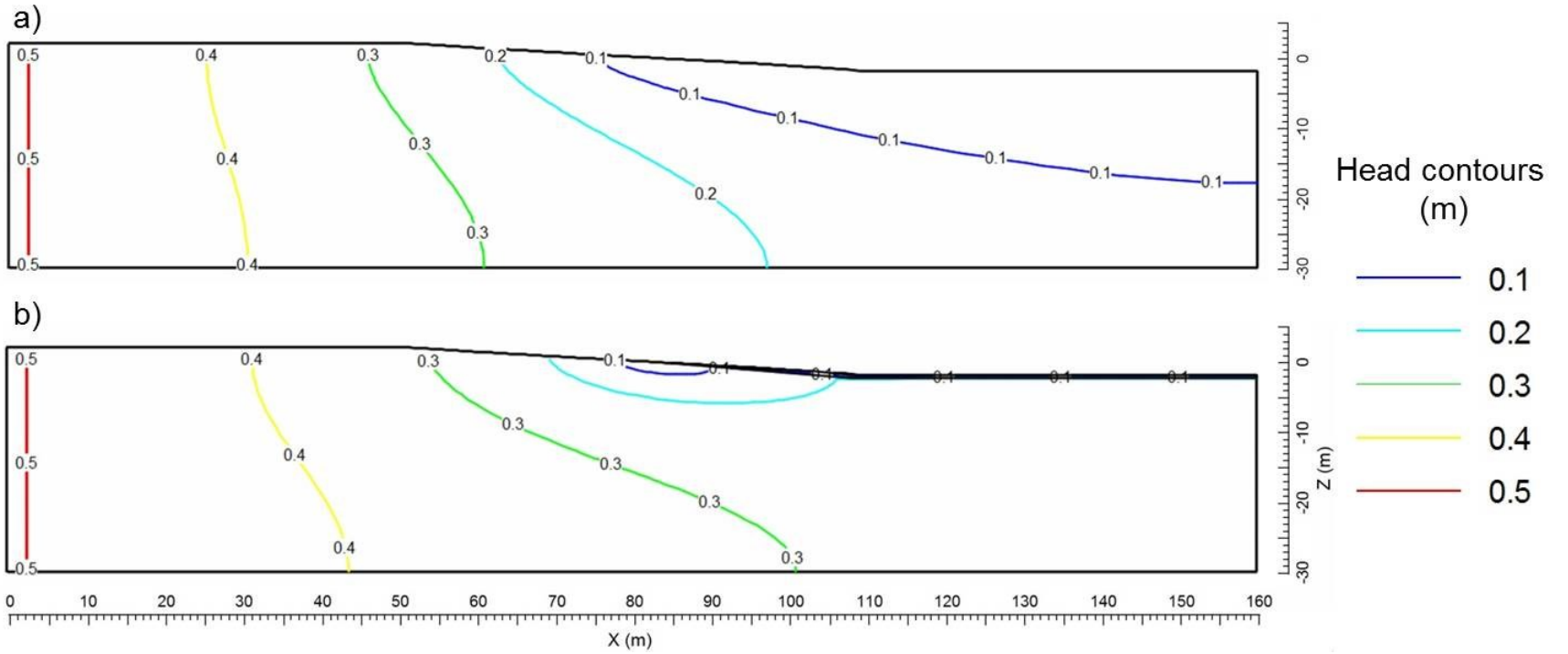

Figure 13. Equipotential distribution (in m) for Stony Brook Harbor steady state model without (a) and with (b) the low-permeability mud layer, shown as the bolded black line.

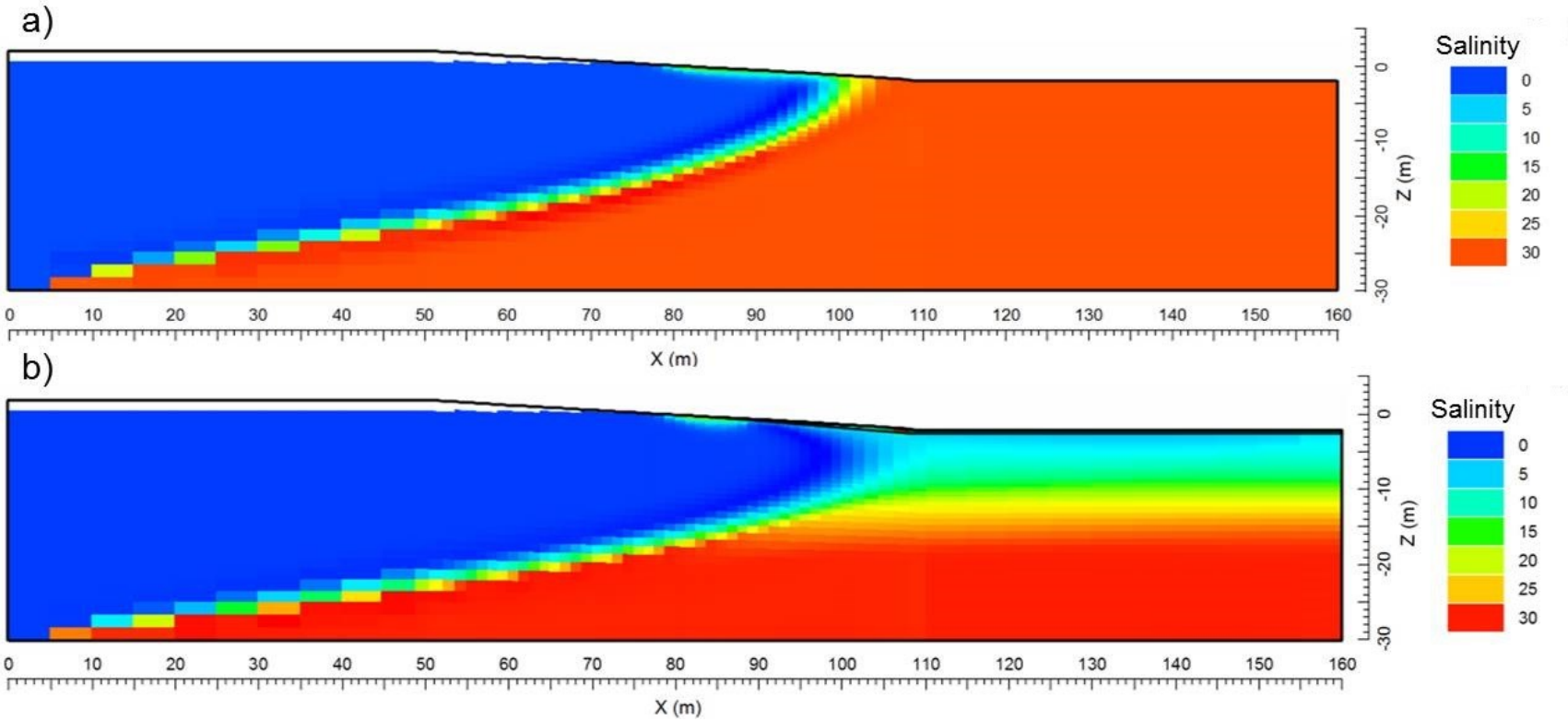

Figure 14. Salinity distribution for Stony Brook Harbor steady state model without (a) and with (b) the low-permeability the mud layer, plotted as a black bold line.

Chapter 4: Time-lapse electrical resistivity survey of the intertidal zone and implications for submarine ground water discharge

Abstract

Submarine groundwater discharge (SGD) is now widely recognized as a crucial contributor to surface water as it provides a pathway for nutrients and contaminants that can significantly impact coastal ecosystems. Field measurements in the vicinity of the freshwater-seawater interface (FSI) have shown that the spatio-temporal distribution of SGD can be highly heterogeneous. Some numerical models have identified three regions (a density-driven circulation cell offshore, an upper saline plume and a freshwater tube in the intertidal zone) which seem to persist over time, such that the distinct regions can be recognized in simulations that average the numerically predicted salinity profiles over the tidal phases. For each region, the size and shape are influenced by factors such as the tidal and wave loading, inland hydraulic gradient, beach geometry and aquifer properties. There is a paucity of field data about the evolution of the salinity profile in the shallow regions of the FSI during a tidal cycle. To characterize the spatio-temporal heterogeneities of the FSI and compare with numerical predictions, I used electrical resistivity as a proxy for salinity. Electrical resistivity surveys were acquired during a 12-hour cycle in a tidally dominated environment. My measurements indicate fundamentally different scenarios during high and low tide. At low tide, the resistivity data suggest an influx of freshwater from land, forming a plume that rises up and contributes substantially to SGD in the intertidal zone. I also observed the occurrence of three regions somewhat analogous to the numerical predictions. However, at high tide, instead of these distinct regions, I observed a diffuse mixing zone that extended along the water/sediment interface and overlaid the freshwater from land. Point measurements of seepage rates and salinity are in basic agreement with the two scenarios. It should also be noted that the phase-averaged section obtained with the resistivity surveys resembles the high tide resistivity end-member and therefore differs from the phase-averaged simulations.

1. Introduction

The most general definition of submarine groundwater discharge (SGD) includes any fluid crossing the sediment/ocean interface, regardless of its origin, driving-force and composition [*Burnett et al.,* 2003]. Understanding SGD is crucial to quantify chemical fluxes from coastal aquifers to the ocean and to monitor seawater intrusion [*Zektser et al.,* 2006]. SGD provides a pathway for terrestrially-derived contaminants to reach the oceans and impact marine ecosystems [*Johannes,* 1980] by altering coastal nutrient dynamics *[Beck et al., 2007b]*. The mixing of fresh and salt porewater creates geochemically active zones that modify chemical fluxes [*Moore,* 1999; *Moore and Shaw,* 1998; *Valiela and Delia*, 1990]. SGD importance is widely recognized; nevertheless challenges intrinsic to its study persist. Due to its widely distributed and heterogeneous nature, and its spatio-temporal variations at a variety of scales, SGD remains difficult to quantify [*Michael et al.*, 2003]. To address this issue many methods have been developed [*Burnett et al.*, 2006].

A variety of seepage meters are available to measure SGD directly. However, to characterize the high spatial variability requires a large number of point measurements *[Bokuniewicz, 1980; Michael et al., 2003; Russoniello et al., 2013],* or a combination of several complementary methods [*Burnett et al.*, 2006]. Numerical models have significantly contributed to predicting SGD patterns for given conditions, and recent simulations have brought new insight into flux dynamics and chemistry in coastal settings [*Ataie-Ashtiani et al.*, 1999; *Kuan et al.*, 2012; *Li et al.*, 1999; *Robinson et al*., 2006]. Numerical models have identified three distinct hydrological regimes: a density-driven circulation cell offshore, a superficial intertidal saline zone, and a freshwater discharge area between the two. The freshwater-seawater interface (FSI) may fluctuate both in space and time due to variations in tides, waves or hydraulic gradient, among others. While the three regimes and the FSI have been extensively studied over various time scales in numerical simulations [*Robinson et al.*, 2007a; *Robinson et al.*, 2007b; *Robinson et al.*, 2007c], there is still a paucity of field data, especially regarding to the shallow processes and their dynamics over a tidal cycle.

The main goal of this study is to elucidate these processes and the associated variations of porewater salinity distribution in the intertidal zone of a sandy coastal aquifer, in West Neck Bay (Shelter Island, NY) during a semi-diurnal tidal cycle. This study combines stationary time-lapse electrical resistivity (ER) surveys of the intertidal zone and direct seepage measurements at the

sediment/ocean interface in the intertidal and subtidal zones. Salinities measured in the seepage meters are compared to the fluid distribution imaged by the ER surveys, used as proxy for salinity. SGD in West Neck Bay has been extensively studied in a comparative experiment led by working group 112 of the Scientific Committee on Oceanic Research (SCOR) *[Anonymous, 2002; Burnett et al., 2006; Dulaiova et al., 2006; Paulsen et al., 2004; Sholkovitz et al., 2003; Stieglitz et al., 2008b; Stieglitz et al., 2007]* and in other previous studies [*O'Rourke*, 2000; *Paulsen et al.*, 1998]. Some data suggested the existence of a confining unit at that site, but its extent and properties were not characterized [*Stieglitz et al*., 2007]. A secondary goal of this study is to investigate if deeper ER vertical cross-sections can image the extent of the postulated confining layer.

2. Study Site

West Neck Bay is a small embayment located in the southwestern part of Shelter Island, situated between the North and South forks of Long Island, NY, in the Peconic Estuary (figure 1). My study site was identical to the one chosen by the working group 112 of the Scientific Committee on Oceanic Research (SCOR). The bay area is approximately 1 km^2 and its depth varies between 2 and 4 m [*Gobler and Sañudo-Wilhelmy*, 2001]. The bay exchanges water with the Peconic Estuary through a narrow channel called West Neck Creek.

Shelter Island is a relatively simple hydrologic system as there are no significant streams, and therefore all water entering the Peconic Estuary comes from overland run-off and groundwater [*Soren*, 1978]. About half of the precipitation on Shelter Island is estimated to be lost by evaporation; the remaining 5% reaches the estuary as run-off, making groundwater the major contributor of freshwater.

Shelter Island is composed of upper Pleistocene deposits of glacial drifts consisting of clay, silt, outwash sand and gravel, cobbles and boulders [*Soren*, 1978]. These deposits constitute the Upper Glacial Aquifer, under which lays two distinct confining clay units, the Magothy aquifer, the Raritan clay and the Lloyd aquifer. Fresh groundwater is limited to the upper glacial aquifer, as revealed by exploratory drilling. The clay confining unit and the deeper aquifers contain saline water. Thickness of the upper glacial aquifer varies between 23 and 33 m at

Shelter Island. More details about the geology of the island can be found in [*Schubert*, 1998; *Soren,* 1978].

On Shelter Island, hydraulic conductivities range from 60 to 83 m/d, the average porosity is 30% and the hydraulic gradient 0.00115 [*Soren*, 1978]. The anisotropy ratio in the upper glacial aquifer on Long Island was inferred to be 10:1 from numerical modeling *[Buxton and Modica*, 1992]. The saltwater interface is located at about 15 m under sea level, as inferred from geochemical data [*Gobler and Sañudo-Wilhelmy*, 2001].

The shore around West Neck Bay is mainly composed of coarse-grained sand and gravel and has slope of 1:8 (or 7.1°) [*Paulsen et al.*, 2004]. The average salinity in the bay is approximately 26, but was approximately 31 during my study. The average tidal range is around 1.2 m but was measured to be 0.8 m during our data acquisition. Due to the shape of the bay, wave influence is negligible.

3. Methods

The intertidal zone was studied using four different techniques: stationary time-lapse electrical resistivity (ER) surveys providing 2D vertical cross-sections repeated over time, point measurements of conductivity and temperature using a Trident probe, manual and automated seepage measurements, and fluid parameter analysis using a YSI 556 multiprobe hand meter. Each method is described in the following sections; experimental setup is outlined in Figure 2.

3.1 Electrical resistivity survey acquisition and processing

Because electrical resistivity of fluids in coastal settings can vary up to six orders of magnitude, its spatial distribution provides a useful proxy for fluid mixing and dynamics underground. However, the relation between measured bulk resistivity and pore water salinity is not straightforward. The inverted resistivity of saturated sediments from field data and its spatial variation is a function of the geometry of the acquisition setting, salinity, saturation, clay content and porosity [*Olhoeft*, 1981]. The electrodes in most of the intertidal zone were located in fully saturated sediments as indicated by the observed seepage face during ebbing and low tide. Consequently, in the intertidal and subtidal zones, the changes in conductivity can be attributed solely to the electrolyte conductivity and therefore be used as a proxy for salinity [*Telford et al.*, 1990]. Higher ER would indicate relatively lower salinities due to the influx of fresh SGD

[*Swarzenski et al.*, 2007]. The electrodes of the landward portion of the survey located above the high tide mark were coupled with partially saturated sediments, but were not the focus of the present study so no computation of fluid properties were made for this portion of the transect.

ER imaging was performed using an Advanced Geosciences Inc. (AGI) SuperSting 8-channel receiver R8 resistivity meter. The SuperSting system uses a 56 electrode cable with 0.61 m electrode spacing. One preliminary stationary survey was acquired on 09/12/2012 at low tide. The cable was placed perpendicularly to the shore, 4 m northward of the pier, and independent C/T measurements were taken with the Trident probe to assess the reliability of the inversion. On 09/13/12 a 12 hour time-lapse survey was performed at the same location, with transects named A to L, during a semi-diurnal tidal cycle from high tide to the next high tide (Figure 16b). The cable was placed partially on land and partially in the water. All electrodes on land and in the intertidal zone were linked to the ground through springs attached to 0.3 m metallic stakes to ensure good coupling. A mix of swelling bentonite clay and seawater was poured on each land electrode to maximize surface contact with the ground. Exposed electrodes were wet with seawater at the beginning of each ER survey.

Measurements were made using a combination of dipole-dipole and Schlumberger configurations to optimize both vertical and lateral resolutions, and the data were stacked together for the inverse analysis. Data were analyzed using the software package EarthImager 2D [*AGI*, 2009]. Several 2-dimensional finite elements inversion methods are available: a damped least square inversion, a robust inversion that enables relatively sharp contrasts as the distribution of data errors is assumed to be exponential, and a smooth inversion, called Occam's inversion [*Constable et al.*, 1987], that assumes a Gaussian error distribution. All methods were tried; the smooth inversion was selected as it minimized the appearance of artifacts that cannot be real as they are smaller than the resolution of the survey.

Two parameters allow estimating the quality of the inversion: the room mean square error (RMSE) and the Euclidian norm (L2). Both are statistical measures of the residual difference between the inverted model and the data. Typically, a RMSE under 10 % and/or a L2<1 indicate a good fit between the inverted model and the measurements.

Water depth and fixed seawater resistivity values can strongly influence the result of the inversion [*Day-Lewis et al.*, 2006; *Henderson et al.*, 2010]. Preliminary data analysis revealed that fixing the water column resistivity prevented convergence of the model no matter which

inversion technique or initial model was used. Water resistivity was therefore not constrained in our inversion.

The land topography and bathymetry along the profiles were carefully measured using a laser station and a sonic depth sounder, respectively. Water levels were continuously monitored using a Solinst pressure logger to determine tidal depth variations for each individual transect. Inversions were performed using the average water depth measured during acquisition. A sensitivity analysis indicated that water level variation smaller than 0.25 m during data acquisition would not produce significant artifacts in the inverted section when the water resistivity is left unconstrained [*Durand et al.*, 2011]. This amplitude of variation was not attained for any of the 12 ER time-lapse surveys. For easier comparison between resistivity surveys, Trident measurements and YSI readings, the resistivity sections were converted to conductivity sections. One must also keep in mind that the inverted section represents an optimal estimation of the spatial distribution of resistivity on the vertical profile and that the solution is non-unique [*Tarantola*, 2005]. Comparing ER survey results with another method is therefore necessary to provide confidence to the ER interpretation.

3.2 Seepage meters

SGD at selected locations was quantified using an ultrasonic seepage meter, for which detailed description is available in [*Paulsen et al.*, 2001]. SGD was captured in a steel collection chamber (with a square cross section of 0.21 m^2) inserted approximately 10 cm into the sediment. The discharge was directed to a cylindrical flow tube with two piezoelectric transducers that continually generate bursts of ultrasonic signals in opposite directions (periodic waves with a frequency of 1.7 MHz). Arrival of the ultrasonic signals was continuously monitored and allows determination of the flow direction and instantaneous velocity. The meter is capable of measuring SGD at rates as low as ± 0.86 cm/d, with a sampling period as high as 5 minutes during several days.

Two ultrasonic seepage meters U1 and U2 were deployed between 9/11/12 and 9/14/12 at 19 and 23 m from the high tide mark, respectively, in alignment with the electrical resistivity surveys (Figure 16a). Measurements were taken every 5 minutes for 4 days. Two Solinst loggers were placed inside the funnels to measure SGD temperature and conductivity as well as real time tidal level with a 5 minute sampling period.

In addition, 2 manual seepage meters [*Lee*, 1977] M1 and M2 were deployed on 8/14/2012, at 4 and 7 m from the high tide mark, respectively (Figure 16a). SGD rates were measured and water samples collected for 10 hours during the time-lapse resistivity survey, to measure temperature, conductivity and salinity.

3.3 Trident probe

The Trident probe is a direct-push instrument, developed to screen and assess offshore areas where groundwater may be discharging to the surface water body [*Chadwick et al.*, 2003]. The probe integrates two temperature sensors, two electrical conductivity sensors, and two pore water samplers. The subsurface C/T probe measures the electrical conductivity and temperature of the sediments at a chosen depth, whereas the surface C/T sensors measure the electrical conductivity and temperature of the surface water above the sediment-water interface. In this study, the depth was fixed at 0.6 m below the sediment-water interface, but it represents the maximum depth attainable as sediments sometimes did not allow full penetration. The temperature sensor has a measurement range of -5 to +35 °C with an accuracy of 0.001 °C, and a resolution of 0.00025 °C.

The Trident probe was used to provide independent instantaneous measurements to ground-truth the inversion from a preliminary study, the day before the 12h time-lapse survey. Four tridents points were chosen along the survey line and the conductivities were measured at ~0.4 m depth.

3.4 Salinity measurements

Water collected from the seepage meter and the Trident pore water were analyzed for temperature, conductivity and salinity using a YSI 566 handheld multiprobe. Characterizing the actual pore water seeping through the sediment-ocean interface aid in confirming the results from the ER surveys.

Although the Solinst loggers placed in the ultrasonic seepage meters did record temperature variations, the conductivity sensors did not. It is still possible to compute SGD salinity with the Coppens equation [*Coppens*, 1981] using the instantaneous speed of sound recorded by the piezoelectric transducers, the instantaneous temperature and depths from the logger:

$$c(D,S,t) = c(0,S,t) + (16.23 + 0.253t)D + (0.213 - 0.1t)D^2$$
$$+[0.016 + 0.0002\,(S-35)](S-35)tD \qquad \text{(Equation 1)}$$

with:

$$c(0,S,t) = 1449.05 + 45.7t - 5.21t^2 + 0.23t^3 + (1.333 - 0.126t + 0.009t^2)(S-35)$$

- $t = T/10$, where T = temperature in degrees Celsius
- S = salinity in parts per thousand
- D = water depth in kilometers

This equation was developed for temperatures between 0 and 35 °C, salinities between 0 and 45, and depths between 0 and 4 km.

4. Results

4.1 Electrical resistivity surveys and Trident probe

Two methods are used to assess the reliability of the inverted sections. First, the ER section acquired on 9/10/13 is plotted against the conductivity measurements obtained with the trident probe (Figure 17), after conversion to a fluid conductivity section using a formation factor of 3.3 calculated by Paulsen et al. [2004], which is compatible with a sand porosity of 30% and a cementation factor of 1.3, typical of unconsolidated sands [*Archie*, 1942]. There is a good agreement between the two independent data sets; the Trident measurements in the intertidal zone are slightly higher than the inverted values. This could be the result of pore water temperature variations measured by the Trident but ignored by the ER survey, or an artifact of the level of detail created by the interpolation technique used to plot the inverted section. A perfect match is not expected due to the nature of the comparison; agreement within an order of magnitude is satisfactory.

Another method of estimating the reliability of the inversion is to compare the results obtained for different initial conditions [*Oldenburg and Li*, 1999]. Inversions were performed with three initial models to compare the stability of the inversion (Figure 18). The RMSE and L2 values were 7.79% and 0.59, 16.57% and 0.52 and 8.13% and 0.58 for the pseudosection, the average apparent resistivity and the custom resistivity, respectively. The overall results are consistent between methods and do not show any excessive difference at high depths, which

indicates that the inversion is stable over the whole thickness of the section [*Oldenburg and Li*, 1999]. The amount and position of resistive and conductive features are similar, however, the absolute resistivity values vary between methods. This shows that, for this setting, resistivity can be used to image contrasts and changes in subsurface resistivity but is not the most appropriate tool to give an accurate estimate of salinity distribution. However, the use of the apparent resistivity pseudosection as an initial model creates high frequency artifacts after inversion visible on Figure 18(a) for $15 < x < 27$ m. This inversion seems more sensitive to the noise in the data and was therefore not used further on. The overall RMS and L2 values of the inversion with the average apparent resistivity model were lower and this method was therefore chosen for the time-lapse inversion. In spite of the care taken to ensure the minimum amount of noise during acquisition, all sections had to be filtered and about 20% of all data sets were removed.

The results of the 12 time lapse ER surveys conducted during a semi-diurnal tidal cycle are shown in (Figure 19 and Figure 20). Previous studies suggest that the aquifer is not homogeneous in this area and suggested the presence of a confining unit [*Stieglitz et al.*, 2007] or clay lens [*Paulsen et al.*, 2004]. Interpretation of bulk conductivity measurements in term of pore fluid composition must therefore be done with caution. However, lithology and porosity are constant over time and therefore comparing transects at different times still provides information about the pore fluid composition.

At high tide, on transect A, a low conductivity sub-horizontal cell is observed originating from land and extending to almost 20 m in the horizontal direction and down to $z \sim -2$ m depth (Figure 19). A layer of approximately 1 m thickness with high conductivity is observed from the high tide mark to the end of the profile. At depth, for $x \sim 32$ m a region of intermediate conductivities is observed extending from the surface to $z \sim -5$ m. This could be part of the mixing zone formed by the saltwater wedge or just an edge-effect, an artifact of the inversion. Profile B is very similar to profile A, with the development of a low conductivity feature at $x \sim 25$ m and $-6 < z < -4$ m. This feature does not persist on the following sections but reappears more clearly before the next high tide stage on sections I and J. On profile C, the resistivity cell seems less visible and fingering of intermediate conductivities develops in the middle of the section. In D, the resistive cell is in contact with the top of the sediments close to the high tide mark, at $x \sim 10$ m; fingering is amplified. On transect E, the resistive cell looks more continuous and the portion in contact with the sediment interface is growing. A superficial mixing cell forms

landward of the contact point with the sediments. Some high frequency features appear between x = 15 and x = 20 m which are the results of noise in the inversion due to the rapid change in water level. Part of the fingering appears sub horizontal at about -2 m depth. This could be an artifact due to the low conductivity of the feature above preventing adequate penetration of the signal, but the low underlying resistivity contradicts this interpretation. The land resistive structure is now developing a tube-like feature at depth under 4 m that reaches as far as 23 m. The low tide profile F (Figure 20) confirms the structure shown in E. The resistive cell in contact with the sediment interface is becoming wider, almost reaching the low tide mark. In G, the resistive cell reaches its maximum extent, between x = 0 and x = 26m. The superficial mixing cell widens as the tide retreats, but its depth remains very limited. The sub horizontal conductive structure persists until transect J, before the next high tide. This structure could be the results of partially confining clay until described by *Stieglitz et al.* [2008b]; however, the fact that the structure disappears at high tide rules out the presence of the clay unit(DOI index > depth of structure). The tube like portion of the resistive cell appears to move vertically on transect J, at x~25 m, but does not reach the surface. The two parts of the resistivity cell on transect J surround a more conductive structure, which resembles the model from *Robinson et al.* [2006] with a freshwater tube and the upper saline plume. However, the structure is not permanent as simulated by *Robinson et al.* [2006]. High tide profiles K and L look like the initial high tide transect A. The ER sections reveal dynamic flow patterns in the intertidal and subtidal zones, as observed by *Befus et al.* [2013].

Published numerical simulations present salinity distributions that are averaged over a tidal cycle [*Gibbes et al.*, 2007; *Robinson et al.*, 2006; *Robinson et al.*, 2007a; *Robinson et al.*, 2007b]. For comparison, I computed the tidal average of all sections (Figure 21c), a high tide average using the profile A, B and L (Figure 21a) and a low tide average using the profiles F, G and H (Figure 21b). The tidal average looks like the high-tide end-member (Figure 21a), which significantly differs from the numerical predictions. The low-tide end-members (Figure 21b) is closer to the numerical predictions with three zones: a superficial mixing cell centered about the high tide mark $5 < x < 10$ m and $0 < z < 1$ m, a resistive cell originating from land and exiting at the sediment interface in the intertidal zone and finally a diagonally oriented zone with intermediate conductivities that could resemble the upper saline plume, the freshwater discharge tube and the saltwater wedge, respectively, as described in [*Gibbes et al.*, 2007; *Robinson et al.*,

2006; *Robinson et al.*, 2007a; *Robinson et al.*, 2007b]. There are, however, some discrepancies in shape and position of these features between the observations and the model results, as discussed in section 5.

The high-tide end-member indicates a strong freshwater signal from land, but the resistive cell is sub horizontal and extends at depth a couple of meters beyond the low tide mark. The cell does not reach the sediment interface. The freshwater signal persisted over time and was visible at low tide, but seems to be in direct contact with the sediment surface. The zone of contact imaged on the ER sections coincided with a freshwater seepage face identified by rivulets at the surface [*O'Rourke*, 2000], and included the locations of both manual seepage meters. Salinity of water from the seepage face was measured at 0.2.

4.2 SGD in the intertidal zone: manual seepage meters

Specific discharge measured with the manual seepage meters are presented in Figure 22. Seepage rates were very high, varying from 40 to 145 cm/d with an average of 93 cm/d for M1, and varying from 12 to 74 cm/d with an average of 38 cm/d for M2 during the period recorded. Unfortunately, it is not possible to obtain continuous SGD measurements at the intertidal zone, as the seepage meters cannot record data if the water column thickness is insufficient for the bag to float or if the meter is exposed, as shown by the gap in data around low tide. SGD in seepage meter M1 did not exhibit a clear trend relative to the tide; M2 showed higher SGD rates around low tide. In both meters, salinity measurements indicate a progressive freshening from high tide to low tide with initial salinities equal to that of the bay at 33. After the gap in data, salinities in the collection bags average 2 and 7 in A and B, respectively. In seepage meter A, there was a progressive increase in salinity with flooding tide, starting at 0.62 after low tide to 5.2 before high tide. In seepage meter B, the salinity was 6.66 after low tide and increased slightly to 7.2 before high tide.

Conservation of mass in the seepage meter can be described as follow:

$$m_{SM}^{t+1} = m_{SM}^{t} + m_{input}^{t+1} - m_{output}^{t+1} \qquad \text{(Equation 1)}$$

With m_{SM}^{t+1} and m_{SM}^{t} the mass of salt contained in the manual seepage meter at time *t+1* and *t*, respectively; m_{input}^{t+1} the mass of salt entering the seepage meter through SGD at time *t+1*, and m_{output}^{t+1} the mass of salt exiting the seepage meter via the collection bag at time *t+1*.

We have $m = SV$, with m the mass of salt (g), S the salinity (g/L) and V the volume (L). Under the hypothesis of an incompressible fluid, we have $V_{input}^{t} = V_{output}^{t} = V_{bag}^{t}$ and Equation 1 becomes:

$$S_{SM}^{t+1}V_{SM} = S_{SM}^{t}V_{SM} + (S_{input}^{t+1} - S_{output}^{t+1})V_{bag}^{t+1} \qquad \text{(Equation 2)}$$

If we assume that there is full mixing in the seepage meter and that the salinity in the bag is equal to the salinity in the seepage meter, i.e. $S_{output}^{t+1} = S_{SM}^{t+1}$ then we can rearrange equation 2 into equation 3:

$$S_{input}^{t+1} = \frac{S_{ouput}^{t+1}\left(V_{bag}^{t+1}+V_{SM}\right)-S_{SM}^{t}V_{SM}}{V_{bag}^{t+1}} \qquad \text{(Equation 3)}$$

All quantities on the right-hand side of the equation were measured and it is therefore possible to remove the artifact due to the dilution of surface water trapped during the seepage meter installation and to compute the salinity of SGD (Figure 23b). Assuming conservative mixing, a freshwater salinity of 0.1 (Jonathan Wanlass, pers. comm.) and a surface water salinity of 33, measured by a YSI probe, it is possible to estimate the percentage of freshwater contained in SGD and in the collection bag (Figure 23).

For both seepage meters, the initial salinity measured in the collection bags is close to the bay, 31, which corresponds to almost 98% of seawater. As the water level decreases, so does the salinity. The rates of freshening are very similar for both seepage but after low tide the percentage of freshwater is approximately 98 % in seepage meter A versus 80% in B. The decrease in freshwater content observed in seepage meter A is absent in B.

The computation of SGD salinity and freshwater content according to equation 3 are presented in Figure 23b. Computed SGD salinities in A are close to 20 corresponding to 66% of freshwater and decrease slowly towards low tide. After low tide, SGD salinity is approximately 10 and increases quickly. High-frequency oscillations are visible before low tide and are even stronger after low tide. Some computed salinities for A and SGD salinities for B are negative which is unreliable. Possible explanations for these observations are presented in the discussion, section 5b.

4.3 SGD in the subtidal zone: ultrasonic seepage meters

Ultrasonic seepage meter (USM) U1, located at 19 m form the high tide mark, recorded both positive and negative fluxes that correspond to discharge and seawater infiltration,

respectively. SGD varies between -80 and 28 cm/d with an average of -7 cm/d and a clear correlation with the tide is visible, as observed in previous studies [*Anonymous*, 2002; *Paulsen et al.*, 2004; *Taniguchi*, 2002]. A peak in tide is followed by strong seawater infiltration and a low tide is followed by a positive discharge. An observed delay of ~ 1h has been previously characterized by P*aulsen et al.* [2004]. Salinities computed using Coppens equation [*Coppens*, 1981] are approximately 12 with variation less than 1. This indicates a 60% freshwater content using the bay water and the well water as salinity end-members. The minimum salinity values were attained during rising tide when positive SGD reached its maximum. A diurnal signal is clearly visible on the salinity curve. The peaks coincide with the warmer air temperatures between 9 am and 6 pm and reveal the influence of temperature on the salinity computation (equation 1).

USM U2, located at 23 m from the high tide mark, did not measure any discharge from the sediments to the ocean but only seawater infiltration as indicated by the strictly negative values. SGD varies between -20 and -9 cm/d with an average of -13 cm/d. There is no correlation with the diurnal tidal signal marking the horizontal limit of the zone of tidal influence. Salinity is high and similar to that of the bay. Diurnal peaks in salinity occur between 12 PM and 8 PM, which is later than U1. The delay is probably due to the thicker water column above U2 that delays the propagation of the heat signal.

The salinities differences measured in U1 and U2 are in good agreement with the pore water composition inferred from the resistivity section. The constant negative discharge in U2 correlates with the position of higher conductivity features extending at depth, on the seaward end of the profiles. The agreement between both data sets indicate that this feature is not an edge-effect of the inversion, but is most likely the density driven circulation cell termed the salt-water wedge [*Kohout*, 1960]. The density-driven circulation cell appears closer to land than previously observed with bulk conductivity profiles at x ~ 45 m from the mean tide mark [*Paulsen et al.*, 2004].

5. Discussion

5.1 Comparison with other studies: SGD rates

A summary of SGD estimates in West Neck Bay is presented in Table 2. No measurements were previously done in the intertidal zone but our values from the manual

seepage meters are in remarkable agreement with the ones performed by *Paulsen et al.* [2004] in the subtidal zone. Values recorded by the ultrasonic seepage meter 19 m offshore of the high tide mark are in good agreement with all other methods. I observed a decay in SGD rate with increasing distance from the shore, and a negative correlation between SGD and tidal level, in agreement with all previous observations [*Anonymous*, 2002].

My study, however, is the only one which recorded negative seepage values offshore, indicating seawater intrusion. All experiments for the SCOR project were made in spring when precipitations rates are high (35.3 cm cumulated from March-May 2002) and evapotranspiration has not reached its peak yet whereas our data were acquired in fall (12.2 cm cumulated from July to September 2012). The inland hydraulic gradient is relatively smaller during the fall season and as suggested by numerical simulations, position of the freshwater-seawater interface varies seasonally [*Michael et al.*, 2005], which is in agreement with the location of the saltwater wedge on our ER survey results.

As mentioned in [*Stieglitz et al.*, 2008b; *Stieglitz et al.*, 2007] such high SGD rates are unusual in an unconfined aquifer and could be indicative of a confined or partially confined aquifer.

5.2 Interpretation of SGD composition

The similar salinities measured in manual SM A and B at the beginning of the experiment are significantly different from the salinities measured after low tide, in spite of nearly identical freshening rates during ebbing tide. This suggests that the salinity variations in the seepage chambers could be mostly due to the progressive dilution of seawater trapped during installation. The lack of symmetry between salinities recorded at both high tide stages also point in this direction. If a full seepage meter volume, i.e. 39 L, were to be pushed into the sediments during installation, this volume would only be completely flushed after 6 h in A and 12 h in B thus invalidating most of the salinity measurements. The manual seepage meters used are each equipped with a 10 cm diameter rubber plug that is installed only after the chamber is inserted into the sediments, in order to minimize the amount of seawater that can be trapped. The almost constant salinities observed in the collection bag from B after only 6 h indicate that this scenario is unlikely and show that, at least the salinities measured after low tide are not affected by the dilution effect. The lack of symmetry between salinity can be a consequence of the incomplete

sampling time; we did not capture a full tidal cycle but 9.5 hours, if we exclude the first bag due to seepage meter equilibration. If the rate of salinity increase observed in A during flooding tide is constant, salinity would increase by 24 and reach 29, i.e. a freshwater content of 12% at the end of the 12 hours; seepage meter B salinity would remain constant at 8 or 78% freshwater. The increase in seawater content observed in A after low tide is much faster than the freshening observed during ebbing tide. The beach saturates more easily than it drains, which is due to the slope of the beach and the asymmetrical transient response of the inland hydraulic head to the tidal stimulation, as predicted by an analytical model [*Turner et al.*, 1997] and previously observed at this site [*Paulsen et al.*, 2004].

An attempt to derive SGD salinity and composition over time, using manual seepage meters in the intertidal zone, yielded results that were not consistently interpretable. This indicates that some of the assumptions made for the calculations were not justified. One assumption was that the fluid was incompressible. Even if this is not entirely accurate, the compressibility of water cannot account for the magnitude of errors observed. A second hypothesis is that water in the seepage chamber is well mixed and that salinity measured in the bag at a given moment is representative of the salinity inside the seepage meter at the same moment. In spite of the density difference between fresh and sea waters, it is very unlikely that any significant salinity layering could develop in such a small volume and short amount of time. The last assumption states that the volume of SGD entering the seepage meter is equal to the one collected in the bag. This can only be true if the flow is unidirectional. Prefilling the bags can allow for groundwater recharge but is not recommended if water quality analyses are performed [*Libelo and MacIntyre*, 1994; *Shaw and Prepas*, 1989]. We did not prefill the bags to avoid introducing external water in the system and could therefore only record positive SGD. As the bag volume is directly used in equation 3, it appears that unrecorded bidirectional exchanges of flow and solutes within the seepage meters are responsible for the negative calculated salinity values and complicate estimates of SGD composition.

West Neck Bay is a relatively wave-free environment. Hydraulic head oscillations attenuate very rapidly at this site, a 90 % decay was observed between wells situated approximately 50 m apart for a 12 hour period signal [*Paulsen et al.*, 2004], hence higher frequencies should attenuate even faster. The high-frequency oscillations observed in the

computed SGD salinities are not therefore not the results of waves and are most likely an artifact of the bidirectional fluxes not accounted for in the calculations.

5.3 Impact of sediment heterogeneities on SGD

The ER cable was installed 4 m north of the jetty present at our site to avoid the disturbance created by the perforation of a suspected but unconfirmed confining layer [*Stieglitz et al.*, 2007]. The seepage meters were placed 1 m north of the ER cable. The very high seepage rates measured in the intertidal zone are similar to previous peak values obtained close to the pier [*Paulsen et al.*, 2004], and these high rates are consistent between spring and fall which is consistent with the existence of a confining layer. However, the inferred depth of the confining layer varied between 0.2 and 0.5 m which is deeper than the penetrating depth of the manual SM of ~ 0.10 m. Surface bulk conductivities did not indicate any interruption in the confining layer close to the shore [*Paulsen et al.*, 2004]. If the layer restricts the vertical water exchanges, the water collected in the intertidal zone might therefore come from lateral fluxes from the jetty, which disagrees with the surface bulk conductivities suggesting that the influence of the jetty extended farther laterally than previously thought. Yet, discharge rate predictions using an analytical model for an unconfined anisotropic aquifer [*Rumer and Shiau*, 1968] were in agreement with the observations even if tidal forcing was not accounted for [*Paulsen et al.*, 2004].

Surface bulk conductivity measurements in the subtidal zone indicated that the position of the superficial mixing zone did not vary significantly between high and low tide [*Stieglitz et al.*, 2008b], which is in agreement with the results from our time-lapse ER survey.

5.4 Interpretation of ER time-lapse survey

In spite of some inherent limitations of the electrical resistivity method, our data suggest a partial agreement with current numerical models developed for a homogeneous isotropic aquifer [*Robinson et al.*, 2006] and field measurements in unconfined sandy aquifers [*Gibbes et al.*, 2008b]. At low tide, 3 regions similar to the ones predicted by simulations, i.e. an upper saline plume, freshwater tube and saltwater wedge are observed. However, there are some discrepancies: our low tide end-member conductivity section resembles the published model, however, a 12 hr. phase-average does not and is more similar to our high-tide end-member. The

shape and position of the FSI in the intertidal zone differ from the model. The intertidal shallow mixing zone and the freshwater discharge area appear to be mobile. Several factors can explain the apparent discrepancies between our data and the model: the curvature of the shoreline is known to focus flow, the anisotropy and sediment heterogeneity of the aquifer, and 3D geometric complexity due to the presence of the jetty.

Vertical movements of the fresh water discharge zone suggested by the ER sections are in agreement with the salinity variations recorded in the manual seepage meters. The ER results, however, do not confirm the presence of a confining unit as described by [*Stieglitz et al.*, 2007]. In theory, clay formations are less resistive due to strong surface conduction [*Archie*, 1942; *Revil*, 1998]. However, in coastal settings it is likely that conductivity occurs mostly in the porous medium saturated with saline water. Furthermore, to be imaged by the ER survey a feature needs a minimum contrast of 20 % between its resistivity and the surroundings, and its dimensions must be larger than at least on spacing between electrodes, 0.6 m in our case. It is therefore possible that the confining unit cannot be resolved by the ER survey. Nevertheless, even if that layer is invisible on the cross-sections it should be possible to observe its hydrological effects. Temporal variations in conductivity distribution down to 6 m below grade do not seem to indicate any segregation between an upper and a lower portion of the aquifer. Sub-horizontal movements do not appear to be favored by other factors than aquifer anisotropy and no horizontal feature is sufficiently consistent over time to be interpreted as a structure in the sediments. A confining unit thicker than 6 m would prevent SGD as high as measured.

6. Conclusion

The geophysical techniques used in this study did not find definitive evidence of the existence of a confining unit as previously suggested; however, my data do not completely rule out its presence either. High SGD rates found in the intertidal zone are in favor a partially confined aquifer; however, the dynamic conductivity distribution at depth disagrees with the presence of a continuous low permeability unit at depth. Core measurements are necessary to determine the hydrogeological setting at this location. Numerical models for homogeneous isotropic straight-beach aquifer cannot predict the observations, revealing the need for anisotropic and heterogeneous models. This would enable us to better characterize flow and

solute transport that determine the biogeochemical reactions occurring in the subterranean estuary and impact chemical fluxes associated with SGD.

References

AGI (2009), Instruction Manual for EarthImager 2D, Version 2.4.0, Resistivity and IP Iversion Software, Austin, Texas, *Report.*

Anonymous (2002), Submarine Groundwater discharge assessment intercomparison experiment, , International Hydrological Program (IHP), Scientific Commitee on Oceanic Research (SCOR), Land Ocean Interactions in the Coastal Zone (LOICZ), *Report*, 26 pp.

Archie, G. (1942), The electrical resistivity log as an aid in determining some reservoir characteristics, *Trans. AIME*, *146*(99), 54-62.

Ataie-Ashtiani, B., R. Volker, and D. Lockington (1999), Tidal effects on sea water intrusion in unconfined aquifers, *Journal of Hydrology*, *216*(1-2), 17-31.

Beck, A. J., Y. Tsukamoto, A. Tovar-Sanchez, M. Huerta-Diaz, H. J. Bokuniewicz, and S. A. Sañudo-Wilhelmy (2007b), Importance of geochemical transformations in determining submarine groundwater discharge-derived trace metal and nutrient fluxes, *Applied Geochemistry*, *22*(2), 477-490.

Befus, K. M., M. B. Cardenas, D. V. Erler, I. R. Santos, and B. D. Eyre (2013), Heat transport dynamics at a sandy intertidal zone, *Water Resources Research*, *49*(6), 3770-3786.

Bokuniewicz, H. (1980), Groundwater seepage into Great South Bay, New York, *Estuarine and Coastal Marine Science*, *10*(4), 437-444.

Burnett, W. C., H. Bokuniewicz, M. Huettel, W. S. Moore, and M. Taniguchi (2003), Groundwater and pore water inputs to the coastal zone, *Biogeochemistry*, *66*(1-2), 3-33.

Burnett, W. C., et al. (2006), Quantifying submarine groundwater discharge in the coastal zone via multiple methods, *Science of the Total Environment*, *367*(2-3), 498-543.

Buxton, H. T., and E. Modica (1992), Patterns and rates of ground-water movement on Long Island, New York, *Ground Water*, *V. 30*(No. 6), p. 857-866.

Chadwick, D. B., A. Gordon, J. Groves, C. Smith, R. Paulsen, and B. Harre (2003), New tools for monitoring coastal contaminant migration, *Sea technology*, *44*(6), 17-22.

Constable, S. C., R. L. Parker, and C. G. Constable (1987), Occam's inversion: A practical algorithm for generating smooth models from electromagnetic sounding data, *Geophysics*, *52*(3), 289-300.

Coppens, A. B. (1981), Simple equations for the speed of sound in Neptunian waters, *The Journal of the Acoustical Society of America*, *69*(3), 862-863.

Day-Lewis, F., E. White, C. Johnson, J. Lane Jr, and M. Belaval (2006), Continuous resistivity profiling to delineate submarine groundwater discharge--examples and limitations, *The Leading Edge*, *25*(6), 724.

Dulaiova, H., W. C. Burnett, J. P. Chanton, W. S. Moore, H. Bokuniewicz, M. A. Charette, and E. Sholkovitz (2006), Assessment of groundwater discharges into West Neck Bay, New York, via natural tracers, *Continental Shelf Research*, *26*(16), 1971-1983.

Durand, J. M., J. Wanlass, N. Stark, R. Paulsen, and T.-f. Wong (2011), Study of submarine groundwater discharge on the west shore of Forge River using electrical resistivivty measurements and seepage meters, paper presented at Geology of Long Island and Metropolitan New York, 18th proceedings, Stony Brook, NY, USA, April 9th 2011.

Gibbes, B., C. Robinson, L. Li, and D. Lockington (2007), Measurement of hydrodynamics and pore water chemistry in intertidal groundwater systems, *Journal of Coastal Research, SI*, *50*, 884-894.

Gibbes, B., C. Robinson, H. Carey, L. Li, and D. Lockington (2008b), Tidally driven pore water exchange in offshore intertidal sandbanks: Part I. Field measurements, *Estuarine, Coastal and Shelf Science*, *79*(1), 121-132.

Glover, R. (1959), The pattern of fresh-water flow in a coastal aquifer, *Journal of Geophysical Research*, *64*(4), 457-459.

Gobler, C. J., and S. A. Sañudo-Wilhelmy (2001), Temporal variability of groundwater seepage and brown tide blooms in a Long Island embayment, *Marine Ecology Progress Series*, *217*, 299-309.

Henderson, R. D., F. D. Day-Lewis, E. Abarca, C. F. Harvey, H. N. Karam, L. B. Liu, and J. W. Lane (2010), Marine electrical resistivity imaging of submarine groundwater discharge: sensitivity analysis and application in Waquoit Bay, Massachusetts, USA, *Hydrogeology Journal*, *18*(1), 173-185.

Johannes, R. (1980), Ecological significance of the submarine discharge of groundwater, *MARINE ECOL.- PROG. SER.*, *3*(4), 365-373.

Johnson, A. G., C. R. Glenn, W. C. Burnett, R. N. Peterson, and P. G. Lucey (2008), Aerial infrared imaging reveals large nutrient-rich groundwater inputs to the ocean, *Geophysical Research Letters*, *35*(15), L15606.

Kohout, F. (1960), Cyclic flow of salt water in the Biscayne aquifer of southeastern Florida, *Journal of Geophysical Research*, *65*(7), 2133-2141.

Kuan, W. K., G. Jin, P. Xin, C. Robinson, B. Gibbes, and L. Li (2012), Tidal influence on seawater intrusion in unconfined coastal aquifers, *Water Resources Research*, *48*(2), W02502.

Lee, D. R. (1977), A device for measuring seepage flux in lakes and estuaries, *Limnology and Oceanography*, 140-147.

Li, L., D. Barry, F. Stagnitti, and J. Parlange (1999), Submarine groundwater discharge and associated chemical input to a coastal sea, *Water Resources Research*, *35*(11), 3253-3259.

Libelo, E. L., and W. G. MacIntyre (1994), Effects of surface-water movement on seepage-meter measurements of flow through the sediment-water interface, *Applied Hydrogeology*, *2*(4), 49-54.

Michael, H. A., J. S. Lubetsky, and C. F. Harvey (2003), Characterizing submarine groundwater discharge: A seepage meter study in Waquoit Bay, Massachusetts, *Geophys. Res. Lett*, *30*(6), 1297.

Michael, H. A., A. E. Mulligan, and C. F. Harvey (2005), Seasonal oscillations in water exchange between aquifers and the coastal ocean, *Nature*, *436*(7054), 1145-1148.

Moore, W. S. (1999), The subterranean estuary: a reaction zone of ground water and sea water, *Marine Chemistry*, *65*(1), 111-125.

Moore, W. S., and T. J. Shaw (1998), Chemical signals from submarine fluid advection onto the continental shelf, *Journal of Geophysical Research: Oceans (1978–2012)*, *103*(C10), 21543-21552.

O'Rourke, D. (2000), Quantifying specific discharge into West Neck Bay, Shelter Island, New York using a three-dimensional finite-difference groundwater flow model and continuous measurements with an ultrasonic seepage meter, 88 pp, State University of New York, Stony Brook.

O'Rourke, D., P. R., and W. T-f. (1999), Measuring Submarine Groundwater Seepage Using an Ultrasonic Flow meter and the "Drum Method"- A Comparative study, in *Geology of Long Island and Metropolitan New York*, edited, Stony Brook, NY, USA.

Oldenburg, D. W., and Y. Li (1999), Estimating depth of investigation in dc resistivity and IP surveys, *Geophysics*, *64*(2), 403-416.

Olhoeft, G. (1981), Electrical properties of rocks, *Physical properties of rocks and minerals*, *2*, 298-305.

Paulsen, R., C. Smith, and T.-f. Wong (1998), Defining freshwater outcrops in West Neck Bay, Shelter Island, New York using direct contact resistivity measurements and transient underflow measurements, paper presented at Geology of Long Island and Metropolitan New York, Stony Brook, NY, USA, April, 18th 1998.

Paulsen, R. J., C. F. Smith, D. O'Rourke, and T. F. Wong (2001), Development and evaluation of an ultrasonic ground water seepage meter, *Ground Water*, *39*(6), 904-911.

Paulsen, R. J., D. O'Rourke, C. F. Smith, and T. F. Wong (2004), Tidal Load and Salt Water Influences on Submarine Ground Water Discharge, *Ground Water*, *42*(7), 990-999.

Revil, A. (1998), Nature of surface electrical conductivity in natural sands, sandstones, and clays, *Geophys Res Lett*, *25*(5), 691-694.

Robinson, C., B. Gibbes, and L. Li (2006), Driving mechanisms for groundwater flow and salt transport in a subterranean estuary, *Geophys. Res. Lett*, *33*, L03402.

Robinson, C., L. Li, and H. Prommer (2007a), Tide-induced recirculation across the aquifer-ocean interface, *Water Resources Research*, *43*(7), W07428.

Robinson, C., L. Li, and D. Barry (2007b), Effect of tidal forcing on a subterranean estuary, *Advances in Water Resources*, *30*(4), 851-865.

Robinson, C., B. Gibbes, H. Carey, and L. Li (2007c), Salt-freshwater dynamics in a subterranean estuary over a spring-neap tidal cycle, *Journal of Geophysical Research*, *112*(C9), C09007.

Rumer, R. R., and J. Shiau (1968), Salt water interface in a layered coastal aquifer, *Water Resources Research*, *4*(6), 1235-1247.

Russoniello, C. J., C. Fernandez, J. F. Bratton, J. F. Banaszak, D. E. Krantz, A. S. Andres, L. F. Konikow, and H. A. Michael (2013), Geologic effects on groundwater salinity and discharge into an estuary, *Journal of Hydrology*, *498*, 1-12.

Schubert, C. E. (1998), Areas contributing ground water to the Peconic estuary, and ground-water budgets for the North and South forks and Shelter Island, Eastern Suffolk County, New York.

Shaw, R., and E. Prepas (1989), Anomalous, short-term influx of water into seepage meters, *Limnology and Oceanography*, *34*(7), 1343-1351.

Sholkovitz, E., C. Herbold, and M. Charette (2003), An automated dye-dilution based seepage meter for the time-series measurement of submarine groundwater discharge, *Limnol. Oceanogr. Methods*, *1*, 16-28.

Soren, J. (1978), Hydrogeologic conditions in the town of Shelter Island, Suffolk County, Long Island, New York., *Water-Resources Investigation Report Rep. 77-77*, U. S. Geological Survey.

Stieglitz, T., J. Rapaglia, and H. Bokuniewicz (2008b), Estimation of submarine groundwater discharge from bulk ground electrical conductivity measurements, *Journal of Geophysical Research*, *113*(C8), C08007.

Stieglitz, T. C., J. Rapaglia, and S. C. Krupa (2007), An effect of pier pilings on nearshore submarine groundwater discharge from a (partially) confined aquifer, *Estuaries and coasts*, *30*(3), 543-550.

Swarzenski, P. W., F. W. Simonds, A. J. Paulson, S. Kruse, and C. Reich (2007), Geochemical and geophysical examination of submarine groundwater discharge and associated

nutrient loading estimates into Lynch Cove, Hood Canal, WA, *Environmental Science & Technology*, *41*(20), 7022-7029.

Taniguchi, M. (2002), Tidal effects on submarine groundwater discharge into the ocean, *Geophysical Research Letters*, *29*(12).

Tarantola, A. (2005), *Inverse problem theory and methods for model parameter estimation*, siam.

Telford, W. M., L. Geldart, and R. E. Sheriff (1990), *Applied geophysics*, Cambridge Univ Pr.

Turner, I. L., B. P. Coates, and R. I. Acworth (1997), Tides, waves and the super-elevation of groundwater at the coast, *Journal of Coastal Research*, 46-60.

VALIELA, I., and C. DELIA (1990), Special issue-groundwater inputs to coastal waters-introduction, edited, Kluwer Academic Publ Spuiboulevard 50, PO Box 17, 3300 AA Dordrecht, Netherlands.

Zektser, I. S., L. G. Everett, and R. G. Dzhamalov (2006), *Submarine groundwater*, CRC Press Inc.

Tables

Table 2. Comparison of SGD measurements in West Neck Bay from different studies.

Study	Method	Distance from high tide mark (m)	SGD range (cm/d)
Present	Manual seepage meter	4	12 to 73
		7	40 to 145
	Ultrasonic seepage meter	19	-80 to 28
		23	-20 to -9
[*Dulaiova et al.*, 2006]	Radon	20 m from the shoreline	0 to 34
	Radium		15
[*Sholkovitz et al.*, 2003]	Dye (WHOI) seepage meter	Close to the shore	2 to 30
		Offshore	2 to 8
[*O'Rourke et al.*, 1999]	Ultrasonic and manual	-	29 to 40
[*Paulsen et al.*, 2004]	Ultrasonic	10	14 to 168
[*Taniguchi et al.*, 2002]	Heat pulse	50	4 to 11

Figures and captions

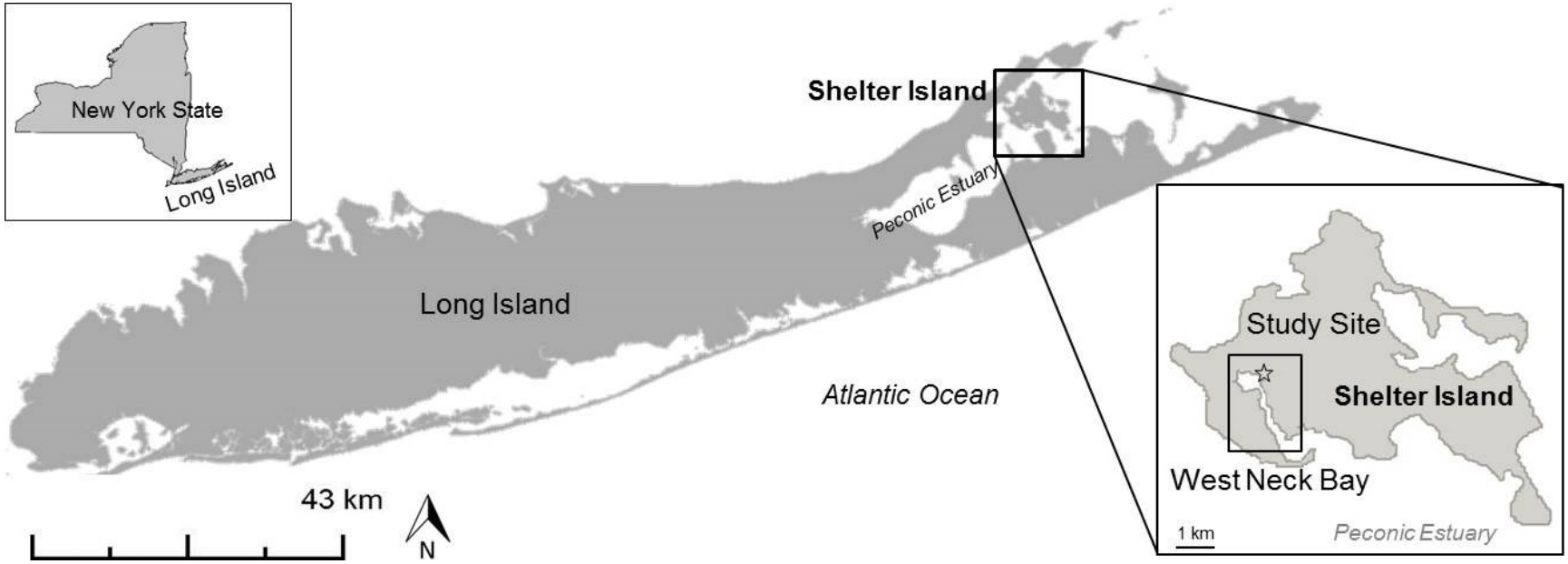

Figure 15. Location map of Shelter Island and position of study site.

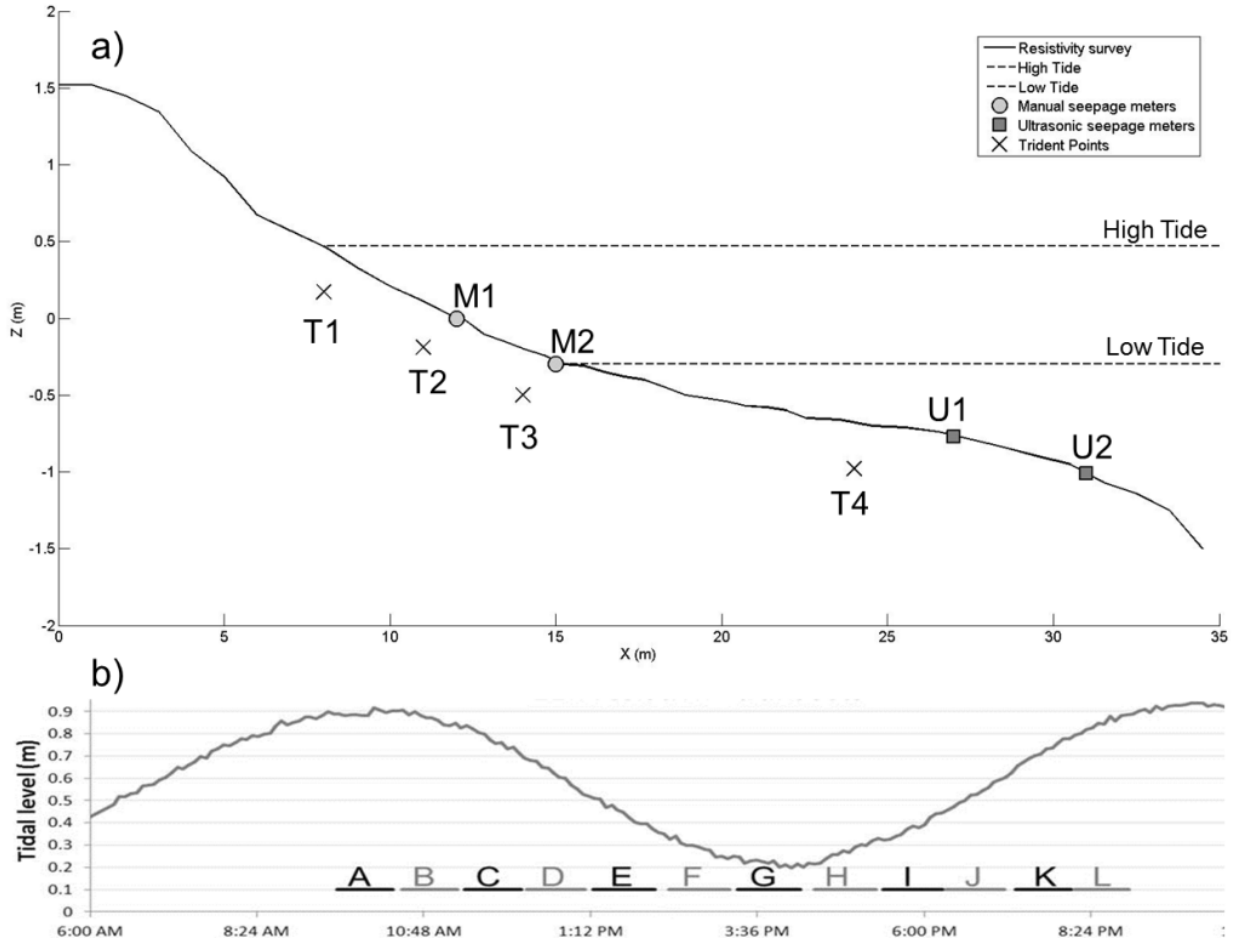

Figure 16. Experimental setting in West Neck Bay. (a) Relative positions of data sampling locations. The position of the first electrode is taken as origin of the framework. (b) Time-lapse ER surveys and associated tidal level.

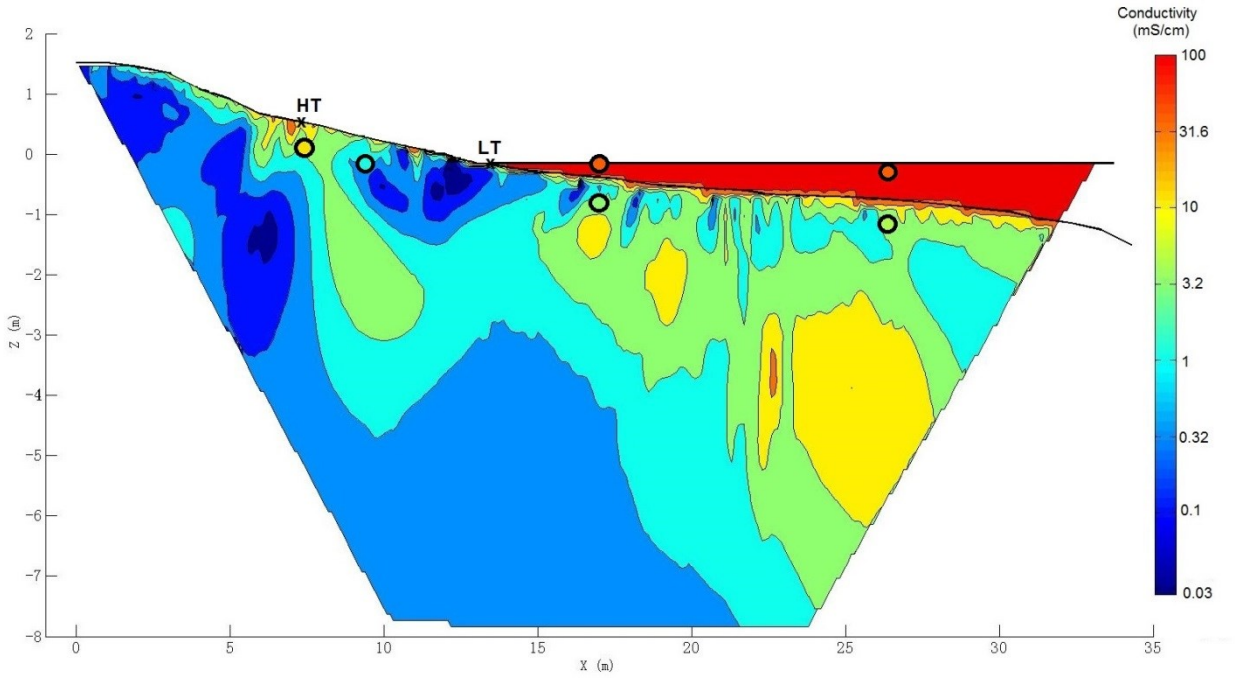

Figure 17. Comparison between the inverted conductivity section and the Trident probe conductivity measurements (filled in circles). The resistivity cable is shown as a solid black line. The black crosses indicate the position of the high tide (HT) and low tide (LT) marks. Conductivities are plotted on a log scale.

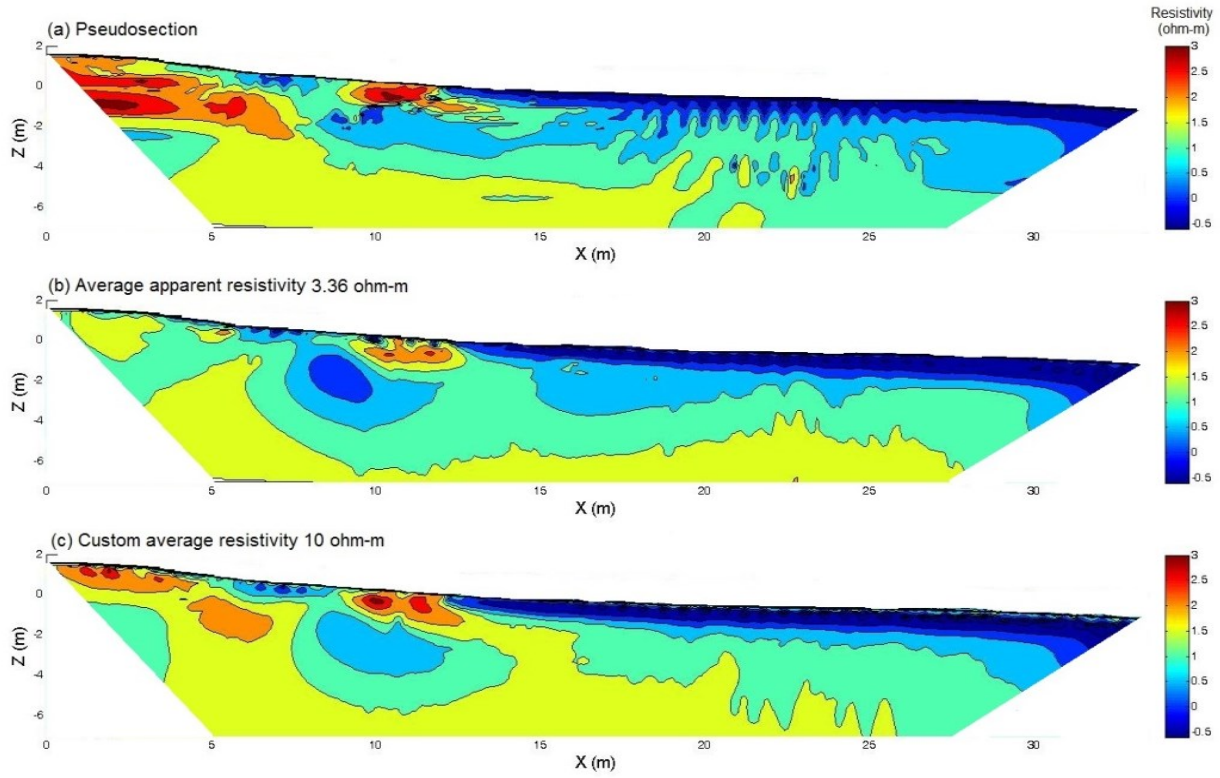

Figure 18. Comparison of inverted resistivity sections obtained from 3 different initial models: the apparent resistivity pseudosection (a), the average apparent resistivity homogeneous model (b) and a custom homogeneous resistivity model (c). Resistivities, in ohm-m, are plotted on a log scale.

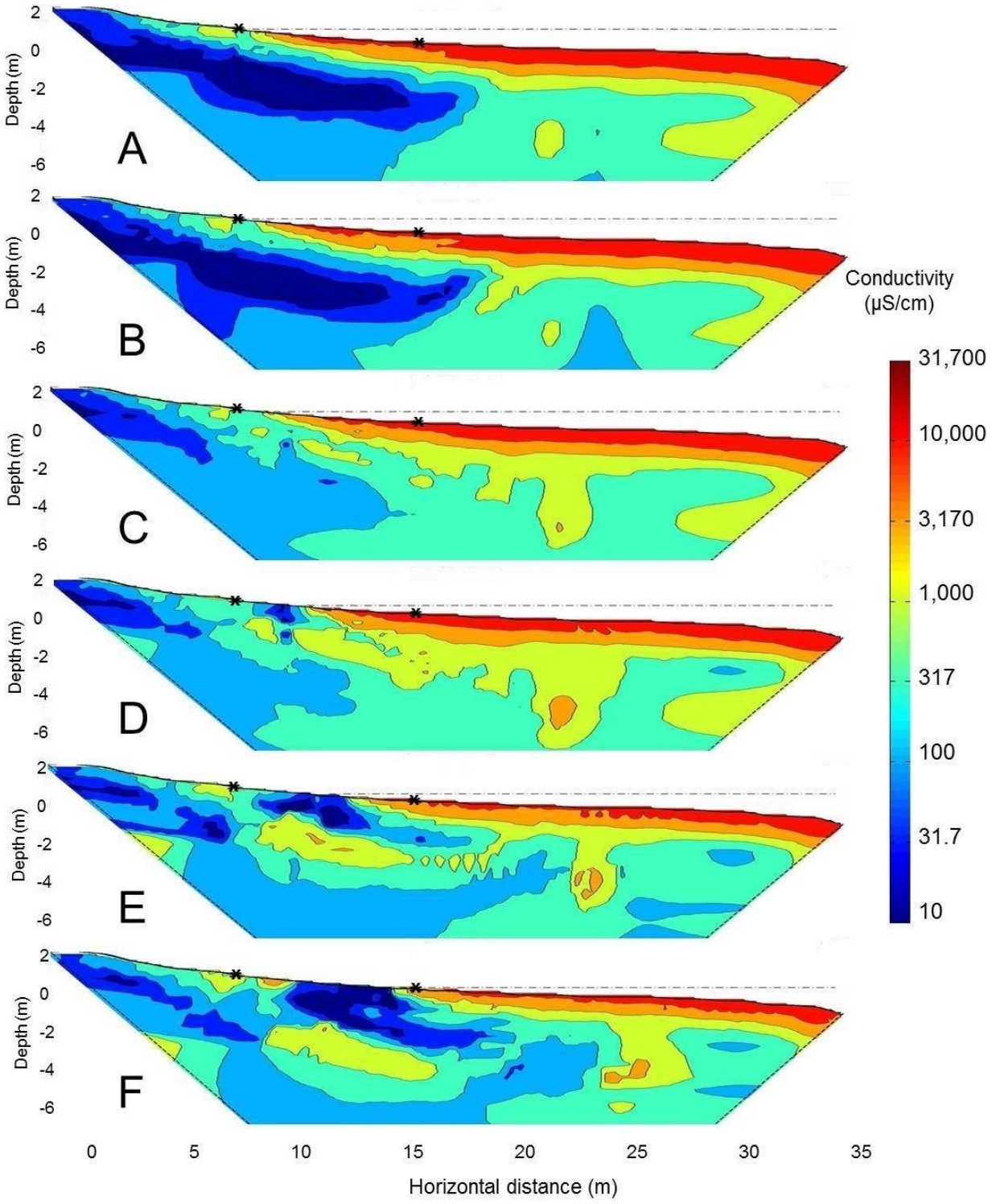

Figure 19. Inverted conductivity sections of time lapse survey, profiles A to F. Bulk conductivity is plotted on a log scale in µS/cm. High tide and low tide marks are indicated by black crosses (x), the dashed line shows the water level.

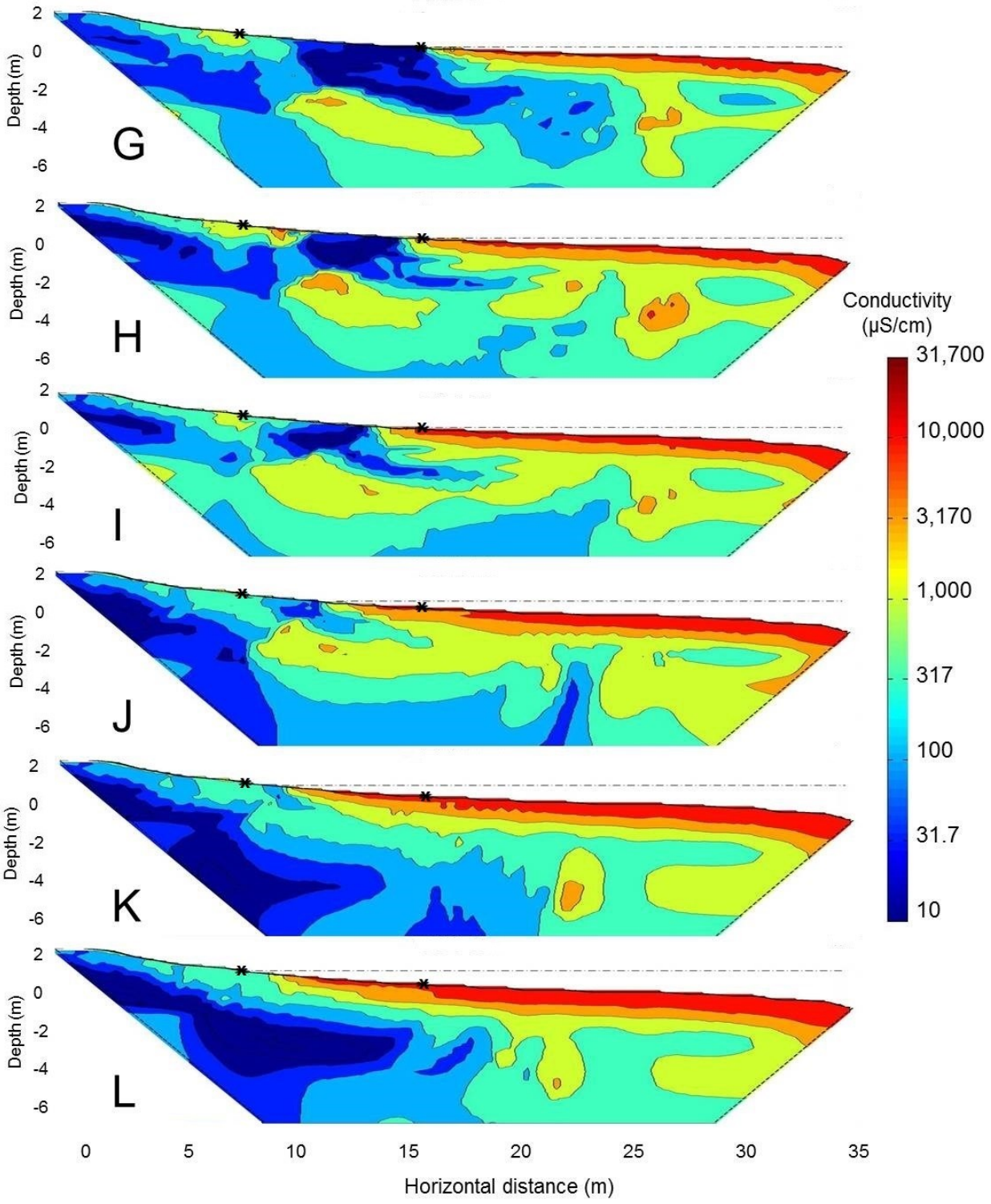

Figure 20. Inverted conductivity sections of time lapse survey, profiles G to L. Bulk conductivity is plotted on a log scale in µS/cm. High tide and low tide marks are indicated by black crosses (x), the dashed line shows the water level.

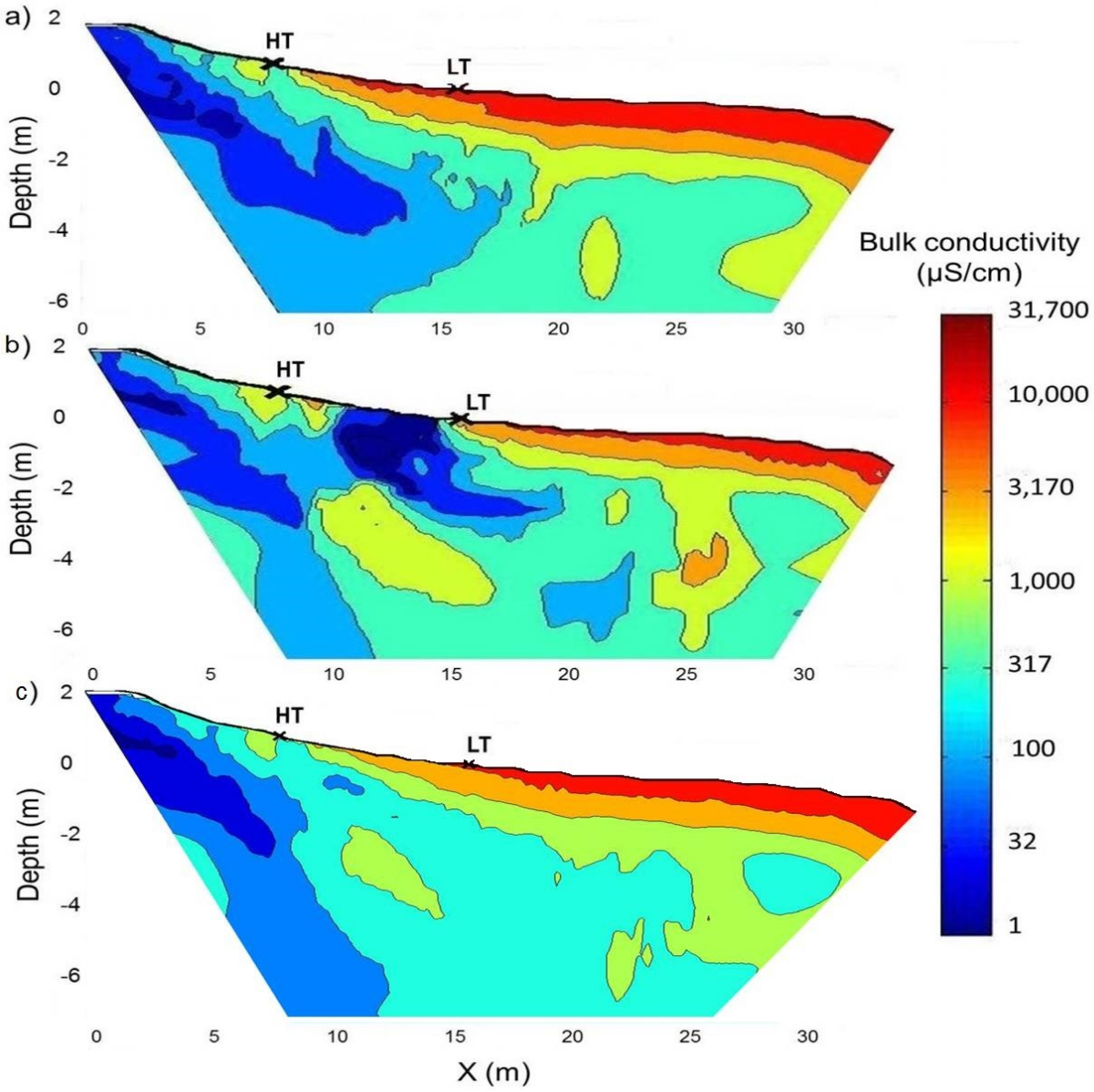

Figure 21. Average conductivity sections for the high tide (a) and low tide (b) end-members, and for the phase-averaged profile (c), in µS/cm. Conductivities are plotted on a log scale.

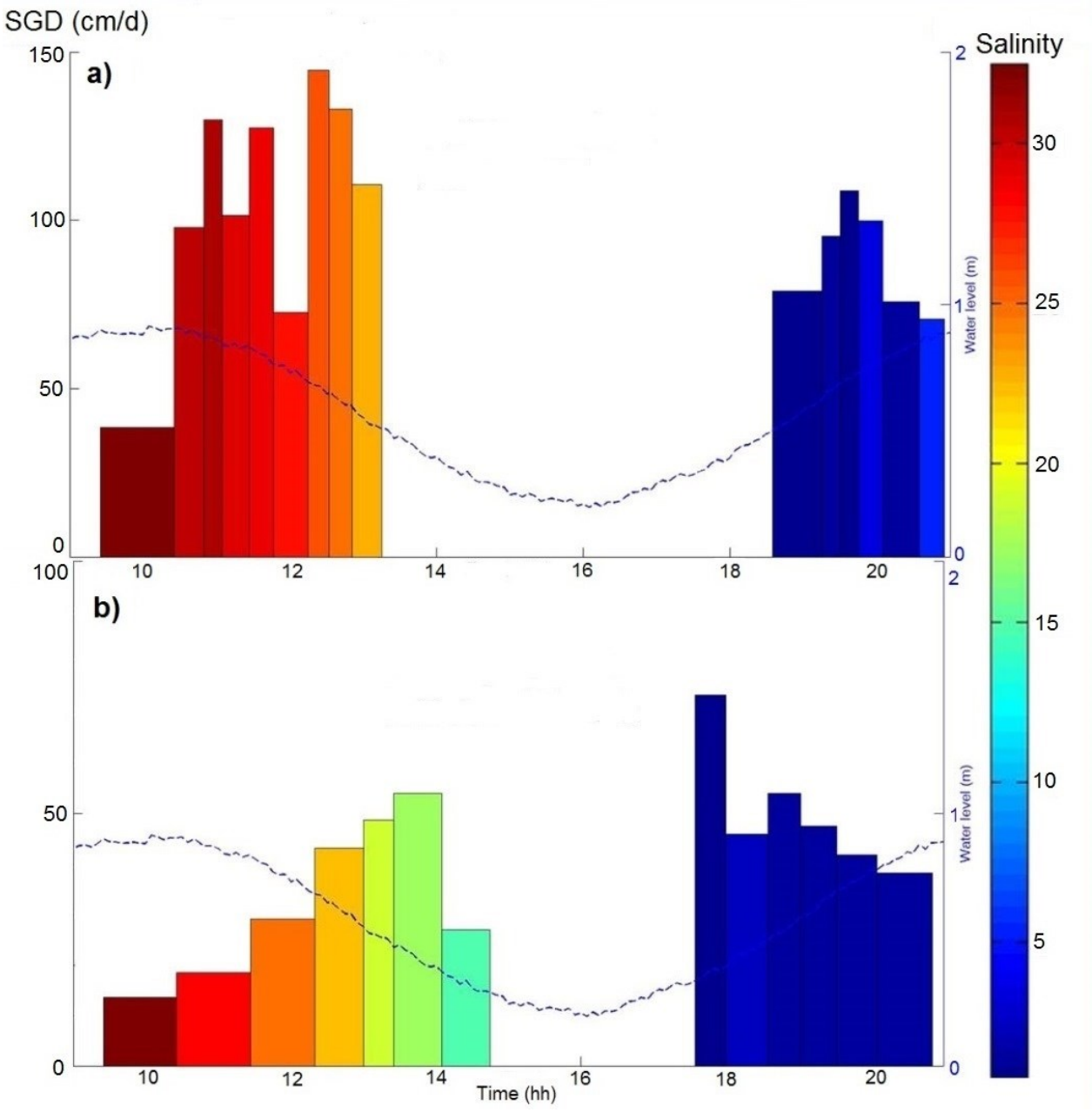

Figure 22. Seepage rates and salinity measured with the manual seepage meters M1 (a) and M2 (b) in the intertidal zone.

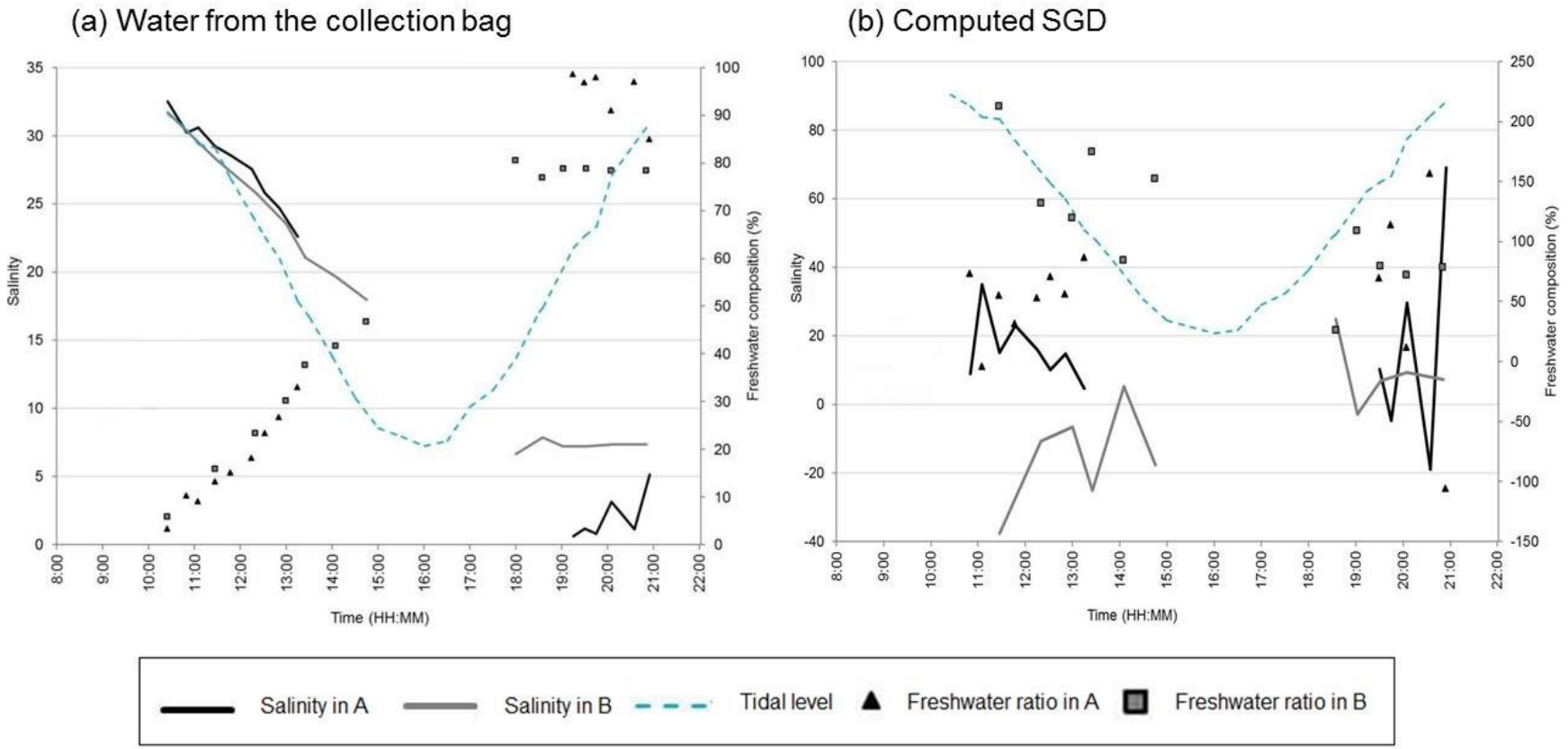

Figure 23. Salinities and freshwater content (%) measured in the manual seepage collection bags (a) and computed for SGD entering the seepage meters (b).

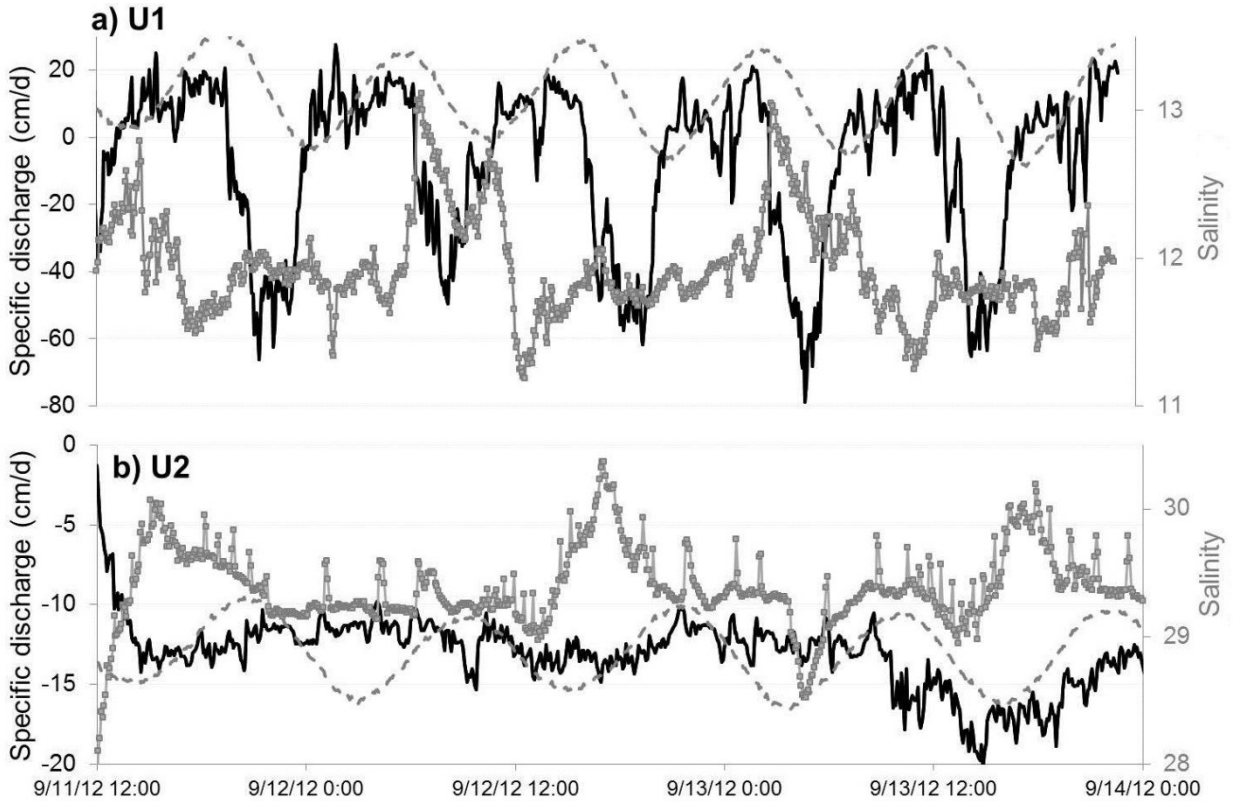

Figure 24. Seepage rates measured with the ultrasonic seepage meters U1 (a) and U2 (b), in cm/d (black solid line). The relative tidal level is plotted with a grey dashed line; salinity, is plotted in grey with square markers.

Chapter 5: Nutrient loading associated with submarine groundwater discharge in Forge River

Abstract

Forge River, a tidal river located on the south shore of Long Island, has experienced chronic hypoxia due to excessive nitrogen input for almost a decade. A significant portion of nitrogen is entering the river through submarine groundwater discharge (SGD). Management and ecological restoration of the Forge River watershed hinge upon a comprehensive understanding of where and how nutrient loading is occurring. An integrated approach combining electrical resistivity surveys, conductivity/temperature and seepage point measurements, and pore water analysis was used to map out SGD distribution and provide water quality data. We found that nitrogen speciation and concentration are linked to different SGD regimes distributed in 3 main zones. The first zone is composed of near shore sandy areas with high SGD. They present little nitrate reduction and constitute the major source of nitrogen input to surface waters. The second zone encompasses offshore areas rich in silt and organic matter. They exhibit low SGD and higher denitrification. Finally, in zone 3, dredging activities have altered the sediment distribution and subsequently created preferential flow paths focusing freshwater discharge in the center of the river.

1. Introduction

1.1 Background

The Forge River is located between the hamlets of Mastic and Moriches, in southern Suffolk County, NY (Figure 25). A major tributary of Moriches Bay on the south shore of Long Island, Forge River has played an important role in producing natural resources for both commercial and recreational users for many decades. For several decades it has experienced chronic hypoxia due to excessive nitrogen input from a number of natural and anthropogenic sources, including submarine discharge that contains effluent from unsewered high-density residential housing and wastewater from a commercial duck farm upstream. An alarming fish-kill occurred in the summer of 2006, which increased the concern about a general decline in its state of health and, consequently, Forge River was added to the 2006 New York State 303(d) List of Impaired Water Bodies. To date many surface waters along the south shore and east end of Long Island have areas of severe eutrophication and harmful algal blooms [*Burson et al.*, 2008; *Laroche et al.*, 1997; *Ryther*, 1954]. Although recent improvement has been observed in the river due to closure of the upriver duck farms and recent dredging, concern remains that excessive nitrogen is entering the river.

Management and ecological restoration of the Forge River watershed hinge upon a comprehensive understanding of where and how nutrient loading is occurring. As is typical of Long Island streams, a significant portion of the freshwater flow of Forge River derives from groundwater, which may transport nutrients from the underground aquifer by submarine groundwater discharge (SGD). Since this SGD can transport nutrients and contaminants from inland sources, it plays a key role in controlling the water quality of the surface waters with significant impact on the ecological condition in these waters [*Johannes*, 1980; *Zektser et al.*, 2006]. A recent study of the benthic fluxes of Forge River observed that the flux related to groundwater is relatively high, representing up to 73% of the total external supply of nitrogen [*Aller*, 2009]. As this flux is largest on the more densely populated western side of the Forge watershed, it has probably contributed to the greater hypoxia and nitrogen, as well as lower oxygen levels observed in the tributaries and shorelines along this portion of the Forge River.

1.2 Objective of the project

By its very nature, the mixing zone between Forge River and Moriches Bay is a dynamic system that evolves with the interaction between bay water from tidal loading and fresh surface water, which may involve significant spatial and temporal complexity.

An integrated study was designed to map out areas of pronounced SGD and acquire water quality data within these zones. I adopted the methodology and protocol that were established by *Paulsen et al.* [2008] in the Coastal Contaminant Migration Monitoring Assessment of Forge River, which integrated the ultrasonic seepage meter with the Trident Probe, a screening probe that uses electrical conductivity and temperature sensors for mapping out the extent of groundwater seepage, and the SuperSting, a geophysical tool for mapping out the spatial distribution of electricity resistivity as a proxy for fresh water discharge. Guided by the spatial extent of SGD that had been inferred from the SuperSting and Trident Probe measurements, cluster wells were also positioned in transects across the river to provide *in situ* nitrogen speciation and concentration measurements in groundwater. Ultrasonic seepage meters were also used to measure SGD fluxes at key locations.

Results of past studies revealed that significant concentrations of nitrogen were present in near-shore groundwater discharging into the Forge River, mostly along the western shoreline [*Paulsen et al.*, 2008; *Wanlass*, 2009]. Those studies found that high nutrients inputs were located in the portion of Forge River analyzed in the present report i.e. transects FR2 and FR1, as shown in Figure 29. Some ammonia was present in the hypoxic levels (DO < 2 mg/L) at concentrations varying between 0.02 and 2.25 mg/L, indicating a possible conversion of nitrate into ammonia in oxygen-depleted areas.

The overall objective of this study is to quantify the nitrogen load related to groundwater influx across the hyporheic zone at two locations on Forge River. These sites were selected because they have significant groundwater input, according to previous hydrogeological investigations and interpretation of well data [*Paulsen et al.*, 2008; *Wanlass*, 2009]. It should be noted that a third transect was also investigated at Wills Creek (Figure 29), but is not presented here as the results were similar to the ones obtained at FR1 and FR2 [*Durand and Paulsen*, 2014].

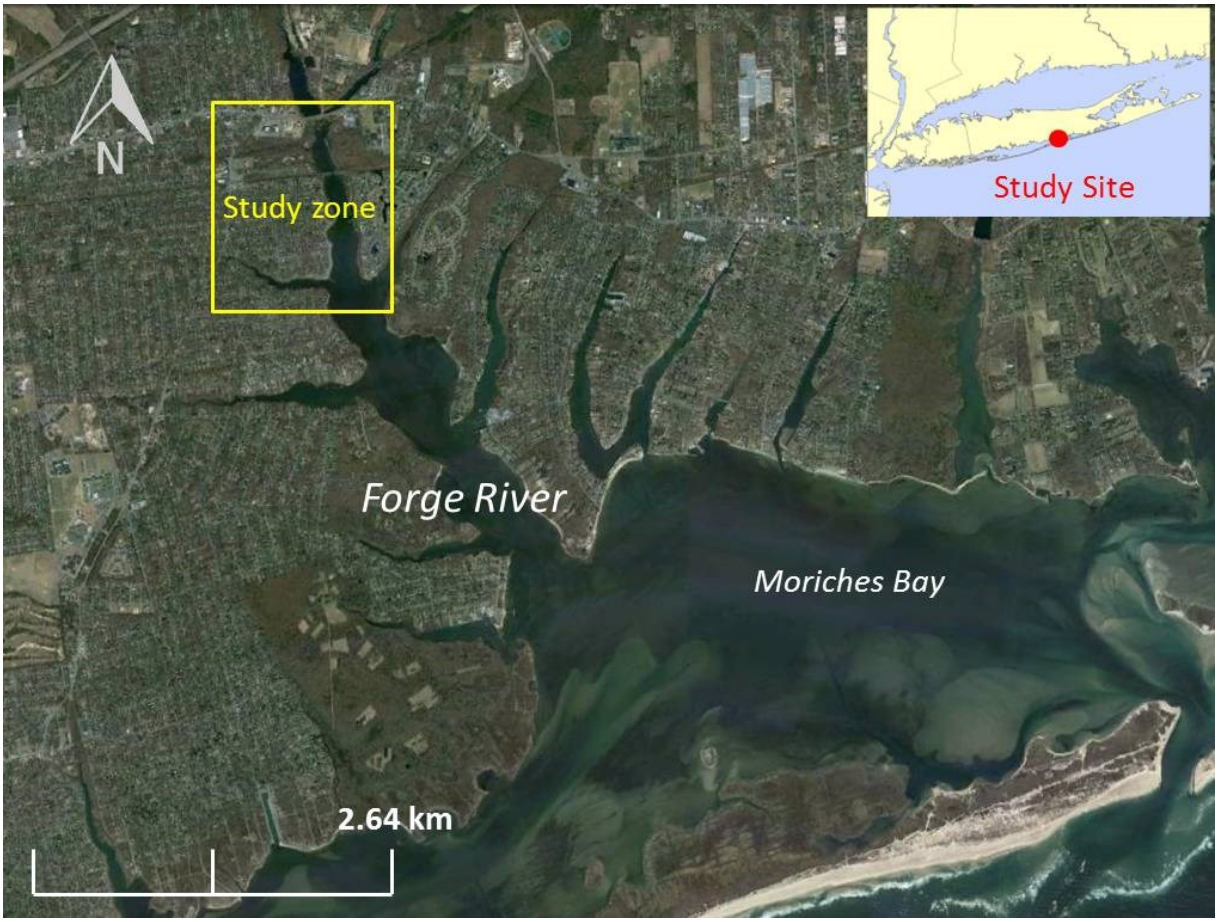

***Figure 25**: Site map with general location inclusion in upper right corner. The study zone includes two transects in the Forge River and another in Wills Creek.*

2. Methodology: equipment and field procedure

2.1 Equipment

Several techniques were used to characterize the near shore and offshore groundwater conditions, as well as characteristics present within the hyporheic zone. The techniques include: well installation near shore, well clusters and the installation of offshore wells and geophysical measurements. Offshore wells were installed using a Geoprobe barge operated by the Suffolk County Department of Health Services (SCDHS) and near shore wells were installed using an auger drill rig with hollow stem augers. The locations of these wells were determined from past work, current geophysical characterization and knowledge of the local hydrogeologic conditions. Figure 28 presents the detailed sampling design of the offshore wells. In addition to the wells, three different types of geophysical measurements were employed in the field. The Trident Probe was used near the surface to map out the spatial distribution of electrical conductivity and temperature as proxies for SGD. The SuperSting system was used to image subsurface profiles

of electrical resistivity along selected vertical sections transverse to the shoreline. The ultrasonic seepage meter system was deployed at selected locations to quantify SGD.

2.1.1 Trident Probe

The Trident probe is a direct-push instrument developed to screen and assess offshore areas where groundwater may be discharging to the surface water body [*Chadwick et al.*, 2003]. The probe integrates two temperature sensors, two electrical conductivity sensors, and two pore water samplers. The subsurface conductivity/temperature (C/T) probe measures the electrical conductivity and temperature at depth, whereas the surface C/T sensors measure the electrical conductivity and temperature of the water in the vicinity of the Trident probe. The subsurface C/T probe and the dual pore water samplers are collocated in a triangular pattern with a spacing of about 10 cm on an aluminum stopper/sealer plate that rests on the sediment-water interface. By adjusting the position of the mounting plate relative to the subsurface probes, measurements can be conducted at different depths. In this study, the depth was typically fixed at 45.7 cm (18”) below the sediment-water interface.

Each conductivity sensor is made up of two pairs of stainless steel electrodes that make up a Wenner array. A known current is imposed on the outer pair of electrodes, while the voltage through the inner pair is monitored. The apparent conductivity of the saturated sediments and its spatial variation is primarily a function of changes in salinity, and secondarily of clay content and porosity. In this setting, it is likely that an area with relatively low conductivity is associated with SGD. The temperature sensor consists of a customized digital oceanographic thermometer with a ruggedized titanium probe. It has a measurement range of -5 to +35 °C at an accuracy of 0.001 °C, and a resolution of 0.00025 °C. Areas of groundwater seepage may appear either as warm or cold contrast to the surface water, depending on the seasonal and site characteristics.

Once such a likely area of groundwater impingement has been identified, the dual water-sampling probes can be used to collect samples for on-site field parameter characterization (salinity, DO, ORP, pH) and for detailed analysis of chemical constituents by off-site laboratories. The head of the push-pole of the Trident probe is fitted with a global positioning system (GPS) unit with wide-area augmentation system (WAAS) capability. Hence the data logger also captures spatial coordinates of the location where subsurface and surface measurements of electrical conductivity and temperature are measured.

2.1.2 Supersting Resistivity system

Electrical resistivity imaging was performed using the SuperSting R8 system, and the acquired data were analyzed using the software package EarthImager 2D. The SuperSting system uses a cable of length 33 m (112'), with 56 electrodes separated by a uniform spacing of 0.61 m (2'). It is capable of simultaneously measuring 8 channels using a high-power transmitter. The control box injects current in the cable every 3 seconds, and 8 apparent resistivity values representing 8 depth levels are read for each current injection. The control box assigns which electrode shall be the current injector and which shall be the potential reader, in accordance with the specific array configuration that has been selected. In this study, measurements were made using both the dipole-dipole and Schlumberger configurations at each site, and the data were stacked together for the inverse analysis. The dipole-dipole configuration is useful to study shallow variations; the Schlumberger allows a deeper penetration and a greater lateral resolution.

Using 2-dimensional resistivity inversion, the software package EarthImager2D interprets the apparent resistivity data acquired by the SuperSting array and provides optimal estimation of the spatial distribution of resistivity on the vertical profile. In this study the software has been implemented following the procedure described by [*Durand et al.*, 2011].

2.1.3 Ultrasonic seepage meter

SGD was quantified using an ultrasonic seepage meter developed by [*Paulsen et al.*, 2001]. SGD is captured by a steel collection chamber (with a diameter of 45.72 cm (18") and a round cross section of 0.164 m^2), inserted approximately 10 cm into the sediment. The discharge so captured is directed to a cylindrical flow tube with two piezoelectric transducers mounted at opposite ends. The transducers continually generate bursts of ultrasonic signals (periodic waves with a frequency of 1.7 MHz) from one end of the meter to the other end, while arrival of the ultrasonic signals is continuously monitored by the piezoelectric transducers. If velocity of the flow induced by the SGD in the tube is small relative to the ambient sound velocity and if the fluctuations of temperature and salinity are negligible, then the flow velocity is directly proportional to the difference between the upstream and downstream arrival times. Taking into account the areal ratio between flow tube and collection chamber, the specific discharge of the submarine ground water can be calculated from the flow velocity in the tube. The meter is capable of continuously measuring SGD at rates as low as ±0.07 μm/s (0.25 cm/d). In parallel,

the water temperature and conductivity are collected using a solinst level logger attached to the underside of the seepage funnel. The sampling rate is 10 seconds and is used to determine the specific discharge.

The ultrasonic groundwater seepage meter was deployed following the protocol described in [*Chadwick et al.*, 2003; *Chadwick et al.*, 2003]. Data calibration for the ultrasonic seepage meter requires to record null fluxes before and after each deployment and are called prezero and postzero. The prezero and postzero allow checking the stability of the meter during deployment, their average is deducted from the discharge measured in the field to remove the error created by the seepage meter itself.

2.2 Field procedure

2.2.1 Trident probe

In some cases, the lithology and geological conditions were such that the subsurface probes of the Trident met with significant resistance at a depth less than the target depth of 45.7 cm, which required relocating the sampling point by a lateral distance of approximately 30-60 cm for another trial to penetrate the probes down to the target depth. Occasionally it was necessary to repeat the process up to three times before a successful installation was accomplished. In sediments that were silty, it was sometimes difficult to extract water samples. The locations of Trident stations were chosen according to knowledge of the site acquired from previous studies. Pore water was pumped using the water-sampling probe powered by a low-flow peristaltic pumping system, for nutrients analyses. Prior to sampling, the system was purged by first pumping and discharging approximately 60 ml (3 sampler volumes using a 10 m sample tube). Conductivity and temperature of collected pore water were simultaneously measured using a YSI multimeter probe. Readings were monitored until they were stable, then logged over a sixty second interval and averaged by the recording software. Records also include the time, date and location of the station. After the station was logged, samples were collected for water quality measurements using the YSI 556 hand-held probe for temperature, conductivity, salinity, dissolved oxygen, pH and oxydo-reduction potential (ORP).

Samples for phosphate analysis were collected in 250 ml amber glass bottles. Samples for standard inorganic analysis (nitrogen series, phosphate and silica) were collected in HDPE, 250 ml screw cap bottles. Between points, the screen zone was disassembled, brushed to remove

attached sediments, rinsed with seawater and deionized water (DI) and put back in place. The entire sampling system was flushed with a series of solutions including: a 1/10 alcanox aqueous solution, surface water, and DI water. All samples were unfiltered. Care was taken during the pumping process to minimize the amount of suspended solids in the samples.

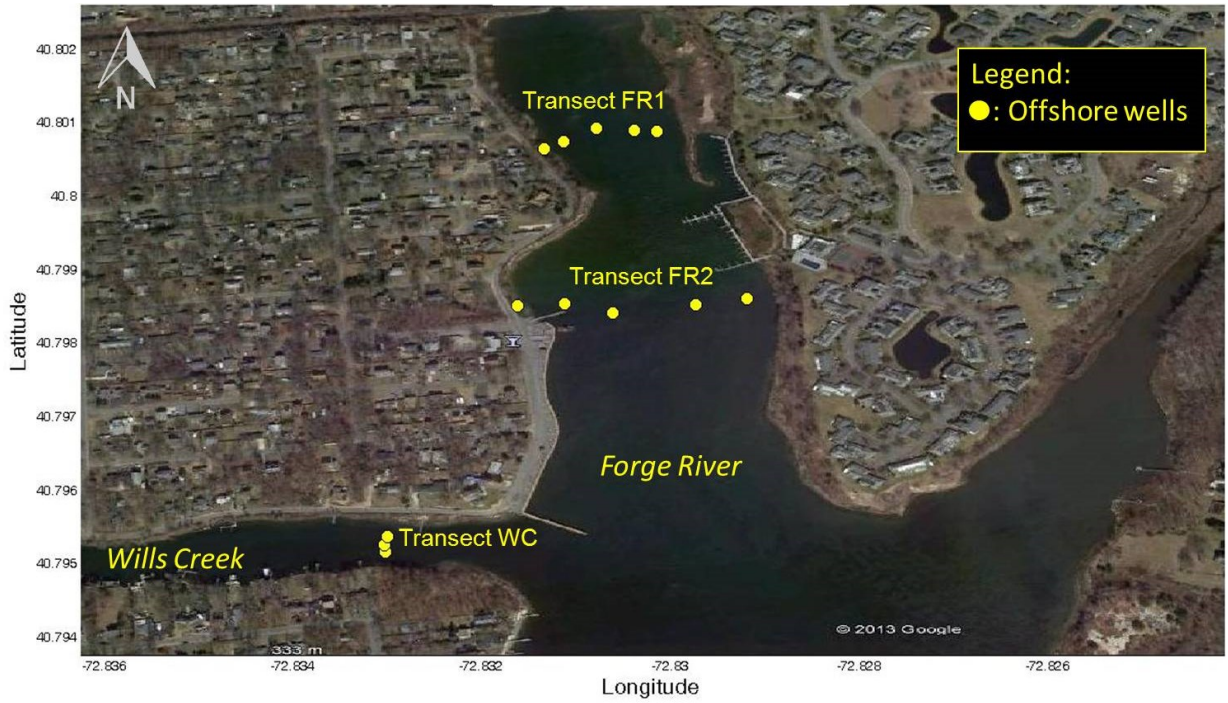

***Figure 26**: Site map showing Trident point locations associated with the wells, in Wills Creek and Forge River.*

Trident transect were acquired at three locations: FR1, FR2 and WC between 6/19/13 and 7/9/13 to explore the shallow pore water temperature and conductivity distribution (Figure 26). Two tables summarizing the Trident records are available in appendix (Appendix 1 and Appendix 2).

2.2.2 Supersting resistivity and EarthImager2D

The SuperSting cable was deployed on the sediment bottom along transects running perpendicular to the shoreline, north/south for Wills Creek and west/east for Forge River. If part of the cable was exposed, additional electrode spikes were added and coupled to the cable to ensure proper contact with the ground. All resistivity surveys were acquired at low tide. At two transect locations on FR1 and FR2 a high tide measurement of resistivity was performed in order to capture tidal variability. To limit the variations of the overlying surface water layer during a

given resistivity survey, the acquisition was scheduled so that the minimum or maximum tidal stage would occur at the middle of the data acquisition period.

Bathymetry profiles and muck layer profiles were always performed simultaneously to the electrical resistivity surveys. Trident points were associated with ER measurements for ground-truthing. The positions of the electrical resistivity surveys for Forge River are shown in Figure 27. The offset observed between the transects FR1A, FR1B and the wells results from various difficulties encountered in the field. Due to some problems with the SuperSting, the acquisition of electrical resistivity transects had to be repeated several times at different location before obtaining satisfying results. Anchoring the boat was also challenging in this area, so it was not possible to position it as accurately as for the other sites. Finally, malfunction of the GPS forced us to use a different unit with slightly different accuracy.

2.2.3 Ultrasonic seepage meter

Guided by the other measurements on the spatial distribution of SGD, two locations along the transect FR2 were selected for deployment of the ultrasonic seepage meters in Forge River: close to the shore and in the middle of the river. The seepage meters were left in place for a period of two days on July 24th and 25th, 2013. Technical difficulties only allowed us to obtain data from the location closest to the shore (Figure 27). For both the ultrasonic seepage meter deployment and the electrical resistivity measurements a Solinst pressure logger was deployed at the marina to monitor the tidal level. By plotting the measured tidal variation along with the predicted tides given by the MapTech ProChart Navigation software, we observed that the tidal variations in the creek and the river have about 65 % the amplitude of the predictions at the Moriches Coast Gard Station and a lag of ~1h. Solinst multiloggers were deployed in the funnels to record pressure, temperature and conductivity of seepage but technical problems (erratic readings by logger or incomplete record) did not allow recovering the data. The software predictions were then corrected and used as tidal level indicator.

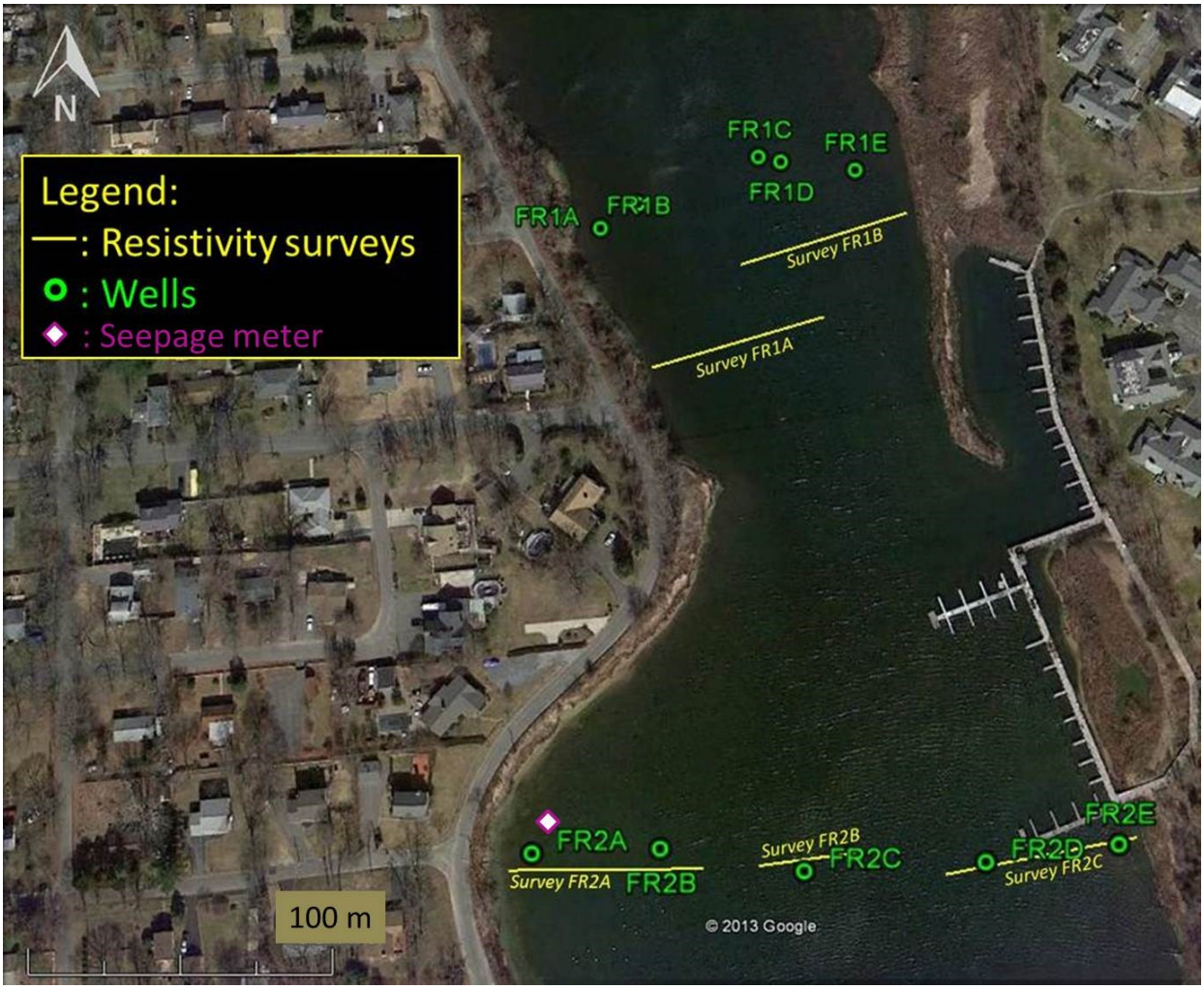

***Figure 27**: Site map of electrical resistivity surveys and well profiles at FR1 and FR2 and ultrasonic seepage meter location, in Forge River.*

2.2.4 Water sampling

2.2.4.1 Well design

The sampling design of the offshore sediment bottom included 5 sample points at depth along five stations transecting the river at three locations. Typically, there is a muck/silt layer overlying a layer of sand and gravel (Figure 28). The upper pore fluids were collected using temporary Trident Probe at two points located at 0.3 to 0.7 m (1 to 2 ft) bellow the sediment/water interface. The third temporary point was set at the interface between the underlying sandy bottom and the silt/muck layer. Typically the sample point was set 0.3 m (1 ft) into the sandy bottom. The deeper pore fluids were collected using offshore semi-permanent one inch piezometers. The 4th and 5th points were set at 3 and 6 m (10 and 20 ft) below the sandy/muck interface. Figure 28 provides the conceptual sampling design. Although slightly

different at each station, the sample points were consistently place in each sediment horizon. The thickness of the silty/muck layer above the sand substrate was the only variable that dictated the position of sample points 3 through 5.

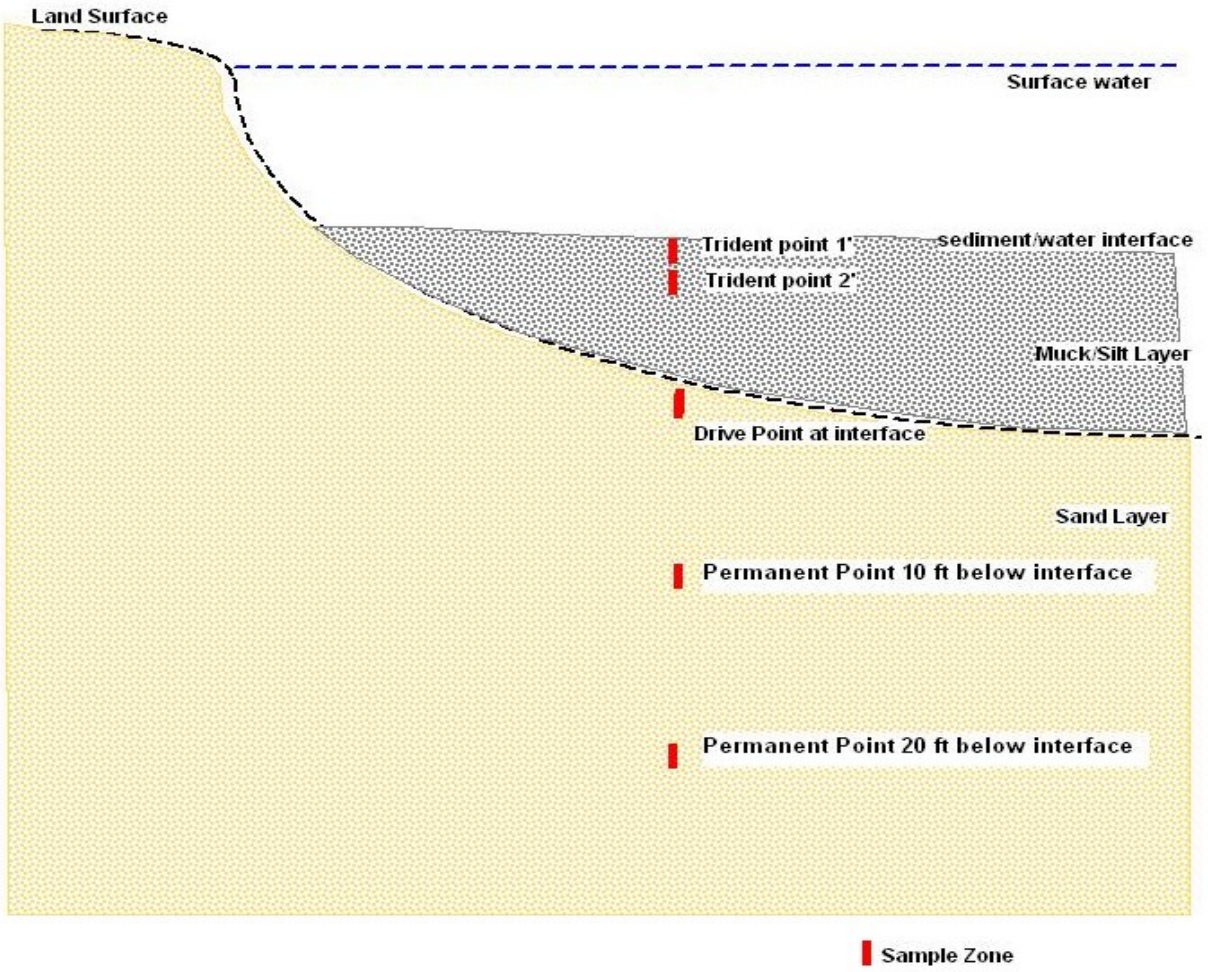

***Figure 28**: Conceptual sampling design in the hyporheic zone.*

Locations of profile wells are shown in Figure 29. Profile wells were also sampled up-gradient of each transect: RD2 in Wills Creek, FR1-land and FR2-land in Forge River. Samples were drawn from the up-gradient profile wells and analyzed for: nitrate, nitrite, Total Kjeldahl Nitrogen (TKN), phosphate, silica and chloride for the well RD2 during fall 2012. Surface water samples were also tested for total phosphorus, orthophosphate, biochemical oxygen demand (BOD) and silica. At Forge River and for Wills Creek during the summer 2013 sampling campaign, the water samples were analyzed for the presence of nitrogen series i.e. nitrate-nitrite, ammonia and TKN. The total nitrogen values were calculated as the sum of TKN and nitrate-nitrite. The two associated land wells were also analyzed for silica and BOD. A detailed

discussion of the findings is presented in Section 3 of the report. Field parameters (temperature, conductivity, salinity, DO, pH and ORP) were also measured for each pore water sample.

***Figure 29**: Site map showing pore water points inland and offshore wells in Wills Creek and Forge River.*

2.2.4.2 Nutrients analysis

Samples from the monitoring wells were analyzed by a private certified lab (H2M Labs Inc.) following the "Standard Operating Procedure for Sampling for Inorganic Compounds in Aqueous Samples" (US EPA, 2002). The samples were stored on ice at 4oC and transported to the SCPEHL for validation analysis by US EPA method SM4500-NH3H for Ammonia, US EPA method E351.2 for Total Kjeldahl Nitrogen, M4500-N C for total nitrogen. Samples collected in the fall of 2012 were analyzed by Long Island Analytical using the following techniques: EPA 200.7 Rev 4.4 for dissolved silica, ASTM D3590-89 &02 (A) for TKN, EPA 300.0 Rev. 2.1 for chloride, nitrate as N, nitrite as N and orthophosphate as P, SM 18-20 5210B (01) for BOD and SM 18-21 4500-P E for total phosphorus.

2.2.4.3 *In situ* pore water analysis

Samples obtained from the Trident and from the wells were analyzed on-site using a YSI 556 hand-held multi probe. The YSI probe detects temperature, conductivity, salinity, pH, DO and ORP. The YSI probe was calibrated to specific conductivity standards prior to the beginning of each survey. In addition, the Trident system measured temperature and conductance in the sediment bottom.

3. Results

3.1 Trident mapping and pore water conductivity sections

Electrical conductivity and temperature data from the Trident surveys associated with the offshore wells are presented in Appendix 2. As noted earlier, the data were typically acquired at a fixed depth of 45.7 cm (18") below the sediment-water interface. The subsurface C/T probe measures the electrical conductivity and temperature of the saturated sediment at depth, whereas the surface C/T sensors measure the reference electrical conductivity and temperature of the surface water in the vicinity of the Trident probe. The properties measured with the C/T probe in the shallow sediments depend on both porous medium and the saturating fluid properties.

The results from the Trident point transects associated with the well sampling at Forge River are presented in *Figure 30*. The difference in surface water temperature between FR1 and FR2 is the results of different acquisition weeks (*Figure 30*a). Bulk temperatures and conductivities for transect FR1 vary slightly around 20°C and 8 mS/cm, respectively, indicating some mixing between fresh groundwater and surface water. Surface water conductivities are lower close to both shores and in the center of the river, revealing freshwater discharge (*Figure 30*d). The conductivity difference, defined as $\Delta C = C_{porewater} - C_{surface\ water}$, is smaller close the shores indicating some limited mixing with the surface water. The analysis of FR2 is slightly different. The bulk conductivity distribution is more homogeneous and all the values are very low < 5 mS/cm which reveals the presence of fresh groundwater, isolated under the muck layer, across the whole river. A relatively low value of surface water conductivity, 25 mS/cm, close to the east shore, indicates significant freshwater discharge in the area. Previous studies had found that seepage was found mostly on the west shore [*Wanlass*, 2009], but our data suggest that the discharge on the east shore is not negligible.

Points at the center of the river in transects FR1 and FR2 stand out from the other sampling points: they have low bulk and surface water conductivities, i.e. < 5 mS/cm and < 10 mS/cm, respectively (*Figure 30*c), which results in very small conductivity and temperature differences (*Figure 30*e). This indicates that the reference probe (or surface water probe), located a few inches above the probe inserted into the sediments, is sampling seeping groundwater fluid that has not been mixed with the overlying surface water. Two scenarios can explain the low conductivities of the overlying water at the center of the river: a strong fresh SGD flux or a misplacement of the reference probe inside the muck layer, enabled by the fluidity of that layer. High SGD rates are unexpected in areas where the low permeability muck layer is at least 1.5 m (5 ft) thick.

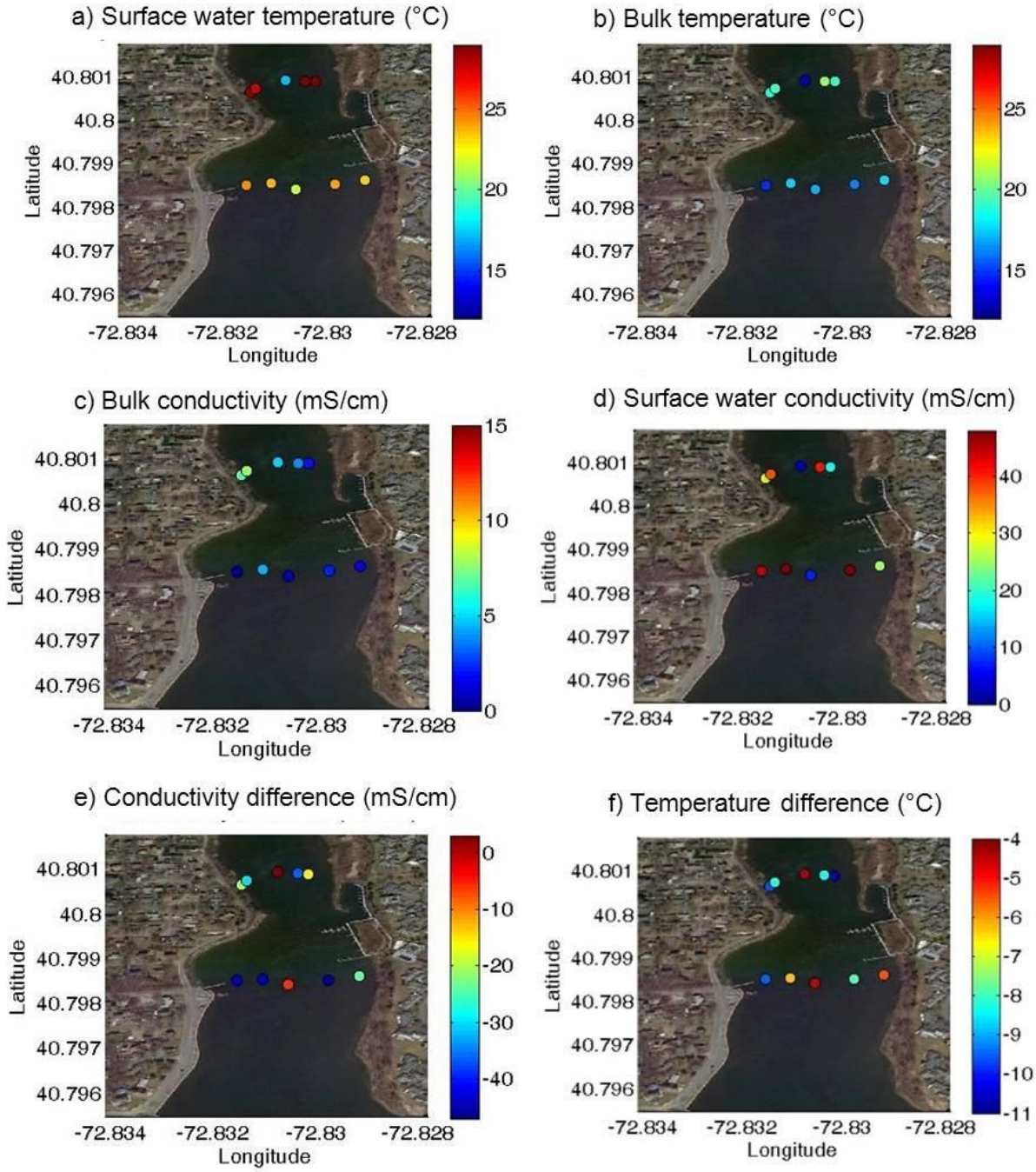

Figure 30. *Temperature results for the Trident points associated with the wells in Forge River. Conductivity difference is computed as follow:* $\Delta C = C_{porewater} - C_{surface\ water}$. *Temperature difference is computed as follow:* $\Delta T = T_{porewater} - T_{surface\ water}$.

These findings contradict the results from seepage meter profiles in a previous study that stipulated that most freshwater discharge was focused at the shorelines and more specifically on

the west shore [*Wanlass*, 2009]. It is possible that the muck layer presents some discontinuities thus allowing some strong freshwater discharge away from the shores. The consistency of the centered location of these discontinuities at FR1 and FR2, argues against the probe misplacement hypothesis. It is likely that this is the result of prior dredging activities that occurred during late 2012, post Super Storm Sandy, which created some preferential flow paths by removing the confining mud layer in the center of the river. I will next present the results from the well pore water conductivity analyses (Figure 31 and Figure 32) which confirm the existence of these flow paths and rule out the second hypothesis. Accordingly, my conclusion is that there appears to be three distinct zones of SGD present in the hyporheic zone: the near shore zone of significant SGD discharge and mixing (Zone 1), the sloping area toward the center containing significant layering of silts and organic matter with very low SGD (Zone 2), and the central area with highly fluidized, less dense sediments associated with significant SGD upwelling (Zone 3).

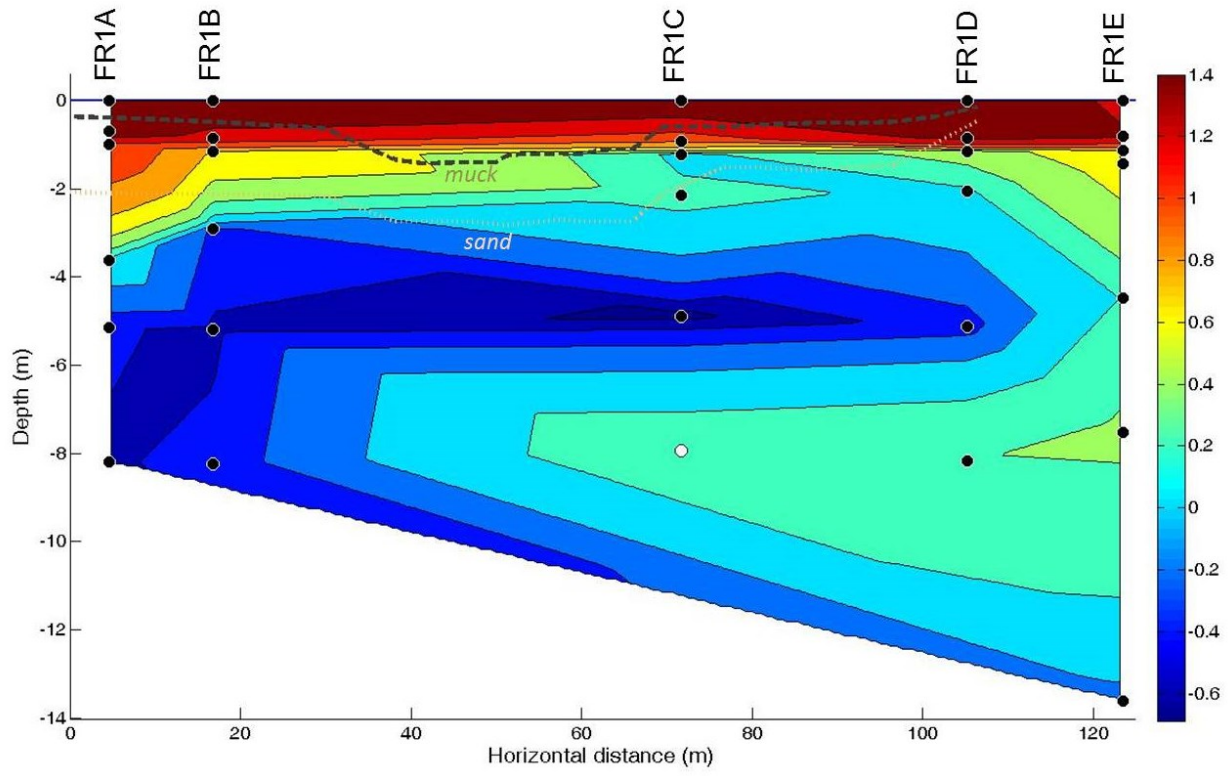

Figure 31. *Logarithmic scale of pore water conductivity measurements (in mS/cm) for transects FR1 in Forge River. The black dots show the sampling locations. The white dot indicates an unreported conductivity value. In the section, that value was replaced by the linear interpolation of directly adjacent values.*

Figure 31 shows an interpolated section of *in situ* pore water conductivities measured with the YSI probe during water collection, at FR1. All sample locations show high conductivity values at their superficial levels indicating intrusion of the overlying seawater. This intrusion however is very limited as most of the water is fresh at depth greater than 1 m (3 ft). A strong fresh water plume coming from the west shore is clearly visible and moves sub horizontally towards the east shore due to the presence of the low permeability silt layer. A second trend is observed in the center of the river where part of the fresh water plume is moving upward and reaches the superficial level of well FR1C, in agreement with the superficial Trident probe measurements. This vertical flow path is believed to result from the dredging activities that may have fluidized the muck layer in the center of the river, increasing its permeability. This is in agreement with inverted resistivity sections to be presented later and the Trident point measurements discussed earlier. Diver observation made during equipment deployment indicated a silty and highly fluidized bottom, with significant groundwater upwelling, also observed in the water samples from wells FR1C-a and FR2C-a.

The extrapolated conductivity section for FR2 (Figure 32) is qualitatively similar to that for FR1 in the first 6 m depth. A strong freshwater signal originating from the west shore of the river moves towards the center of the section and rises to reach the surface in the center of the section, where the muck layer is more fluid. Saline surface water does not infiltrate beneath the muck layer. In FR2, closer to the bay, the freshwater-seawater interface is visible in the center of the section at depth beyond 6 m.

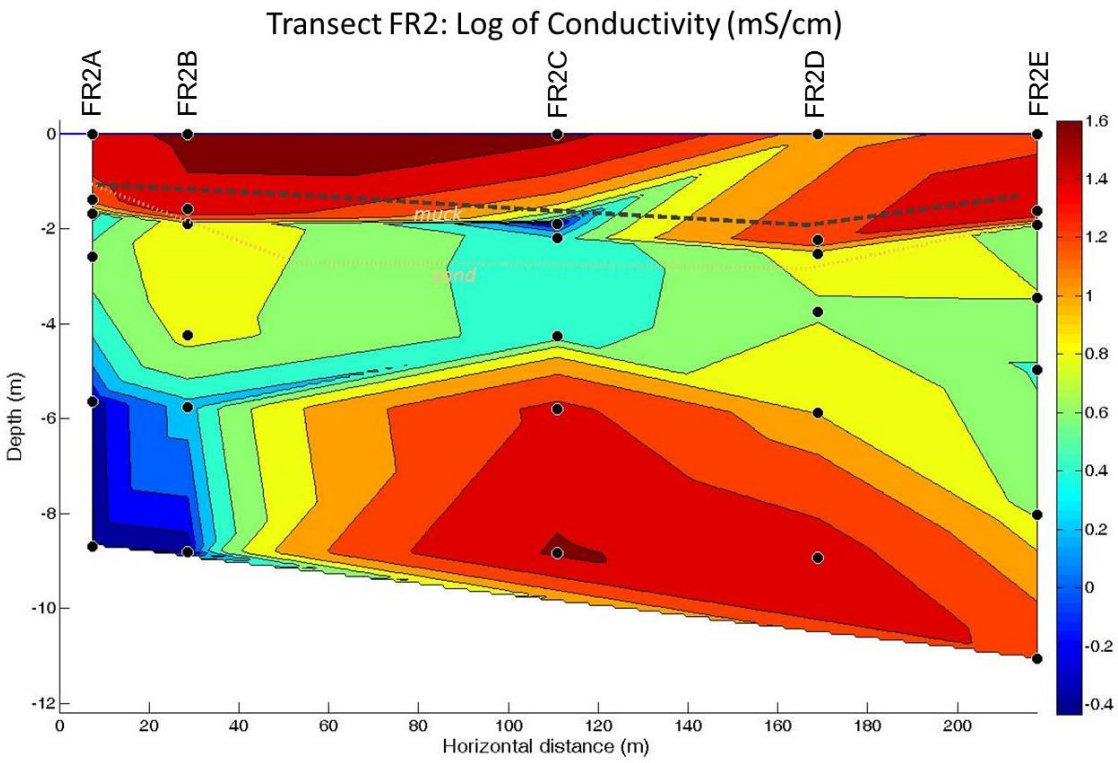

***Figure 32**. Logarithmic scale of conductivity measurements (in mS/cm) for transect FR2 in Forge River. The black dots show the sampling locations.*

3.2 Electrical resistivity surveys

The inverted conductivity sections for transect FR1, located in the upper section of the Forge river, show that there is a diffuse zone of very low conductivity (between 0.04 and 0.5 mS/cm), that reveals the presence of fresh water (Figure 33). The freshwater signal is stronger on the west shore of Forge River. The plume extends under most of this river section, likely due to the hydraulic confinement exerted by the low-permeability muck layer, also present in most of this section. Two significant areas of fresh groundwater are detected around x ~ 28 m and x ~ 55 m offshore and extend down to a depth of 10 m.

The inverted conductivity sections for transect FR2 is quantitatively similar. There is a diffuse zone of very low conductivity (between 0.04 and 0.5 mS/cm) (Figure 34, Figure 35 and Figure 36). The freshwater signal is stronger on the west shore of Forge River but a significant amount of freshwater is present in the middle area at various locations. The freshwater cell also extends under most of this river section, likely due to the hydraulic confinement by the muck layer. Two areas of fresh groundwater were detected at ~ 35 and 60 m offshore (measured from

western shoreline) and extended down to a depth of 16 m. A third area with freshwater is visible at x ~ 30 m offshore of the eastern shoreline.

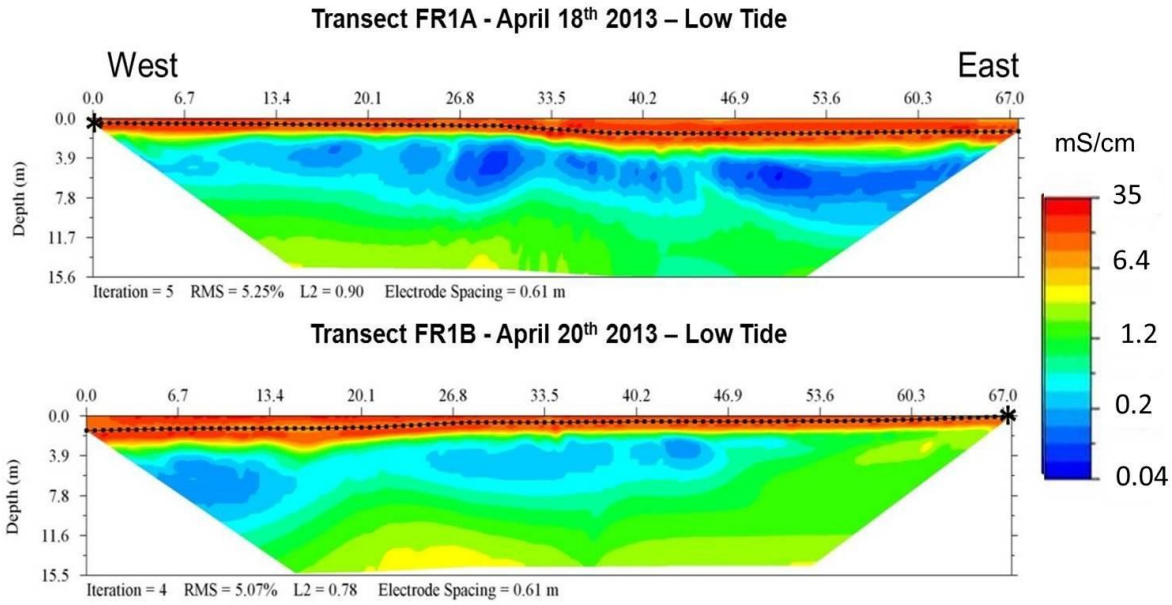

***Figure 33**: Inverted conductivity sections of profile FR1A and FR1B at the west and east shore of Forge River, respectively.*

The survey FR2A was repeated at low and high tide to study the tidal influence on the freshwater distribution (Figure 34). The two surveys are consistent, and there is not much difference in the horizontal extent of the freshwater plume. However, the freshwater plume seems to be focused closer to the shore at high tide and farther offshore at low tide. Given the limited influence of tidal variations on the resistivity profiles, surveys FR2B and FR2C were only acquired at low tide.

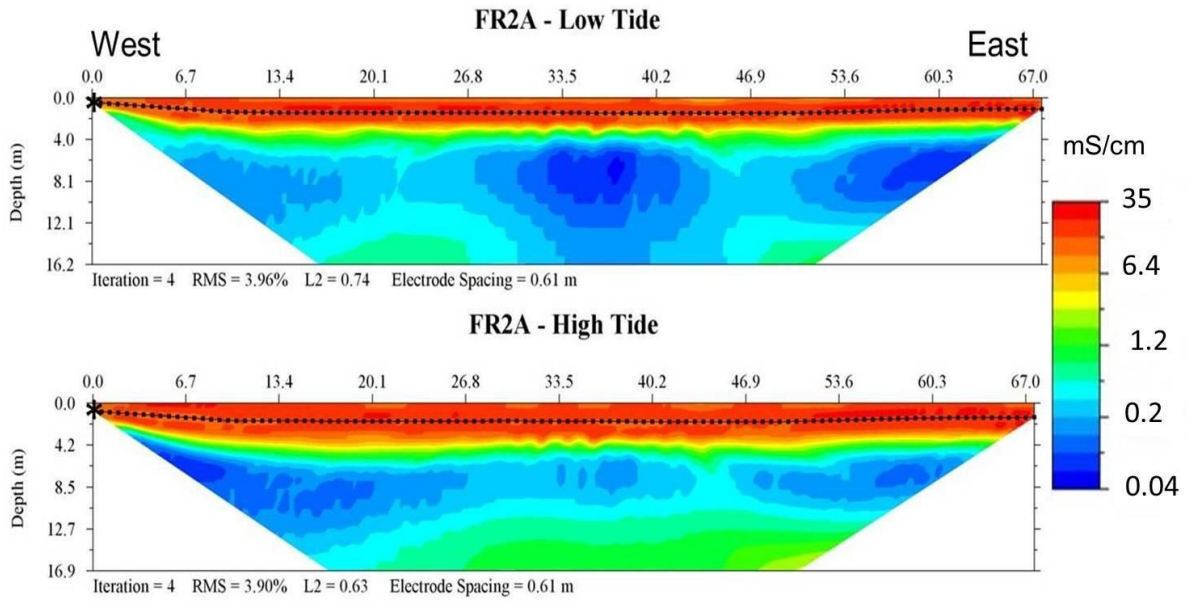

***Figure 34**: Inverted conductivity section of profile FR2A at the west shore of Forge River on April 11th 2013 at low and high tide.*

The transect FR2B was located in the center of the river, where the muck layer is the thickest. A layer of high conductivity appears right below the electrodes, down to 4 m. This could be due to the very high porosity of the muck layer or the effect of saturation by surface water. Under this layer, the water is relatively homogeneous and fresh (1.2 mS/cm). A fresher portion with a conductivity under 0.5 mS/cm can be noticed at depth for $6 < z < 9$ m in the center of the section. The signal is not as strong as the one observed at the shores, due the decay of SGD flux with increasing distance from the shores indicated by seepage measurements in a previous study [*Wanlass*, 2009].

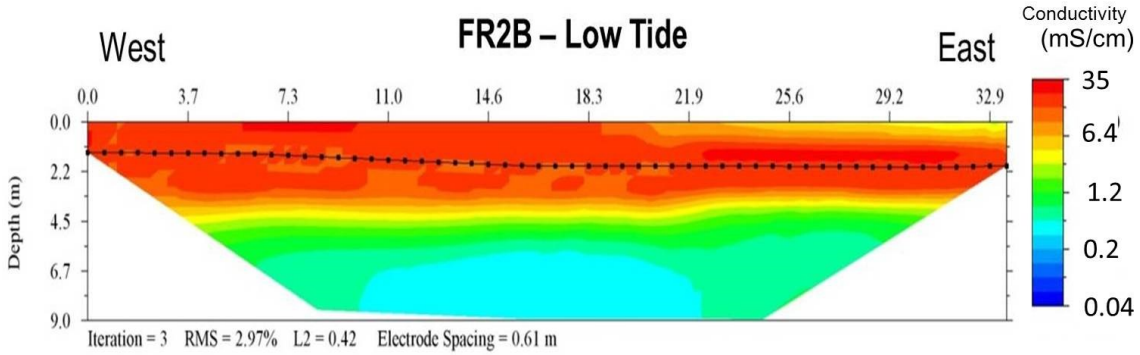

***Figure 35**: Inverted conductivity section of profile FR2B in the middle of Forge River on April 20th 2013 at low tide.*

On the electrical conductivity section FR2C (Figure 36), a zone of very low conductivity is present close to the east shore, for 13< x<58 m and no deeper than 10 m. It reveals the presence of a freshwater plume that does not spread as far offshore and as deep as the one observed at FR2A on the west shore. There is fresh groundwater along each shore but in bigger quantity on the west shore. This is in agreement with the known flow paths and hydraulic gradients for the area [*Paulsen et al*., 2008; *Wanlass*, 2009].

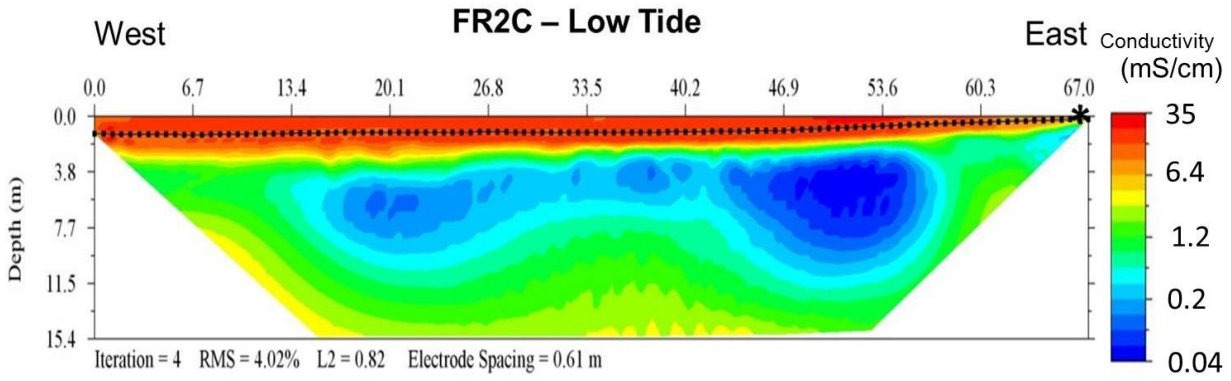

Figure 36*: Inverted conductivity section of profile FR2C on the east shore of Forge River on April 8th 2013 at low tide.*

3.3 Ultrasonic seepage meter

We present in Figure 37 the seepage data acquired at location FR2C for a duration of 17 hours. The continuous increase of discharge from negative to positive during the first 5 hours was related to the transient perturbations as the seepage meter stabilized. Beyond this stabilization stage, the seepage data over approximately one tidal cycle seem uncorrelated to the tidal level, in contrast to typical measurements in sandy coastal areas [*Paulsen et al.*, 2004; *Taniguchi*, 2002]. This could be due to the presence of the muck layer that provides hydraulic insolation from tidal forcing. An almost continuous discharge has also been observed in similar setting such as Stony Brook Harbor but the discharge rate through the muck layer was an order of magnitude lower, i.e. 3 cm/d (see chapter 3). The average SGD recorded at this location after stabilization is 42 cm/d (Figure 37), with a maximum discharge of 59 cm/d. Specific discharge measured in the sandy portion in Wills Creek (not presented here, see [*Durand and Paulsen*, 2014]) varied between 10 and 48 cm/d, with an average of 28 cm/d and showed a tidal dependence.

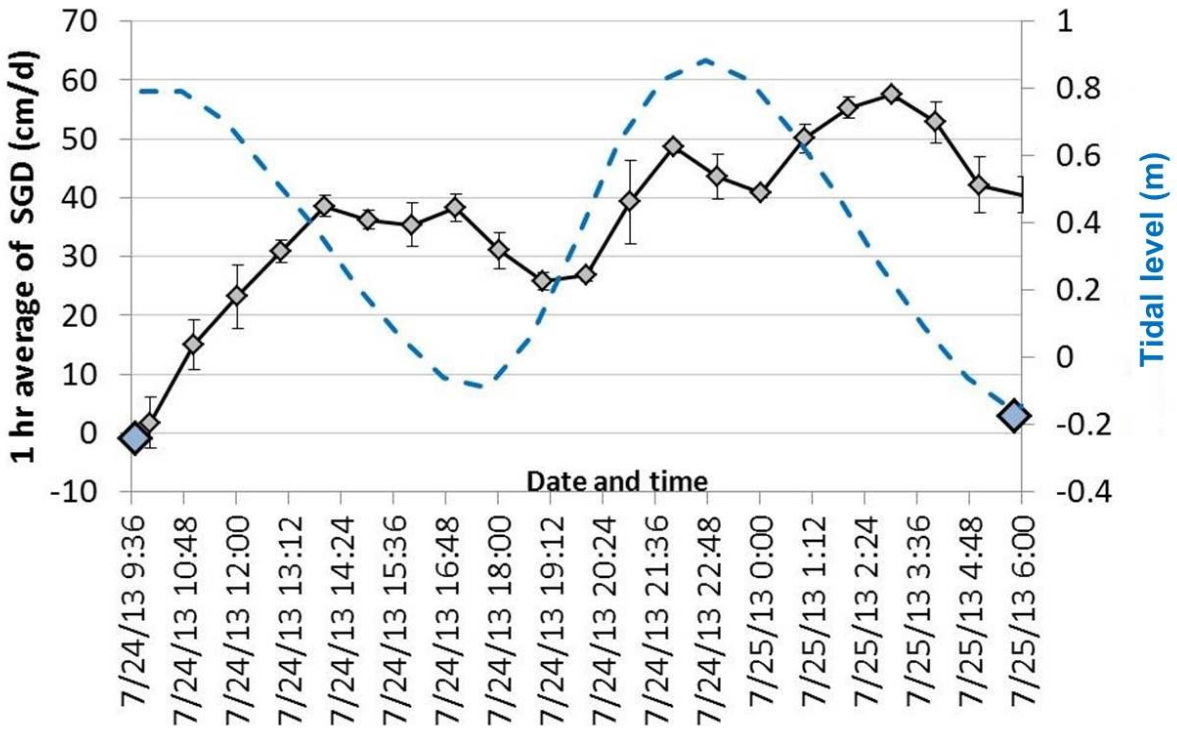

Figure 37*. 1-hour average of specific discharge recorded by the ultrasonic seepage flow meter (in cm/d), at FR2. Error bars were calculated as standard deviations. The blue dotted line indicates the tidal level (in m). The blue diamonds indicate the zero levels of the seepage meter before and after deployment.*

3.4 Well profiles

The results of nutrient analyses are presented in Figures 38 to 42 for transect FR1 and in figures 43 to 47 for transect FR2. The sampling locations are shown as black dots. When the concentrations are under the detection limits, the data are plotted as small squares with color indicating the detection limit (see lower left corner of plots for legend). A white dot indicates a sampling point for which field values were not reported. A summary of the numerical values of nutrient analyses and field parameter measurements for each well is presented in (Appendix 4 and 5).

3.6.1 Results of nutrients analysis for transect FR1

The only significant nitrate-nitrite concentrations ranged from 5 to 10 mg/L, and were found under 2 m depth at sampling levels c to e, for the offshore sampling points FR1A and FR1B located on Forge River west shore (Figure 38). The concentrations decreased progressively towards the surface and reached values under the detection limit in the muck layer and above. A surface water nitrate concentration of 0.49 mg/L was detected at station FR1A-s.

No nitrates were found in the surface water at other surface water stations. All values from the center of the river to the east shore were low, under 2 mg/L. The nitrate plume was localized to the western shore of Forge River.

Denitrification is defined as the reduction of nitrate by heterotrophic organisms leading to the production of molecular nitrogen ($N_2(g)$) through a series of intermediate gaseous nitrogen oxide products [*Zumft*, 1997]. These microorganisms use nitrate when the concentration of oxygen is low enough (under 2mg/L), and also require organic carbon as a source for energy.

A number of microorganisms reduce nitrate to ammonia which is assimilated as a source of nitrogen for biosynthesis [*Payne*, 1973]. Several heterotrophic bacteria (*E. coli, Azospirillum*) are capable of converting nitrates to nitrites and nitrites to ammonia. This process called ammonification is associated with sediments containing a high organic content, such as those in the Forge River. It has been suggested that the pathway of nitrate reduction to ammonia is important in coastal sediments [*Koike and Hattori*, 1978]. Nitrate reduction normally occurs under anaerobic soil conditions (water logged soils). This process is not considered to be the major denitrification process in the Forge but may be a secondary process and explains elevated concentrations of ammonia in areas where significant organic nitrogen was present. Dissolved organic nitrogen can form inside the microbial cells and may be excreted and/or liberated from the cells after their death [*Koike and Hattori*, 1978].

The ammonia distribution was also very localized, and limited to the muck layer (Figure 39). Relatively high values were found in the two upper levels of wells FR1A, B and D, where concentrations varied between 10 to 18 mg/L. The rest of the section exhibits very low ammonia concentrations, typically under 2 mg/L. The high incidence of ammonia in the muck layer, coincides with low nitrate values, and suggests potential ammonification of nitrogen (organic or nitrate) by microbial organisms. This is also consistent with the dissolved oxygen section (Figure 42) showing that the high values of ammonia match low levels of dissolved oxygen, under 2-3 mg/L, since oxygen would prevent denitrification as nitrate is a less favorable electron acceptor. It is likely that the microbial activity is enhanced in the muck layer as the organic matter provides energy to the microorganisms [*Koike and Hattori*, 1978].

Total Kjeldahl Nitrogen (TKN) is defined as the sum of organic nitrogen, ammonia (NH_3) and ammonium (NH_4^+). The total nitrogen concentrations are not measured by the laboratory but calculated as the sum of TKN and nitrate-nitrite values (Figure 41). The results show that the TKN concentrations match the distribution of ammonia (Figure 40). However, it is possible to calculate the amount of organic nitrogen and ammonium by subtracting the concentrations of ammonia from TKN. For most locations, the values of organic nitrogen are very low and vary between 0 – 2 mg/L but in some locations (well FR1A upper level and FR1C limit of muck layer) the amount of organic nitrogen reaches 6 – 8 mg/L. This argues in favor of ammonification of nitrates by microbes, as dissolved organic nitrogen can form inside the microbial cells and may be excreted and/or liberated from the cells after their death [*Koike and Hattori*, 1978].

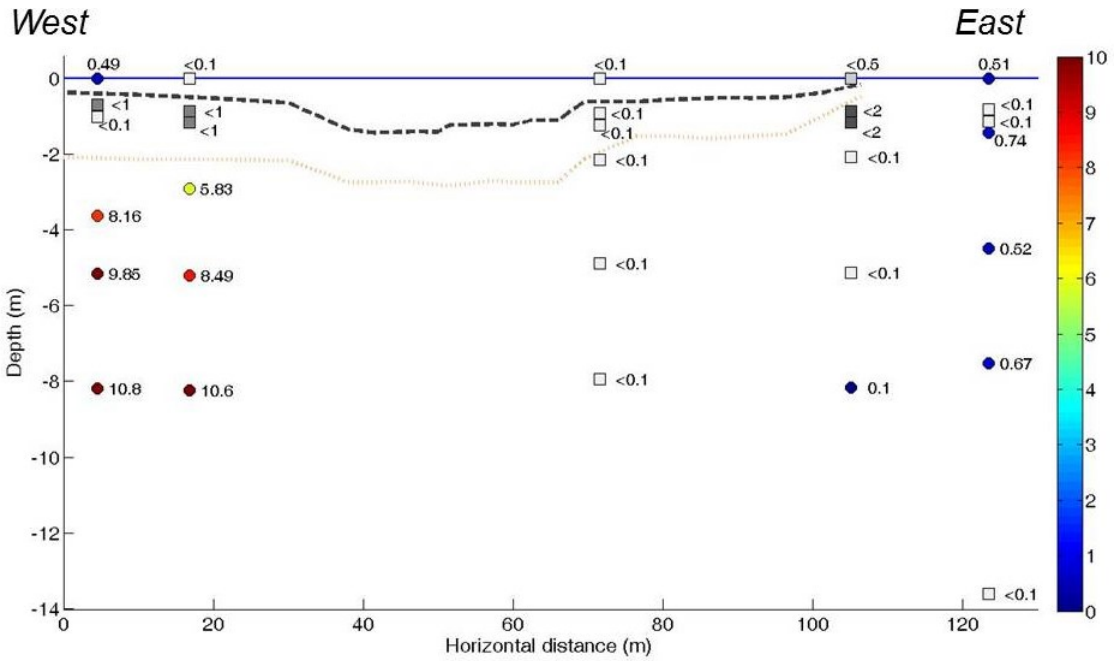

***Figure 38**: Nitrate-Nitrite concentrations (in mg/L) from transect FR1 in Forge River.*

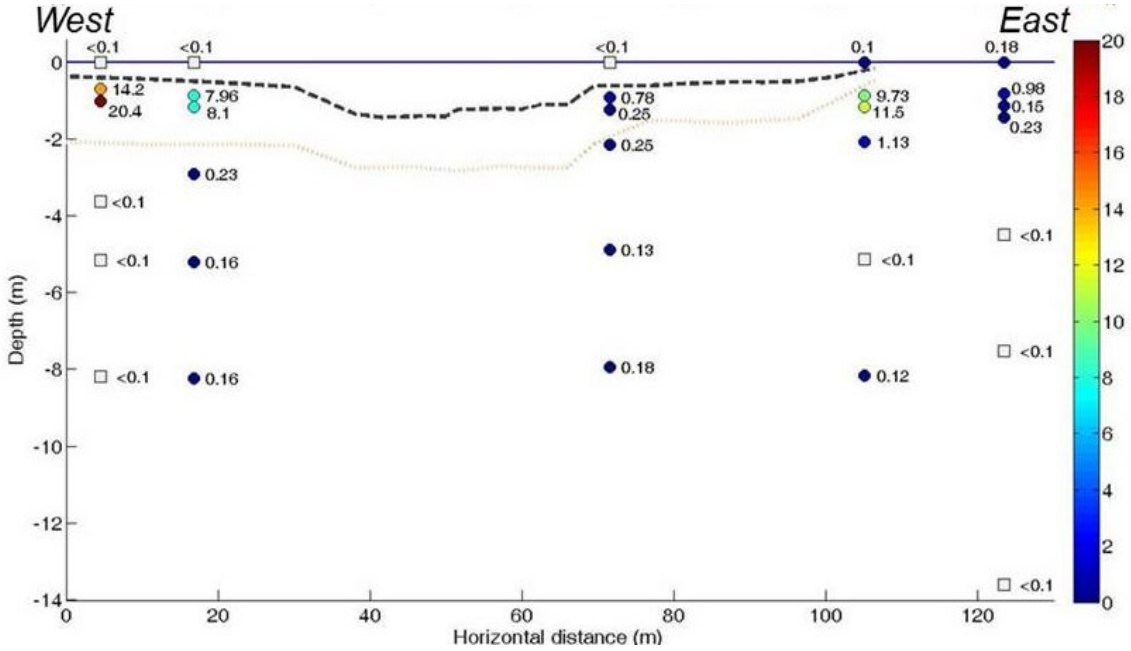

***Figure 39**: Ammonia concentrations (in mg/L) from transect FR1 in Forge River.*

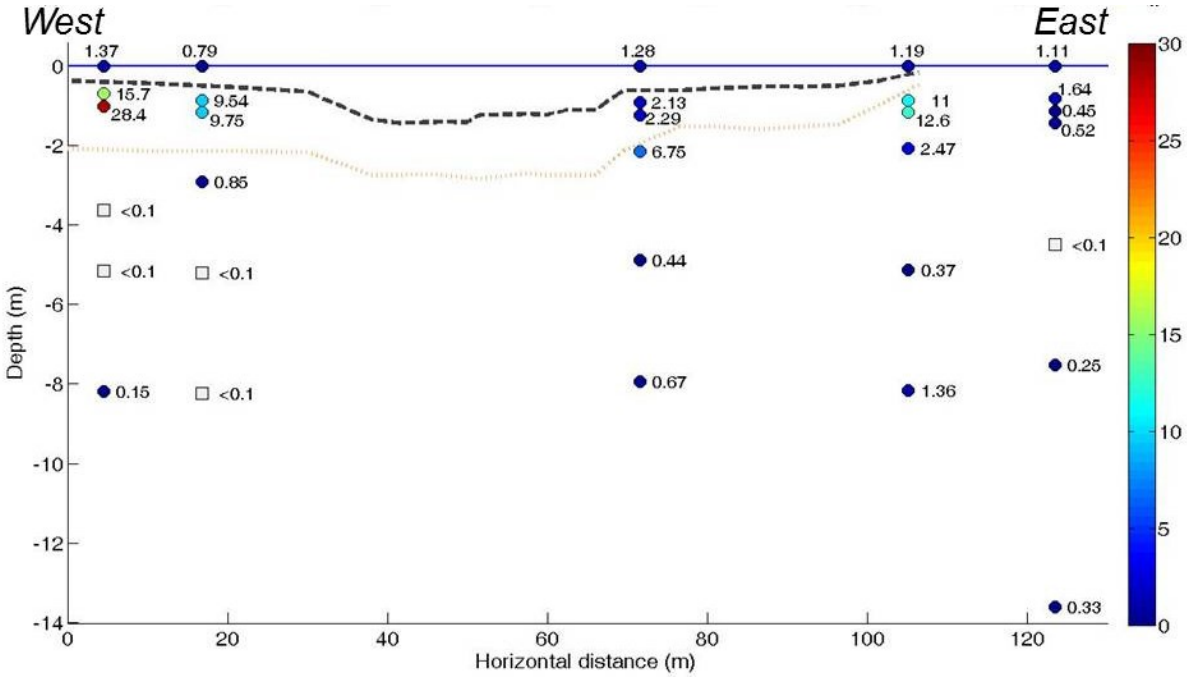

***Figure 40**: TKN concentrations (in mg/L) from transect FR1 in Forge River.*

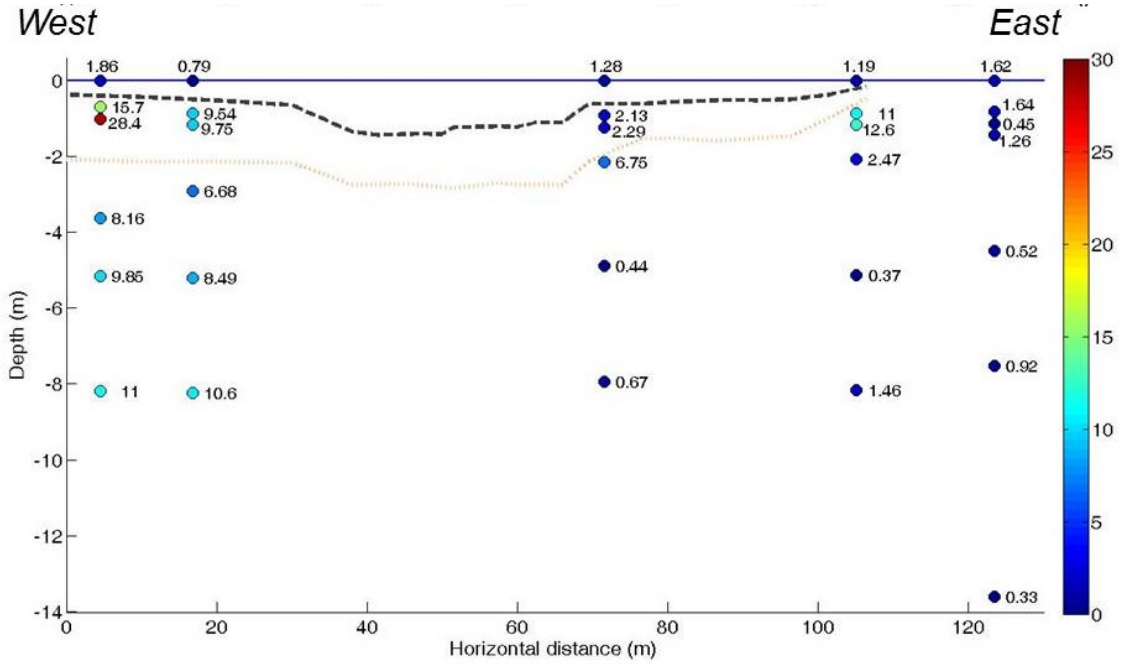

***Figure 41**: Total nitrogen concentrations (in mg/L) for transect FR1 in Forge River.*

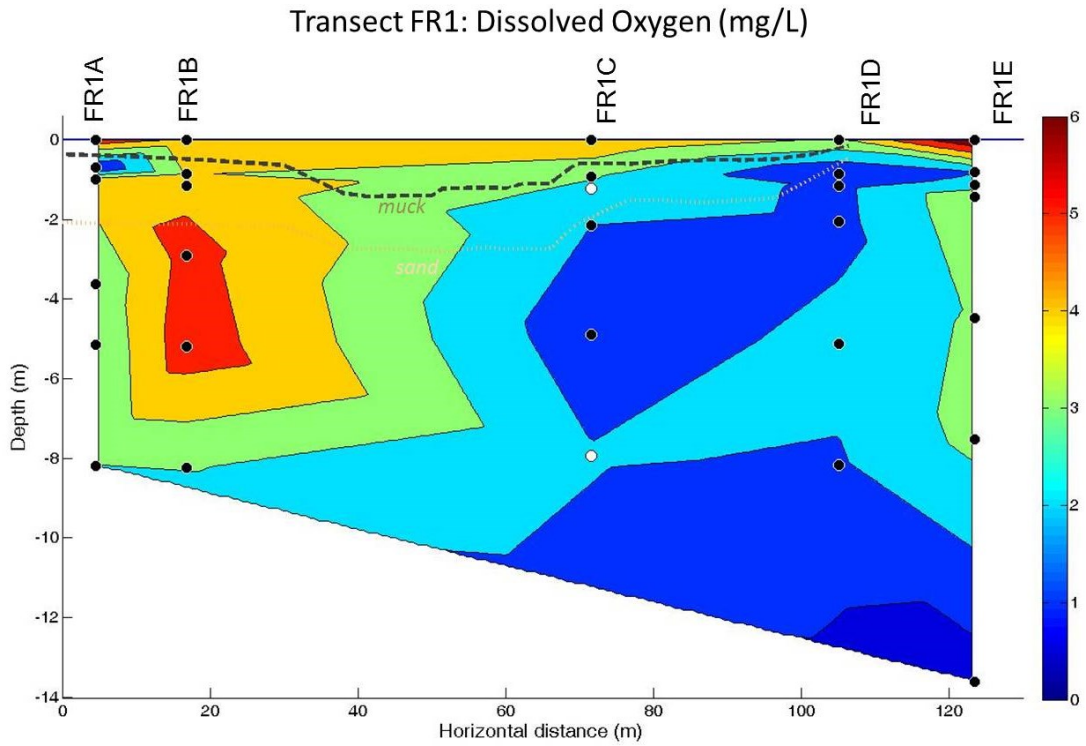

***Figure 42**: Dissolved oxygen measurements (in mg/L) for transect FR1 in Forge River. The dots indicate the position of the measurements, the colors show the interpolated values.*

The dissolved oxygen concentrations are strongly zoned across the river (Figure 42). Surface waters and the west portion of the section are rich in oxygen. For the rest of the section, from the center of the river to the east shore and a shallow level of well FR1A in the muck layer, the groundwater is depleted in oxygen. The low levels of oxygen observed in the vicinity of the muck layer, at FR1A-a and FR1D-b, coincide with the high level of ammonia and delineate where denitrification is possible and/or the production of ammonia from organic matter rich muck layer.

In conclusion, it appears that the hyporheic zone is divided into three zones with distinct SGD characteristics and nutrient fluxes, as described in section 3.1.4. The near shore zone 1 (~10 m) has significant advective flows and is an area where denitrification and mixing are likely occurring. The evidence for this is the decreasing values of nitrates coming from inland groundwater that are not present in upper section of this zone as wells as the low DO in these sediments. Looking solely at the water quality results at each station in zone 1, there is evidence that nitrogen is being reduced in this zone, ranging of 0 to 25%. Based on station FR2A levels e through b we see a 24.5% reduction in nitrate concentration within the zone, but compared to the inland well data, there appears to be evidence of further reduction. Since the flow paths and time of sampling may not coincide, it is hard to verify further reduction. In general the groundwater near shore has consistently shown nitrogen concentrations in the 5 to 10+ mg/L range. Considering only the samples within zone we present the reduction of nitrates to be ranging from 0 to 25%.This zone, however, is also a mixing zone when surface water infiltrates the sediments during high tides. Ammonia and organic nitrogen are present in the zone, likely due to organic matter mixing and/or microbial activity in the sandy sediments. Ammonia production is likely in areas with organic nitrogen and low DO, these conditions are present in this area. The area immediately offshore (10 to 90 m) is characteristic of zone 2 with significant layer of organic rich sediments (muck layer) and little SGD present. The area has lower concentration of total nitrogen than near shore sediments and has little nitrogen at depth, which suggests denitrification occurring and/or mixing of groundwater flow paths. The low DO concentration supports this. The flux of nitrogen to the river is likely benthic flux in organic forms. A similar zone is present along in the near shore area along the eastern shoreline (~10 to 20 m offshore). The third area (90 to 110 m) has the characteristic of zone 3 in that the presence of SGD is significant at the sediment surface and sediments are highly fluidized. The concentrations of total nitrogen are low

and no nitrate is detected at the surface or at depth, suggesting denitrification or strong dilution. Low concentrations of ammonia and organic nitrogen are present in the upper fluidized sediments, as previously mentioned, and likely due to organic nature of sediments and denitrification processes.

3.6.2 Results of nutrients analysis for transect FR2

Nitrate concentrations at the section FR2 are localized near the west shore of the Forge River (Figure 43). The concentrations at sample points FR2A and FR2B range between 0.8 and 3.88 mg/L, under the muck layer. The rest of the section, however, present low nitrate concentrations, generally under the detection limit. Nitrate concentrations in the surface water are also low and do not exceed 1 mg/L. It appears that there is some denitrification/mixing occurring at this location since up-gradient well concentrations of nitrates range from 2.8 to 9.53 mg/L.

Ammonia concentrations are high relative to nitrate, ranging between <0.1 and 45 mg/L, but extremely localized (Figure 44). Ammonia is mostly distributed in the muck layer, away from the shores that are sandy areas with significant SGD. The center of the section is free of ammonia as this coincides with the strong SGD upwelling, likely due to dredging, and may have washed out the organic nitrogen layer. The high ammonia concentrations detected in the organic rich muck layer appear, as previously observed in FR1, seem to be the result of ammonification of the organic nitrogen by microbial organisms in anoxic conditions. This process is considered to be more or a benthic flux than SGD related. In contrast, the rest of the section has low ammonia concentrations under 1 mg/L. There is a potential pathway for the production of ammonia through the ammonification of organic nitrogen in an anaerobic environment though microbial activity, and may explain relatively high concentrations of ammonia at several sample points in the Forge river. It is however unlikely that such high and localized concentration of ammonia results from groundwater transport or microbial activity. It is most likely due to localized residual accumulation of organic matter from the duck farms. The location of this accumulation is consistent with the high ammonia values observed at the transect FR1 in the muck layer close to the shores (see sampling points FR1A-a, FR1A-b and FR1D-b in Figure 39).

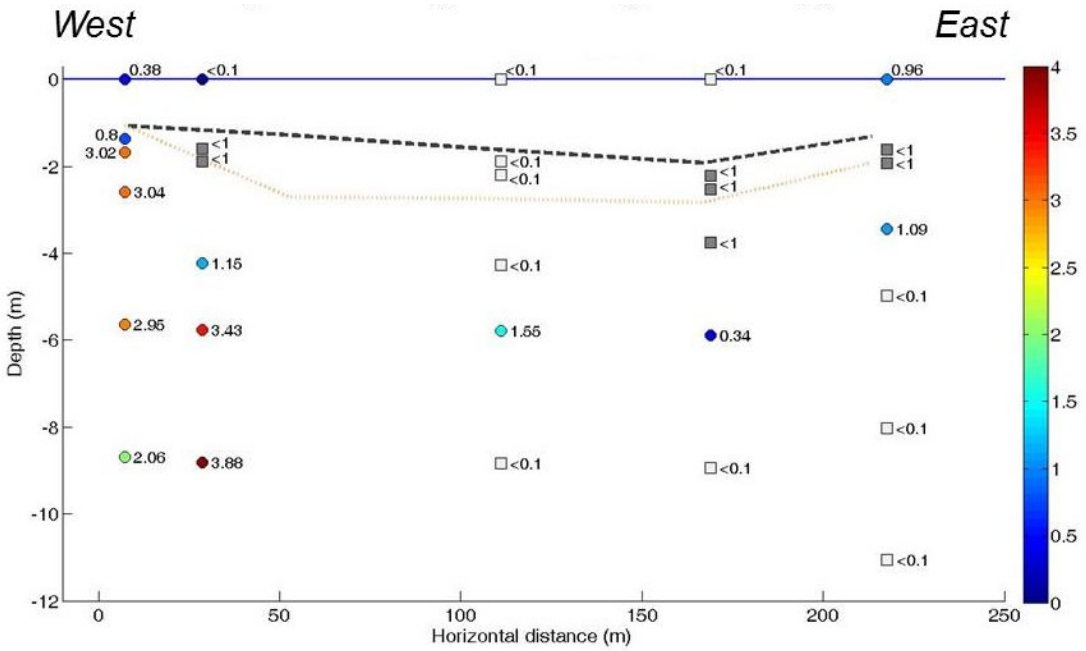

***Figure 43**: Nitrate-Nitrate concentrations (in mg/L) from transect FR2 in Forge River.*

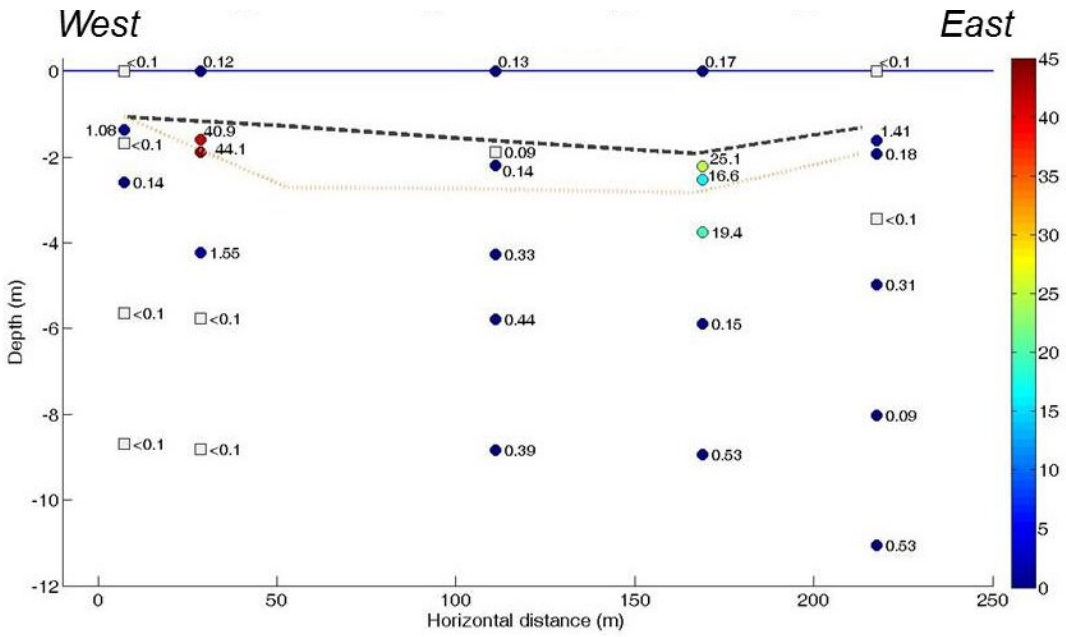

***Figure 44**: Ammonia concentrations (in mg/L) from transect FR2 in Forge River.*

Concentrations of TKN as high as 88 mg/L are found in the same areas as the ammonia accumulation (Figure 45), meaning that ammonium as well as other organic nitrogen species are present in concentrations exceeding 40 mg/L (Figure 44). As previously mentioned, these

elevated concentrations are found in the areas where a lot of organic material is present. The total nitrogen distribution is mostly controlled by the ammonia, ammonium and other organic nitrogen species (Figure 46).

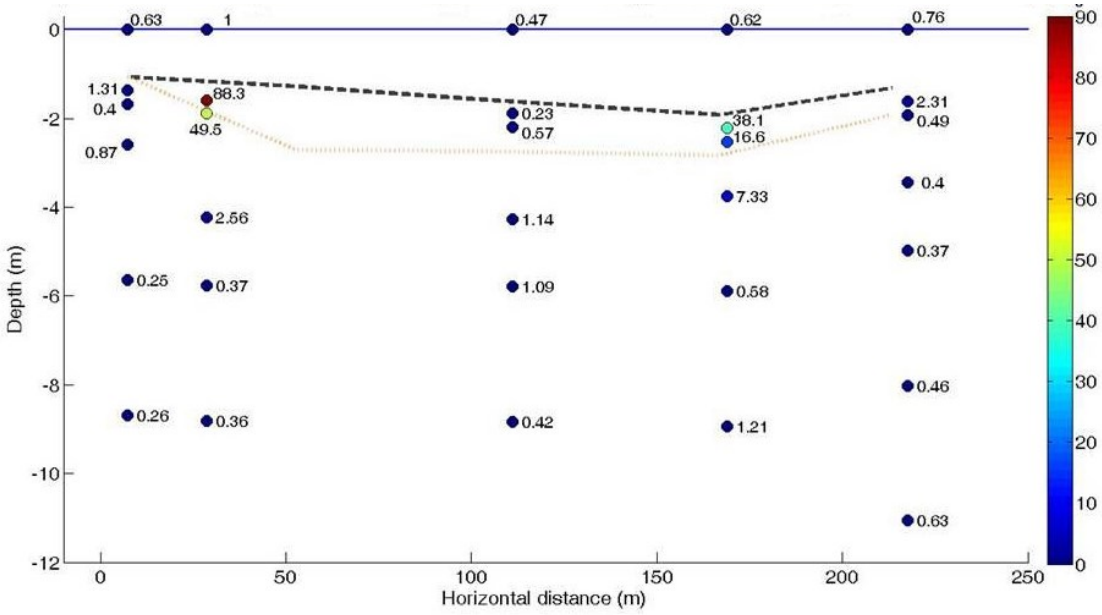

***Figure 45**: TKN (in mg/L) from transect FR2 in Forge River.*

Most of the groundwater within the hyporheic zone appears depleted in dissolved oxygen (Figure 47). Intermediate dissolved oxygen concentrations can be found at depth, in the center of the section. The highest concentrations are found at the interface of the muck/silt layer and co-located with the SGD pulses revealed in the resistivity measurement plots. The dissolved oxygen concentrations in these zones are similar to the values found in groundwater that is the origin of the water in these zones.

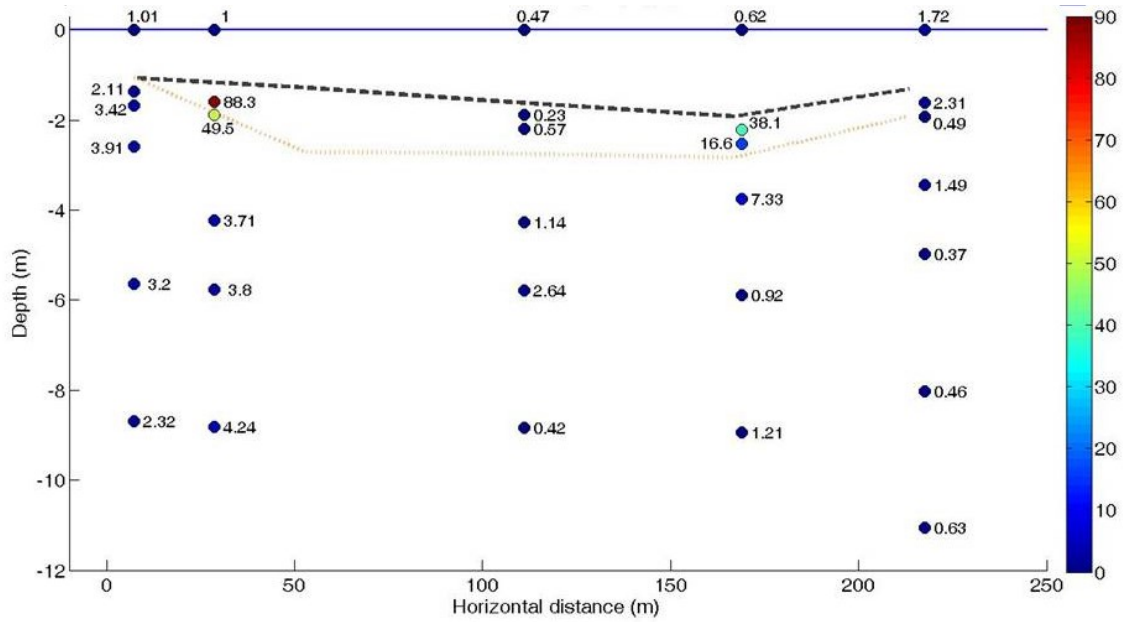

***Figure 46**: Total nitrogen concentrations (in mg/L) from transect FR2 in Forge River.*

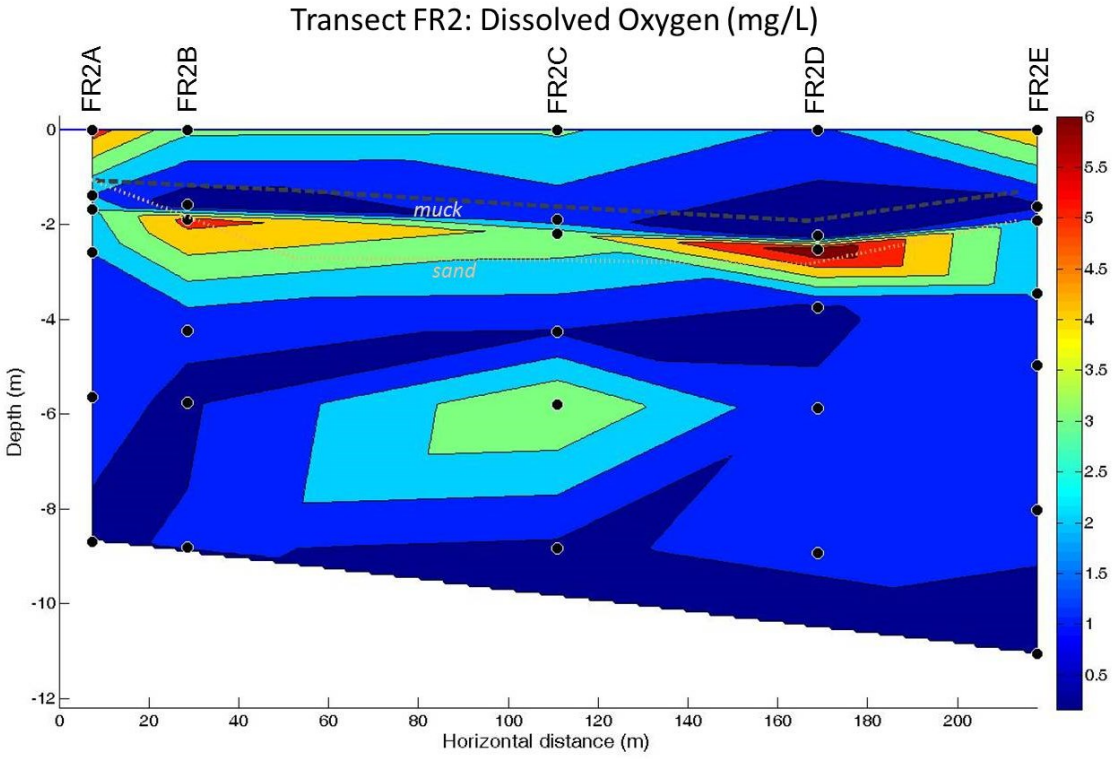

***Figure 47**: Dissolved Oxygen measurements (in mg/L) for transect FR2 in Forge River. The dots indicate the location of the measurements and the colors the interpolated values.*

The mixing process between the fresh groundwater and the salt water at depth can contribute to diluting the nitrate present in groundwater, but since the mixing zone is fairly limited, as indicated by the conductivity data, dilution alone cannot account for the low nitrate concentrations observed. The center freshwater beneath the river is also influenced by the converging of deep and shallow groundwater flow paths, essentially mixing waters with lower and higher nitrogen concentrations. It is likely that several processes occur simultaneously in a zoned manner.

3.4.3 Results of nutrients analysis for inland wells

The nutrients and DO concentrations for the inland wells are plotted in Figure 48. High nitrate concentrations above 7 mg/L are observed in each inland well but they appear to be focused within 8 meters of the ground surface. At depth, nitrate concentrations decrease below 4.5 mg/L. The well RD2 in Wills Creek shows the highest total nitrogen concentrations. The TKN concentrations are low for FR1 and FR2, 1.38 mg/L and under. The well RD2 exhibits slightly higher organic nitrogen concentrations ranging between 1 and 3.1 mg/L. This can be explained by lower DO values. For the inland wells, the total nitrogen concentrations are mostly controlled by the nitrate distribution.

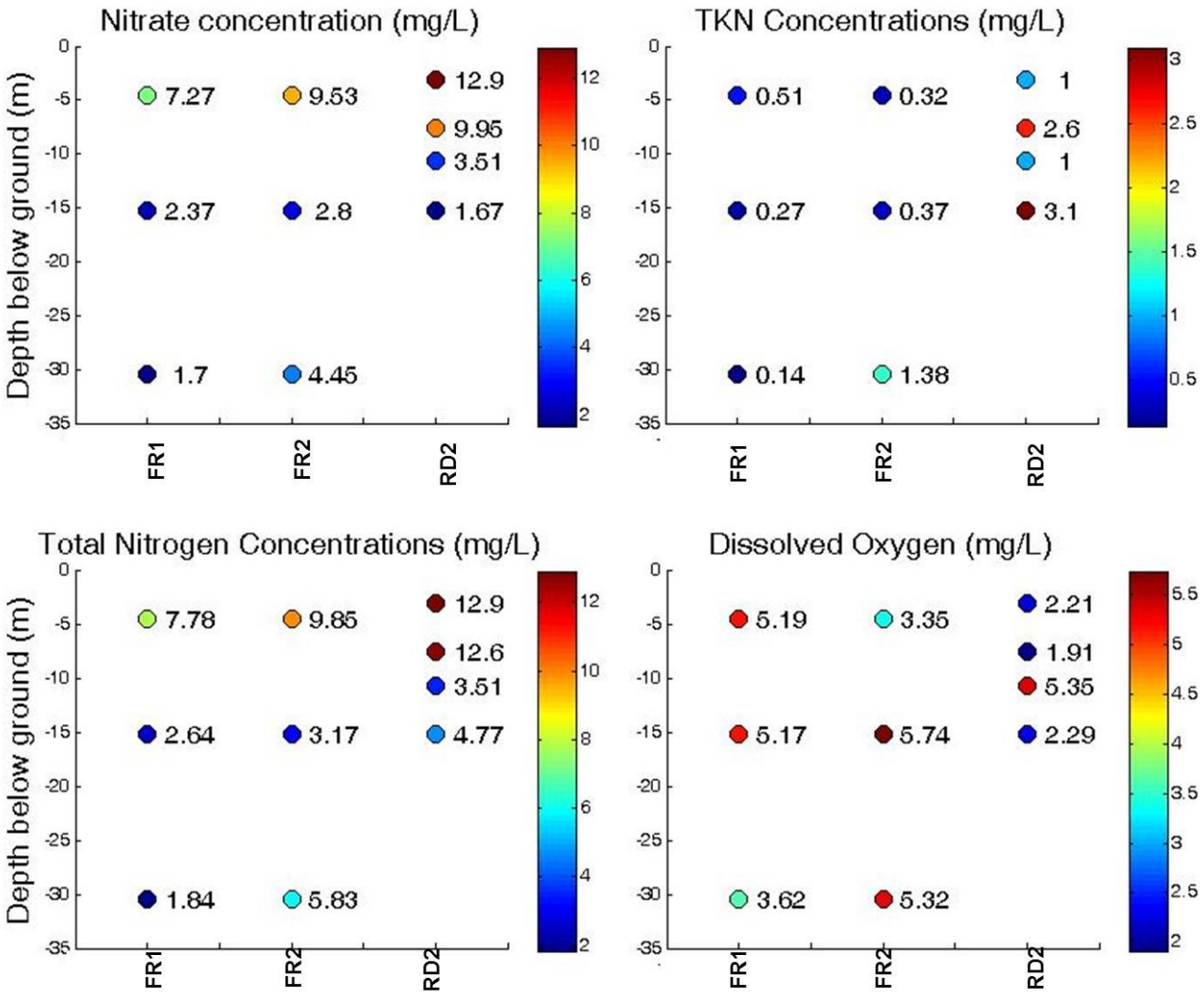

Figure 48*: Nutrients analysis results for the inland wells RD2 in Wills Creek, and FR1 and FR2 at Forge River.*
Note: Ammonia results are not shown as all samples were under the detection limit of 0.1 mg/L.

4. Conclusion

A significant portion of the freshwater flow of Forge River derives from groundwater, which is transporting high concentrations of nutrients from the upland area to the river through SGD. The complex nature of this discharge, its impact on the hyporheic zone and ultimately on the surface waters are challenging to characterize. This study was able to define the most predominant zones of SGD within the river as well as determine the distribution of different nitrogen species and concentrations in these zones. Three distinct zones were identified and exist

in varying degrees along each of the studied sections of the Forge River. The zones are defined as followed:

- Zone 1 is the near shore advective zone observed in all sections. Sediments in these zones are sandy but contain significant organic matter as well as silt. Hydraulically, they are mixing zones with strong SGD present at low tides and significant mixing and bank storage of seawater at high tide. Specific discharges are as high as 59 cm/d. There is also mixing of nitrogen rich groundwater and nitrogen present in organic matter in sediments. Typically, the dissolved oxygen concentration is low allowing potential denitrification. Conservative estimates of relative nitrate concentration attenuation, using sample points without mixing influence (FR1A levels C to E, FR2A levels B to E), indicate nitrate attenuation of up to 24% for F1 and 32% for F2. This zone is the major advective area of the river and where most of groundwater-derived nitrogen enters the river.

- Zone 2 is an area offshore of zone 1 and represents the largest zone. This zone contains sediments rich in organic material and silts that can be as thick as 8 feet. Hydraulically, it is not an area of significant SGD and the nitrogen flux from these sediments is likely to be a diffuse flux of the organic species. In some areas of zone 2, relatively high concentrations of ammonia are detected and are likely due to ammonification of the organic nitrogen rather than related to groundwater input. The sandy area beneath the organic/silty area is typically low in nitrogen and dissolved oxygen (less than 2 mg/l). This suggests that there may be some denitrification occurring. Zone 2 in FR1 and FR2 shows evidence of denitrification in the low portions of the organic muck layer. Maximum nitrate attenuation is approximately 45% for FR1 and 70% for FR2. The deeper portion of zone 2 shows low concentrations of nitrates which likely results from dilution of shallow porewater by deeper groundwater flow paths that contain lower nitrogen concentrations.

- Zone 3 is located in the central section of the river and contains highly fluidized sediments of organic matter and silts. Hydraulically, this area has SGD upwelling present. Upwelling areas are preferential flow paths that were likely formed through dredging or erosion of the bottom confining sediments. The flux of nitrogen as nitrate in this area is low in concentration and in most cases under the detection limit of laboratory analyses. The nitrogen present is usually low level of organic forms and the levels of dissolved oxygen are low

suggesting denitrification and again are areas where deep and shallow flow paths converge and mix.

The major contributor of nitrogen to the river appears to be focused in zone 1 areas and, in some instances, along zone 2 in the organic forms. Zone 3 is an advective zone but the flux of nitrogen is very low. These fluxes are temporally and spatially variable. The magnitude and extent of these three zones are constantly changing but their existence and basic characteristics will likely persist. This study emphasizes the complexity of processes occurring within the hyporheic zone in Forge River. The estimates of nitrate concentration attenuation given here are only preliminary values. The multiple nitrogen species found and their distribution demonstrate the high complexity of biogeochemical reactions taking place in the hyporheic zone at Forge River. Sediment incubation experiments would provide valuable information regarding the kind of micro-organisms involved. Nitrogen gas measurements would also enable more accurate quantification of denitrification in each zone.

The hydraulic changes from seasonal changes in groundwater gradients, tidal fluctuations and the porosity variations within the bottom sediments contribute to SGD high variability. The same can be said for the chemical analysis of the pore fluids within the hyporheic zone. Various forms of nitrogen are present, including those present in the organic rich sediments and those entering through groundwater discharge of terrestrial groundwater. Characterizing SGD in Forge River at a given time is, however, possible through an integrated study combining several geophysical and geochemical techniques. The understanding of the various mechanisms at play and the changing inland conditions will require continued detailed efforts of monitoring in order to evaluate the impact of remediation of groundwater inland.

Table 3: Summary of zone characteristics at three locations studied.

Zone	Characteristics	Forge FR1	Forge FR2	Wills RD2
Zone 1	Extent (m)	0-15	0-20	0-7
	SGD	high	high	high
	Nitrogen flux (nitrate/organic)	High /Low	High /Low	Medium/Low
	Denitrification	Nitrate medium ~24.5%	Nitrate high ~ 32%	Nitrate medium ~30%
Zone 2	Extent (m)	15-100, 110-130	20-100, 130-200	7-70
	SGD	Very low	Very low	Very low
	Nitrogen flux (nitrate/organic)	Low/Low	Low/High	Low/Low
	Denitrification Ammonification	Ammonification present	Ammonification present	Ammonification present
Zone 3	Extent (m)	100-110	100-130	Not present
	SGD	Low	Low	
	Nitrogen flux (nitrate/organic)	Low/low	Low/low	
	Denitrification	Low	Low	

Note: Levels of estimates for denitrification: low 0-10%, medium 10-30% and high 30-100%.

References

Aller, R. C., C. J. Gobler, and B. J. Brownawell (2009), Data report on benthic flux studies and the effect of organic matter remineralization in sediments on nitrogen and oxygen cycling in the Forge River, New York: Task #1 and 2. Prepared for Suffolk County Department of Health Services, *Report*, 62 pp.

Brownawell, B., D. Wang, J. Ruggieri, S. Sañudo-Wilhelmy, and R. L. Swanson (2009), Sediment Quality Characterization for the Forge River, Long Island*Rep.*, 21 pp, Prepared for the Town of Brookhaven.

Burson, A. M., S. C. Talmage, and C. T. Gobler (2008), Linking the dynamics of nutrient cycling and primary producers to hypoxia in Forge River, Mastic, NY, in *SCERP Environmental Symposium*, edited, Stony Brook- Southampton, NY, USA.

Cameron Engineering and Associates (2012), Forge river management plan, LLP in association with CH2MHill, prepared for the town of Brookhaven, *Report.*

Chadwick, D. B., J. Groves, C. Smith, and R. Paulsen (2003), Hardware description and sampling protocols for the Trident Probe and UltraSeep systems: Technology to evaluate contamination transfer between groundwater and surface water.*Rep.*, United States Navy, SSC San Diego.

Chadwick, D. B., A. Gordon, J. Groves, C. Smith, R. Paulsen, and B. Harre (2003), New tools for monitoring coastal contaminant migration, *Sea technology*, *44*(6), 17-22.

Durand, J. M., J. Wanlass, N. Stark, R. Paulsen, and T.-f. Wong (2011), Study of submarine groundwater discharge on the west shore of Forge River using electrical resistivivty measurements and seepage meters, paper presented at Geology of Long Island and Metropolitan New York, 18th proceedings, Stony Brook, NY, USA, April 9th 2011.

Johannes, R. (1980), Ecological significance of the submarine discharge of groundwater, *MARINE ECOL.- PROG. SER.*, *3*(4), 365-373.

Koike, I., and A. Hattori (1978), Denitrification and ammonia formation in anaerobic coastal sediments, *Applied and Environmental Microbiology*, *35*(2), 278-282.

Laroche, J., R. Nuzzi, R. Waters, K. Wyman, P. Falkowski, and D. Wallace (1997), Brown Tide blooms in Long Island's coastal waters linked to interannual variability in

Paulsen, R. J., C. F. Smith, D. O'Rourke, and T. F. Wong (2001), Development and evaluation of an ultrasonic ground water seepage meter, *Ground Water*, *39*(6), 904-911.

Paulsen, R. J., C. F. Smith, J. Wanlass, and N. H. Stark (2008), Forge River Groundwater Flow Rate and Nutrient Contaminant Load Site Investigation Draft Report*Rep.*, 67 pp, Suffolk County Department of Health Services.

Payne, W. (1973), Reduction of nitrogenous oxides by microorganisms, *Bacteriological Reviews*, *37*(4), 409.

Ryther, J. H. (1954), The ecology of phytoplankton blooms in Moriches Bay and Great South Bay, Long Island, New York, *The Biological Bulletin*, *106*(2), 198-209.

Wanlass, J. S. (2009), Development of an integrated geophysical and hydrological approach to study submarine ground water discharge into Forge River, Stony Brook University, Stony Brook.

Zektser, I. S., L. G. Everett, and R. G. Dzhamalov (2006), *Submarine groundwater*, CRC Press Inc.

Zumft, W. G. (1997), Cell biology and molecular basis of denitrification, *Microbiology and Molecular Biology Reviews*, *61*(4), 533-616.

Appendices

Appendix 1: Trident values associated with the electrical resistivity surveys at FR1 and FR2 in Forge River.

Site ID	Date	Time	Longitude (deg.)	Latitude (deg.)	Probe				Reference				ΔT (°C)	ΔC (mS/cm)
					Average T (°C)	Stdev. T (°C)	Average C (mS/cm)	Stdev. C (mS/cm)	Average T (°C)	Stdev. T (°C)	Average C (mS/cm)	Stdev. C (mS/cm)		
FR1A_1	4/18/13	11:44:57	-72.831	40.80023	13.102	N/A	33.932	N/A	14.620	N/A	37.204	N/A	-1.518	-3.272
FR1A_2	4/18/13	10:45:30	-72.8309	40.80026	12.742	0.017	41.399	0.074	12.397	0.018	36.078	0.015	0.345	5.321
FR1A_3	4/18/13	11:15:58	-72.8309	40.80028	11.526	0.004	32.624	0.374	11.393	0.003	34.756	0.014	0.133	-2.133
FR1B_2	4/20/13	12:00:14	-72.8305	40.80065	14.165	0.101	8.659	0.018	15.407	0.012	47.948	3.862	-1.242	-39.289
FR1B_1	4/20/13	12:57:07	-72.8304	40.80067	12.838	0.011	6.189	0.127	15.796	0.022	44.126	0.022	1.946	-37.937
FR1B_3	4/20/13	14:37:20	-72.8301	40.80073	14.618	0.017	11.869	0.029	16.864	0.005	36.422	0.606	-2.246	-24.554
FR2A_HT1	4/11/13	9:59:20	-72.8315	40.79848	11.54	0.042	42.63	0.104	14.45	0.003	54.65	0.054	-2.91	-12.02
FR2A_HT2	4/11/13	10:48:53	-72.8313	40.79849	11.26	0.108	41.38	0.215	14.47	0.006	53.32	0.093	-3.21	-11.93
FR2A_HT3	4/11/13	10:36:05	-72.8312	40.7985	11.41	0.009	41.39	0.235	14.75	0.001	52.21	0.117	-3.34	-10.82
FR2A_LT1	4/11/13	15:11:30	-72.8316	40.79848	12.74	0.022	36.06	0.162	16.44	0.008	47.06	0.133	-3.70	-11.00
FR2A_LT2	4/11/13	15:33:28	-72.8314	40.79849	13.06	0.046	29.49	0.192	12.79	0.004	49.01	0.055	0.27	-19.52
FR2A_LT3	4/11/13	16:02:15	-72.8312	40.7985	11.88	N/A	39.55	N/A	16.65	N/A	45.29	N/A	-4.76	-5.74
FR2B1	4/20/13	10:10:44	-72.8304	40.79855	12.40	0.02	14.53	0.027	14.51	0.001	51.47	0.137	-2.06	-46.39
FR2C_1	4/8/13	12:36:59	-72.8294	40.79862	10.76	0.065	54.41	2.169	11.326	0.064	33.252	0.189	-0.566	21.159
FR2C_2	4/8/13	12:59:53	-72.8297	40.79855	10.323	0.023	87.737*	0.508	11.094	0.001	35.788	0.123	-0.771	51.949

Notes:

- * Erroneous values indicative of interactions between the cable and the Trident probe. In the plots, these values are replaced by the conductivity of pore water measured by the YSI probe at the same location. The YSI value is higher than the surface water value measured, which is most likely the result of an increase in fluid temperature due to the friction with the sampling tube during pumping. Where the sediments are extremely muddy it is possible that some surface conduction, due to very fine particles, contributes to enhance the bulk conductivity value.
- $\Delta T = T_{probe} - T_{reference}$ and $\Delta C = C_{probe} - C_{reference}$.
- N/A indicates a missing value due to technical difficulties.

Appendix 2: Trident results associated with the wells for transects FR1 and FR2, in Forge River.

Site ID	Date	Time	Longitude (deg.)	Latitude (deg.)	Probe				Reference				ΔT (°C)	ΔC (mS/cm)
					Average T (°C)	Stdev T (°C)	Average C (mS/cm)	Stdev. C (mS/cm)	Average T (°C)	Stdev T (°C)	Average C (mS/cm)	Stdev. C (mS/cm)		
FR1A	6/25/13	15:37:05	-72.8315	40.80065	18.851	0.001	6.655	0.03	28.491	0.022	27.444	0.617	-9.64	-20.789
FR1B	6/26/13	12:17:07	-72.8314	40.80075	19.436	0.020	7.927	0.033	27.653	0.026	38.249	0.593	-8.218	-30.322
FR1C	6/27/13	14:51:18	-72.8308	40.80093	12.812	0.002	4.804	0.006	17.165	0.002	2.43	0.002	-4.354	2.374
FR1D	7/9/13	11:23:18	-72.8304	40.80091	20.876	0.011	3.919	0.011	29.165	0.007	40.514	0.098	-8.289	-36.595
FR1E	7/9/13	13:10:49	-72.8302	40.8009	19.097	0.007	1.958	0.001	29.884	0.006	17.552	1.218	-10.79	-15.594
FR2A	6/20/13	9:48:14	-72.8316	40.79852	14.846	0.001	0.407	0.001	24.402	0.032	44.665	1.871	-9.556	-44.258
FR2B	6/19/13	11:19:30	-72.8311	40.79855	17.528	0.007	4.363	0.047	23.746	0.020	48.683	0.121	-6.218	-44.320
FR2C	6/24/13	14:54:30	-72.8306	40.79842	16.929	1.511	0.902	0.518	21.442	0.420	6.950	0.070	-4.513	-6.320
FR2D	6/21/13	11:08:27	-72.8298	40.79853	16.103	0.002	2.240	0.027	23.983	0.001	48.311	0.089	-7.880	-46.071
FR2E	6/20/13	12:17:04	-72.8292	40.79862	17.817	0.001	1.786	0.002	23.345	0.023	25.467	1.338	-5.527	-23.681

Notes:

- The name of a Trident station is built as follow: FR1/2 indicates the transect number, the letter A-E the associated well.
- C and T refer to conductivity and temperature, respectively.
- $\Delta T = T_{probe} - T_{reference}$, and $\Delta C = C_{probe} - C_{reference}$.

Appendix 3: Piezometer wells description at FR1 and FR2, in Forge River.

Wells	Latitude (deg.) N	Longitude (deg.) W	Date sampled	Well and level description
FR2-land	40.798358	72.83198	1/16/13	S: shallow (15') / M: medium (50') D: deep (100')
FR1-land	40.800538	72.83182	7/16/13	
FR2A	40.79852	72.83163	6/20/13	a: (1') into muck or sand layer b: (2') into muck or sand layer c: (5') below top of sand layer d: (10') below top of sand layer e: (20') below top of sand layer
FR2B	40.79855	72.8311	6/19/13	
FR2C	40.798531	72.83046	6/24/13	
FR2D	40.79855	72.82975	6/21/13	
FR2E	40.79862	72.8292	6/20/13	
FR1A	40.800636	72.83147	6/25/13	
FR1B	40.80075	72.83135	6/26/13	
FR1C	40.0093	72.83082	6/27/13	
FR1D	40.800914	72.83017	7/9/13	
FR1E	40.800892	72.83036	7/9/13	

Appendix 4: Results of pore water analysis for transect FR1 in Forge River.

Transect FR1	***Laboratory analysis***				***Field parameters***						
Forge River water quality data	**Nitrate-nitrite**	**Ammonia**	**Total Nitrogen**	**TNK**	**Temperature**	**Conductivity**	**Salinity**	**DO**	**DO**	**pH**	**ORP**
Sample	(mg/L)	(mg/L)	(mg/L)	(mg/L)	(°C)	(mS/cm)		(%)	(mg/L)		(mV)
FR1A-a	<1.00	14.2	15.7	15.7	30.15	35.58	22.3	14.3	0.94	7.22	-392.8
FR1A-b	<0.1	20.4	28.4	28.4	35.39	14.52	8.29	67.1	4.44	6.85	-396.6
FR1A-c	8.16	<0.1	8.16	<0.1	24.05	1.35	0.67	39.1	3.24	6.08	-242.4
FR1A-d	9.85	<0.1	9.85	<0.1	24.43	0.421	0.2	38	3.09	5.75	-186.5
FR1A-e	10.8	<0.1	11	0.15	22.18	0.377	0.18	34.4	2.97	5.69	-141.1
FR1A-s	0.49	<0.1	1.86	1.37	29.05	25.9	15.73	81.8	5.68	7.78	-84.1
FR1B-a	<1.00	7.96	9.54	9.54	27.45	20.12	11.96	55.5	4.06	6.88	-330.4
FR1B-b	<1.00	8.1	9.75	9.75	28.83	6.016	3.25	62.7	4.75	6.77	-340.1
FR1B-c	5.83	0.23	6.68	0.85	23.17	0.59	0.29	62.8	5.34	6.06	-198.2
FR1B-d	8.49	0.16	8.49	<0.1	23.56	0.358	0.17	65.9	5.57	5.77	-111.5
FR1B-e	10.6	0.16	10.6	<0.1	23.25	0.449	0.22	36	3.05	6.13	-93.8
FR1B-s	<0.1	<0.1	0.79	0.79	28.35	39.63	25.19	71.9	4.83	7.91	-52.9
FR1C-a	<0.1	0.78	2.13	2.13	27.36	10.53	5.93	40.9	3.08	6.67	-101.2
FR1C-b	<0.1	0.25	2.29	2.29	29.43	1.362	0.67	36.5	2.81	6.87	-52.7
FR1C-c	<0.1	0.25	6.75	6.75	22.26	1.798	0.91	23	2	6.39	-29.6
FR1C-d	<0.1	0.13	0.44	0.44	21.89	0.203	0.1	15.4	1.34	6.45	-35
FR1C-e	<0.1	0.18	0.67	0.67	24.40	2.14	1.10	25.21	2.08	7.03	-74.42
FR1C-s	<0.1	<0.1	1.28	1.28	27.46	35.65	22.42	70.9	4.94	7.95	10.3
FR1D-a	<2.00	9.73	11	11	32.01	28.01	17.09	14.5	0.95	6.93	-305.6
FR1D-b	<2.00	11.5	12.6	12.6	26.29	3.051	1.58	22.4	1.76	6.93	-179.9
FR1D-c	<0.1	1.13	2.47	2.47	29.99	1.416	0.7	22.8	1.71	6.77	-148.5
FR1D-d	<0.1	<0.1	0.37	0.37	25.09	0.494	0.24	28.7	2.32	7.39	-107.7
FR1D-e	0.1	0.12	1.46	1.36	24.62	2.461	1.27	23.2	1.9	7.2	-70.8
FR1D-s	<0.5	0.1	1.19	1.19	29.81	39.42	25	58.7	3.85	7.65	-41.6
FR1E-a	<1.00	0.98	1.64	1.64	28.03	26.63	16.24	27.2	1.92	6.33	-155.1
FR1E-b	<1.00	0.15	0.45	0.45	27.68	5.532	2.97	32.2	2.49	6.14	-32.2
FR1E-c	0.74	0.23	1.26	0.52	26.2	4.891	2.61	47.3	3.7	6.5	-50
FR1E-d	0.52	<0.1	0.52	<0.1	25.35	1.612	0.81	38.6	3.12	6.68	-25.6
FR1E-e	0.67	<0.1	0.92	0.25	23.06	2.723	1.41	38.6	3.26	6.43	-14.9
FR1E-f	<0.1	<0.1	0.33	0.33	24.18	0.867	0.42	5.8	0.47	7.77	-76.3
FR1E-s	0.51	0.18	1.62	1.11	29.58	21.98	13.13	100	7.05	7.83	-7.6
FR1S	7.27	<0.1	7.78	0.51	18.25	0.184	0.09	55.9	5.19	5.38	48.7
FR1M	2.37	<0.1	2.64	0.27	16.32	0.156	0.07	53.6	5.17	5.92	38.9
FR1D	1.7	<0.1	1.84	0.14	14.6	0.147	0.07	36.9	3.62	5.64	41.5

Appendix 5: Results of pore water analysis for transect FR2 in Forge River.

Transect FR2	***Laboratory analysis***				***Field parameters***						
Forge River water quality data	**Nitrate-nitrite**	**Ammonia**	**Total Nitrogen**	**TNK**	**Temperature**	**Conductivity**	**Salinity**	**DO**	**DO**	**pH**	**ORP**
Sample	(mg/L)	(mg/L)	(mg/L)	(mg/L)	(°C)	(mS/cm)		(%)	(mg/L)		(mV)
FR2A-a	0.8	1.08	2.11	1.31	24.75	20.72	12.39	26.2	2	5.94	8.4
FR2A-b	3.02	<0.1	3.42	0.4	23.73	1.989	1.01	34	2.85	5.9	49.1
FR2A-c	3.04	0.14	3.91	0.87	23.91	5.062	2.72	24.8	2.03	5.78	60.5
FR2A-d	2.95	<0.1	3.2	0.25	20.24	0.439	0.21	13.4	1.22	5.8	51.7
FR2A-e	2.06	<0.1	2.32	0.26	19.57	0.369	0.18	9.6	0.87	5.78	55.6
FR2A-s	0.38	<0.1	1.01	0.63	24.41	33.19	20.78	74.4	5.51	7.2	49.7
FR2B-a	<1.00	40.9	88.3	88.3	26.42	35.9	22.61	4.1	0.3	7.02	-374
FR2B-b	<1.00	44.1	49.5	49.5	27.93	8.045	4.44	66.9	5.36	7.12	-342.6
FR2B-c	1.15	1.55	3.71	2.56	21.76	7.16	3.93	13.9	1.11	6.13	-80
FR2B-d	3.43	<0.1	3.8	0.37	21.68	1.92	0.98	10	0.87	5.99	-30
FR2B-e	3.88	<0.1	4.24	0.36	20.24	0.431	0.21	11.4	1.09	6.12	-35
FR2B-s	<0.1	0.12	1	1	24.61	43.86	28.29	45.5	3.21	7.35	-45.7
FR2C-a	<0.1	<0.1	0.23	0.23	28.43	0.371	0.18	16.9	1.3	6.46	4.4
FR2C-b	<0.1	0.14	0.57	0.57	27.21	2.624	1.34	51.4	3.68	7.64	3.1
FR2C-c	<0.1	0.33	1.14	1.14	27.12	2.869	1.48	12	0.94	6.52	12.6
FR2C-d	1.55	0.44	2.64	1.09	25.31	27.77	17.06	54	4.03	6.89	-211.4
FR2C-e	<0.1	0.39	0.42	0.42	26.58	41.78	26.75	11.3	0.79	7.14	-129.7
FR2C-s	<0.1	0.13	0.47	0.47	32.18	44.66	28.37	60.1	3.14	7.69	-10.7
FR2D-a	<1.00	25.1	38.1	38.1	28.79	22.68	13.61	2.1	0.14	7.43	-400.8
FR2D-b	<1.00	16.6	16.6	16.6	27.1	7.369	4.51	88.8	6.85	7.76	-278.1
FR2D-c	<1.00	19.4	7.33	7.33	24.5	5.899	3.2	10.9	0.86	6.95	-312.9
FR2D-d	0.34	0.15	0.92	0.58	21.43	9.855	5.56	13.4	1.1	6.66	-248.1
FR2D-e	<0.1	0.53	1.21	1.21	23.44	30.9	19.21	18.8	1.4	6.89	-221.3
FR2D-s	<0.1	0.17	0.62	0.62	24.63	11.04	28.42	25.3	1.79	7.15	-192.7
FR2E-a	<1.00	1.41	2.31	2.31	24.19	38.03	24.15	11.6	0.84	7.01	-218.3
FR2E-b	<1.00	0.18	0.49	0.49	23.18	5.847	3.17	27.1	2.26	6.81	-130.1
FR2E-c	1.09	<0.1	1.49	0.4	24.62	6.363	3.47	25.4	2.06	6.82	-14.1
FR2E-d	<0.1	0.31	0.37	0.37	22.49	3.693	1.95	18.4	1.56	6.73	2.5
FR2E-e	<0.1	<0.1	0.46	0.46	20.84	5.803	3.16	17	1.49	6.63	-5.4
FR2E-f	<0.1	0.53	0.63	0.63	21.53	22.51	13.6	3	0.24	7.35	-141.5
FR2E-s	0.96	<0.1	1.72	0.76	24.37	20.57	12.29	62.5	4.87	7.07	16.1
FR2S	9.53	<0.1	9.85	0.32	17.73	0.268	0.13	35.9	3.35	4.6	77.7
FR2M	2.8	<0.1	3.17	0.37	15.72	0.172	0.08	60.3	5.74	5.95	41.9
FR2D	4.45	<0.1	5.83	1.38	16.12	0.723	0.35	55.2	5.32	5.97	40.1

Chapter 6: Conclusion and path forward

Conclusion

Spatio-temporal variations of submarine groundwater discharge (SGD) were investigated using a suite of geophysical techniques. SGD distribution was characterized at the embayment scale in Stony Brook Harbor, NY, a tidally-dominated low-energy environment with active mud sedimentation. Numerical modelling simulations were utilized to verify the observed field measurements in Stony Brook Harbor. Temporal variations of SGD in the intertidal zone were investigated over a semi-diurnal tidal cycle in a partially confined sandy aquifer at West Neck Bay, Shelter Island, NY. Finally, the relationship between nutrient fluxes and SGD were studied at multiple locations along a contaminated tidal river, Forge River, NY.

To address the high spatial variability of SGD [*Michael et al.*, 2005], we used an integrated approach combining three or more hydrogeophysical methods [*Burnett et al.*, 2006]. Electrical resistivity (ER) surveys procured high spatial resolution 2D vertical cross-sections of conductivity distribution, used as a proxy for salinity [*Swarzenski et al.*, 2007; *Swarzenski et al.*, 2004]. Repeated over-time, ER surveys also delivered high temporal resolution images. A hand-push conductivity and temperature (C/T) probe served to screen large areas by providing point measurements used to identify zones of potentially fresh SGD, but also to obtain independent measurements and verify the results of ER surveys [*Chadwick et al.*, 2003]. Direct flow rate measurements were collected using both ultrasonic [*Paulsen et al.*, 2001] and manual [*Lee*, 1977] seepage meters, which allowed a high resolution investigation of tidally-driven SGD variations. When possible, pore water samples were collected through piezometers to provide *in situ* salinities and nutrients concentrations [*Charette and Allen*, 2006]. Finally, 2D density-dependent steady-state numerical models of 2 contrasting sites in Stony Brook Harbor were developed [*Guo and Langevin*, 2002; *Zheng and Wang*, 1999b].

Major conclusions of this thesis are summarized below:

1) My integrated approach using a direct-push probe ER surveys, C/T and seepage point measurements, and porewater analyses was successful in identifying SGD spatio-temporal variations at different scales and in various settings. Comparison between

methods revealed good agreement; *in situ* porewater conductivities confirmed the reliability of ER surveys as a useful tool for studies in coastal environments.

2) Active deposition of low permeability mud sediments in low-energy coastal environments has a significant impact on SGD distribution, as observed in Stony Brook Harbor, NY. The mud layer acts as a cap: it restricts SGD at the shoreline, prevents mixing with seawater and channels a significant volume of freshwater offshore. Areas without mud show enhanced SGD and mixing with the overlying seawater. SGD volume through the mud cap is estimated to reach approximately 30% of SGD discharged at the shoreline. The numerical models developed for two contrasting sites were in agreement with field observations made in Stony Brook Harbor. The models show that a 50 cm thick mud layer with a hydraulic conductivity of 0.01 m/d can significantly alter the groundwater flow pattern, mixing between ground and surface waters and salinity distribution at depth. Investigating the presence and characteristics of such a layer prior to SGD studies in similar environments is necessary before any attempt of SGD estimates at a regional scale.
3) Time-lapse ER surveys revealed important horizontal and vertical variations in groundwater conductivities, which suggest a dynamic salinity distribution in the intertidal zone. This disagrees with standard published numerical models for unconfined isotropic homogeneous aquifers and therefore illustrates the need for more specific numerical models [*Robinson et al.*, 2007b]. At Shelter Island, the ER cross-sections did not provide evidence of the existence of a suggested confining unit [*Stieglitz et al.*, 2007], yet high SGD rates found in the intertidal zone are in favor of a partially confined aquifer. The temporal variability of conductivity distribution at depth, however, disagrees with the presence of a continuous low permeability unit at depth.
4) At Forge River, three zones were identified and characterized in terms of flow rate, porewater conductivity and porewater nitrogen concentrations. The first zone, composed of near shore sandy areas exhibited high SGD and important mixing with saline surface water; this zone also constituted the major area of nitrate input to the river. The second zone included areas covered by low permeability silty and organic-rich sediments which had very low SGD rates and limited mixing. Slower seepage rates were associated with higher denitrification and diffusive nitrogen fluxes. The last zone encompassed highly

fluidized silty and organic-rich sediments located in the center of the river where fresh groundwater upwelling was observed. The low nitrogen concentrations measured in this zone were the result of dilution and mixing with water of longer flow paths. The third zone is the result of anthropogenic activity, primarily dredging, that disturbed the low-permeability silt layer and modified SGD by creating preferential flow paths in the center of the river.

Path forward

The findings described in this work raised questions about certain aspects of SGD that could benefit from further investigation. Suggested directions about future research are presented below.

1) Fine particle low-permeability sediments are common in low-energy environment [*Bratton et al.*, 2007]. Studies have emphasized the role of geologic heterogeneities [*Russoniello et al.*, 2013] and sediment compressibility [*Gardner and Wilson*, 2006] on SGD; however, there is still a paucity of data regarding the influence of active sedimentation on SGD. The development a set of comparative density-difference transient models including tidal forcing would enable researchers to determine which conditions, i.e. combination of thickness and hydraulic conductivity, would significantly affect SGD distribution in such settings. These models, coupled with particle-tracking algorithms, could also provide valuable information on flow paths and residence times which impact chemical budgets [*Kuan et al.*, 2012].
2) Embayments are common on the USA Atlantic coast and elsewhere in the world and account for a significant portion of the coast. Curved shorelines have been shown to focus hydraulic gradients and enhance groundwater flow in lake settings [*Mc Bride and Pfannkuch*, 1975]. Development of 3D models that combine the effect of a concave shoreline and density-driven phenomena would highlight the fundamental differences between discharge processes and composition in coastal embayments compared to straight ocean shorelines and would therefore contribute to improved chemical mass balances at regional scale.

3) The highly variable and widely distributed occurrence of SGD has hindered accurate large scale mass balances. An integrated approach that combines modeling, regional field data, such as thermal infrared remote sensing techniques, and ground-truthing detailed field measurements would provide an excellent framework to better locate and quantify SGD on a regional scale [*Johnson et al.*, 2008; *Kelly et al.*, 2013].

References

Bratton, J. F., W. Sanford, C. Langevin, M. Polemio, and P. Povinec (2007), The importance of shallow confining units to submarine groundwater flow, paper presented at Proceedings of the Symposium" A New Focus on Groundwater-Seawater Interactions" at the 24th General Assembly of the International Union of Geodesy and Geophysics, Perugia, Italy, 2-13 July 2007., IAHS Press.

Burnett, W. C., et al. (2006), Quantifying submarine groundwater discharge in the coastal zone via multiple methods, *Science of the Total Environment*, *367*(2-3), 498-543.

Chadwick, D. B., A. Gordon, J. Groves, C. Smith, R. Paulsen, and B. Harre (2003), New tools for monitoring coastal contaminant migration, *Sea technology*, *44*(6), 17-22.

Charette, M. A., and M. C. Allen (2006), Precision Ground Water Sampling in Coastal Aquifers Using a Direct-Push, Shielded-Screen Well-Point System, *Ground Water Monitoring & Remediation*, *26*(2), 87-93.

Gardner, L. R., and A. M. Wilson (2006), Comparison of four numerical models for simulating seepage from salt marsh sediments, *Estuarine, Coastal and Shelf Science*, *69*(3), 427-437.

Guo, W., and C. D. Langevin (2002), *User's Guide to SEWAT: A Computer Program for Simulation of Three-Dimensional Variable-Density Ground-Water Flow*, United States Geological Survey.

Johnson, A. G., C. R. Glenn, W. C. Burnett, R. N. Peterson, and P. G. Lucey (2008), Aerial infrared imaging reveals large nutrient-rich groundwater inputs to the ocean, *Geophysical Research Letters*, *35*(15), L15606.

Kelly, J. L., C. R. Glenn, and P. G. Lucey (2013), High-resolution aerial infrared mapping of groundwater discharge to the coastal ocean, *Limnol. Oceanogr.: Methods*, *11*, 262-277.

Kuan, W. K., G. Jin, P. Xin, C. Robinson, B. Gibbes, and L. Li (2012), Tidal influence on seawater intrusion in unconfined coastal aquifers, *Water Resources Research*, *48*(2), W02502.

Lee, D. R. (1977), A device for measuring seepage flux in lakes and estuaries, *Limnology and Oceanography*, 140-147.

Mc Bride, M. S., and H. O. Pfannkuch (1975), The distribution of seepage within lakebeds, *Jounral of Research of U.S. Geological Survey*, *3*(5), 8.

Michael, H. A., A. E. Mulligan, and C. F. Harvey (2005), Seasonal oscillations in water exchange between aquifers and the coastal ocean, *Nature*, *436*(7054), 1145-1148.

Paulsen, R. J., C. F. Smith, D. O'Rourke, and T. F. Wong (2001), Development and evaluation of an ultrasonic ground water seepage meter, *Ground Water*, *39*(6), 904-911.

Robinson, C., L. Li, and H. Prommer (2007a), Tide-induced recirculation across the aquifer-ocean interface, *Water Resources Research*, *43*(7), W07428.

Russoniello, C. J., C. Fernandez, J. F. Bratton, J. F. Banaszak, D. E. Krantz, A. S. Andres, L. F. Konikow, and H. A. Michael (2013), Geologic effects on groundwater salinity and discharge into an estuary, *Journal of Hydrology*, *498*, 1-12.

Stieglitz, T. C., J. Rapaglia, and S. C. Krupa (2007), An effect of pier pilings on nearshore submarine groundwater discharge from a (partially) confined aquifer, *Estuaries and coasts*, *30*(3), 543-550.

Swarzenski, P. W., F. W. Simonds, A. J. Paulson, S. Kruse, and C. Reich (2007), Geochemical and geophysical examination of submarine groundwater discharge and associated nutrient loading estimates into Lynch Cove, Hood Canal, WA, *Environmental Science & Technology*, *41*(20), 7022-7029.

Swarzenski, P. W., W. Burnett, C. Reich, H. Dulaiova, R. Peterson, and J. Meunier (2004), Novel geophysical and geochemical techniques used to study submarine groundwater discharge in Biscayne Bay, Florida.

Zheng, C., and P. P. Wang (1999b), MT3DMS: a modular three-dimensional multispecies transport model for simulation of advection, dispersion, and chemical reactions of contaminants in groundwater systems; documentation and user's guide*Rep.*, DTIC Document.

List of References

AGI (2009), Instruction Manual for EarthImager 2D, Version 2.4.0, Resistivity and IP Iversion Software, Austin, Texas*Rep.*

Aller, R. C., C. J. Gobler, and B. J. Brownawell (2009), Data report on benthic flux studies and the effect of organic matter remineralization in sediments on nitrogen and oxygen cycling in the Forge River, New York: Task #1 and 2. Prepared for Suffolk County Department of Health Services*Rep.*, 62 pp.

Anderson, M. P. (2005), Heat as a ground water tracer, *Groundwater*, *43*(6), 951-968.

Anderson, W. P., and R. E. Emanuel (2010), Effect of interannual climate oscillations on rates of submarine groundwater discharge, *Water Resources Research*, *46*(5).

Anonymous (2002), Submarine Groundwater discharge assessment intercomparison experiment, International Hydrological Program (IHP), Scientific Commitee on Oceanic Research (SCOR), Land OCean Interactions in the Coastal Zone (LOICZ). *Rep.*, 26 pp

Archie, G. (1942), The electrical resistivity log as an aid in determining some reservoir characteristics, *Trans. AIME*, *146*(99), 54-62.

Ataie-Ashtiani, B., R. Volker, and D. Lockington (1999), Tidal effects on sea water intrusion in unconfined aquifers, *Journal of Hydrology*, *216*(1-2), 17-31.

Badon-Ghyben, W. (1888), Notes on the probable results of well drilling near Amsterdam, *Tijdschrift van het Koninklijk Inst. van Ing. Den Haag*, 21.

Bear, J. (1999), *Seawater intrusion in coastal aquifers: Concepts, methods, and practices*, Springer Netherlands.

Beck, A. J., J. P. Rapaglia, J. K. Cochran, and H. J. Bokuniewicz (2007a), Radium mass-balance in Jamaica Bay, NY: Evidence for a substantial flux of submarine groundwater, *Marine Chemistry*, *106*(3), 419-441.

Beck, A. J., Y. Tsukamoto, A. Tovar-Sanchez, M. Huerta-Diaz, H. J. Bokuniewicz, and S. A. Sañudo-Wilhelmy (2007b), Importance of geochemical transformations in determining submarine groundwater discharge-derived trace metal and nutrient fluxes, *Applied Geochemistry*, *22*(2), 477-490.

Befus, K. M., M. B. Cardenas, D. V. Erler, I. R. Santos, and B. D. Eyre (2013), Heat transport dynamics at a sandy intertidal zone, *Water Resources Research*, *49*(6), 3770-3786.

Bokuniewicz, H. (1980), Groundwater seepage into Great South Bay, New York, *Estuarine and Coastal Marine Science*, *10*(4), 437-444.

Bokuniewicz, H., M. Taniguchi, T. Ishitoibi, M. Charette, M. Allen, and E. A. Kontar (2008), Direct measurements of submarine groundwater discharge (SGD) over a fractured rock aquifer in Flamengo Bay Brazil, *Estuarine Coastal and Shelf Science*, *76*(3), 466-472.

Bratton, J. F. (2010), The three scales of submarine groundwater flow and discharge across passive continental margins, *The Journal of Geology*, *118*(5), 565-575.

Bratton, J. F., S. M. Colman, E. R. Thieler, and R. R. Seal (2002), Birth of the modern Chesapeake Bay estuary between 7.4 and 8.2 ka and implications for global sea-level rise, *Geo-Marine Letters*, *22*(4), 188-197.

Bratton, J. F., J. K. Böhlke, F. T. Manheim, and D. E. Krantz (2004), Ground Water Beneath Coastal Bays of the Delmarva Peninsula: Ages and Nutrients, *Ground Water*, *42*(7), 1021-1034.

Bratton, J. F., W. Sanford, C. Langevin, M. Polemio, and P. Povinec (2007), The importance of shallow confining units to submarine groundwater flow, paper presented at Proceedings of the Symposium" A New Focus on Groundwater-Seawater Interactions" at the 24th General Assembly of the International Union of Geodesy and Geophysics, Perugia, Italy, 2-13 July 2007., IAHS Press.

Bugna, G. C., J. P. Chanton, J. E. Cable, W. C. Burnett, and P. H. Cable (1996), The importance of groundwater discharge to the methane budgets of nearshore and continental shelf waters of the northeastern Gulf of Mexico, *Geochimica et Cosmochimica Acta*, *60*(23), 4735-4746.

Burnett, W. C., H. Bokuniewicz, M. Huettel, W. S. Moore, and M. Taniguchi (2003), Groundwater and pore water inputs to the coastal zone, *Biogeochemistry*, *66*(1-2), 3-33.

Burnett, W. C., et al. (2006), Quantifying submarine groundwater discharge in the coastal zone via multiple methods, *Science of the Total Environment*, *367*(2-3), 498-543.

Burson, A. M., S. C. Talmage, and C. T. Gobler (2008), Linking the dynamics of nutrient cycling and primary producers to hypoxia in Forge River, Mastic, NY, in *SCERP Environmental Symposium*, edited, Stony Brook- Southampton, NY, USA.

Buxton, H. T., and E. Modica (1992), Patterns and rates of ground-water movement on Long Island, New York, *Ground Water*, *V. 30*(No. 6), p. 857-866.

Cable, J. E., J. B. Martin, and J. Jaeger (2006), Exonerating Bernoulli? On evaluating the physical and biological processes affecting marine seepage meter measurements, *Limnology and Oceanography: Methods*, *4*, 172-183.

Cameron Engineering and Associates (2012), Forge river management plan, LLP in association with CH2MHill, prepared for the town of Brookhaven, *Report.*

Chadwick, D. B., J. Groves, C. Smith, and R. Paulsen (2003), Hardware description and sampling protocols for the Trident Probe and UltraSeep systems: Technology to evaluate contamination transfer between groundwater and surface water.*Rep.*, United States Navy, SSC San Diego.

Chadwick, D. B., A. Gordon, J. Groves, C. Smith, R. Paulsen, and B. Harre (2003), New tools for monitoring coastal contaminant migration, *Sea technology*, *44*(6), 17-22.

Charette, M., W. Moore, and W. Burnett (2008), Uranium-and thorium-series nuclides as tracers of submarine groundwater discharge, *U-Th series nuclides in aquatic systems. Elsevier*, 155-191.

Charette, M. A., and K. O. Buesseler (2004), Submarine groundwater discharge of nutrients and copper to an urban subestuary of Chesapeake Bay (Elizabeth River), *Limnology and Oceanography*, 376-385.

Charette, M. A., and M. C. Allen (2006), Precision Ground Water Sampling in Coastal Aquifers Using a Direct-Push, Shielded-Screen Well-Point System, *Ground Water Monitoring & Remediation*, *26*(2), 87-93.

Cherkauer, D. S., and P. F. McKereghan (1991), Ground-Water Discharge to Lakes: Focusing in Embayments, *Ground Water*, *29*(1), 72-80.

Constable, S. C., R. L. Parker, and C. G. Constable (1987), Occam's inversion: A practical algorithm for generating smooth models from electromagnetic sounding data, *Geophysics*, *52*(3), 289-300.

Cooper Jr, H. H. (1959), A hypothesis concerning the dynamic balance of fresh water and salt water in a coastal aquifer, *Journal of Geophysical Research*, *64*(4), 461-467.

Coppens, A. B. (1981), Simple equations for the speed of sound in Neptunian waters, *The Journal of the Acoustical Society of America*, *69*(3), 862-863.

Corbett, D. R., and J. E. Cable (2003), Seepage meters and advective transport in coastal environments: Comments on “Seepage meters and Bernoulli's revenge” by EA Shinn, CD Reich, and TD Hickey. 2002. Estuaries 25: 126–132, *Estuaries and Coasts*, *26*(5), 1383-1387.

Cross, V., D. S. Foster, and J. F. Bratton (2010), Continuous resistivity profiling and seismic-reflection data collected in 2006 from the Potomac River estuary, Virginia and Maryland*Rep.*

Day-Lewis, F., E. White, C. Johnson, J. Lane Jr, and M. Belaval (2006), Continuous resistivity profiling to delineate submarine groundwater discharge--examples and limitations, *The Leading Edge*, *25*(6), 724.

Dimova, N. T., P. W. Swarzenski, H. Dulaiova, and C. R. Glenn (2012), Utilizing multichannel electrical resistivity methods to examine the dynamics of the fresh water–seawater interface in two Hawaiian groundwater systems, *Journal of Geophysical Research*, *117*(C2), C02012.

Dulaiova, H., W. C. Burnett, J. P. Chanton, W. S. Moore, H. Bokuniewicz, M. A. Charette, and E. Sholkovitz (2006), Assessment of groundwater discharges into West Neck Bay, New York, via natural tracers, *Continental Shelf Research*, *26*(16), 1971-1983.

Durand, J. M., and R. Paulsen (2014), Flow Patterns and Nutrient Loading Associated With Submarine Groundwater Discharge in Forge River and Wills Creek*Rep.*, Town of Brookhaven, CDM Smith.

Durand, J. M., J. Wanlass, N. Stark, R. Paulsen, and T.-f. Wong (2011), Study of submarine groundwater discharge on the west shore of Forge River using electrical resistivivty measurements and seepage meters, paper presented at Geology of Long Island and Metropolitan New York, 18th proceedings, Stony Brook, NY, USA, April 9th 2011.

Fetter, C. (2001), Applied Hydrogeology (4 th), edited, New Jersey.

Gardner, L. R., and A. M. Wilson (2006), Comparison of four numerical models for simulating seepage from salt marsh sediments, *Estuarine, Coastal and Shelf Science*, *69*(3), 427-437.

Gibbes, B., C. Robinson, L. Li, and D. Lockington (2007), Measurement of hydrodynamics and pore water chemistry in intertidal groundwater systems, *Journal of Coastal Research, SI*, *50*, 884-894.

Gibbes, B., C. Robinson, L. Li, D. Lockington, and H. Li (2008a), Tidally driven pore water exchange within offshore intertidal sandbanks: Part II numerical simulations, *Estuarine, Coastal and Shelf Science*, *80*(4), 472-482.

Gibbes, B., C. Robinson, H. Carey, L. Li, and D. Lockington (2008b), Tidally driven pore water exchange in offshore intertidal sandbanks: Part I. Field measurements, *Estuarine, Coastal and Shelf Science*, *79*(1), 121-132.

Glover, R. (1959), The pattern of fresh-water flow in a coastal aquifer, *Journal of Geophysical Research*, *64*(4), 457-459.

Gobler, C. J., and S. A. Sañudo-Wilhelmy (2001), Temporal variability of groundwater seepage and brown tide blooms in a Long Island embayment, *Marine Ecology Progress Series*, *217*, 299-309.

Gonneea, M. E., A. E. Mulligan, and M. A. Charette (2013), Climate-driven sea level anomalies modulate coastal groundwater dynamics and discharge, *Geophysical Research Letters*, *40*(11), 2701-2706.

Gross, M. G. (1972), Characteristics and environmental quality of six north shore bays: Nassau and Suffolk Counties, Long Island, New York*Rep. 14*, Stony Brook, New York: Marine Science Research Center, State University of New York.

Guo, W., and C. D. Langevin (2002), *User's Guide to SEWAT: A Computer Program for Simulation of Three-Dimensional Variable-Density Ground-Water Flow*, United States Geological Survey.

Harbaugh, A. W., E. R. Banta, M. C. Hill, and M. G. McDonald (2000), *MODFLOW-2000, the US Geological Survey modular ground-water model: User guide to modularization concepts and the ground-water flow process*, US Geological Survey Reston, VA, USA.

Heiss, J. W., W. J. Ullman, and H. A. Michael (2014), Swash zone moisture dynamics and unsaturated infiltration in two sandy beach aquifers, *Estuarine, Coastal and Shelf Science*, *143*, 20-31.

Henderson, R. D., F. D. Day-Lewis, E. Abarca, C. F. Harvey, H. N. Karam, L. B. Liu, and J. W. Lane (2010), Marine electrical resistivity imaging of submarine groundwater discharge: sensitivity analysis and application in Waquoit Bay, Massachusetts, USA, *Hydrogeology Journal*, *18*(1), 173-185.

Herzberg, D. (1901), *Die wasserversorgung einiger nordseebäder*.

Hirsch, J., and A. Randazzo (2000), Hydraulic seepage within an astatic karst lake, North-Central Florida'.

Howarth, R. W., et al. (1996), Regional nitrogen budgets and riverine N & P fluxes for the drainages to the North Atlantic Ocean: Natural and human influences, *Biogeochemistry*, *35*(1), 75-139.

Hwang, D.-W., G. Kim, Y.-W. Lee, and H.-S. Yang (2005), Estimating submarine inputs of groundwater and nutrients to a coastal bay using radium isotopes, *Marine Chemistry*, *96*(1), 61-71.

Johannes, R. (1980), Ecological significance of the submarine discharge of groundwater, *MARINE ECOL.- PROG. SER.*, *3*(4), 365-373.

Johnson, A. G., C. R. Glenn, W. C. Burnett, R. N. Peterson, and P. G. Lucey (2008), Aerial infrared imaging reveals large nutrient-rich groundwater inputs to the ocean, *Geophysical Research Letters*, *35*(15), L15606.

Kelly, J. L., C. R. Glenn, and P. G. Lucey (2013), High-resolution aerial infrared mapping of groundwater discharge to the coastal ocean, *Limnol. Oceanogr.: Methods*, *11*, 262-277.

Kohout, F. (1960), Cyclic flow of salt water in the Biscayne aquifer of southeastern Florida, *Journal of Geophysical Research*, *65*(7), 2133-2141.

Kohout, F. (1965), Section of geological sciences: a hypothesis concerning cyclic flow of salt water related to geothermal heating in the floridan aquifer, *Transactions of the New York Academy of Sciences*, *28*(2 Series II), 249-271.

Koike, I., and A. Hattori (1978), Denitrification and ammonia formation in anaerobic coastal sediments, *Applied and Environmental Microbiology*, *35*(2), 278-282.

Konikow, L., M. Akhavan, C. Langevin, H. Michael, and A. Sawyer (2013), Seawater circulation in sediments driven by interactions between seabed topography and fluid density, *Water Resources Research*, *49*(3), 1386-1399.

Koppelman, L. E., P. K. Weyl, M. G. Gross, and D. S. Davies (1976), *The urban sea: Long Island Sound*, viii+223 pp., Praeger Publishers, New York.

Kroeger, K., and M. Charette (2008), Nitrogen biogeochemistry of submarine groundwater discharge, *Limnology and Oceanography*, *53*(3), 1025-1039.

Krupa, S. L., T. V. Belanger, H. H. Heck, J. T. Brock, and B. J. Jones (1998), Krupaseep—The next generation seepage meter, *Journal of Coastal Research*, 210-213.

Kuan, W. K., G. Jin, P. Xin, C. Robinson, B. Gibbes, and L. Li (2012), Tidal influence on seawater intrusion in unconfined coastal aquifers, *Water Resources Research*, *48*(2), W02502.

Langevin, C. D., W. B. Shoemaker, and W. Guo (2003), *MODFLOW-2000, the US Geological Survey Modular Ground-Water Model--Documentation of the SEAWAT-2000 Version with the Variable-Density Flow Process (VDF) and the Integrated MT3DMS Transport Process (IMT)*, US Department of the Interior, US Geological Survey.

Laroche, J., R. Nuzzi, R. Waters, K. Wyman, P. Falkowski, and D. Wallace (1997), Brown Tide blooms in Long Island's coastal waters linked to interannual variability in groundwater flow, *Global Change Biology*, *3*(5), 397-410.

Lee, D. R. (1977), A device for measuring seepage flux in lakes and estuaries, *Limnology and Oceanography*, 140-147.

Lewandowski, J., K. Meinikmann, T. Ruhtz, F. Pöschke, and G. Kirillin (2013), Localization of lacustrine groundwater discharge (LGD) by airborne measurement of thermal infrared radiation, *Remote Sensing of Environment*, *138*, 119-125.

Lewis, E., and R. Perkin (1981), The practical salinity scale 1978: Conversion of existing data, *Deep Sea Research Part A. Oceanographic Research Papers*, *28*(4), 307-328.

Lewis, J. B. (1987), Measurements of groundwater seepage flux onto a coral reef: Spatial and temporal variations, *Limnology and Oceanography*, *32*(5), 1165-1169.

Li, L., D. Barry, F. Stagnitti, and J. Parlange (1999), Submarine groundwater discharge and associated chemical input to a coastal sea, *Water Resources Research*, *35*(11), 3253-3259.

Libelo, E. L., and W. G. MacIntyre (1994), Effects of surface-water movement on seepage-meter measurements of flow through the sediment-water interface, *Applied Hydrogeology*, *2*(4), 49-54.

Lubke, E. R. (1964), Hydrogeology of the Huntington-Smithtown area, Suffolk County, New York, *U. S. Geological Survey Water-Supply Paper*(1669-D), 68 p.

Mango, A. J., M. W. Schmeeckle, and D. J. Furbish (2004), Tidally induced groundwater circulation in an unconfined coastal aquifer modeled with a Hele-Shaw cell, *Geology*, *32*(3), 233-236.

Manheim, F. T., D. E. Krantz, and J. F. Bratton (2004), Studying ground water under Delmarva coastal bays using electrical resistivity, *Groundwater*, *42*(7), 1052-1068.

Mao, X., P. Enot, D. Barry, L. Li, A. Binley, and D. S. Jeng (2006), Tidal influence on behaviour of a coastal aquifer adjacent to a low-relief estuary, *Journal of Hydrology*, *327*(1-2), 110-127.

Marshall, T. J., J. W. Holmes, and C. W. Rose (1996), *Soil physics*, Cambridge University Press.

Martin, J. B., J. E. Cable, P. W. Swarzenski, and M. K. Lindenberg (2004), Enhanced Submarine Ground Water Discharge from Mixing of Pore Water and Estuarine Water, *Ground Water*, *42*(7), 1000-1010.

Mc Bride, M. S., and H. O. Pfannkuch (1975), The distribution of seepage within lakebeds, *Jounral of Research of U.S. Geological Survey*, *3*(5), 8.

Michael, H. A., J. S. Lubetsky, and C. F. Harvey (2003), Characterizing submarine groundwater discharge: A seepage meter study in Waquoit Bay, Massachusetts, *Geophys. Res. Lett*, *30*(6), 1297.

Michael, H. A., A. E. Mulligan, and C. F. Harvey (2005), Seasonal oscillations in water exchange between aquifers and the coastal ocean, *Nature*, *436*(7054), 1145-1148.

Michael, H. A., M. A. Charette, and C. F. Harvey (2011), Patterns and variability of groundwater flow and radium activity at the coast: a case study from Waquoit Bay, Massachusetts, *Marine Chemistry*, *127*(1), 100-114.

Moore, W. S. (1999), The subterranean estuary: a reaction zone of ground water and sea water, *Marine Chemistry*, *65*(1), 111-125.

Moore, W. S., and T. J. Shaw (1998), Chemical signals from submarine fluid advection onto the continental shelf, *Journal of Geophysical Research: Oceans (1978–2012)*, *103*(C10), 21543-21552.

Moore, W. S., J. L. Sarmiento, and R. M. Key (2008), Submarine groundwater discharge revealed by 228Ra distribution in the upper Atlantic Ocean, *Nature Geoscience*, *1*(5), 309-311.

Mulligan, A. E., and M. A. Charette (2006), Intercomparison of submarine groundwater discharge estimates from a sandy unconfined aquifer, *Journal of Hydrology*, *327*(3-4), 411-425.

Mulligan, A. E., R. L. Evans, and D. Lizarralde (2007), The role of paleochannels in groundwater/seawater exchange, *Journal of hydrology*, *335*(3), 313-329.

Mulligan, A. E., C. Langevin, and V. E. A. Post (2011), Tidal Boundary Conditions in SEAWAT, *Ground Water*.

Murphy III, W., W. B. Ward, B. Boyd, G. Fleming, W. Murphy IV, R. Nolen-Hoeksema, M. Art, and D. A. Rosales (2011), High-resolution shallow geophysics and geology in the Hudson-Raritan Estuary Ecosystem Restoration, New Jersey, *The Leading Edge*, *30*(2), 182-190.

O'Rourke, D. (2000), Quantifying specific discharge into West Neck Bay, Shelter Island, New York using a three-dimensional finite-difference groundwater flow model and continuous measurements with an ultrasonic seepage meter, 88 pp, State University of New York, Stony Brook.

O'Rourke, D., P. R., and W. T-f. (1999), Measuring Submarine Groundwater Seepage Using an Ultrasonic Flow meter and the "Drum Method"- A Comparative study, in *Geology of Long Island and Metropolitan New York*, edited, Stony Brook, NY, USA.

Oldenburg, D. W., and Y. Li (1999), Estimating depth of investigation in dc resistivity and IP surveys, *Geophysics*, *64*(2), 403-416.

Olhoeft, G. (1981), Electrical properties of rocks, *Physical properties of rocks and minerals*, *2*, 298-305.

Park, M. J. (1985), Prediction of tidal hydraulics and sediment transport patterns in Stony Brook Harbor, State University of New York, Stony Brook.

Paulsen, R., C. Smith, and T.-f. Wong (1998), Defining freshwater outcrops in West Neck Bay, Shelter Island, New York using direct contact resistivity measurements and transient underflow measurements, paper presented at Geology of Long Island and Metropolitan New York, Stony Brook, NY, USA, April, 18th 1998.

Paulsen, R. J., C. F. Smith, D. O'Rourke, and T. F. Wong (2001), Development and evaluation of an ultrasonic ground water seepage meter, *Ground Water*, *39*(6), 904-911.

Paulsen, R. J., D. O'Rourke, C. F. Smith, and T. F. Wong (2004), Tidal Load and Salt Water Influences on Submarine Ground Water Discharge, *Ground Water*, *42*(7), 990-999.

Paulsen, R. J., C. F. Smith, J. Wanlass, and N. H. Stark (2008), Forge River Groundwater Flow Rate and Nutrient Contaminant Load Site Investigation Draft Report*Rep.*, 67 pp, Suffolk County Department of Health Services.

Payne, W. (1973), Reduction of nitrogenous oxides by microorganisms, *Bacteriological Reviews*, *37*(4), 409.

Post, V. (2011), A new package for simulating periodic boundary conditions in MODFLOW and SEAWAT, *Computers & Geosciences*, *37*(11), 1843-1849.

Post, V. E. A. (2005), Fresh and saline groundwater interaction in coastal aquifers: Is our technology ready for the problems ahead?, *Hydrogeology Journal*, *13*(1), 120-123.

Prieto, C., and G. Destouni (2005), Quantifying hydrological and tidal influences on groundwater discharges into coastal waters, *Water resources research*, *41*(12).

Revil, A. (1998), Nature of surface electrical conductivity in natural sands, sandstones, and clays, *Geophys Res Lett*, *25*(5), 691-694.

Robbins, S. K. (1977), Stony Brook Harbor: an interdisciplinary analysis., *Special report Rep. 9*, SUNY Stony Brook, Marine Sciences Research Center.

Robinson, C., B. Gibbes, and L. Li (2006), Driving mechanisms for groundwater flow and salt transport in a subterranean estuary, *Geophys. Res. Lett*, *33*, L03402.

Robinson, C., L. Li, and D. Barry (2007a), Effect of tidal forcing on a subterranean estuary, *Advances in Water Resources*, *30*(4), 851-865.

Robinson, C., L. Li, and H. Prommer (2007b), Tide-induced recirculation across the aquifer-ocean interface, *Water Resources Research*, *43*(7), W07428.

Robinson, C., B. Gibbes, H. Carey, and L. Li (2007c), Salt-freshwater dynamics in a subterranean estuary over a spring-neap tidal cycle, *Journal of Geophysical Research*, *112*(C9), C09007.

Robinson, C., P. Xin, L. Li, and D. A. Barry (2014), Groundwater flow and salt transport in a subterranean estuary driven by intensified wave conditions, *Water Resources Research*, *50*(1), 165-181.

Rosenberry, D. O. (2008), A seepage meter designed for use in flowing water, *Journal of Hydrology*, *359*(1), 118-130.

Rosenberry, D. O., and R. H. Morin (2004), Use of an electromagnetic seepage meter to investigate temporal variability in lake seepage, *Groundwater*, *42*(1), 68-77.

Rumer, R. R., and J. Shiau (1968), Salt water interface in a layered coastal aquifer, *Water Resources Research*, *4*(6), 1235-1247.

Russoniello, C. J., C. Fernandez, J. F. Bratton, J. F. Banaszak, D. E. Krantz, A. S. Andres, L. F. Konikow, and H. A. Michael (2013), Geologic effects on groundwater salinity and discharge into an estuary, *Journal of Hydrology*, *498*, 1-12.

Ryther, J. H. (1954), The ecology of phytoplankton blooms in Moriches Bay and Great South Bay, Long Island, New York, *The Biological Bulletin*, *106*(2), 198-209.

Schubert, C. E. (1998), Areas contributing ground water to the Peconic estuary, and ground-water budgets for the North and South forks and Shelter Island, Eastern Suffolk County, New York.

Shaw, R., and E. Prepas (1989), Anomalous, short-term influx of water into seepage meters, *Limnology and Oceanography*, *34*(7), 1343-1351.

Shinn, E. A., C. D. Reich, and T. D. Hickey (2002), Seepage meters and Bernoulli's revenge, *Estuaries*, *25*(1), 126-132.

Sholkovitz, E., C. Herbold, and M. Charette (2003), An automated dye-dilution based seepage meter for the time-series measurement of submarine groundwater discharge, *Limnol. Oceanogr. Methods*, *1*, 16-28.

Slomp, C. P., and P. Van Cappellen (2004), Nutrient inputs to the coastal ocean through submarine groundwater discharge: controls and potential impact, *Journal of Hydrology*, *295*(1), 64-86.

Smith, A. J. (2004), Mixed convection and density-dependent seawater circulation in coastal aquifers, *Water Resources Research*, *40*(8).

Soren, J. (1978), Hydrogeologic conditions in the town of Shelter Island, Suffolk County, Long Island, New York., *Water-Resources Investigation Report Rep. 77-77*, U. S. Geological Survey.

Stark, N., J. M. Durand, T.-f. Wong, J. Wanlass, and R. Paulsen (2012a), Submarine Groundwater Discharge in Relation to the Occurrence of Submerged Aquatic Vegetation, Data Report for Site 2, Gardiners Bay*Rep.*, Peconic Estuary Program of the Suffolk County Department of Health Services.

Stark, N., J. M. Durand, T.-f. Wong, J. Wanlass, and R. Paulsen (2012b), Submarine Groundwater Discharge in Relation to the Occurrence of Submerged Aquatic Vegetation, Data Report for Site 4, Bullhead Bay*Rep.*, Peconic Estuary Program of the Suffolk County Department of Health Services.

Stark, N., J. M. Durand, T.-f. Wong, J. Wanlass, and R. Paulsen (2012c), Submarine Groundwater Discharge in Relation to the Occurrence of Submerged Aquatic Vegetation, Data Report for Site 1, Three Mile Harbor*Rep.*, Peconic Estuary Program of the Suffolk County Department of Health Services.

Stark, N., J. M. Durand, T.-f. Wong, J. Wanlass, and R. Paulsen (2012d), Submarine Groundwater Discharge in Relation to the Occurrence of Submerged Aquatic Vegetation, Data Report for Site 3, Cedar Point*Rep.*, Peconic Estuary Program of the Suffolk County Department of Health Services.

Stieglitz, T., M. Taniguchi, and S. Neylon (2008a), Spatial variability of submarine groundwater discharge, Ubatuba, Brazil, *Estuarine Coastal and Shelf Science*, *76*(3), 493-500.

Stieglitz, T., J. Rapaglia, and H. Bokuniewicz (2008b), Estimation of submarine groundwater discharge from bulk ground electrical conductivity measurements, *Journal of Geophysical Research*, *113*(C8), C08007.

Stieglitz, T. C., J. Rapaglia, and S. C. Krupa (2007), An effect of pier pilings on nearshore submarine groundwater discharge from a (partially) confined aquifer, *Estuaries and coasts*, *30*(3), 543-550.

Swarzenski, P. W., F. W. Simonds, A. J. Paulson, S. Kruse, and C. Reich (2007), Geochemical and geophysical examination of submarine groundwater discharge and associated nutrient loading estimates into Lynch Cove, Hood Canal, WA, *Environmental Science & Technology*, *41*(20), 7022-7029.

Swarzenski, P. W., W. Burnett, C. Reich, H. Dulaiova, R. Peterson, and J. Meunier (2004), Novel geophysical and geochemical techniques used to study submarine groundwater discharge in Biscayne Bay, Florida.

Swarzenski, P. W., W. C. Burnett, W. J. Greenwood, B. Herut, R. Peterson, N. Dimova, Y. Shalem, Y. Yechieli, and Y. Weinstein (2006), Combined time-series resistivity and geochemical tracer techniques to examine submarine groundwater discharge at Dor Beach, Israel, *Geophysical Research Letters*, *33*(24).

Taniguchi, M. (2002), Tidal effects on submarine groundwater discharge into the ocean, *Geophysical Research Letters*, *29*(12).

Taniguchi, M., and Y. Fukuo (1993), Continuous Measurements of Ground-Water Seepage Using an Automatic Seepage Meter, *Groundwater*, *31*(4), 675-679.

Taniguchi, M., and H. Iwakawa (2001), Measurements of submarine groundwater discharge rates by a continuous heat-type automated seepage meter in Osaka Bay, Japan, *Journal of Groundwater Hydrology*, *43*(4), 271-278.

Taniguchi, M., and H. Iwakawa (2004), Submarine groundwater discharge in Osaka Bay, Japan, *Limnology*, *5*(1), 25-32.

Taniguchi, M., W. C. Burnett, J. E. Cable, and J. V. Turner (2002), Investigation of submarine groundwater discharge, *Hydrological Processes*, *16*(11), 2115-2129.

Taniguchi, M., T. Ishitobi, W. C. Burnett, and G. Wattayakorn (2007), Evaluating ground water–sea water interactions via resistivity and seepage meters, *Ground Water*, *45*(6), 729-735.

Taniguchi, M., W. C. Burnett, H. Dulaiova, E. A. Kontar, P. P. Povinec, and W. S. Moore (2006), Submarine groundwater discharge measured by seepage meters in Sicilian coastal waters, *Continental Shelf Research*, *26*(7), 835-842.

Tarantola, A. (2005), *Inverse problem theory and methods for model parameter estimation*, siam.

Taylor, R. W., and D. S. Cherkauer (1984), The application of combined seismic and electrical measurements to the determination of the hydraulic conductivity of a lake bed, *Groundwater Monitoring & Remediation*, *4*(4), 78-85.

Telford, W. M., L. Geldart, and R. E. Sheriff (1990), *Applied geophysics*, Cambridge Univ Pr.

Top, Z., L. E. Brand, R. D. Corbett, W. Burnett, and J. Chanton (2001), Helium and radon as tracers of groundwater input into Florida Bay, *Journal of Coastal Research*, 859-868.

Turner, I. L., B. P. Coates, and R. I. Acworth (1997), Tides, waves and the super-elevation of groundwater at the coast, *Journal of Coastal Research*, 46-60.

Valiela, I., and C. Delia (1990), Special issue-groundwater inputs to coastal waters-introduction, edited, Kluwer Academic Publ Spuiboulevard 50, Po Box 17, 3300 Aa Dordrecht, Netherlands.

Valiela, I., J. M. Teal, S. Volkmann, D. Shafer, and E. J. Carpenter (1978), Nutrient and particulate fluxes in a salt marsh ecosystem: Tidal, *Limnol. Oceanogr*, *23*(4), 798-812.

Valiela, I., K. Foreman, M. LaMontagne, D. Hersh, J. Costa, P. Peckol, B. DeMeo-Andreson, C. D'Avanzo, M. Babione, and C. H. Sham (1992), Couplings of watersheds and coastal waters: sources and consequences of nutrient enrichment in Waquoit Bay, Massachusetts, *Estuaries and Coasts*, *15*(4), 443-457.

Wanlass, J. S. (2009), Development of an integrated geophysical and hydrological approach to study submarine ground water discharge into Forge River, Stony Brook University, Stony Brook.

Weinstein, Y., W. C. Burnett, P. W. Swarzenski, Y. Shalem, Y. Yechieli, and B. Herut (2007), Role of aquifer heterogeneity in fresh groundwater discharge and seawater recycling: An example from the Carmel coast, Israel, *Journal of Geophysical Research-Oceans*, *112*(C12).

Wilson, A. M., and L. R. Gardner (2006), Tidally driven groundwater flow and solute exchange in a marsh: numerical simulations, *Water Resources Research*, *42*(1).

Winter, T., and H. Pfannkuch (1984), Effect of anisotropy and groundwater system geometry on seepage through lakebeds: 2. Numerical simulation analysis, *Journal of Hydrology*, *75*(1), 239-253.

Xin, P., C. Robinson, L. Li, D. A. Barry, and R. Bakhtyar (2010), Effects of wave forcing on a subterranean estuary, *Water Resources Research*, *46*(12), W12505.

Young, C. R. (2013), Fate of Nitrogen during Submarine Groundwater Discharge into Long Island North Shore Embayments, 165 pp, Stony Brook University.

Zektser, I. S., L. G. Everett, and R. G. Dzhamalov (2006), *Submarine groundwater*, CRC Press Inc.

Zheng, C., and P. P. Wang (1999a), MT3DMS, *A modular three-dimensional multi-species transport model for simulation of advection, dispersion and chemical reactions of contaminants in groundwater systems*.

Zheng, C., and P. P. Wang (1999b), MT3DMS: a modular three-dimensional multispecies transport model for simulation of advection, dispersion, and chemical reactions of contaminants in groundwater systems; documentation and user's guide*Rep.*, DTIC Document.

Zumft, W. G. (1997), Cell biology and molecular basis of denitrification, *Microbiology and Molecular Biology Reviews*, *61*(4), 533-616.